Photodegradation of Polyester Films

Fiona Jane Horne

A thesis submitted to the Department of Pure and Applied Chemistry, University of Strathclyde in part fulfilment of the requirements for the degree of Doctor of Philosophy.

February 2019

Declaration

This thesis is the result of the author's original research. It has been composed by the author and has not been previously submitted for examination which has led to the award of a degree.

The copyright of this thesis belongs to the author under the terms of the United Kingdom Copyright Acts as qualified by University of Strathclyde Regulation 3.50. Due acknowledgment must always be made to the use of any material contained in, or derived from, this thesis.

Signed: Date:

Acknowledgments

Firstly, I would like to thank my supervisor, Dr John J. Liggat, for welcoming me into his research group and for all his support and guidance throughout the duration of my PhD. He is a pleasure to work with and I couldn't have done this without you!

I am grateful to DuPont Teijin Films for providing the funding for this research. Further appreciation and thanks go to my industrial supervisors Professor Bill MacDonald and Dr Stephen Sankey for their appreciated support and advice.

Within the chemistry department, I would like to thank Neil Hodgson for his excellent glassblowing skills and Dr Brian McMillan for his advice and support. In addition, thanks must also go to Dr P. L Tang for his help with the IR instruments, and his invaluable help and support.

I would like to extend my thanks to all the postgraduate students in TG 521, past and present, for their kindness and advice throughout the years.

Finally, special thanks must go to my husband Stuart and my parents for their continued love, support, and encouragement. I couldn't have got through this without you and for that, I dedicate this thesis to you.

Abstract

Poly(ethylene terephthalate) (PET) is well known for its excellent properties, but when exposed to ultra-violet (UV) light PET films have the tendency to degrade, which in some applications can be a shortcoming. Many groups have studied the different degradation pathways that can occur in PET during outdoor exposure, however, the effect of specific narrow band wavelength ranges of light have received little attention.

To begin, this research programme was concerned with understanding the effects of exposing PET films to narrow and broad band wavelength ranges of light. The narrow band wavelength ranges used were 302 and 365 nm light and the broad band wavelength range was 290-800 nm. Single films were analysed as well as stacks of films, to investigate whether these could be used to depth profile a single film of the same thickness, during exposure. When using narrow band wavelength ranges, oxidative and non-oxidative conditions (under nitrogen) were used. This fundamental study concluded that PET degrades more extensively under short wavelength light (302 nm) compared to longer wavelength light (365 nm) of the same intensity and when exposed under oxidative conditions compared to non-oxidative conditions. During exposure, various degradation products were proven to be produced, including carboxylic acid end groups, dimers, quinone species, monohydroxy terephthalate groups and mono-substituted terephthalic rings.

Another area of this research was focused on using a novel way to study the reactions that take place as a consequence of different wavelengths of light, while still replicating outdoor exposure. Exposing samples to the full spectrum of light means that photodegradation reactions taking place as a consequence of short and long wavelengths of light, happen simultaneously. Whereas, if samples were exposed to different wavelengths of light consecutively, the reactions that happen simultaneously outdoors could be studied. Samples were therefore exposed to one wavelength of light followed by another wavelength of light (302 nm light followed by 365 nm light and vice versa). This study showed that long wavelength light (365 nm) can cause more damage to a film than previously reported, especially when a film has already been photodegraded using short wavelength light (302 nm) before being exposed to longer wavelength light.

Finally, the photodegradation behaviour of poly(diethylene glycol terephthalate) (PDEGT) homopolymer was studied. Although the thermal degradation of PDEGT has been previously reported, the photodegradation of PDEGT has received no attention. The effects of temperature, atmosphere, and wavelength of light were considered, resulting in the PDEGT showing a higher extent of degradation compared to PET, exposed under the same conditions. A mechanistic pathway for the photodegradation reactions occurring in PDEGT during exposure has been proposed.

Table of Contents

1 Photodegradation of terephthalate polymers 1
1.1 Photovoltaics 1
1.2 Photochemistry of polyesters 4
1.3 Photodegradation of Poly(ethylene terephthalate) 13
1.3.1 Photolysis 15
1.3.2 Photo-oxidation 25
1.4 Summary of literature for PET 35
1.5 Photodegradation of Poly(ethylene naphthalate) 36
1.5.1 Photolysis 37
1.5.2 Photo-oxidation 43
1.6 Poly(diethylene glycol) terephthalate 45
1.7 Focus of research 46
1.8 References 48

2 Experimental 56
2.1 Materials 56
2.1.1 PET film samples 56
2.1.2 PDEGT thin films 56
2.2 Sample exposure 56
2.2.1 Atlas Suntest Weatherometer XLS+ 57
2.2.3 Hönle Cube 100 Lamps 62
2.2.4 Exposure under a non-oxidative atmosphere 63
2.3 Infra-red 63
2.3.1 Attenuated Total Reflectance Fourier Transform Infrared 65
2.3.2 Diffuse Reflectance Infrared Fourier Transform 70
2.4 Differential Scanning Calorimetry 72
2.4.1 Theory 72
2.4.2 Experimental conditions 75
2.5 Ultraviolet-visible Spectroscopy 76

2.5.1 Theory 76
2.5.2 Experimental conditions 79
2.6 Fluorescence Spectroscopy 80
2.6.1 Theory 80
2.6.2 Experimental conditions 81
2.7 Ultraviolet-visible-near infrared spectroscopy 82
2.7.1 Theory 82
2.7.2 Experimental conditions 82
2.8 Contact Angle 83
2.8.1 Theory 83
2.8.2 Experimental conditions 85
2.9 Scanning Electron Microscopy 85
2.9.1 Theory 85
2.9.2 Experimental conditions 87
2.10 Calculation of errors 87
2.11 References 91

3 Fundamental photodegradation studies of PET 93
3.1 Characterisation of PET film 93
3.2 Stacked films 100
3.2.1 Intensity Measurements 100
3.2.2 Scattering Model 102
3.2.3 Conclusions 106
3.3 Weatherometer irradiations 106
3.3.1 ATR FT-IR 106
3.3.2 DRIFT 117
3.3.3 UV-visible spectroscopy 124
3.3.4 Fluorescence spectroscopy 127
3.3.5 DSC 130
3.3.6 Contact angle 136
3.3.7 Scanning Electron Microscopy 138
3.3.8 General Conclusions 141

3.4 Effect of specific wavelengths on the photodegradation of PET 141
3.4.1 ATR FT-IR 142
3.4.2 DRIFT 153
3.4.3 UV-visible spectroscopy 159
3.4.4 DSC 162
3.4.5 Scanning Electron Microscopy 171
3.4.6 General Conclusions 171
3.5 Exposing PET to high intensity 365 nm light 173
3.5.1 Infrared 173
3.5.2 UV-visible spectroscopy 176
3.5.3 General Conclusions 177
3.6 Effect of degradation atmosphere on the photodegradation of PET 178
3.6.1 Exposing PET to 302 nm light under nitrogen 178
3.6.2 General Conclusions 187
3.7 References 188

4 The effect of UV light pre-treatment on the photo-oxidation of PET 192
4.1 Exposure to 302 nm followed by 365 nm 193
4.1.1 ATR FT-IR 193
4.1.2 DRIFT 205
4.1.3 UV-visible spectroscopy 212
4.1.4 Fluorescence spectroscopy 213
4.1.5 DSC 215
4.1.6 Contact Angle 221
4.1.7 Scanning Electron Microscopy 224
4.1.8 Conclusions 226
4.2 Exposure to 365 nm followed by 302 nm 227
4.2.1 ATR FT-IR 227
4.2.2 DRIFT 234
4.2.3 UV-visible spectroscopy 239
4.2.4 Fluorescence spectroscopy 240
4.2.5 DSC 242

4.2.6 Contact Angle 249
4.2.7 Scanning Electron Microscopy 251
4.2.8 Conclusions 253
4.3 References 254

5 Investigating the role of wavelength, temperature, and atmosphere on the photodegradation of PDEGT 257
5.1 Characterisation of PDEGT 257
5.2 Weatherometer irradiations 262
5.2.1 Weekly weatherometer exposures 262
5.2.2 Shorter weatherometer exposures 281
5.2.3 UV-Vis-NIR 287
5.2.4 Conclusions 288
5.3 Effect of wavelength on the photodegradation of PDEGT 289
5.3.1 ATR FT-IR 289
5.3.2 DRIFT 298
5.3.3 UV-Vis-NIR 305
5.3.4 Conclusions 306
5.4 Exposing PDEGT to high intensity 365 nm light 307
5.4.1 Infrared 307
5.4.2 UV-Vis-NIR 310
5.4.3 Images of exposed PDEGT 311
5.4.4 Conclusions 313
5.5 Effect of temperature 314
5.5.1 Infrared results 314
5.5.2 UV-Vis-NIR 324
5.5.3 Conclusions 325
5.6 Effect of degradation atmosphere 326
5.6.1 Infrared results 326
5.6.2 Conclusions 336
5.7 Mechanistic pathways for the photodegradation of PDEGT 336
5.7.1 Oxidative conditions 336

5.7.2 Non-oxidative conditions 336
5.8 References 339

6 Conclusions and Future Work 341
6.1 Conclusions 341
6.2 Future Work 344

1 Photodegradation of terephthalate polymers

1.1 Photovoltaics

Photovoltaics is the technology that generates electrical power by converting sunlight directly into electricity. When photons of light are absorbed there is a release of electrons. When those free electrons are captured, electric current results. This can be used as an immediate power source or stored for later. An illustration of how solar energy works is shown in *Figure 1.01*.[1]

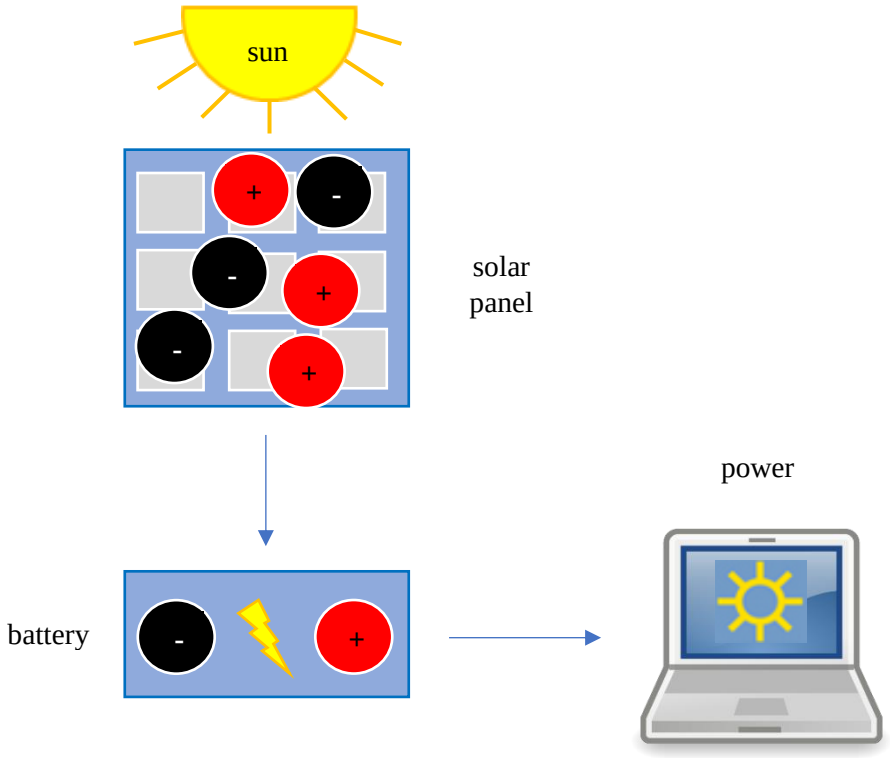

Figure 1.01: Illustration of how solar energy works.[1]

The first functional large area solar cell was made by Fritts in 1883. The twentieth century saw major developments in this area, including the production of the first efficient solar cell from the Bell Lab, USA in 1954 and the world's first solar-powered building at the University of Delaware, USA in 1973. By 2002, the cumulative

worldwide installed photovoltaics reached 2000 MW. This was an important improvement as it had taken 25 years to reach the first 1000 MW but only 3 years to double it.[2]

The International Energy Agency reported that 2016 was a record-breaking year with a 50% growth bringing the market to approximately 75 GW. Many regions of the world are now contributing to PV development with 1.8% of the world's electricity generation covered by PV.[3]

Within the solar panel, there are several different layers, shown in the illustration in *Figure 1.02.* A layer of glass is generally used as the top layer to protect the solar panel, allowing the transmission of light and providing mechanical strength. The solar cells are the most important part of the device as they convert sunlight to electrical current and are protected by the encapsulant.

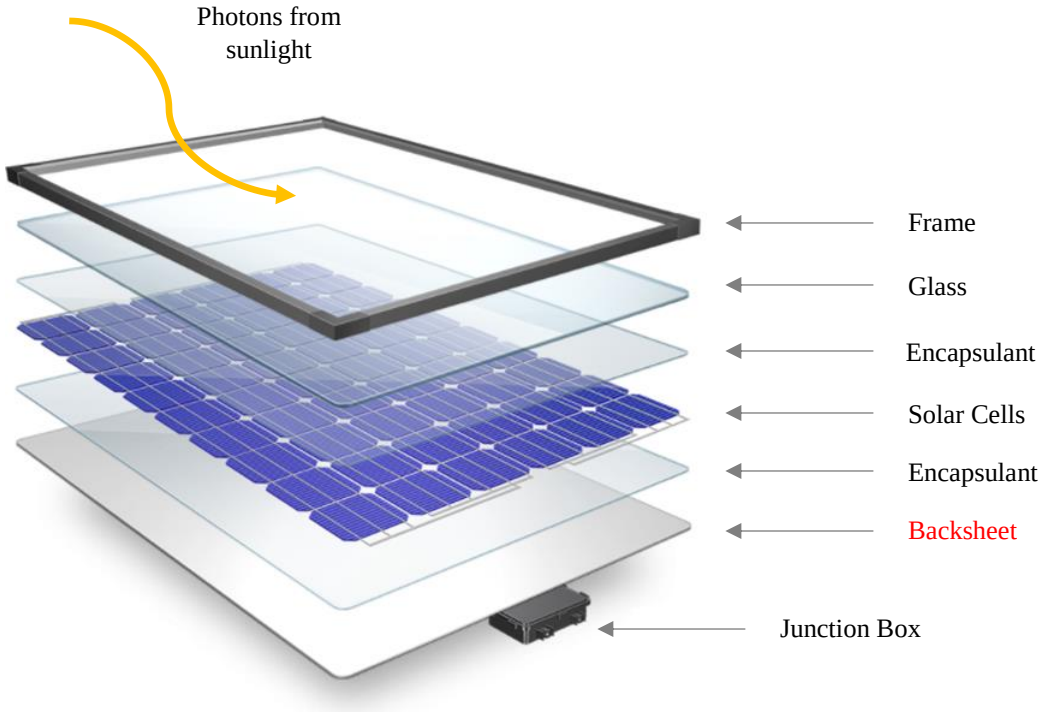

Figure 1.02: Illustration of a solar panel.[1]

A commonly used encapsulant is ethylene-vinyl acetate (EVA), which provides long-term protection of the solar cells and allows the transmission of sunlight. The purpose of the backsheet is to protect the active layer and encapsulant against environmental degradation, while also acting as an electrical insulator. Therefore, it is important that the backsheet does not degrade when exposed to any of the above environments.

Figure 1.03 gives illustrations of two different photovoltaic module structures which shows that when a backsheet is used, light is reflected and transmitted through this single backsheet layer. Again, showing that it is essential that the backsheet does not degrade when exposed outdoors.

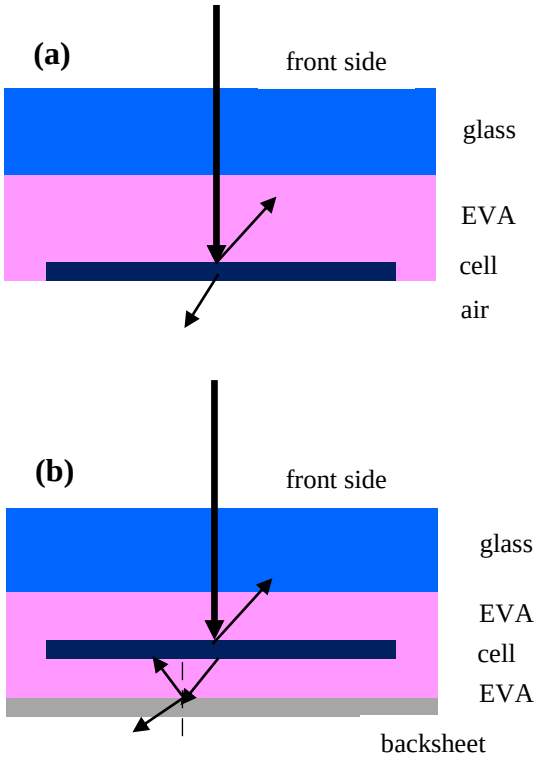

Figure 1.03: Illustration of PV structures (a) glass/cell and (b) glass/cell/backsheet.[4]

Polymeric backsheets are typically made up of three layers of laminated polymer films. An illustration of the structure of a typical backsheet is given in *Figure 1.04.* The core layer is commonly made of PET, providing high mechanical strength and electrical insulation, sandwiched between the inner and outer layers. The inner layer is often EVA or low-density polyethylene (LDPE), while the outer layer is a fluoro-containing polymeric material. The backsheet is essential for long-term durability.[5,6]

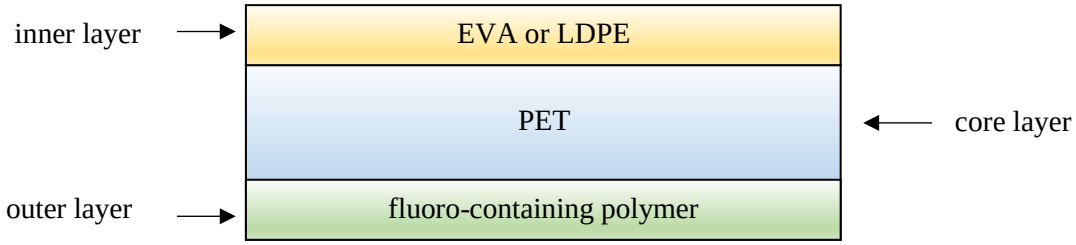

Figure 1.04: Illustration of a three-layer, ABA structure, polymeric backsheet.

Some advantages of photovoltaics are that they have low operating costs, they operate at ambient temperature (so no elevated temperature corrosion), they provide clean – green energy, and they are extremely reliable. However, there are still some disadvantages of photovoltaics, including high installation costs and the fact that the sun does not shine 24 hours a day, meaning the PV cell stops producing electricity when the sun goes down or is reduced in overcast skies.

1.2 Photochemistry of polyesters

Photochemistry is the study of chemical reactions brought about by the interaction of a light quantum and a molecule which result in chemical changes.[7–9] The vital part of a photochemical process is the absorption of a photon which activates the reaction. Photochemical reactions are valuable as their activation differs from thermal reactions in that they may be more precise; light could be absorbed by a specific chromophore

within the molecule.[7] The majority of polymers can absorb UV radiation <300 nm but if a chromophore is present, such as a carbonyl group, they can absorb at even longer wavelengths.[10] The mechanism by which a polymer photodegrades depends highly on the concentration and type of chromophore that is present.

The likelihood of a polymer undergoing photodegradation is down to its ability to absorb photons of suitable energy and if there are photochemical pathways that can utilise this energy.[10] Grotthus and Draper formulated the first law of photochemistry at the start of the 19th century. This state's 'only the light absorbed by a molecule can produce photochemical change in the molecule.'[8,10,11] Stark and Einstein developed and modified this law with the evolution of quantum theory; the second law of photochemistry thus states 'if a species absorbs radiation, then one particle is excited for each quantum of radiation absorbed.'[8]

Figure 1.05 shows a model of a photochemical reaction and that for Stark and Einstein's law to be true all of the excited molecules must form photoproducts and not be lost by any of the alternative processes.[12]

Photochemistry is an important process in polymers as on exposure to UV light, degradation of the polymers useful properties, such as flexibility, strength and the capability of the polymer to endure extreme temperatures and chemicals, can occur.[13,14,15,16] There are many types of degradation processes which polymers undergo; thermal, mechanical, ultrasonic, hydrolysis, chemical, biological and radiation.[13,14] The type of degradation process that takes place depends on the environmental conditions in which the polymer is used, the structure of the polymer and its manufacturing history.[14]

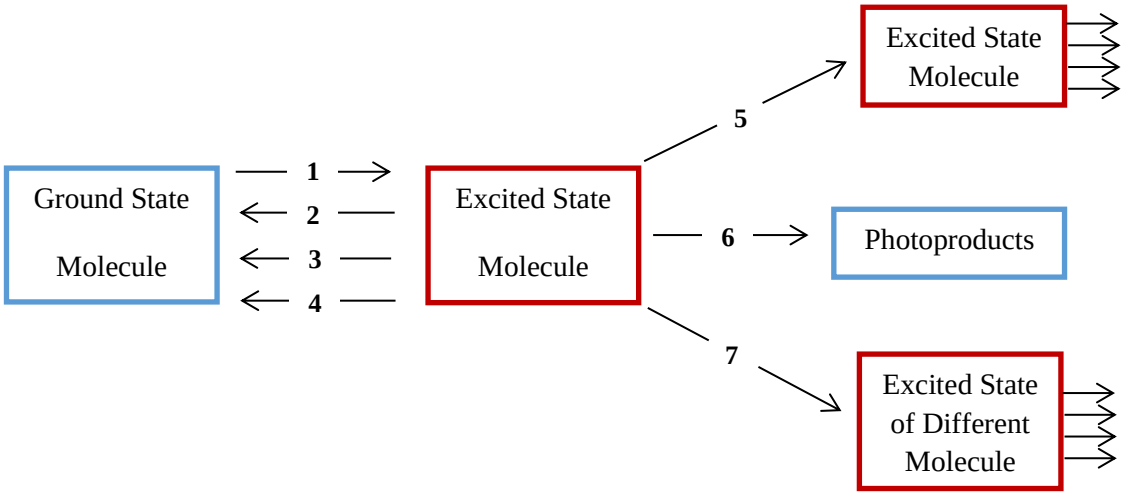

Figure 1.05: Modified model for a photochemical reaction. 1 = Absorption of light, 2 = Emission of light: fluorescence, 3 = Internal conversion of energy, 4 = Reaction with a different molecule losing energy, 5 = Intersystem Crossing, 6 = Decomposition, 7 = Reaction with a different molecule losing energy & photosensitisation.[12]

The poor stability of polymers to weathering, particularly UV light, has caused problems within polymer applications and has limited their lifetime.[17,18] UV light is split into three different ranges; UV-A (320-400 nm), UV-B (290-320 nm) and UV-C(190-290 nm). However, UV-C does not reach the earth's surface and therefore UV-A and UV-B are important in studying the photo-degradation reactions of polymers.[19]

Electronic transitions are caused by the reaction of UV and visible light with matter. The electrons are promoted from the ground state to an excited singlet or triplet electronic state which subsequently changes the occupation of electron orbitals. These electronically excited states can be more reactive than the ground state molecule as they will have new electronic arrangements so can participate in different reactions and possess more energy. Some of the reactions that the excited molecule could undergo are shown in *Figure 1.06*. [7]

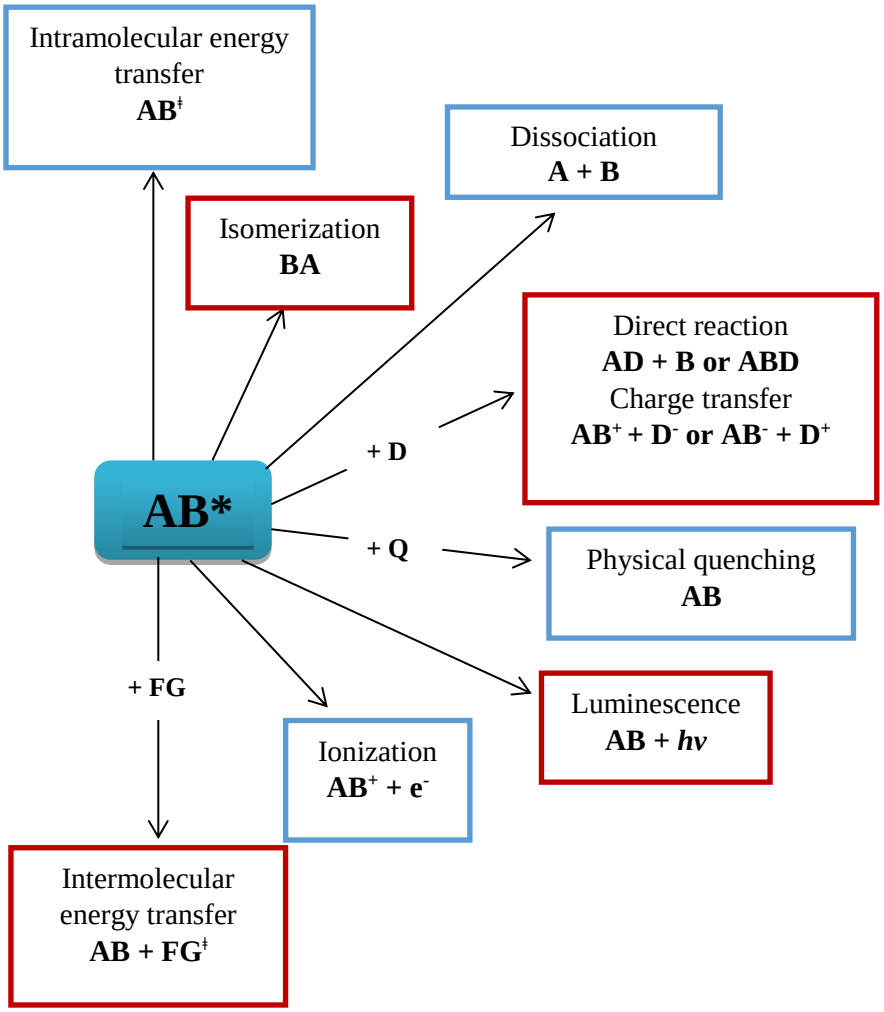

Figure 1.06: Modified schematic of possible routes for excited molecules to loss electronic excitation.[8]

Absorbing a photon means a molecule has enough energy to react, but not every molecule that is excited forms a specific primary product as excitation may be lost in several ways. Therefore we use the primary quantum yield which, for each photon absorbed, is the number of reactant molecules producing specified primary products.[21] Equation 1 defines the primary quantum yield as the number of events that lead to primary products divided by the number of photons absorbed by the molecule in the same interval.[21]

$$\phi = \frac{number\ of\ events}{number\ of\ photons\ absorbed}$$ **Equation 1**

The lifetime that is observed for the excited state is related to the rate constant of emission and the quantum yield.[21]

The electronic transitions that are possible are: π – π*, n – π*, σ – σ* and n – σ*, shown in *Figure 1.07*[12] The energetically most favoured electron promotion is from the highest occupied molecular orbital (HOMO) to the lowest unoccupied molecular orbital (LUMO) which results in an excited state and is also the lowest possible energy transition.[7]

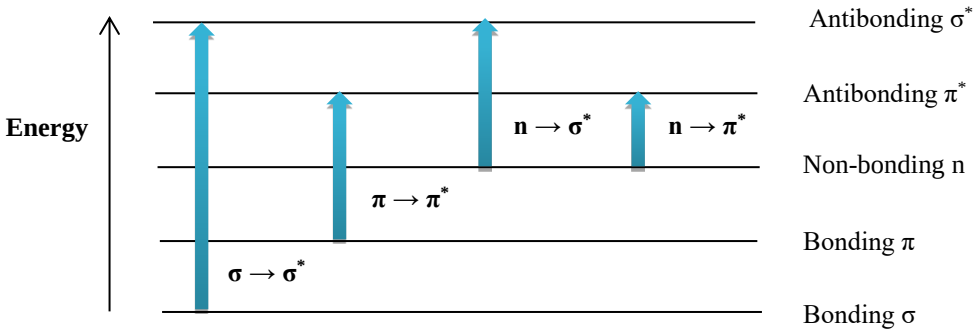

Figure 1.07: Modified schematic of possible electronic transitions.[12]

The ester carbonyl chromophoric groups, in polyesters, are primarily responsible for the absorption of UV light (290 – 400 nm); absorption increases with lowering of the HOMO-LUMO gap.[22]

In PET the carbonyl group acts as a chromophore and can undergo n – π*and π – π* and transitions, in the UV-visible region. This is due to the fact that this chromophore contains both π electrons and non-bonding n-electrons, shown in *Figure 1.08*.[23,24]

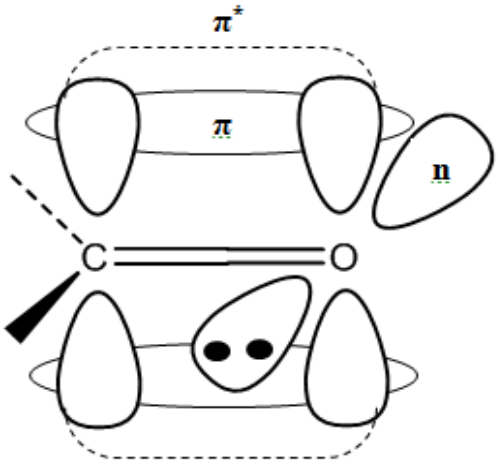

Figure 1.08: Orbital diagram for carbonyl chromophore showing π and n electrons.[25]

The n – π* transition, where n represents a non-bonding orbital, is due to the lone pairs of electrons on the oxygen atom. One of these n electrons can be excited into an empty π* orbital.[23,24] *Figure 1.09* shows a schematic of this transition.[21]

The n – π* transitions in carbonyls are symmetry forbidden and therefore the absorptions are weak. The typical absorption energies are approximately 4 eV at a wavelength of 290 nm.[21] This forbidden transition is only observed due to the molecular symmetry that prohibits it is broken by molecular vibrations. Whereas π – π* transitions are more allowed, due to special overlaps. The values of ε_{max} for forbidden transitions are less than 10^4 but for allowed transitions values of ε_{max} are usually more than 10^4. The intensities of the transitions within PET depend on the allowedness of the transition.[23,24]

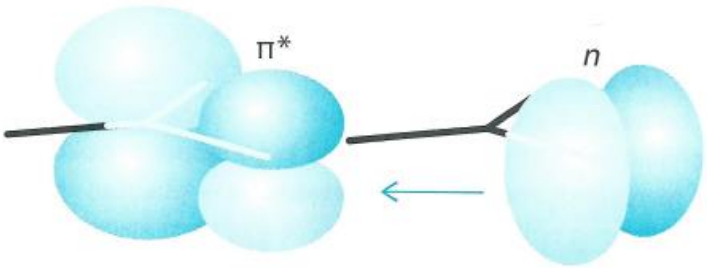

Figure 1.09: n - π* transition, in PET, due to the carbonyl group acting as a chromophore.[21]

Using different wavelengths of UV light to irradiate a sample means that the absorption energies will also be different. Energies can be calculated, for different wavelengths, using Equation 2.

$$E = \frac{h\,c}{\lambda} \qquad \textbf{Equation 2}$$

Where E is the energy of a photon, h is Planck's constant, c is the speed of light and λ is the wavelength of light used.

The absorption characteristics of some typical chromophoric groups, including the carbonyl chromophore, as seen in PET, are shown in Table 1.[21]

Table 1: Absorption characteristics of chromophore groups.[21]

Group	$\bar{\nu}$ (cm^{-1})	λ_{max} (nm)	Ɛ (dm^3 mol^{-1} cm^{-2})
C=C ($\pi \rightarrow \pi^*$)	61000	163	15000
	57300	174	5500
C=O ($n \rightarrow \pi^*$)	35000 – 37000	270 – 290	10 – 20
H_2O ($n \rightarrow \pi^*$)	60000	167	7000

In PET the states responsible for absorption and emission are shown in the schematic in *Figure 1.10*. The figure also indicates the energies needed, in electron volts, for transitions to occur between these states. At different irradiation wavelengths, the energy of the transitions change as previously shown in *Equation 2*.[26]

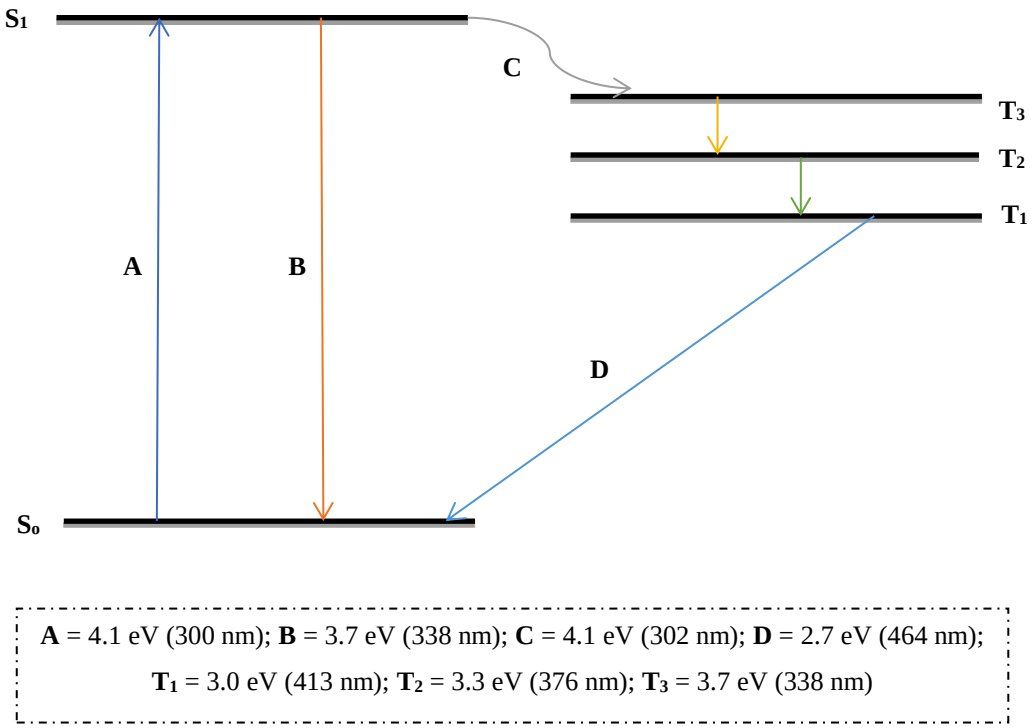

Figure 1.10: Modified diagram of the state's responsible for absorption and emission in PET.[26]

UV-visible absorption spectra of PET and PEN, shown in *Figure 1.11*, show the wavelength dependence of absorption for both polymers. From the absorption spectrum of PET, the λ_{max} is approximately 310 nm. The spectra show that longer wavelengths (315 - 400 nm) are absorbed weakly whereas the shorter wavelengths (250- 315 nm) are strongly absorbed.[27,28]

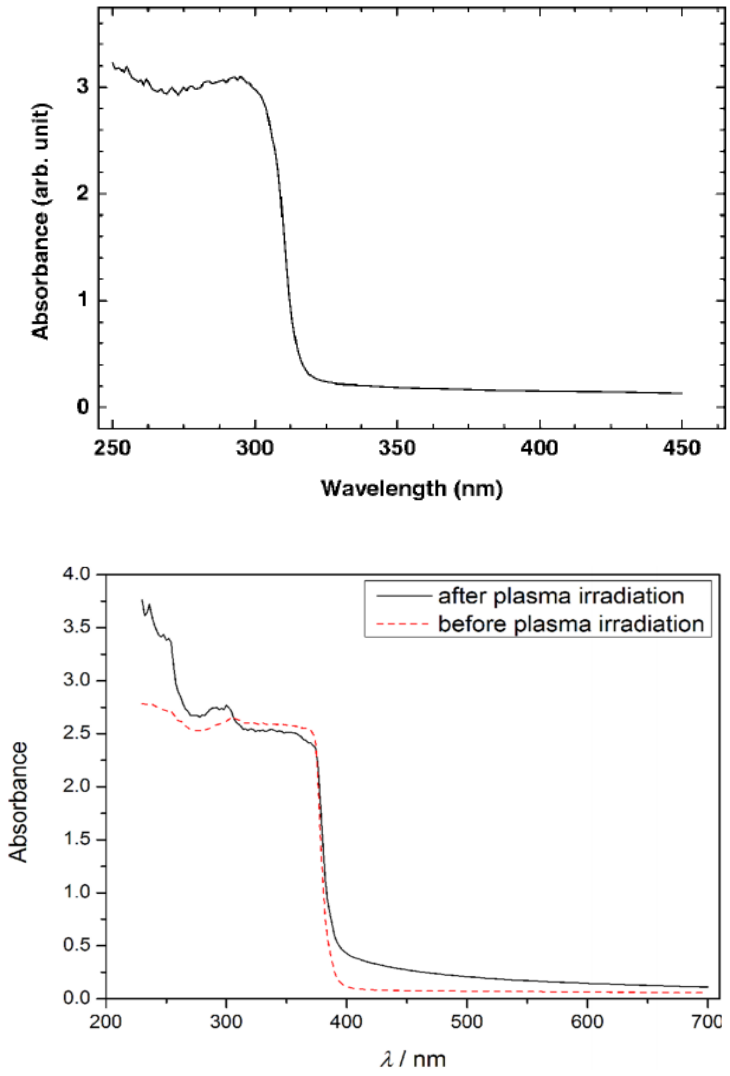

Figure 1.11: UV-visible absorption spectra of PET (a) and PEN (b).[27,28]

The absorptions can also be considered using the Beer-Lambert Law, shown in Equation 3.

$$A = \varepsilon\, b\, c \qquad \textbf{Equation 3}$$

Where A is the absorption of light, b is the path length, c is the concentration of absorbing species and Ɛ is the molar absorption coefficient. For strongly absorbing

chromophores the molar absorptivities can be very large but if absorption is weak the molar absorptivity can be very small. The probability that a certain wavelength of light will be absorbed and the size of the chromophore are both parameters that would affect the magnitude of ε.[21] Dobashi *et al.* stated that photodegradation would be expected to depend on ε and λ_{max} but went on to report that the wavelength is the most important issue.[19]

This review will center on the progress made in understanding the photochemical reactions taking place in PET and PEN on exposure to UV light.

1.3 Photodegradation of Poly(ethylene terephthalate)

PET is a linear, semi-crystalline, synthetic, thermoplastic polymer[29,30] commonly synthesised from the polyesterification reaction between terephthalic acid and ethylene glycol, with a by-product of water; ethylene glycol is removed during esterification to prevent a back reaction.

PET was first synthesised by Carothers in the 1930s and in 1941 Whinfield and Dickson patented the synthesis of PET.[31,32] The structural repeat unit of PET is given in *Figure 1.12*.

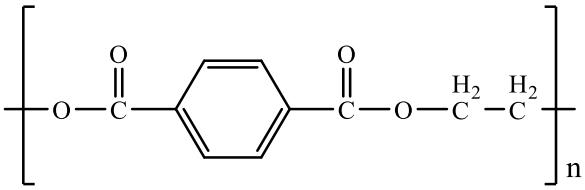

Figure 1.12: Structural repeat unit of PET.

In 2016 the global yearly production of PET was approximately 50.01 million metric tonnes with 1.9 million tonnes of PET bottles collected for recycling in Europe, which

is an increase of 2.1% compared to the previous year.[30] *Figure 1.13* shows the European plastic demand by polymer type for 2016.[33]

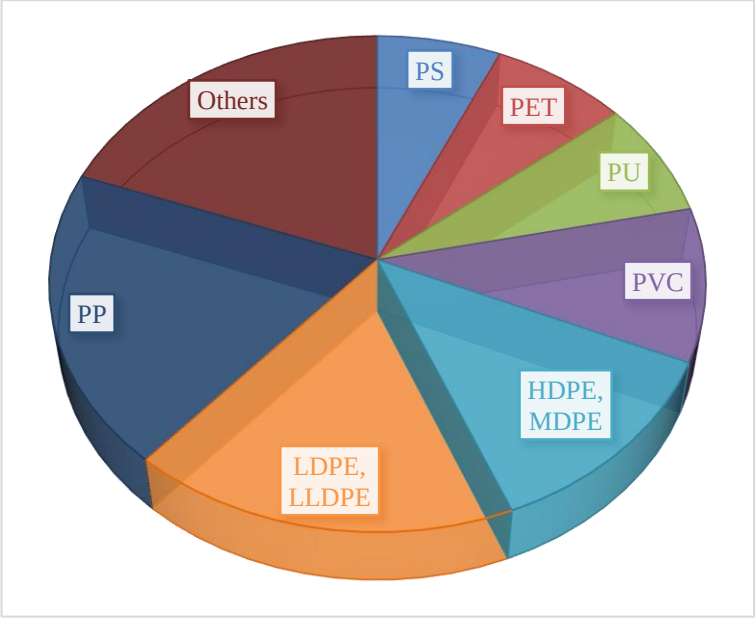

Figure 1.13: European plastic demand by polymer type in 2016.

The increasing interest in recycling PET is due to its use in a wide range of markets such as cards, electronics, packaging, soft-drink bottles and photovoltaics.[29] It is very important as an engineering plastic because it has an unusual balance of physical, chemical, thermal and electrical properties.[34]

PET has been reported to have a much longer lifetime than polyolefins[35] but on exposure to UV light PET films still tend to degrade, which often leads to brittleness and loss of transparency.[36–38] The photodegradation of PET has been studied by different groups[39–46] under a range of artificial light sources,[41,42,47–55] and a small number of papers have been published.

During photodegradation of PET, chemical groups are formed, such as hydroperoxides carbonyls and carboxylic acids.[56,57] The degree of chemical degradation is not the only

factor that should be evaluated when considering the durability of polymer products; the depth profile of degradation and surface deterioration are also important parameters.[58–62] Studying the photodegradation process of PET involves analysing the photolysis and photo-oxidative reactions taking place during exposure.[63]

1.3.1 Photolysis

In a series of papers, Stephenson *et al.* have reported the effects of exposing PET to UV light.[41,42,49,50,64] The samples studied were placed in quartz tubes and irradiated in nitrogen and under vacuum to a wavelength of 253.7 nm; below the λ_{max} of PET. Using a chromatographic instrument, used for analysis of gases, the authors noted that the principal decomposition products identified were CO, H_2, and CH_4.

Analysing the gaseous decomposition products of irradiated PET showed that, in nitrogen, significant amounts of CO and CH_4 were produced. Whereas, under vacuum, the amount of methane formed had considerably decreased and the amount of CO had increased. In both nitrogen and under vacuum H_2 was produced in very small amounts compared with CO and CH_4.[41]

It was reported that the ratio of scission to crosslinking is higher in nitrogen than under vacuum. To explain this, the authors noted that much more hydrogen was produced when irradiations were performed under vacuum than nitrogen. They suggested that the C-H bond rupture that produces hydrogen is affected by the presence of nitrogen; the nitrogen is thought to affect the ability of the hydrogen to migrate out of the polymer. When bond rupture occurs, free radicals are produced which can either recombine or combine with another radical; in this case, the mobile hydrogen atom. If the free radical combines with the hydrogen atom, then recombination will be prevented, and scission will result. Taking this into consideration, it is understandable why the authors noted an increase in the ratio of scission to crosslinking in nitrogen compared with irradiations performed under vacuum.[41,64]

Stephenson *et al.* made some assumptions before the mechanism could be proposed: the polymer was a pure compound, the reactions took place in an oxygen-free atmosphere, the photochemical reactions proceeded through free radical reactions and atomic hydrogen was more mobile than any of the other products in the polymer.[41] The proposed mechanism, inferred from the end products of the decomposition, is shown in *Figure 1.14*.[41]

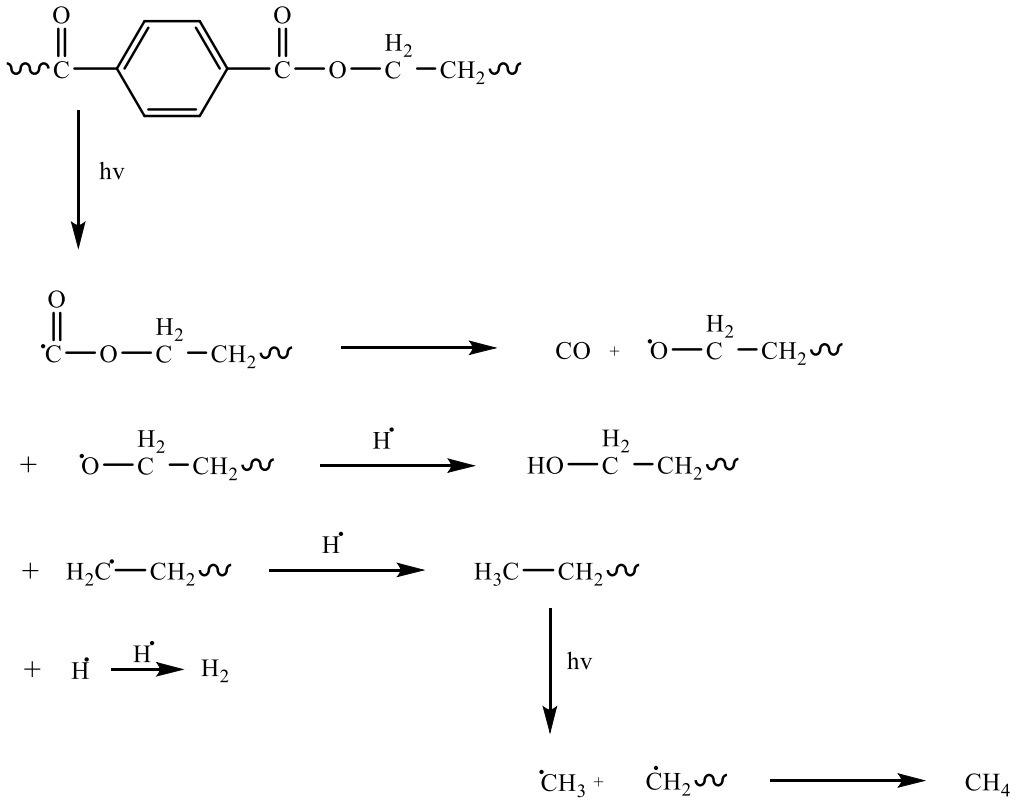

Figure 1.14: Proposed mechanism for photodegradation of PET.[41]

Marcotte *et al.* used a variety of techniques to study the photolysis of PET and proposed a mechanism for the primary reaction that leads to the formation of CO and CO_2 in 1967. Light of wavelengths 253.7 nm and 313 nm were used to study the photolysis of PET films under vacuum. A germicidal lamp was used as more than

90% of its light is emitted at 253.7 nm and the source rich in 313 nm was a medium pressure mercury arc.

UV-visible results, of un-irradiated PET, showed that a thin sample of PET absorbed near 310 nm, transmitted light of wavelengths >320 nm and was opaque to wavelengths <302.5 nm.[51] It had already been noted that PET has an absorption edge at 310 nm and degrades most significantly when irradiated under light of this wavelength.[22,40,47,51,65] Using a thinner cast film in experiments exposed a strong absorption maximum near 240 nm and a weaker absorption near 290 nm. Similar absorption maxima were found in several solutions of phthalate esters and therefore it was concluded that, in the range of 240-320 nm, the main chromophore was the group –O-CO-C_6H_4-CO-O-. This was important as it meant that PET's photochemical changes could be directly related to the photochemistry of the repeat unit, whereas if initiation was due to impurities this would not be the case [51]

Marcotte *et al.* reported that the principal products of the degradation, when irradiated with both wavelengths of light, were CO and CO_2 with rates of formation decreasing with irradiation time. A few percent of methane was also observed in the CO fraction.[51] This is dissimilar to the results of Stephenson *et al.* who reported that CO was the main product along with methane and a small amount of hydrogen; thus a major discrepancy in the formation of CO_2.[41] It was also observed that there were fractures and crosslinking of the polymer molecules and formation of radicals which were identified by ESR spectra: *p*-$C_6H_3^{\cdot}$ and $^{\cdot}$O-CH_2-CH_2-.[51] Marcotte *et al.* proposed a mechanism for the primary reactions, consistent with these observations, which is shown in *Figure 1.15*.

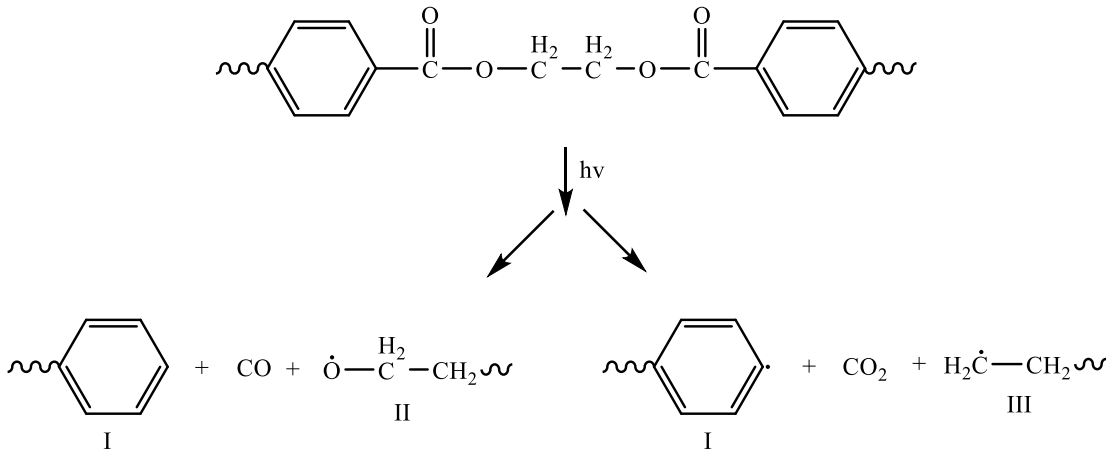

Figure 1.15: Primary reactions leading to the formation of CO and CO_2.[51]

Radicals I, II and III, from *Figure 1.15*, can combine to form groups of the type *p*-O-O-CO-C_6H_4-X- or undergo disproportionation or hydrogen abstraction which would both result in chain fracture.[51] Hydrogen abstraction from a neighbouring molecule would also cause the formation of free radicals which could be responsible for crosslinking in the polymer.[32,51] A crosslinking reaction was therefore proposed and is shown in *Figure 1.16*.[51]

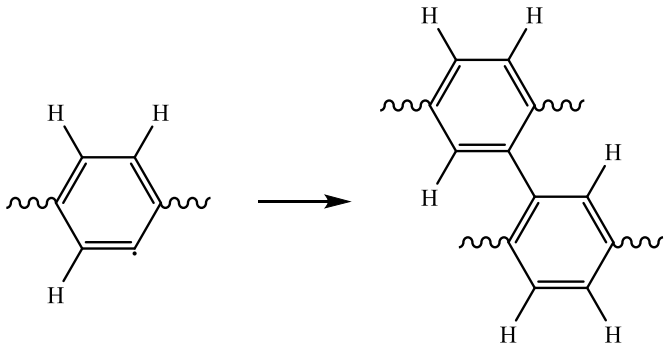

Figure 1.16: Crosslinking of free radicals in the polymer.[46,103]

At room temperature, it was expected that some of the more stable radicals would be trapped in PET because of its rigid medium. Radicals I and III, in *Figure 1.15*, are expected to be more reactive than radical II.[51]

A mechanism for the photolysis of PET was proposed by Buxbaum in 1968 using results obtained by Stephenson *et al.*[41,64] and Marcotte *et al.*[51] They showed that after exposure to light of wavelengths 253.7 and 313 nm the PET film would turn an amber colour, become brittle and evolve gas. Buxbaum, therefore, suggested a probable reaction sequence which is shown in *Figure 1.17*.[67]

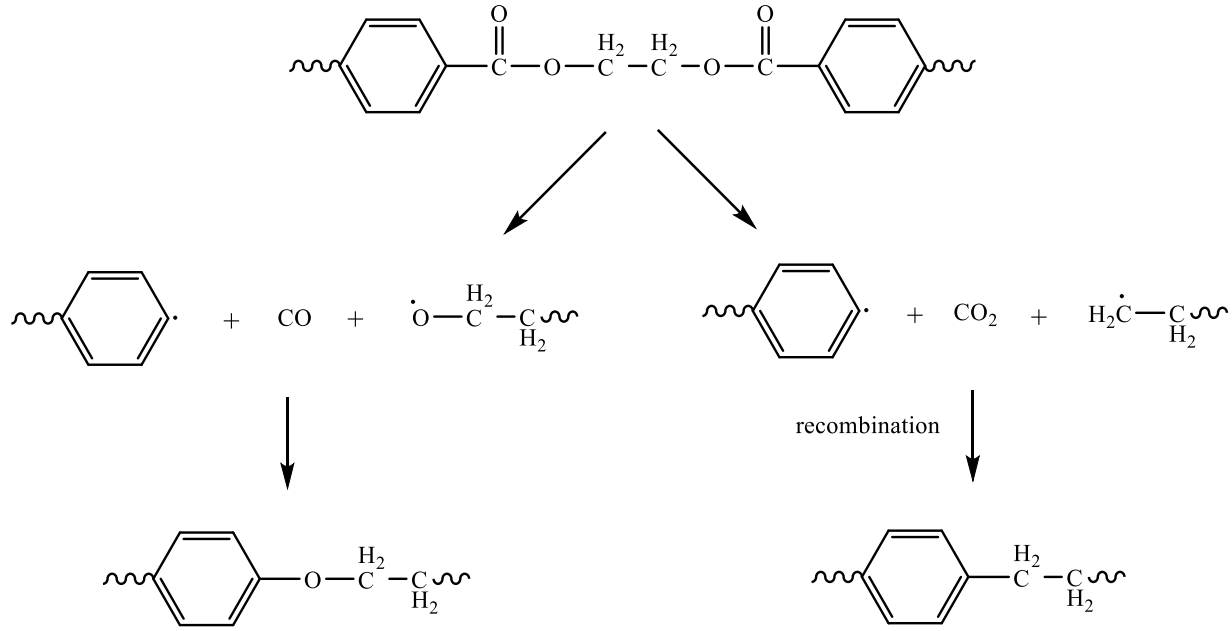

Figure 1.17: Reaction sequence for photolysis of PET.[67]

The formation of radicals can occur if hydrogen abstraction, from neighbouring molecules, has taken place. These radicals could also recombine to form crosslinks. Examples of such radicals are shown in *Figure 1.18*.[67,68]

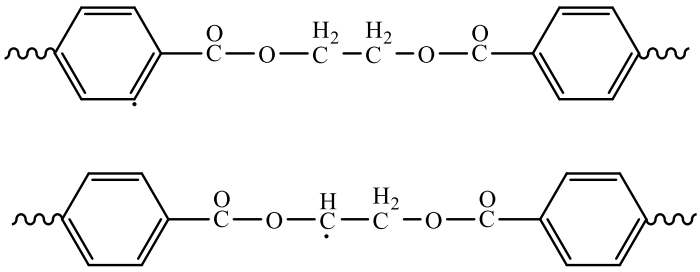

Figure 1.18: Radicals formed due to hydrogen abstraction.[67,68]

Day and Wiles proposed a mechanism, in the early 1970s, of CO and CO_2 production through absorption of UV light which is still generally accepted.[47] Samples were placed in quartz cells under vacuum and irradiated using a mercury lamp. Using filters, two wavelength ranges were used; 300-420 nm and 225-420 nm.

In the first paper of the series, Day and Wiles reported that the number-average molecular weights were decreasing with irradiation time and thus, degradation was evident; the number-average molecular weights were derived from viscometric data[22] and were used to measure the extent of degradation.[69] It was also reported that the formation of carboxylic acid end groups in PET was increasing with exposure to UV light;[22] this is now used as a way to indirectly measure the degree of damage.[45,47,58,63,70] Using ATR measurements it was shown that there was a lower concentration of carboxylic acid end groups in the bulk of the film than on the surface. The build-up of carboxylic acid end groups was not only present at the surface but also at the side of the film that was not facing the UV light source. It was suggested that long wavelengths (>315 nm) are responsible for the build-up of carboxylic acid end groups at the rear side of the film, due to PET's strong absorption of short wavelength light; PET would absorb the short wavelength light and therefore it would not reach the rear surface.[22] Filters were used to prove that long wavelengths of light were indeed responsible for this build-up at the rear surface of the film.[40]

The second paper, in Day and Wiles series, shows the effect of wavelength on the photochemical degradation of PET. They showed, using filters, that the wavelength of UV light influences the rate and nature of photodegradation. When using a filter

with a cut-off at 315 nm it induced a negligible change in the films properties, whereas using shorter wavelengths of light showed significant changes. This indicated that short wavelengths (<315 nm) were a very important parameter in the photodegradation of PET.[40]

Day and Wiles also undertook experiments under vacuum to develop the mechanistic pathway for the photolysis of PET. For both wavelength ranges, mass-spectrometric and gas-chromatographic analyses were used to examine the major products. These analyses indicated that CO and CO_2 were the major volatile products with other minor products such as H_2, CH_4, water, and formaldehyde. The measurements showed that yields of CO and carboxylic acid end groups were higher than those for CO_2. They concluded that the formation of CO and carboxylic acid end groups were part of the primary initial photolytic reaction, whereas CO_2 formation was only important later in the decomposition process.[47] Size Exclusion Chromatography was also employed by Fechine *et al.* to show that the formation of carboxylic acid end groups and chain scission both occurred during the photodegradation of PET materials.[38]

Using the wavelength range of 225-420 nm to irradiate the sample, Day and Wiles proposed a mechanism for the degradation of PET under vacuum, shown in *Figure 1.19*. This shows that for CO to form, reactions 3 and 8 need to take place (Norrish Type I reaction)[47,71] and reactions 1 and 4 must take place for the formation of carboxylic acid end groups to occur. Reactions 1, 3 and 5 result in chain scission.[38,47] Reaction 4 and 5 are comparable and so should have the same rate, however, this is not the case as carboxylic acid end groups are produced in higher yields than CO_2. Therefore Day and Wiles suggested that an alternative route to produce carboxylic acid end groups must be possible; they proposed a further two reactions, shown in *Figure 1.20*.[47]

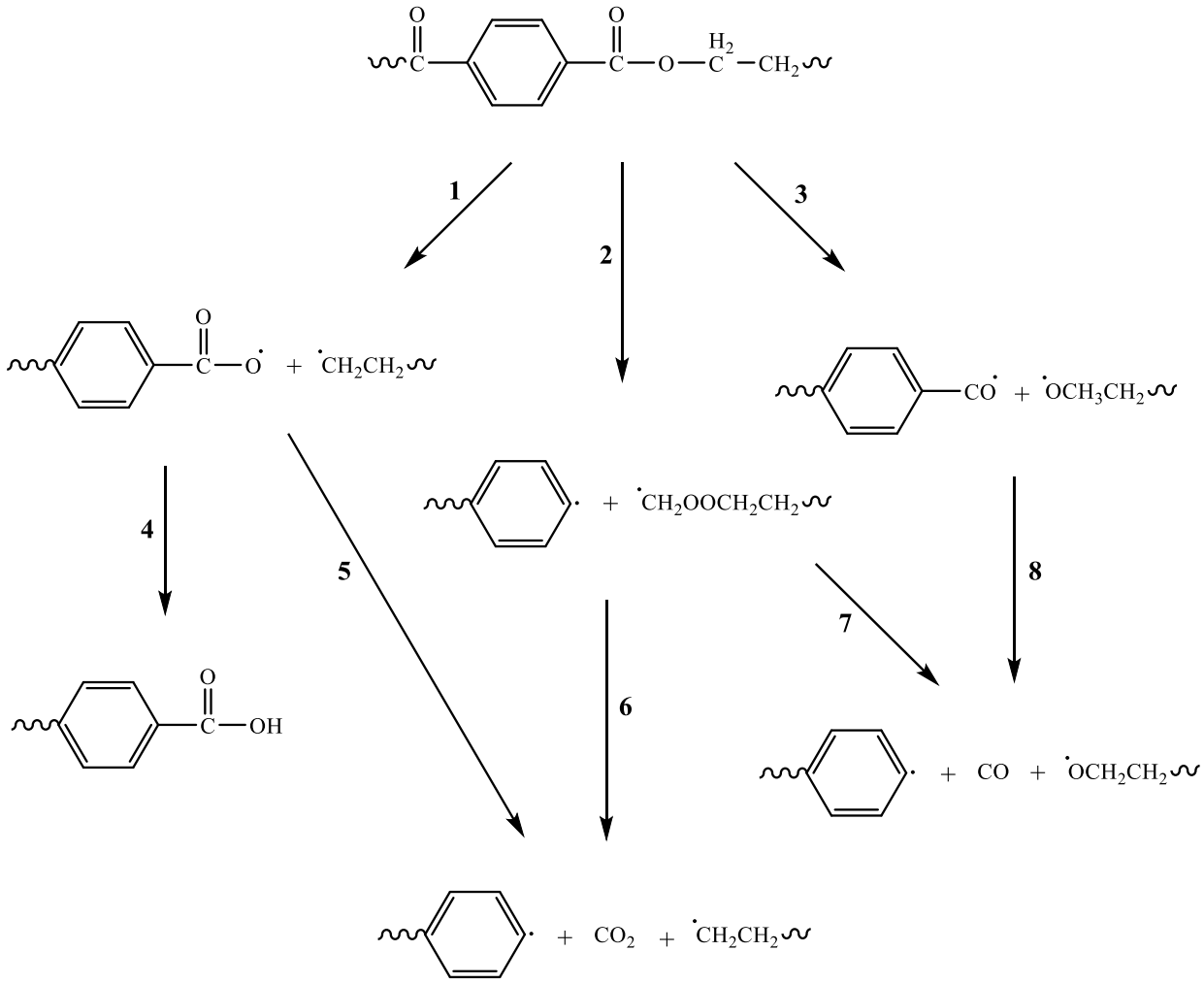

Figure 1.19: Mechanism proposed by Day and Wiles for degradation of PET under vacuum.[47,72,73]

From *Figure 1.20*, reaction 1 shows the intermolecular hydrogen abstraction while reaction 2 is an intramolecular hydrogen abstraction. Day and Wiles suggested that reaction 2, the Norrish Type II intramolecular rearrangement,[47,71] would be most feasible.[47] The authors based this on the fact that aliphatic[74] and aromatic esters[75] that contain a γ-hydrogen atom decompose through an intramolecular rearrangement.

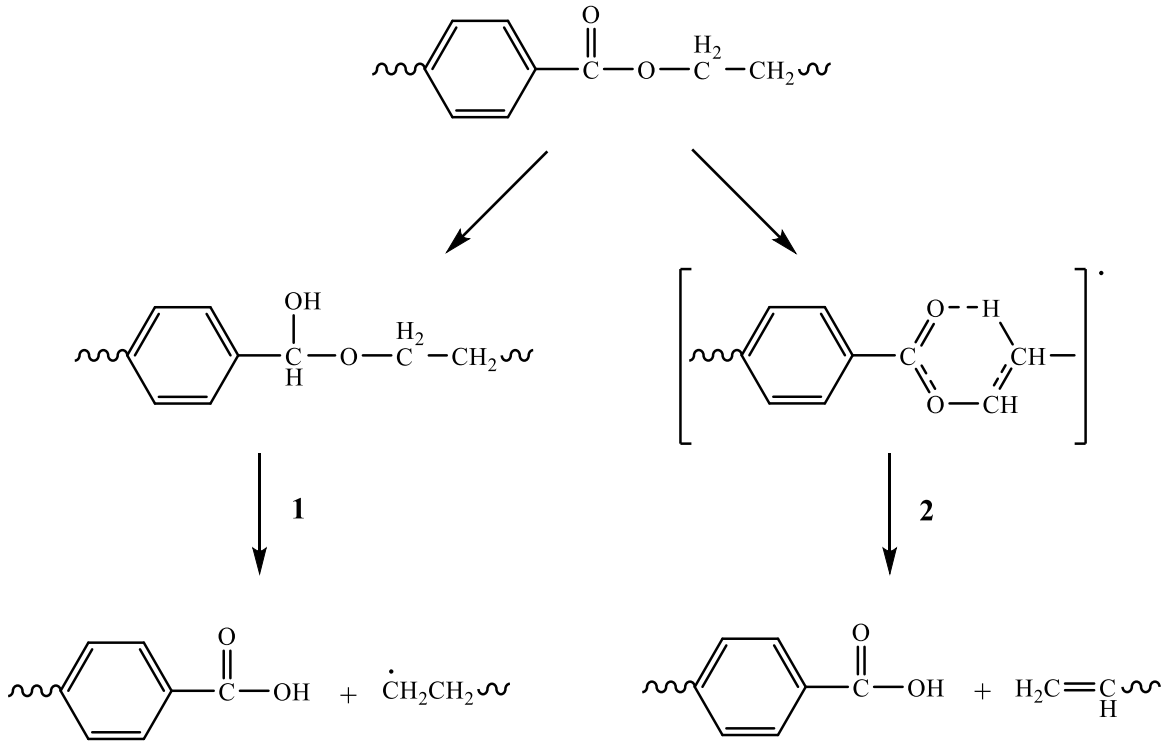

Figure 1.20: Day and Wiles alternative mechanism for the formation of carboxylic acid end groups.[47,72,73]

Using the wavelength range of 300-420 nm to irradiate the sample, under vacuum, showed that the rate of formation of CO_2 was produced in lesser amounts until the induction period was over and the rate of CO_2 production increased. The authors assumed that CO_2 was produced by reactions 1 and 4 initially but later in the reaction was formed by the build-up of an intermediates concentration with irradiation time.[47,41] This adjustment in the CO/CO_2 ratio has also been reported by Marcotte *et al.*, during vacuum photolysis of PET.[51] The wavelength range of 225-420 nm, in comparison, showed a higher initial yield of CO_2, which is thought to be because of an improved efficiency of reactions 1 and 4 at shorter wavelengths.[47]

Grassie and Scott studied the degradation and stabilisation of polymers and reported that in PET, chain scission was predominant. They observed that the initial chain scission could occur in the ester group but at any one of the three points shown in *Figure 1.21* by the dotted lines.

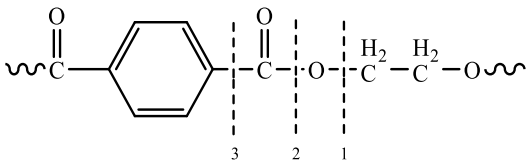

Figure 1.21: Repeat unit of PET with dotted lines showing the three different points in which chain scission can occur.[76]

Scission at dotted lines 1 and 2 would mean the formation of CO and CO_2 and all radicals formed would be capable of hydrogen abstraction. The fact that vinyl groups are formed in the polymer during degradation indicated that an alternative chain scission reaction must be taking place; a Norrish Type II scission reaction, shown in *Figure 1.22*.[76]

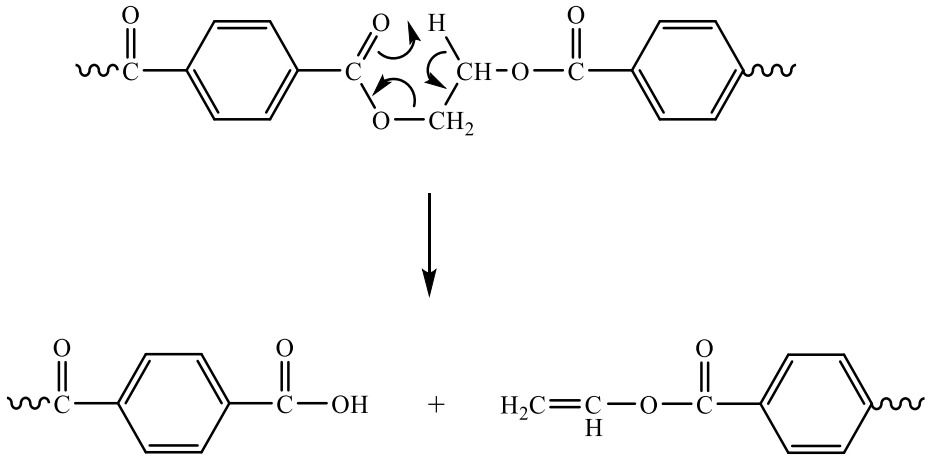

Figure 1.22: Alternative Norrish Type II chain scission reaction.[76]

1.3.2 Photo-oxidation

Photo-oxidation reactions take place in the presence of air, and polymers tend to degrade faster in these conditions than in an inert environment. *Figure 1.23* shows the radical-based auto-oxidative process by which photo-oxidative degradation takes place.[77]

The initiation reaction generates free radicals which are mostly formed due to one of the chromophores undergoing a photolysis reaction. The effect of UV light generates these free radicals but has little effect on the propagation steps as these are thermal reactions.[76,77] The second step in the propagation reaction is generally used to measure the rate of propagation by determining the ease of hydrogen abstraction. The termination reactions involved in the photo-oxidation process are bimolecular and in an atmosphere sufficient in oxygen, the reaction of two peroxy radicals is the only reaction that needs to be considered; termination depends on the type of peroxy radicals that are present.[77]

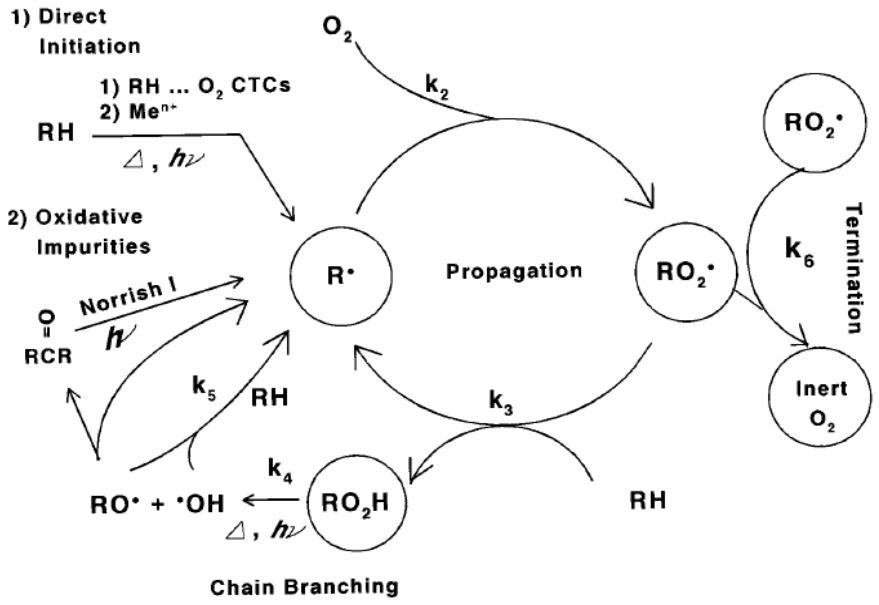

Figure 1.23: Radical-based auto-oxidation process for almost all polymers.[77]

Bolland and Gee from British Rubber Producers Research Association studied auto-oxidation as early as 1946 and proposed a mechanism which is still the basis of the modern theory today, shown in *Figure 1.24*.[78–82] Originally the reaction was developed for rubber and lipids but is now extensively used for all types of polymeric materials.[81]

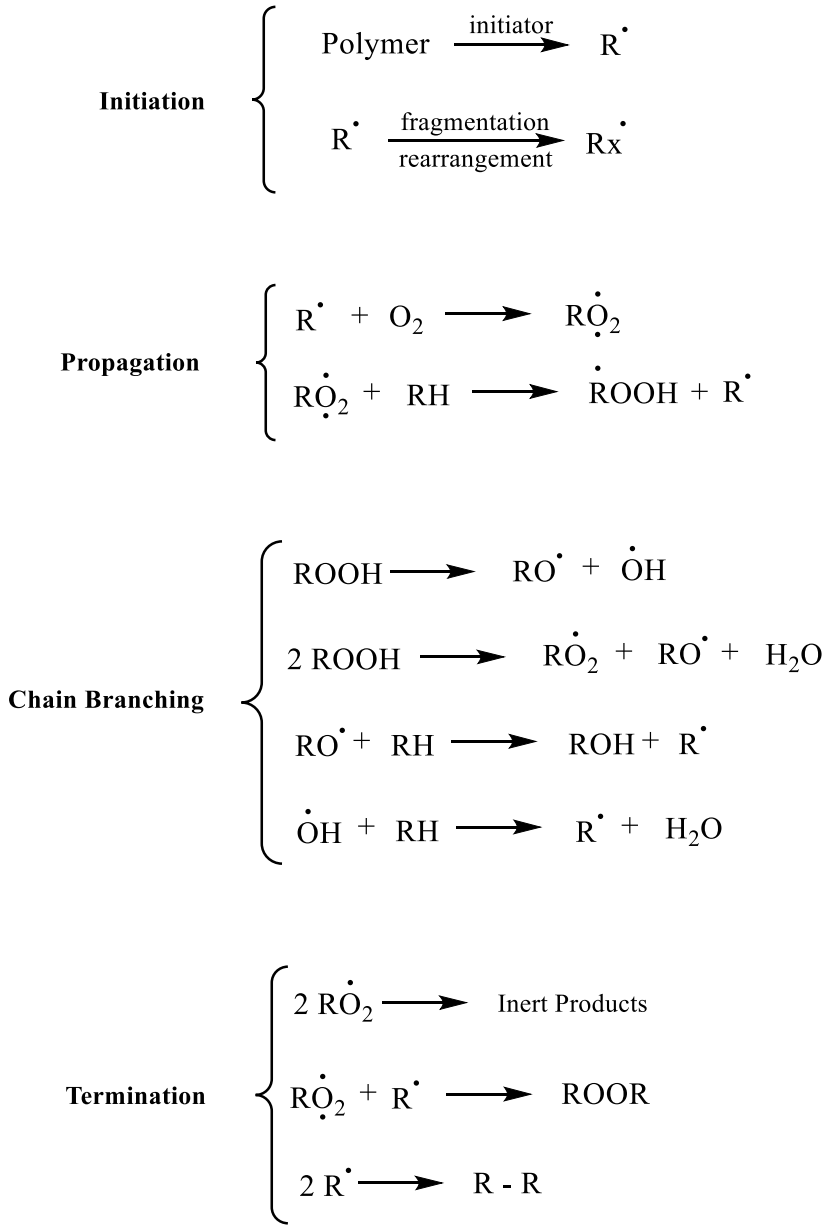

Figure 1.24: Basic auto-oxidation scheme developed by Bolland and Gee.[81]

The basic auto-oxidation scheme, shown in *Figure 1.24*, includes initiation, chain propagation, chain branching and termination steps.[81] The scheme also shows the formation and decomposition of hydroperoxides throughout the process.[83] The propagation step involves hydrogen abstraction by the peroxy radical and is the reason this process is autocatalytic. This step also transforms the reaction from what would be a slow and steady build-up of damage to a rapidly accelerating failure.[81]

In 1983, Davis and Sims proposed reactions for the photo-oxidation of polymers once initiation had occurred (PH → P·).[58,83,84] The propagation and chain branching reactions are shown in *Figure 1.25*.[83,84]

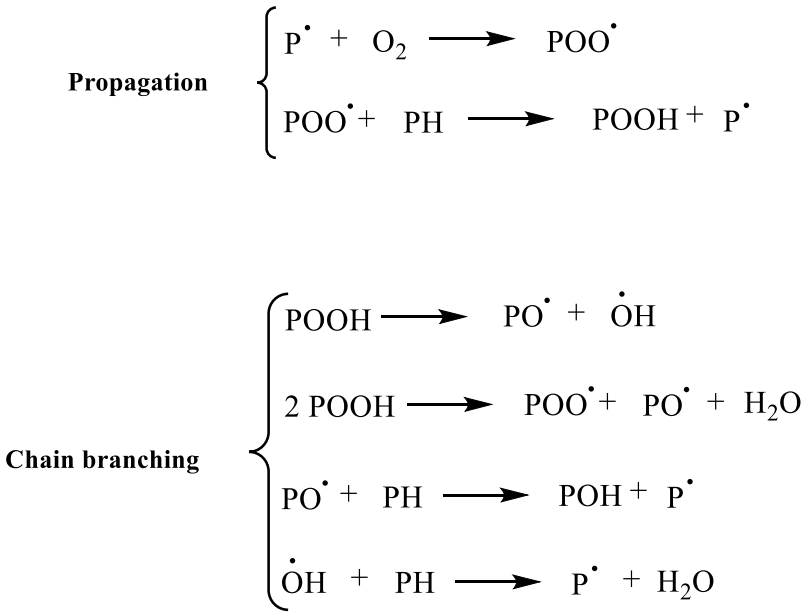

Figure 1.25: Photo-oxidation reactions of polymers after initiation proposed by Davis and Sims.[83,84]

Alternative reactions, to those proposed by Davis and Sims, were also given by other authors and are shown in *Figure 1.26*.[58,85,86]

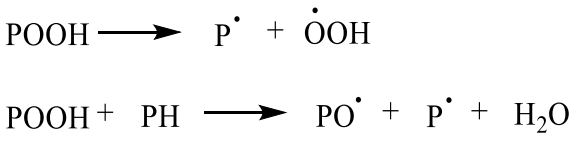

Figure 1.26: Alternative reactions proposed by other authors.[83]

Typically, the termination process is through the combining of a pair of radicals. Degradation occurs here because the radicals produced are unstable and so could undergo scission reactions.[83]

The differences in environment, with oxygen present, have been reported to show several significant differences. Irradiations performed in non-oxidative conditions showed discoloration[32,40] and crosslinking to the extent that the material was insoluble in o-chlorophenol.[40,73] Performing irradiations in an oxidative atmosphere showed chain scissions and fluorescent species build up, but there was no crosslinking and only minor discoloration. It was assumed that the presence of oxygen would suppress crosslinking as radicals produced could react with oxygen to form peroxy radicals and therefore, radicals recombining to form crosslinks could be reduced. Based on these differences in results, from the two environments, Day and Wiles suggested that there was the possibility of a photo-oxidative reaction.[40]

Day and Wiles, therefore, studied the photodegradation of PET with oxygen present and proposed a pathway for the photo-oxidation reaction occurring in PET. The samples were placed in quartz cells, with air present at a pressure of 1 atm, and irradiated with an Osram superpressure mercury lamp (SP500W). Using filters, two wavelength ranges were used; 300-420 nm and 225-420 nm. It was reported that no major differences were identified in the products, compared with the results under vacuum, apart from the substantial increase in CO_2 production. Although, under oxidative conditions, photolysis was still a significant feature of the reaction.[47]

Using 300-420 nm light showed that the yields of CO and carboxylic acid end groups were very similar and indicated that in both vacuum and air the same primary reactions take place. However, in air, the production of CO_2 was considerably higher,

comparable to the production of CO. This suggested that oxygen was participating in the reaction.[47,87] Therefore Day and Wiles proposed a photo-oxidation mechanism which is shown in *Figure 1.27*.[47,72] It was already known that during the photo-oxidation of polymers there is the formation of hydroperoxides; this means that the mechanism is consistent with previous knowledge.[47,72,88]

Steps 1 and 2 in the mechanism, in *Figure 1.27*, show the chain propagation steps where the initial radical could be regenerated through hydrogen abstraction. Step 3 shows the formation of the hydroxyl and alkoxy radical through photolysis of the hydroperoxides. Monohydroxy terephthalate groups can be formed through the substitution of the hydroxyl radicals in the phenylene ring; these species are thought to be the cause of the observed fluorescence in photo-oxidised PET.[47]

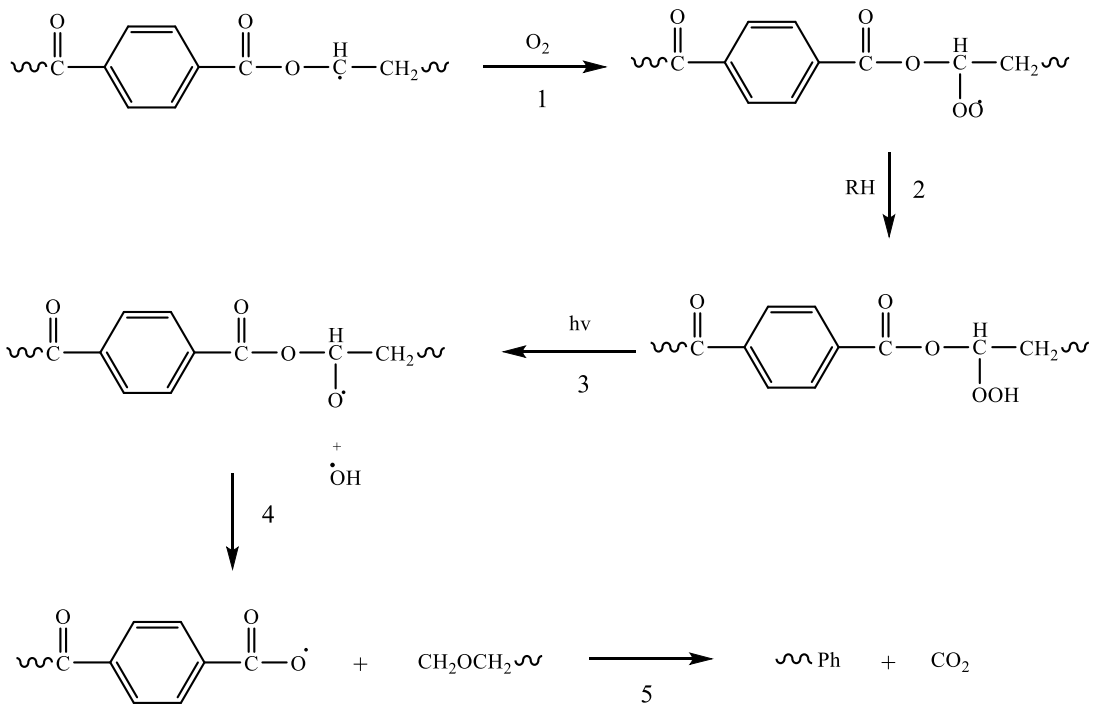

Figure 1.27: Photo-oxidation mechanism proposed by Day and Wiles.[42,84,103]

The observation of blue-green fluorescent material had already been previously reported due to the formation of mono- and di- hydroxy-substituted materials,[52–54] with an excitation of 340 nm and emission of 460 nm; shown in *Figure 1.28*.[40,42] However, in Day and Wiles second paper of the series they reported that the fluorescence emission spectrum was consistent with the existence of the monohydroxy terephthalate species.[40] This species was identified by Pacifici.[54]

Figure 1.28: Mono- and di- hydroxy-substituted materials.[40]

The proposed mechanism by Day and Wiles for the production of the monohydroxy terephthalate species is shown in *Figure 1.29*. The fluorescence species was only observed under photo-oxidative conditions, which mean that the proposed photo-oxidative mechanism is valid.

Using 225-420 nm light Day and Wiles found that the production of carboxylic acid end groups was very similar and therefore proposed it was independent of irradiation wavelength and environment. This shows that the mechanism for the shorter wavelength range, shown in *Figure 1.27*, is also applicable here. However, using a broader wavelength range caused an increase in the production of CO and CO_2.[40] It was concluded that the shorter wavelength light was causing the decomposition of secondary oxidative products that were more susceptible to shorter wavelength light, but no difference was observed in the primary photolytic processes.

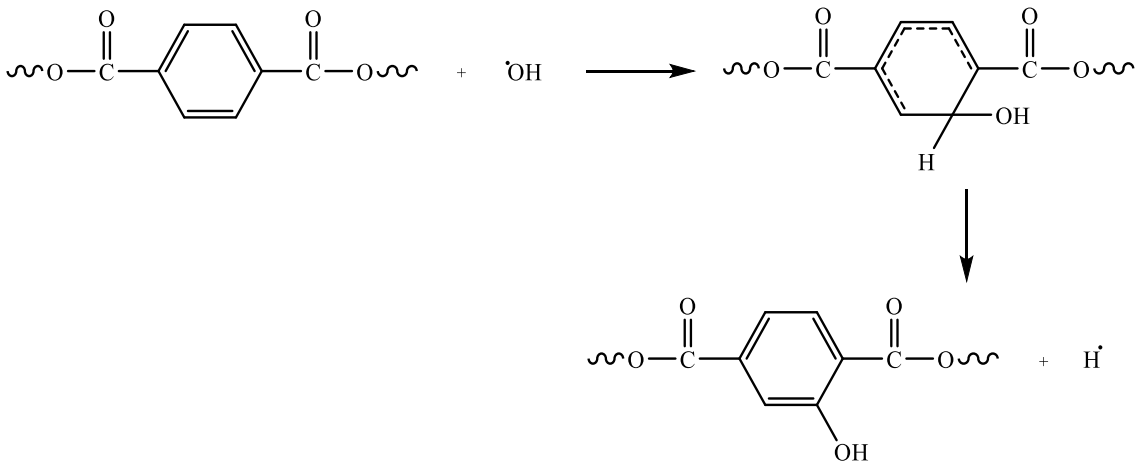

Figure 1.29: Mechanism for the formation of monohydroxy terephthalate groups in the polymer backbone, including hydroperoxide formation and photolysis.[47]

Fechine *et al.* questioned the pathway that was proposed by Day and Wiles, as they argued that the reaction for the formation of carboxylic acid end groups was not affected by the presence of oxygen.[47,89] Whereas, Fechine *et al.* argued that this mechanistic pathway did not explain the differences seen between the bulk and surface of the film, as the UV radiation would be accessible to both. Therefore Fechine *et al.* proposed a mechanism for the photo-oxidative reactions undergone by PET when exposed to UV light, shown in *Figure 1.30.*[89] Carboxylic acid end groups are formed in the reaction and can be used to measure the extent of degradation of the polymer.[90]

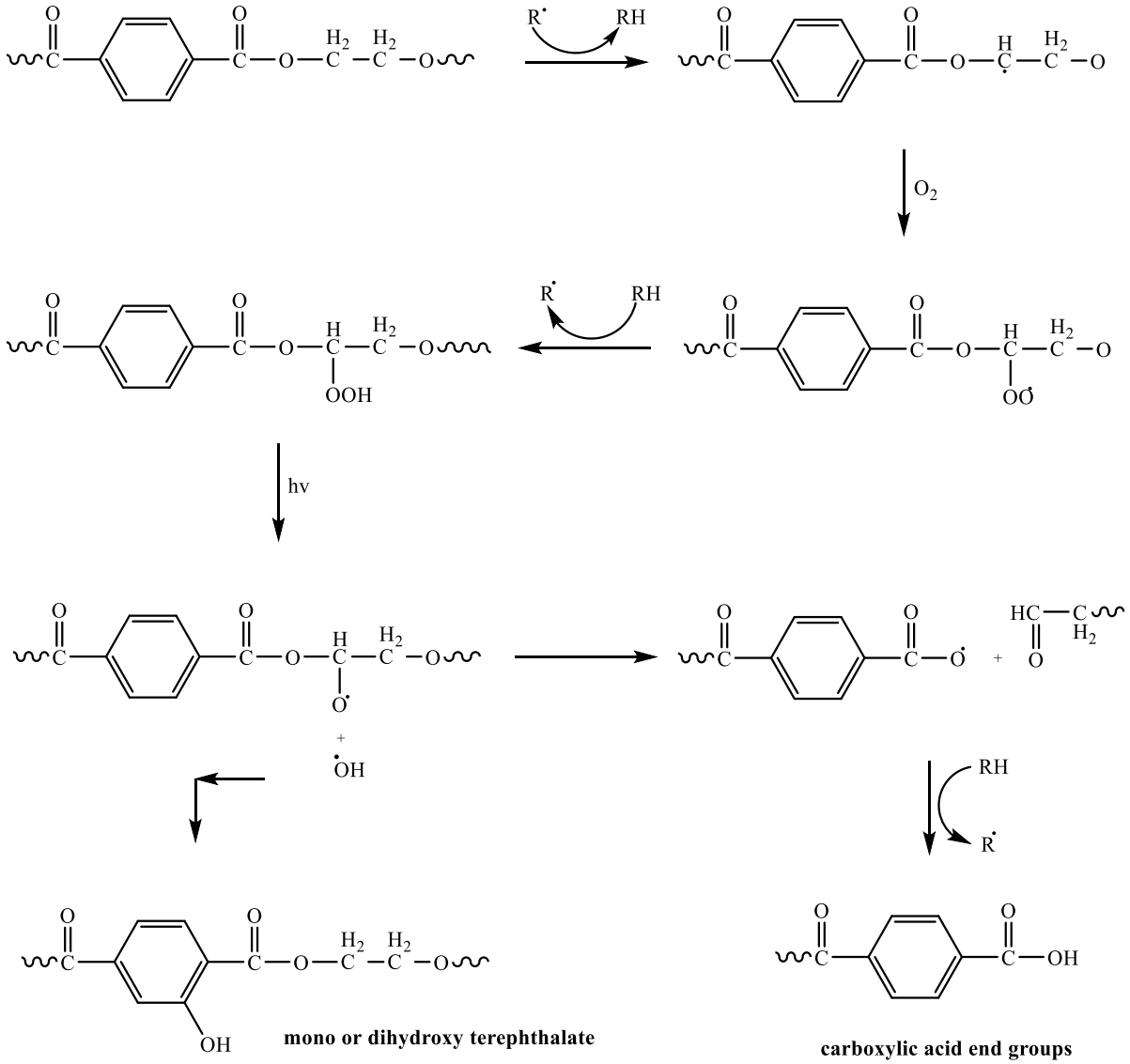

Figure 1.30: Fechine *et al.* proposed photo-oxidation reaction undergone by PET when exposed to UV light. Radicals R can be produced either by a Norrish Type I reaction or in this reaction cycle.[89]

Fechine *et al.* irradiated PET film samples in a weathering chamber using Q-Panel UVA fluorescent lamps with a 290 nm cut-off point.[38,91] The weathering cycle consisted of 4 hours under UV light at 60°C and 4 hours under condensed water at 50°C in the dark; this means that because of the conditions in the chamber the sample could undergo photo-, thermal and hydrolytic degradation.[38]

Fourier transform infrared spectroscopy data and titrations were used to measure the carboxyl index which is related to the concentration of carboxylic acid end groups in the polymer. The carboxyl index showed an increase in carboxylic acid end group concentration with exposure time;[38] this agrees with the fact that carboxylic acid end groups can act as a catalyst to support additional degradation.[92]

The UV-visible spectrum of PET given in *Figure 1.31* shows that there is an increase in absorption at 400 nm which allows the yellowness index to be estimated. This discoloration and increase in absorption were thought to be largely due to the production of quinone and diquinone species during photodegradation.[38,93] A mechanism for the production of these species is shown in *Figure 1.32*.[38]

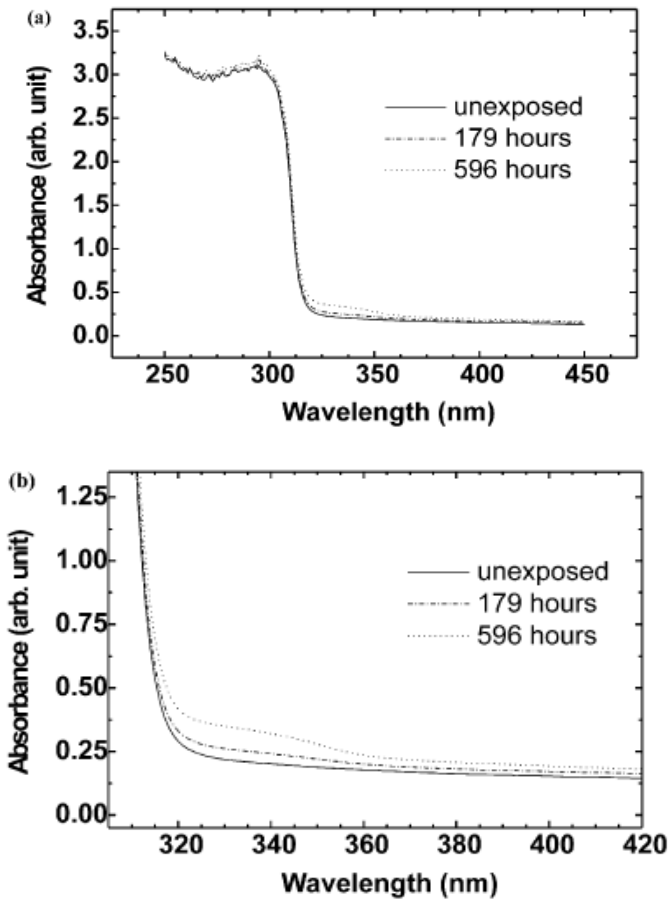

Figure 1.31: UV-visible spectra of (a) unexposed & aged PET and (b) in detail in 400 nm region.[38]

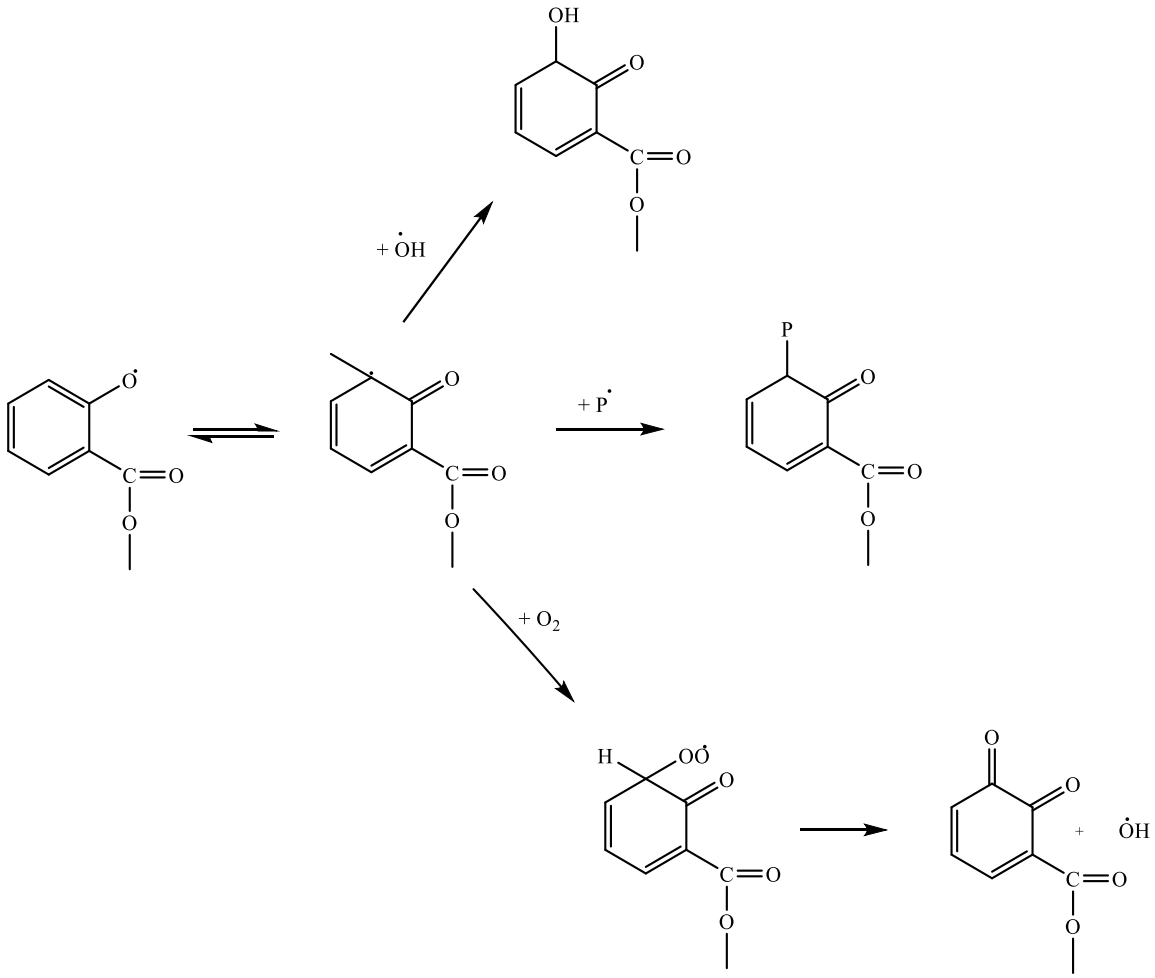

Figure 1.32: Proposed reactions for the formation of quinone and diquinone species.[38]

1.4 Summary of literature for PET

Author	Film	Thickness	Irradiations	Research
Non-oxidative atmosphere				
Stephenson *et al.*	Mylar C	~ 6 µm	253.7 nm germicidal lamp	CO and CH_4 reported as major products and proposed mechanism for production of these groups
Marcotte *et al.*	Mylar C	0.05 µm	253.7 and 313 nm germicidal lamp	Reported CO and CO_2 as major products, as well as fractures, crosslinking and formation of radicals. Mechanistic pathway was proposed.
Day and Wiles	Melinex S and Mylar C	23 µm & 12 µm	Xenon and Carbon arc Weatherometers – two wavelength ranges (300-420 and 225-420 nm)	Reported that short wavelengths of light caused meaningful change and CO and CO_2 were major products, as well as a build-up of COOH end groups. Also reported chain scission and fluorescent species build up. Mechanisms proposed.
Oxidative atmosphere				
Day and Wiles	Melinex S and Mylar C	23 µm & 12 µm	Xenon and Carbon arc Weatherometers – two wavelength ranges (300-420 and 225-420 nm)	Major products reported as CO and CO_2, as well as a build-up of COOH end groups. Under oxidative conditions, CO_2 was produced in higher yields, compared to non-oxidative, as oxygen is now participating in the reaction. Mechanistic pathways produced.
Fechine *et al.*	Bi-orientated films	23 µm	Weathering chamber with UVA fluorescent lamps (cut-off at 290 nm)	Proposed that oxygen affected the formation of COOH end groups as this explained differences seen between bulk and surface of the film. Mechanisms produced for production of quinone groups and COOH end groups.

1.5 Photodegradation of Poly(ethylene naphthalate)

The photodegradation of poly(ethylene naphthalate) (PEN) has been studied by different groups but only a small amount of papers have been published.[37,94–96] During photodegradation of PEN, there is the formation of different chemical groups, such as naphthanoic acid end groups and anhydride groups. The photodegradation of PEN involves both photolysis and photo-oxidative processes and will be discussed here only as a comparison.

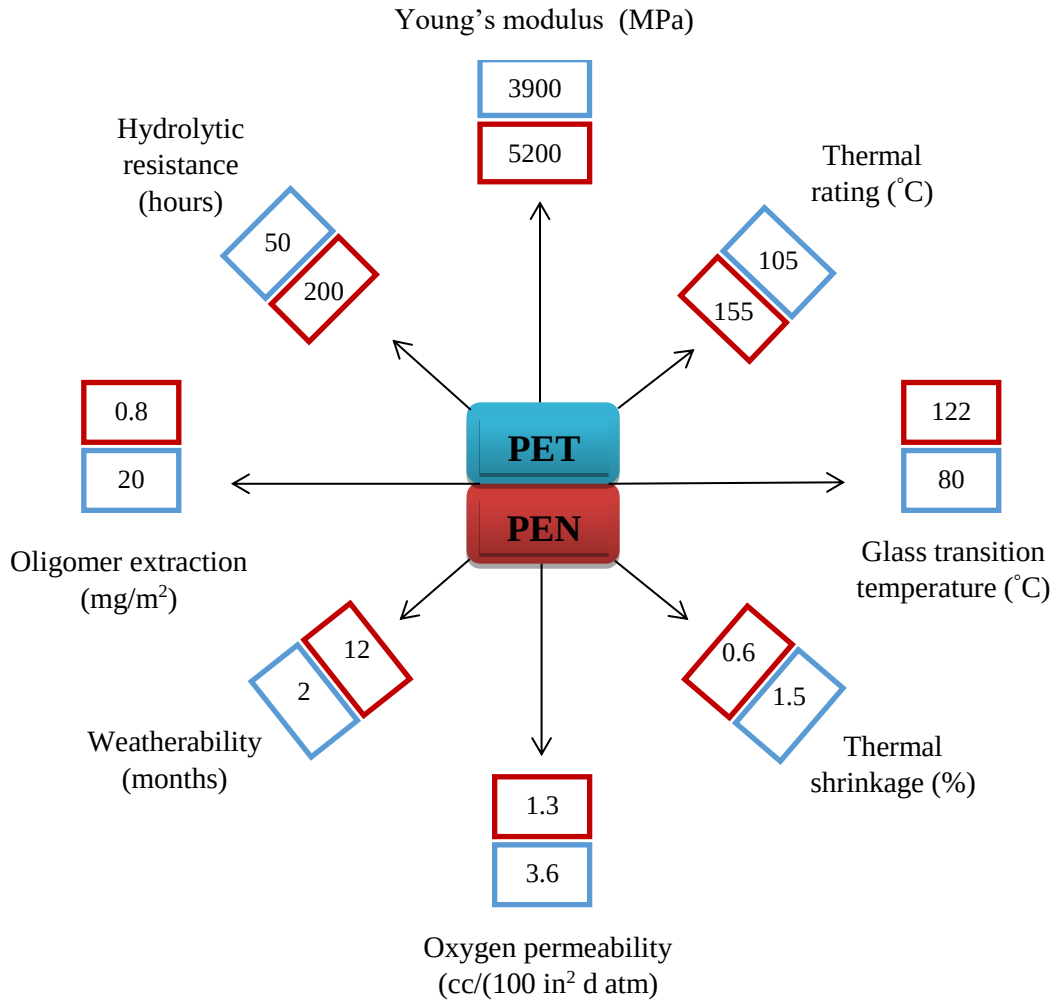

Figure 1.33: Modified comparison of properties of PET and PEN.[97]

PEN is a condensation polymer that was first synthesised by ICI scientists in 1948. The primary starting monomer is dimethyl-2,6-naphthalene dicarboxylate, accompanied by glycol. PEN can be used in an extensive range of applications such as motor insulators, photographic films, and packaging.[97] PEN films have improved properties over PET, for example, their stiffness, UV weathering resistance, thermal stability, tensile strength, and hydrolysis resistance. *Figure 1.33* shows a comparison of these properties.[97] Although PEN shows a higher resistance to UV weathering it still photodegrades when exposed to UV light.

1.5.1 Photolysis

Ouchi *et al.* studied the photodegradation of PEN under vacuum and reported his findings in 1976. A high-pressure mercury lamp was used in this study to expose samples to wavelengths of light <375 nm. It was observed that the photochemical reactions only took place on the surface layers of the film with an insoluble fraction being formed..[37] This was further reinforced by Blais *et al.* who established that in irradiated films the formation of carboxylic acid end groups only occurred on the surface. Thus, the authors concluded that photodegradation of PEN was mostly a surface effect.[39]

In the study by Ouchi *et al.* it was also reported that the absorption spectra of the PEN films showed a sharp rise at approximately 380 nm after irradiation. In the wavelength region less than 380 nm the film was opaque but transparent in the near UV and visible regions. Thus it was believed that prolonged exposure to visible light would not cause any further deterioration of the films properties.[37]

As well as using a high-pressure mercury lamp, Ouchi *et al.* also used a UV carbon arc to irradiate the film samples. In this case, the light penetrated deeply and caused photochemical reactions throughout the complete depth of the sample. The reactions were accompanied by chain scission and an insolubilisation reaction. When PEN was excited with UV light, the authors reported that the sample emitted blue fluorescence. By comparing the fluorescence spectra of PEN with PET it was concluded that the

products of exposing PEN to UV light would not be similar to those produced during the photodegradation of PET.[37]

Allen and McKellar then proposed what they thought was one of the main primary photochemical processes, scission at the naphthyl-carbon bond, shown in *Figure 1.34*.[96,98] It was also noted that this process would agree with the results reported by Ouchi *et al*.[37,96,99] and has been shown to occur through an excited singlet state which is consistent with the reports of strong fluorescence. Allen and McKellar also suggested that the outcome may be the formation of naphthalenic chain ends.[96]

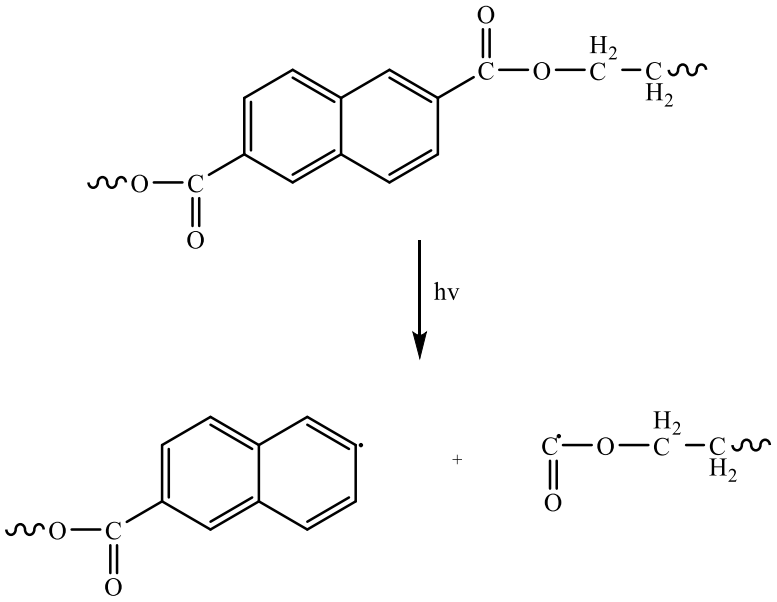

Figure 1.34: Scission of PEN at the naphthyl-carbon bond.[96]

Figure 1.35 shows a radical undergoing a hydrogen abstraction reaction with propan-2-ol; this radical is produced in the chain scission reaction in *Figure 1.33*. This indicates that hydrogen abstraction, from the solvent, is the radicals principal decay process.[96,98]

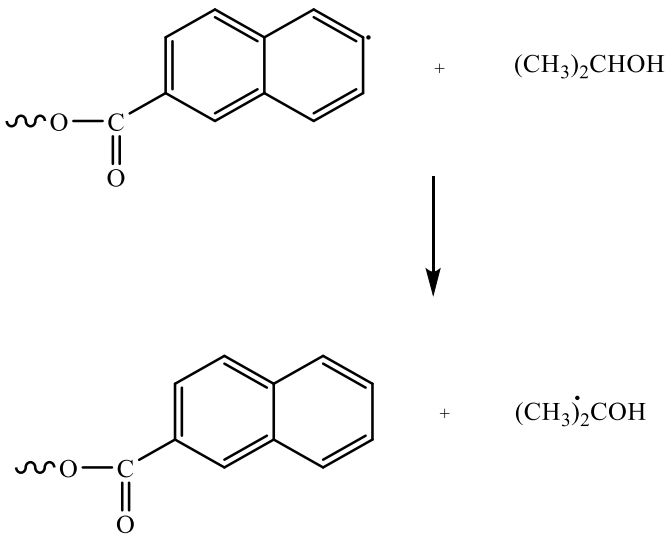

Figure 1.35: Hydrogen abstraction reaction of PEN occurring in propan-2-ol.[96]

Scheirs and Gardette studied the photolysis and photo-oxidation of PEN in 1996 and from their results proposed mechanisms for the photochemical reactions taking place during irradiation. For photolysis experiments, the samples were placed in pyrex tubes, sealed under high vacuum and placed in an irradiation chamber which used mercury-vapour lamps.

The main effect of irradiation on the PEN samples was the apparent yellowing of the film; the UV-visible absorption spectra showed an increase in the optical density at 400 nm. *Figure 1.36* shows a proposed photolysis reaction taking place during the irradiation of PEN. The production of these bis-naphthalene structures was thought to be the likely cause of the discoloration; accompanied with the formation of gel, chain scission and crosslinking reactions.[100,101] The photochemical reactions were reported to be limited to the surface of the polymer film.[101]

Two absorption peaks were also detected by Scheirs and Gardette in the UV-visible spectra; one at 355 nm and the other at 339 nm. Both peaks showed a decrease, after exposure, but complete destruction was noted after prolonged hours of exposure. The authors suggested that the two maxima could, therefore, be arising from the same

chromophoric group. At wavelengths greater than 370 nm there was an increase in absorption intensity and was attributed to the destruction of the naphthalate ester linkages and the formation of chromophoric conversion products.[100] This increase in absorption intensity above 370 nm was further supported by the study published by Fechine *et al.* Fechine *et al.* proposed that this could be due to the production of aromatic hydroxylated species.[90]

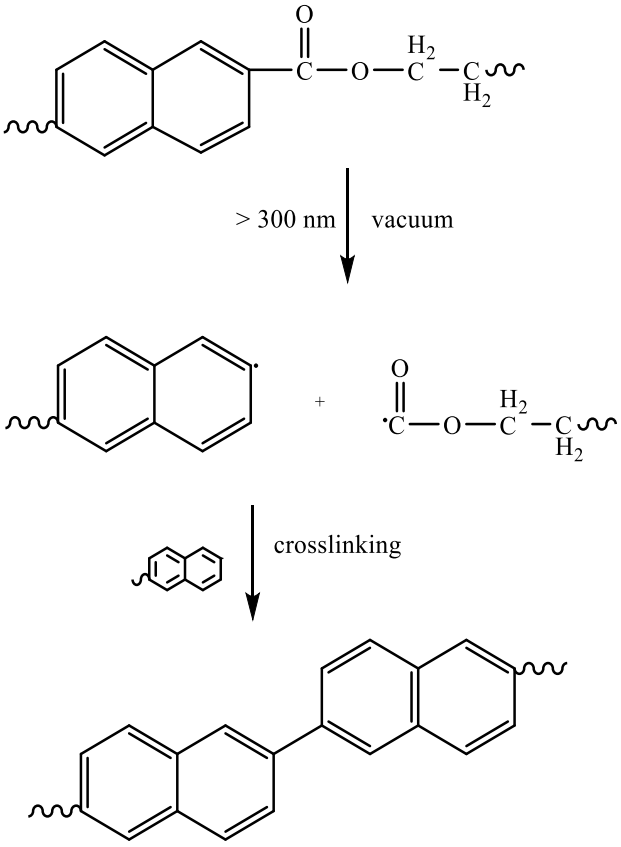

Figure 1.36: Formation of highly coloured conjugated bis-naphthalene structures through radical recombination.[100,101]

Scheirs and Gardette also noted that additional ageing of the samples showed that the 339 nm maximum shifted slightly and a new maximum was identified at 324 nm. These new absorptions were found to match the UV absorption spectrum of 2-

naphthanoic acid. *Figure 1.37* shows the pathway for the production of 2-naphthanoic acid end groups during the exposure of PEN.[100,102]

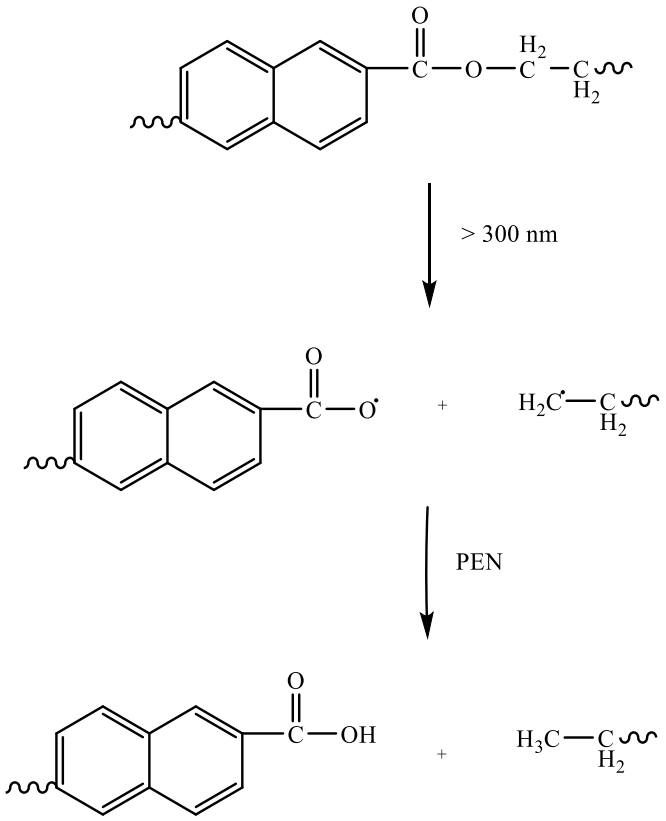

Figure 1.37: Formation of naphthanoic acid end group through chain scission of PEN by photolysis.[100]

Using mass spectrometry, Scheirs and Gardette analysed the volatiles produced during the exposure of PEN to UV light. This showed that CO and CO_2 were the main products of the photolysis process. However, in comparison with PET, PEN produced similar quantities of CO and less carboxylic acid end groups, but an order of magnitude more CO_2. This suggested that a particular chemical or morphological feature in PEN preferred the decarboxylation of carboxylic acid end groups. The gas evolution reaction for PEN is shown in *Figure 1.38*. [100]

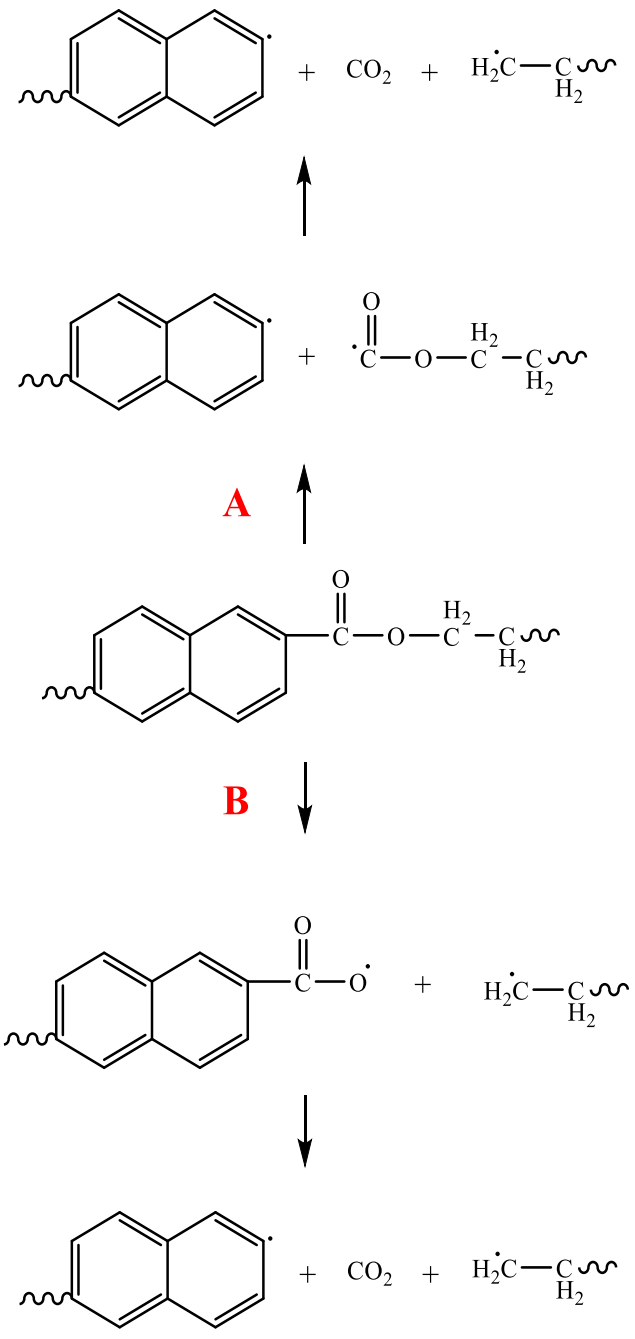

Figure 1.38: Mechanism of gas evolution reaction from PEN.[100]

1.5.2 Photo-oxidation

Scheirs and Gardette studied the photo-oxidation reactions taking place when PEN was exposed to UV light. They showed that 2-naphthanoic acid end groups could also be formed through a photo-oxidative pathway as well as during photolysis. The authors used the same conditions as described for photolysis experiments, the only difference being that air was present.

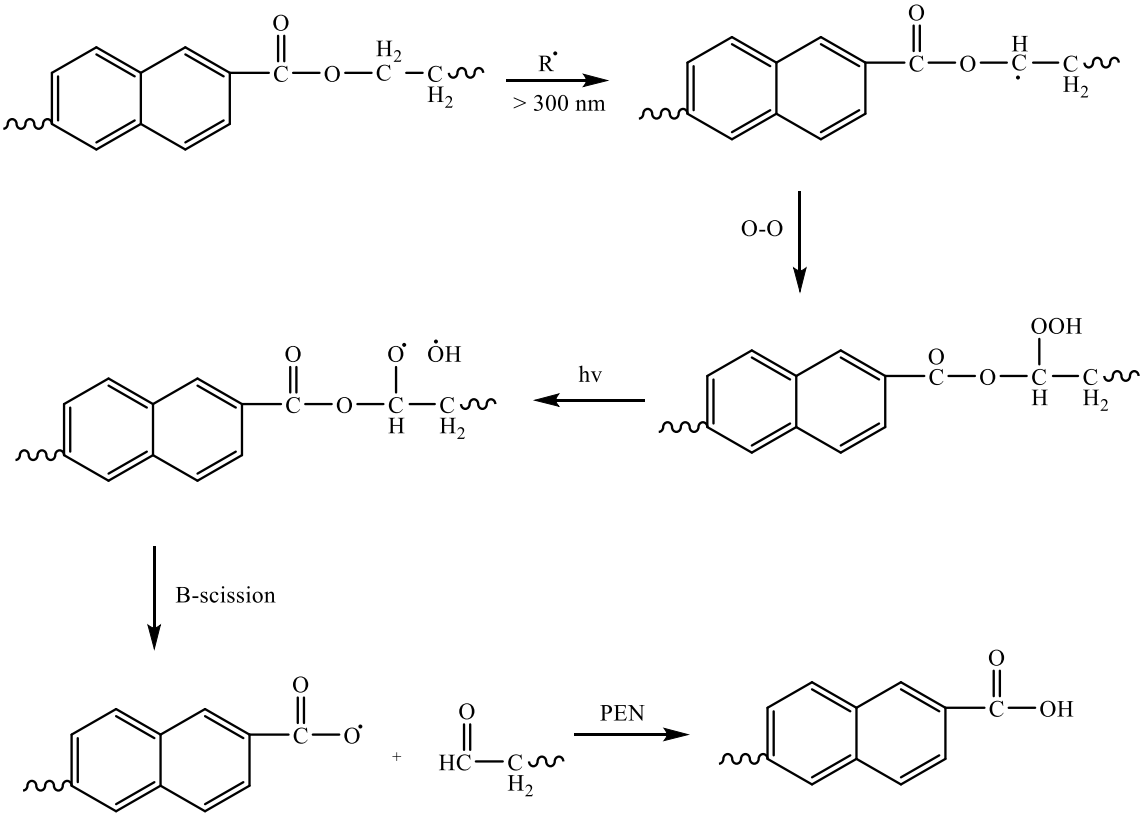

Figure 1.39: Photo-oxidation of PEN to form naphthanoic acid end groups.[90,100].

Figure 1.39 shows that the photo-oxidation of PEN involves peroxidation on the methylene carbon adjacent to the ester and subsequently, β-scission, to yield the naphthanoic acid end group.[90,100] Results also showed that yellowing in PEN was much more of a problem when oxygen was present than under vacuum. Therefore the

chromophores formed could also be due to substituted naphthalene derivatives as well as crosslinked bis-naphthalene structures.[100]

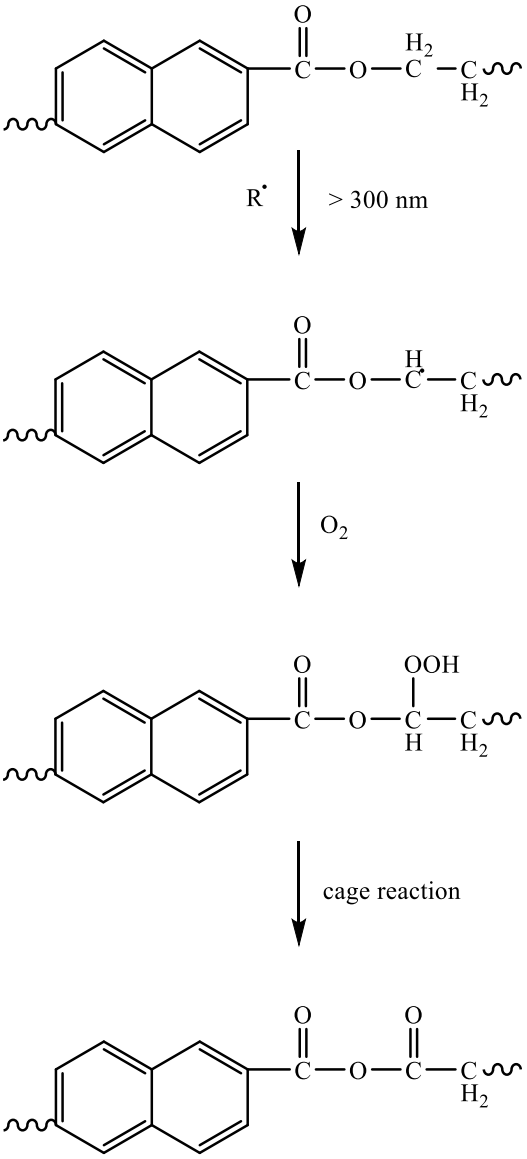

Figure 1.40: Photo-oxidation of PEN to yield an anhydride group.[90,95,100]

IR spectroscopy was used to observe the major changes that occurred in the carbonyl region. It was reported, by several papers, that a peak was identified at 1785 cm^{-1}; this

is due to the formation of anhydride groups.[90,95,100] For the radical formation of anhydrides a cage reaction is a necessary condition, this can be satisfied because of PEN's low molecular mobility, at the exposure temperature, which prevents the radicals from diffusing.[100] The photo-oxidation process in PEN, to yield an anhydride group, is shown in *Figure 1.40*.[90,95,100]

From the analysis of the IR spectra, it was also noted that the rate of carboxylic acid formation was lower for PEN than for PET; chain scission accompanies the formation of carboxylic acid end groups. Hence, the authors concluded that under UV irradiation PEN displays a lower rate of chain scission than PET.[100]

1.6 Poly(diethylene glycol) terephthalate

Another polymer of interest is PDEGT. PDEGT is only distinguishable from PET due to the monomer unit used in synthesis; PDEGT synthesis uses diethylene glycol (DEG), whereas PET uses ethylene glycol (EG). The repeat unit of PDEGT is given in *Figure 1.41*.

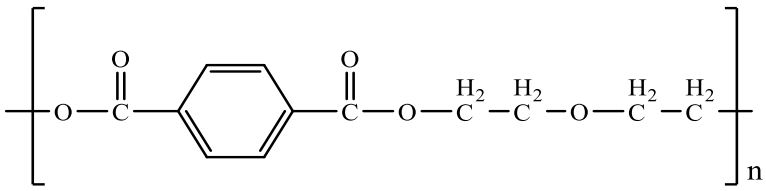

Figure 1.41: Structural repeat unit of PDEGT.

In the production of PET, DEG can be used as a co-monomer to reduce the rate of crystallisation as the DEG group introduces some flexibility in the polymer. For instance, this could be used in the production of drink bottles and would result in a clearer bottle when cooled.[103] Thermal degradation of PDEGT has been studied[103,104], but as far as is known any evidence related to the analysis of the photodegradation of this polymer has not been published.

1.7 Focus of research

DuPont Teijin Films is one of the world's biggest polyester film companies and is the leading producer of PET and PEN polyester films. PET film is used in a wide range of markets such as cards, electronics, packaging and photovoltaics and is very important as an engineering plastic because it has an unusual balance of physical, chemical, thermal and electrical properties.

Environmental factors such as temperature and moisture have been extensively studied and understood by DuPont Teijin Films, but the photodegradation reactions taking place in PET, during exposure to light, is less understood. Therefore, they are interested in the underlying degradation reactions occurring in PET during exposure to narrow and broad band light, especially for PET used in applications where weatherability would be an issue, for example in photovoltaics. In particular, DuPont Teijin Films are concerned that long wavelengths of light could have more of a detrimental effect on the weatherability of PET films, used as backsheets in photovoltaics, than previously reported.

Research was therefore firstly focused on understanding the main reactions occurring in PET during exposure to light. Experiments were undertaken using narrow (302 nm and 365 nm) and broad wavelength ranges of light (290-800 nm). It would be near impossible to determine the role of each wavelength in the degradation when exposing PET to a broad wavelength range of light. For this reason, narrow wavelength ranges of light were used to study the role of different wavelengths in the photodegradation of PET. PET films were also exposed to light under oxidative and non-oxidative environments to understand the reactions occurring when oxygen was not present.

Once the main reactions occurring in PET during exposure to light were understood samples were subject to a novel method of experimentation. Here, samples were exposed to different wavelengths of light sequentially, under oxidative conditions. This method was used to replicate outdoor exposure as exposing samples to different wavelength of light consecutively meant that reactions that happen simultaneously outdoors could be studied.

The reactions occurring in the homopolymer PDEGT when exposed to light were also studied as a comparison to PET and due to the fact that this area of research has never been reported in literature. The effect of wavelength, atmosphere and temperature on the photodegradation of PDEGT were studied.

Thus, the overall aim of this research was to investigate and understand the photochemical reactions occurring in PET, and a related polyester, when exposed to narrow and broad wavelength ranges of light, as well as using a novel method to understand the reactions happening consecutively during outdoor exposure. The findings in this thesis will enable DuPont Teijin Films to improve their understanding of the photodegradation process and benefit their research of protecting PET films against light during outdoor exposure.

This research will also build on previously reported findings, as it will, in particular address the impact of specific wavelengths of UV light and the depth at which UV light can penetrate and cause meaningful change. A novel method for studying consecutive reactions that take place outdoors by exposing the sample to different wavelengths of light sequentially, will also be addressed. The photodegradation reactions occurring during exposure of PDEGT have never been reported before in literature but this research will give an insight into these reactions.

1.8 References

1 http://www.dupont.com/products-and-services/solar-photovoltaic-materials/what-makes-up-solar-panel.html; Accessed March 2018

2 A. Luque and S. Hegedus, *Handbook of Photovoltaic Science and Engineering*, John Wiley and Sons, Ltd, 2003.

3 I. E. Agency, *Snapshot of Global Photovoltaic Markets*, 2016; Accessed April 2018

4 J. P. Singh, S. Guo, I. M. Peters, A. G. Aberle and T. M. Walsh, *IEEE J. PHOTOVOLTAICS*, 2015, 1–9.

5 Y. Voronko, G. C. Eder, M. Knausz, G. Oreski, T. Koch and K. A. Berger, *Prog. Photovoltaics Res. Appl.*, 2015, **23**, 1501–1515.

6 F. Liu, L. Jiang and S. Yang, *Sol. Energy*, 2014, **108**, 88–100.

7 D. R. Arnold, N. C. Baird, J. R. Bolton, J. C. D. Brand, P. W. M. Jacobs, P. de Mayo and W. R. Ware, *Photochemistry: An Introduction*, Academic Press INC., 1974.

8 C. E. Wayne and R. P. Wayne, *Photochemistry*, Oxford science publications, 1996.

9 J. D. Coyle, *Introduction to Organic Photochemistry*, John Wiley and Sons, Ltd, 1986.

10 A. L. Andrady, *Adv. Polym. Sci.*, 1997, **128**.

11 J. Guillet, *Polymer Photophysics and Photochemistry: An introduction to the study of photoprocesses in macromolecules*, Cambridge University Press, 1985.

12 P. Borrell, *Photochemistry: A Primer*, Richard Clay Ltd., 1973.

13 S. Venkatachalam, S. G. Nayak, J. V Labde, P. R. Gharal, K. Rao and A. K.

Kelkar, in *Polyester*, InTech, 2012.

14 N. S. Allen and M. Edge, *Fundamentals of Polymer Degradation and Stabilization*, ELSEVIER SCIENCE PUBLISHERS LTD, 1992.

15 V. B. Bojinov, *Polym. Degrad. Stab.*, 2006, **91**, 128–135.

16 H. Fashandi, a. Zadhoush and M. Haghighat, *Polym. Eng. Sci.*, 2008, **48**, 949–956.

17 N. S. Allen, *Photochemistry and Photophysics of Polymer Materials*, John Wiley and Sons, 2010.

18 A. L. Andrady, S. H. Hamid, X. Hu and A.Torikai, *J. Photochem. Photobiol. B.*, 1998, **46**, 96–103.

19 Y. Dobashi, T. Yuyama and Y. Ohkatsu, *Polym. Degrad. Stab.*, 2007, **92**, 1227–1233.

20 http://www.rsc.org/learn-chemistry/; Accessed May 2018

21 P. Atkins and Julio de Paula, *Elements of Physical Chemistry*, Oxford University Press, Ninth Ed., 2010.

22 M. Day and D. M. Wiles, *J. Appl. Polym. Sci.*, 1972, **16**, 175–189.

23 B. K. Sharma, *Spectroscopy*, GOEL Publishing House, 2007.

24 B. K. Sharma, *Instrumental Methods of Chemical Analysis*, GOEL Publishing House, 2005.

25 J. J. Liggat, *CH576 - Photochemistry Course Notes*, 2014.

26 J. P. LaFemina and G. Arjavalingam, *J. Phys. Chem.*, 1991, **95**, 984–988.

27 G. J. M. Fechine, R. M. Souto-Maior and M. S. Rabello, *J. Mater. Sci.*, 2002, **37**, 4979–4984.

28 S. Wunscher, S. Stumpf, A. Teichler, O. Pabst, J. Perelaer, E. Beckert and U.

S. Schubert, *J. Mater. Chem.*, 2012.

29 G. P. Karayannidis and E. A. Psalida, *J. Appl. Polym. Sci.*, 1999, **77**, 2206–2211.

30 M. E. Tawfik and S. B. Eskander, *Polym. Degrad. Stab.*, 2010, **95**, 187–194.

31 J. R. Whinfield and J. T. Dickson, *Br. Pat.*, 1941, 578 079.

32 J. Scheirs, T. E. Long, B. Hu, R. M. Ottenbrite and J. A. Siddiqui, *Modern Polyesters: Chemistry and Technology and Polyesters and Copolyesters.*, John Wiley and Sons, Ltd, 2003.

33 PlasticsEurope Market Research Group, *Plastics-The Facts 2017*, 2017.

34 A. Macková, V. Havránek, V. Švorčík, N. Djourelov and T. Suzuki, *Nucl. Instruments Methods Phys. Res. Sect. B Beam Interact. with Mater. Atoms*, 2005, **240**, 245–249.

35 G. J. M. Fechine and M. S. Rabello, *Curitiba*, 1998, 3635–43.

36 W. E. I. Wang, A. Taniguchi, M. Fukuhara and T. Okada, *J. Appl. Polym. Sci.*, 1997, **67**, 705–714.

37 I. Ouchi, M. Hosoi and F. Matsumoto, *J. Appl. Polym. Sci.*, 1976, **20**, 1983–1987.

38 G. J. M. Fechine, M. S. Rabello and R. M. Souto-Maior, *Polym. Degrad. Stab.*, 2002, **75**, 153–159.

39 P. Blais, M. Day and D. M. Wiles, *J. Appl. Polym. Sci.*, 1973, **17**, 1895.

40 M. Day and D. M. Wiles, *J. Appl. Polym. Sci.*, 1972, **16**, 191–202.

41 C. V Stephenson, C. Lacey and W. S. Wilcox, *J. Polym. Sci.*, 1961, **55**, 477–488.

42 C. V Stephenson, B. C. Moses and W. S. Wilcox, *J. Polym. Sci.*, 1961, **55**,

451–464.

43 P. Cheung, R. Roberts and K. B. Wagener, *J. Appl. Polym. Sci.*, 1979, **24**, 1809–30.

44 J. Scheirs and J. Gardette, *Polym. Degrad. Stab.*, 1997, **56**, 339.

45 N. S. Allen, M. Edge, M. Mohammadian and K. Jones, *Polym. Degrad. Stab.*, 1994, **43**, 229–37.

46 G. Di Pasquale and F. A. Bottino, *Polymer*, 1996, **37**, 703–705.

47 M. Day and D. M. Wiles, *J. Appl. Polym. Sci.*, 1972, **16**, 203–215.

48 A. R. Shultz and S. M. Leahy, *J. Appl. Polym. Sci.*, 1961, **5**, 64.

49 C. V. Stephenson, B. C. Moses and W. S. Wilcox, *J. Polym. Sci.*, 1961, **55**, 449.

50 C. V Stephenson and W. S. Wilcox, *J. Appl. Polym. Sci. Part A*, 1963, **1**, 2741–2752.

51 F. B. Marcotte, D. Campbell, J. A. Cleaveland and D. T. Turner, *J. Appl. Polym. Sci. Part A-1*, 1967, **5**, 481–501.

52 G. Valk, M. L. Kehren and I. Daamen, *Angew. Makromol. Chem.*, 1969, **7**, 201.

53 G. Valk, M. L. Kehren and I. Daamen, *1Angew. Makromol. Chem.*, 1970, **13**, 97.

54 J. G. Pacifici and J. M. Straley, *Polym. Lett.*, 1969, **7**, 7.

55 K. R. Osborne, *J. Polym. Sci.*, 1959, **38**, 357.

56 D. J. Carlsson and D. M. Wiles, *J. Macromol. Sci. Part C Polym. Rev.*, 1976, **14**, 65–106.

57 J. F. Rabck, *Polymer photodegradation. Mechanims and experimental*

methods., London: Chapman and Hall, 1995.

58 J. R. White and A. Turnbull, *J. Mater. Sci.*, 1994, **29**, 584–613.

59 N. S. Allen, *Eng. Plast.*, 1995, **8**, 247-286.

60 M. S. Rabello and J. R. White, *Polym. Degrad. Stability1*, 1997, **56**, 55–73.

61 M. S. Rabello and J. R. White, *Polym. Compos.*, 1996, **17**, 691–704.

62 L. Ogier, M. S. Rabello and J. R. White, *J. Mater. Sci.*, 1995, **30**, 2364–76.

63 P. Blais, M. Day and D. M. Wiles, *J. Appl. Polym. Sci.*, 1973, **17**, 1895–1907.

64 C. V Stephenson, B. C. Moses and S. Wilcox, *J. Polym. Sci.*, 1961, **55**, 465–475.

65 K. P. Osborn, *J. Polym. Sci.*, 1959, **38**, 357.

66 N. S. Allen, *Developments in Polymer Photochemistry*, Applied Science Publishers, 1982.

67 L. H. Buxbaum, *Angew. Chem. Internat. Ed.*, 1968, **7**, 182–190.

68 D. Coleman, *J. Polym. Sci.*, 1954, **14**, 15.

69 W. Mcmahon, H. A. Birdsall, G. R. Johnson and C. T. Camilli, *J. Chem. Eng. Data*, 1959, 57–79.

70 Y. Nakayama, K. Takahashi and T. Sasamoto, *Surf. Interface Anal.*, 1996, **24**, 711–717.

71 Z. Zhu and M. J. Kelley, *Polymer*, 2005, **46**, 8883–8891.

72 M. Day and D. M. Wiles, *Polym. Lett.*, 1971, **9**, 665–669.

73 C. H. Bamford and C. F. H. Tipper, *Degradation of Polymers*, Elsevier Scientific Pub. Co., 1975.

74 P. Ausloos, *Can. J. Chem.*, 1958, **36**, 383–392.

75 J. A. Barltrop and J. D. Coyle, *J. Chem. Soc.*, 1972, **B**, 251.

76 N. Grassie and G. Scott, *Polymer Degradation and Stabilisation*, Cambridge University Press, 1985.

77 P. Gijsman, G. Meijers and G. Vitarelli, *Polym. Degrad. Stab.*, 1999, **65**, 433–441.

78 J. L. Bolland, *Proc. R. Soc. Lond.*, 1946, 186.

79 J. L. Bolland and G. Gee, *Trans. Faraday. Soc.*, 1946, **42**, 236–243.

80 J. L. Bolland and G. Gee, *Trans. Faraday. Soc.*, 1946, **42**, 244–252.

81 G. Gryn'ova, J. L. Hodgson and M. L. Coote, *Org. Biomol. Chem.*, 2011, **9**, 480–90.

82 N. Grassie, *Developments in Polymer Degradation - 1*, Applied Science Publishers, 1977.

83 A. Rivaton, J.-L. Gardette, B. Mailhot and S. Morlat-Therlas, *Macromol. Symp.*, 2005, **225**, 129–146.

84 A. Davis and D. Sims, *Weathering of Polymers*, Applied Science Publishers, 1983.

85 S. H. Hamid, A. G. Maadhah, F. S. Qureshi and M. B. Amin, *Arab. J. Sci. Eng.*, 1988, **13**, 503.

86 S. G. Kiryushkin and Y. A. Shlyapnikov, *Polym. Degrad. Stab.*, 1989, **23**, 185.

87 E. Balanzat, H. Fuess, C. Trautmann and T. Steckenreiter, *Beam Interact. with Mater. Atoms*, 1997, 159–166.

88 O. Cicchetti, *Adv. Polym. Sci.*, 1970, **7**, 70.

89 G. J. M. Fechine, M. S. Rabello, R. M. Souto Maior and L. H. Catalani, *Polymer*, 2004, **45**, 2303–2308.

90 G. J. M. Fechine, R. M. Souto-Maior and M. S. Rabello, *J. Appl. Polym. Sci.*, 2007, **104**, 51–57.

91 B. O'Donnell and J. R. White, *Polym. Degrad. Stab.*, 1994, **44**, 211–22.

92 D. M. Bikiaris and G. P. Karayannidis, *Polym. Degrad. Stab.*, 1999, **63**, 213–218.

93 M. Edge, N. S. Allen, R. Wiles, R. McDonald and W. Mortlock, *Polymer*, 1995, **36**, 227–34.

94 G. J. M. Fechine, R. M. Souto-Maior and M. S. Rabello, *J. Appl. Polym. Sci.*, 2007, **104**, 51–57.

95 J. Scheirs and J. Gardette, *Polym. Degrad. Stab.*, 1997, **56**, 339.

96 N. S. Allen and J. F. Mckellar, *J. Appl. Polym. Sci.*, 1978, **22**, 2085–2092.

97 J. Scheirs, T. E. Long, B. Hu, R. M. Ottenbrite and J. A. Siddiqui, *Modern Polyesters: Chemistry and Technology of Polyesters and Copolyesters*, John Wiley and Sons, Ltd, 2003.

98 N. Grassie, *Developments in Polymer Degradation - 2*, Applied Science Publishers, 1979.

99 I. Ouchi, H. Aoki, S. Shimotsuma, T. Asai and M. Hosoi, *Congr. Mater. Res.*, 1974, **217**.

100 J. Scheirs and J. L. Gardette, *Polym. Degrad. Stab.*, 1997, **56**, 339–350.

101 Poly(naphthalates), *High Perform. Polym.*, 2014, 255–279.

102 G. Botelho and A. Queiro, *Polym. Degrad. Stab.*, 2000, **70**, 299–304.

103 H. A. Lecomte and J. J. Liggat, *Polym. Degrad. Stab.*, 2006, **91**, 681–689.

104 B. J. Holland and J. N. Hay, *Polymer*, 2002, **43**, 1835–1847.

2 Experimental

2.1 Materials

2.1.1 PET film samples

The PET films investigated in this study were 23 µm and 36 µm Melinex type S and were supplied by DuPont Teijin Films®. The films were reported to contain 0.2 wt% china clay and no UV stabilisers. The films were cut into small squares, 3 cm by 3 cm, and markings were made so that the same area was analysed each time.

2.1.2 PDEGT thin films

The PDEGT homopolymer used was supplied by DuPont Teijin Films®. PDEGT was purified by precipitating from a 10% w/v solution of chloroform in a bath of isopropanol. The polymer was then dried under vacuum. The purified PDEGT was dissolved in dichloromethane (supplied by Sigma Aldrich), solvent cast onto aluminium foil and dried under vacuum. Initially, infrared spectra and the weights of the sample were taken every 4 hours to record the drying process. A digital external micrometer with a range of 0 - 25 mm was used to measure the thickness of each of the dry films.

2.2 Sample exposure

Sunlight is commonly separated into three main wavelength ranges: ultraviolet (UV), visible (VIS), and infrared (IR). Each wavelength range makes up a portion of the solar spectrum, with values given in *Table 1*.

Table 1: Spectral ranges in accordance with CIE.

Range Name	Wavelength Range (nm)	% of Total Solar
Ultraviolet	315 - 400	6.8
Visible	400 – 800	55.4
Infrared	800 – 2450	37.8

ASTM G113-94, *Terminology Relating to Natural and Artificial Weathering Tests of Non-metallic Materials* states that UV is 'radiation for which the wavelengths of the components are shorter than those for visible radiation.'

Although the UV spectral ranges are not well defined the CIE (Commission Internationale de l'Eclairage) committee makes the following distinctions: UV-A is 315 to 400 nm, UV-B is 280 to 315 nm and UV-C is < 280 nm. These will be assumed as the defined spectral ranges in this thesis.[1]

2.2.1 Atlas Suntest Weatherometer XLS+

A materials adverse response to outdoor conditions is known as weathering. In recent years there has been a need for analysis of the weathering resistance of materials used in outdoor applications. Artificial weathering chambers are frequently used to accelerate the degradation. Some common examples of light sources used in these chambers include xenon arc, fluorescent, metal halide and carbon arc. In 1954 the first weathering instrument to use a xenon arc lamp was developed. Xenon arc lamps are preferred when the material to be tested will be exposed outdoors as they have a solar radiation profile that closely resembles that of natural sunlight. Laboratory accelerated weathering tests can also run continuously at a higher irradiance than solar radiation and are not interrupted by the natural day and night cycle.

In this study, sample exposure was carried out in an Atlas Suntest XLS+ Weatherometer with a 1170 cm^2 exposure area. The xenon arc lamp used in the weatherometer operates at high intensity and generates considerable heat, so it is air-

cooled. An illustration of the XLS+ test chamber and lighting system is shown in *Figure 2.01*.[1]

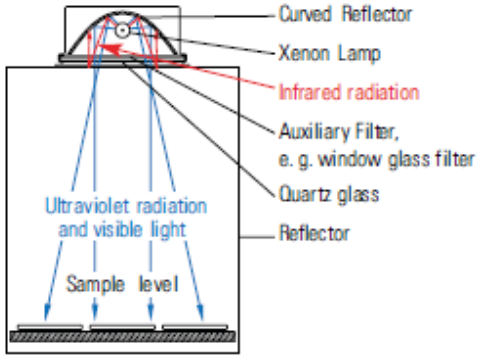

Figure 2.01: Cross section of the XLS+ test chamber and lighting system.[1]

A daylight filter with a cut-off at 290 nm was used with the xenon arc lamp for simulation of outdoor solar radiation. The spectral comparison given in *Figure 2.02* shows that the spectral output of the daylight filter closely matches that of sunlight. The daylight filer meets industry standard ASTM G155 *Operating Xenon Arc Light Apparatus for Exposure of Non-Metallic Materials.*

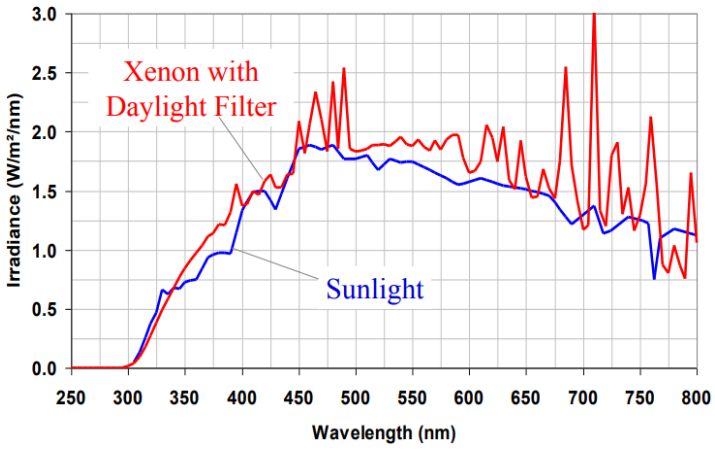

Figure 2.02: Spectral comparison of natural sunlight vs. xenon lamp with a daylight filter.[1]

Irradiance can be controlled between 300-800 nm/Lux as well as automatic control of Black Standard Temperature (BST) and monitoring and display of Chamber Temperature (CHT). A SunCal calibration sensor was used to calibrate the weatherometer before starting a new programme. The sensor allows simultaneous calibration of both irradiance and BST. This weatherometer model follows ISO 4892-1 for measuring and controlling the maximum surface temperature of a black sample.[1]

Exposure was carried out according to ASTM D5071-06 *Exposure to Photodegradable Plastics in a Xenon Arc Apparatus*. The film samples were placed in the chamber using a metal frame and exposed continually to an irradiation intensity of (365 ± 35) W m^{-2}, measured between 300-800 nm, and a temperature of (37.5 ± 2.5)°C.

Equation 1 shows the calculated relationship between the weatherometer, set at 365 W m^{-2}, and outside in Redcar, England.

$$T_{out} = T_{WO}\ x\ 7.5 \qquad \textbf{Equation 1}$$

Where T_{out} is time outside and T_{WO} is time in the weatherometer. This equation is valid for the wavelength range 290 – 800 nm. *Equation 1* was calculated as follows:

$$Weatherometer\ intensity = 365\ W\ m^{-2}$$

$$Intensity\ outside\ (Redcar, England) = 1541x\ 10^{6} J\ m^{-2}$$
$$= 1541\ x\ 10^{6}\ Ws\ m^{-2}$$

$$Change\ units\ to\ W\ m^{-2}\colon\ \frac{1541\ x\ 10^{6}}{365\ x\ 24\ x\ 60\ x\ 60} = 48.86\ W\ m^{-2}$$

$$Therefore\colon\ \frac{365\ W\ m^{-2}}{48.86\ W\ m^{-2}} = 7.5$$

The intensity value for outside in Redcar, England was provided by DuPont Teijin Films.

PET samples were placed on a metal tray for irradiation in the weatherometer. Intensity measurements were carried out at various positions on the tray to determine whether all samples were exposed to the same intensity of light. The spread of intensities across the weatherometer tray are shown in *Figure 2.03*.

94.5%	93.6%	94.5%
100%	98.8%	97.9%
81.4%	79.5%	80.0%

Figure 2.03: Spread of intensities across the weatherometer tray.

A tray with circular holes was made to allow the PET film samples to be attached to the rear side of this tray, meaning each sample could not move during exposure. This tray with attached PET film samples was then placed on the metal sample tray in the weatherometer. Considering that this metal sample tray has a reflective surface, a piece of black material was placed on the tray before the tray with attached samples was placed on top. This meant that back scattering would not be an issue.

Control samples were also added to the tray during exposure experiments to monitor if this spread in intensity affected the rate of degradation.

2.2.2 UVP XX-Series UV Bench Lamps

Exposure to UV light was carried out using XX-Series UV Bench Lamps from Ultraviolet Products (UVP). Two different wavelengths of light were used to irradiate the films; 365 nm (UV-A) and 302 nm (UV-B). The spectra charts for each lamp are given in *Figure 2.04*.[2]

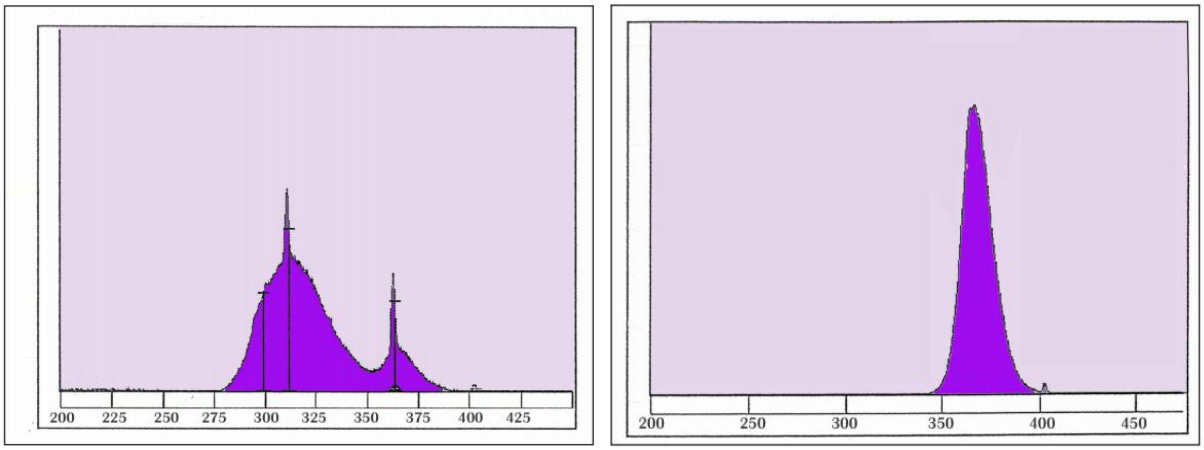

Figure 2.04: Spectral charts of the two UV lamps with filters; 302 nm on the left and 365 nm on the right.[2]

Temperature and intensity could not be controlled on these lamps, but it could be recorded. The intensity of both lamps was measured using an intensity meter and recorded before and after every exposure.

The samples were exposed to an average intensity of (31.7 ± 4.0) W m^{-2} and a temperature of (22.5 ± 2.5)°C.

From *Figure 2.04* it is apparent that the lamps do not emit one single wavelength of light but rather a range of wavelengths. Although, this is the case, in this thesis the lamps will be referred to as the 302 nm lamp and the 365 nm lamp.

2.2.3 Hönle Cube 100 Lamps

Exposure to UV light was also carried out using a Hönle LED Cube 100 from Hönle UV Technology. This lamp exposed samples to high intensity 365 nm (UV-A) light. The spectral chart of the 365 nm lamp is given in *Figure 2.05*.

Temperature could not be controlled but was recorded. Intensity could be adjusted in 1% steps between 2 and 100% irradiance. An intensity measurement was taken before and after every exposure using a hand-held Hönle UV-Meter.

The samples were exposed to an average intensity of (825.5 ± 20) W m^{-2} and a temperature of (43 ± 2.5)°C.

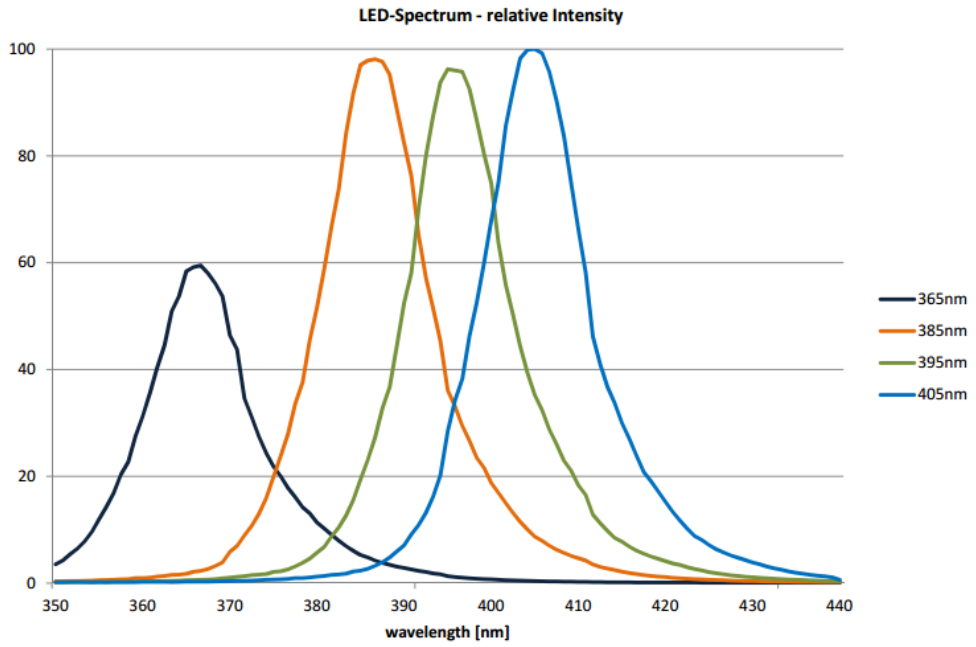

Figure 2.05: Spectral chart for the 365 nm UV lamp use, depicted by the dark blue line.

2.2.4 Exposure under a non-oxidative atmosphere

To expose samples under a non-oxidative atmosphere a photodegradation cell was created, shown in *Figure 2.06*. The cell was made from a borosilicate cone and socket set with a quartz window at the top and two Young's taps on either side. The taps were used for gas inlet and outlet. When a sample was placed inside the cell it could be water cooled or heated, through the water inlet and outlet, shown in *Figure 2.06*. The photodegradation cell was used to control the atmosphere and temperature during exposure experiments.

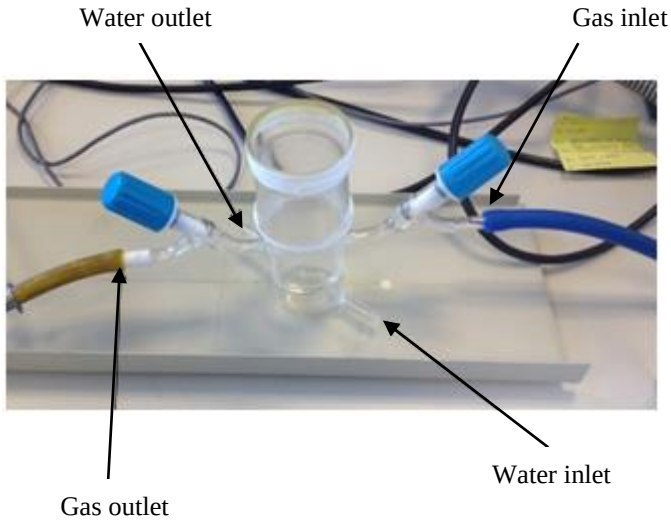

Figure 2.06: Picture of photodegradation cell used for exposing samples under a non-oxidative atmosphere and controlling temperature during exposures.

2.3 Infra-red

IR light is electromagnetic radiation that has a longer wavelength than visible light. IR is the study of interactions of light radiation with matter when electromagnetic waves travel through the medium.[3] For a molecule studied by vibrational spectroscopy, it is essential that its electric dipole moment changes during the

vibration. The molecule does not have to have a permanent dipole; it only needs to have a change in dipole, this could be from zero. Homonuclear diatomic molecules are IR inactive as their electric dipole moment does not change from zero, no matter what length the bond is, whereas heteronuclear diatomic molecules are IR active as their dipole moment changes with lengthening and contracting of the bond.[4] A representation of a vibrating mode of an IR active molecule, CO_2, is shown in *Figure 2.07*.

The number of modes of vibration within a polyatomic molecule can be calculated using *Equations 2 and 3*. *Equation 2* is used if the molecule is linear and *Equation 3* is used if the molecule is non-linear.[4]

$$no.of\ vibration\ modes = 3N - 5 \qquad \textbf{Equation 2}$$

$$no.of\ vibration\ modes = 3N - 6 \qquad \textbf{Equation 3}$$

The equations show that for a non-linear molecule there are 3N – 6 vibrational modes, which also corresponds to 3N – 6 internal degrees of freedom of motion within the molecule.[3,5]

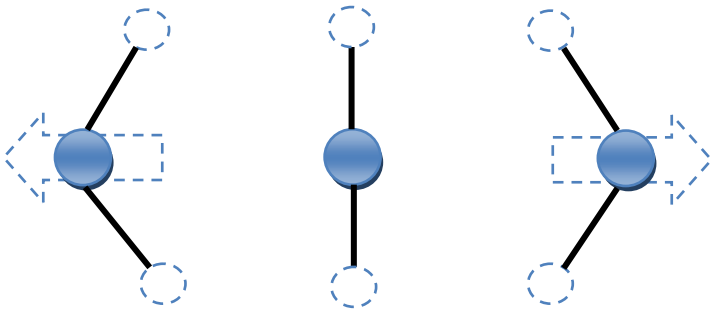

Figure 2.07: Modified representation of the CO_2 bending mode. The arrows signify the molecular dipole moment.[4]

IR energy will be absorbed by a molecule if the vibration of a bond results in a change in dipole moment. Some vibrations that can cause absorptions in the IR region include stretching and bending. In IR the change in absorption with wavenumber is measured, where wavenumber is proportional to the energy or frequency of the vibration of the bond.

There are three main factors that affect the vibrations in a molecule; the type of vibration, the strength of the bond and the mass of the atoms. Absorptions due to stretching occur at higher wavenumbers than bending vibrations. This is because it will generally need more energy to stretch a bond than it is to bend it. This means that, for the same bond, stretching vibrations are of higher energy than bending vibrations. Stronger bonds absorb at higher wavenumbers because more energy will be required to make the bond vibrate. For example, a triple bond will absorb at higher wavenumbers than a single bond. The mass of the atoms on the bond affect the vibration due to lighter atoms vibrating faster than heavier ones. Lighter atoms will vibrate at a higher frequency and will, therefore, absorb at a higher wavenumber.[6]

2.3.1 Attenuated Total Reflectance Fourier Transform Infrared

2.3.1.1 Theory

Attenuated Total Reflectance Fourier Transform Infrared **(**ATR FT-IR) spectroscopy is a useful surface technique in studying polymer degradation as it allows chemical changes in the polymer to be identified.

A representation of how a single bounce diamond crystal ATR works is shown in *Figure 2.08*. In ATR sampling the IR beam is directed into the crystal which totally internally reflects off the internal surface and creates an evanescent wave; if the refractive index of the crystal is not higher than that of the sample then the wave would not be totally internally reflected. *Figure 2.08* shows that this wave is projected orthogonally into the sample in contact with the crystal. The reflected radiation reaches the detector and some of the energy from the evanescent wave has now been absorbed by the sample.[7]

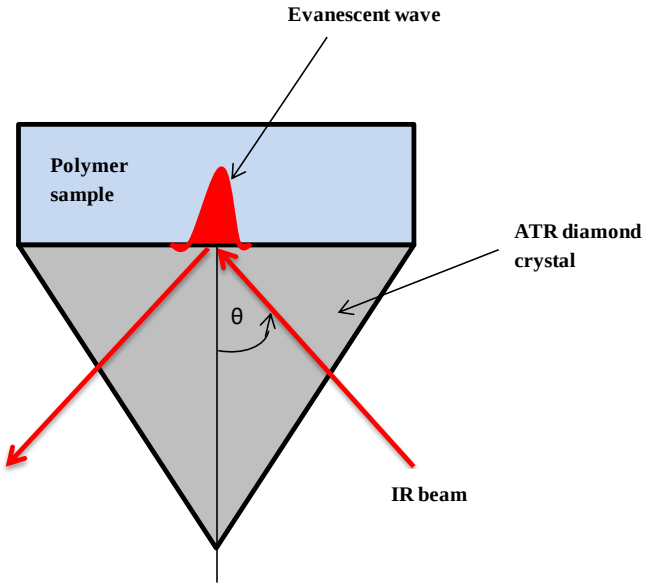

Figure 2.08: Modified representation of a single bounce ATR FT-IR.

When using ATR there are a few experimental factors that are important. Some of these include the refractive indices of the sample and ATR crystal, the angle of incidence of the IR beam, the critical angle, depth of penetration, the wavelength of the IR beam, effective pathlength (EPL), number of reflections and quality of sample contact with the ATR crystal.

Equation 4 shows how the critical angle is related to the refractive indices of the ATR crystal and sample.

$$\theta_c = sin^{-1}\left(\frac{n_2}{n_1}\right) \qquad \textbf{Equation 4}$$

Where θ_c is the critical angle, n_1 is the refractive index of the ATR crystal, and n_2 is the refractive index of the sample.

If the critical angle is exceeded then a pure ATR spectrum will be obtained, whereas if the critical angle is not met then a combined ATR and external reflectance spectra

would result. Three ways in which this can occur are if the refractive index of the sample is too high, if the refractive index of the ATR crystal is too low or if the angle of incidence of the beam is too low.[7]

The depth of penetration of the IR beam into the sample can be defined and calculated using *Equation 5*.

$$d_p = \frac{\lambda}{2\pi\ (n_1^2\ sin^2\ \theta - \ n_2^2)^{\frac{1}{2}}} \qquad \textbf{Equation 5}$$

Where d_p is the depth of penetration, λ is wavelength and θ is the angle of incidence of the IR beam. ATR is a surface technique and only penetrates approximately 0.5 to 5 μm into the sample depending on experimental conditions.

The EPL is another factor which must be taken into consideration. A single reflection ATR is commonly used for qualitative analysis, but when analysing minor components of a sample the EPL is generally increased. The EPL can be derived from *Equation 6.*

$$EPL = N\ x\ d_e \qquad \textbf{Equation 6}$$

Where EPL is the effective path length, N is the number of reflections and d_e is the effective penetration. The EPL can be increased by increasing the number of reflections within the ATR crystal. Increasing the number of reflections means that minor bands become more apparent.

The quality of sample contact with the crystal is usually not a problem with liquid samples but rigid or porous samples can cause issues. Solid samples are usually firmly clamped onto the crystal so that they are in intimate contact. This means that trapped air, between the sample and crystal, is not the medium in which the evanescent wave travels. The pressure applied to the sample can also cause a significant difference in

absorbance due to the difference in sample contact with the crystal. Consistency between spectra could therefore be a problem.

Some advantages of ATR FT-IR spectroscopy are that it is a non-destructive technique, samples that absorb strongly in the IR region can be measured and there is little or no sample preparation required.[8,9] However, a disadvantage of ATR is the sample contact with the ATR crystal.[7] When different degrees of pressure are placed on the sample very different absorbance values, in the spectra, can be obtained.

2.3.1.2 Experimental conditions

An Agilent 5500A Series ATR FT-IR instrument was used to collect spectra of the PET film samples. The following conditions were used:

Background valid time limit:	6 minutes
Y-axis unit:	Absorbance
Minimum Y Threshold:	0.1 Abs
Spectral range (cm^{-1}):	4700 to 650
Background scans:	64
Samples scans:	64
Resolution (cm^{-1}):	2
Sampling technology:	ATR
Sampling subtype:	1-Bounce

ATR FT-IR was used in this research to identify any chemical changes in the PET film samples after exposure to UV light. The front and back sides of the samples were tested at four different points using a template so that the same point was tested each time.

Analysis of the spectra included baseline correction, averaging and normalisation to the peak at 1410 cm^{-1} assigned to aromatic skeletal stretching. This peak has been shown by Ward *et al.* not to change on stretching or crystallisation and therefore it was used as an internal standard.[10]

The film samples tested using ATR FT-IR were not thick enough to give good contact with the crystal, so a piece of non-stick material was placed on top of the sample and better spectra were obtained. *Figure 2.09* shows a spectrum of PET film with and without the non-stick material.

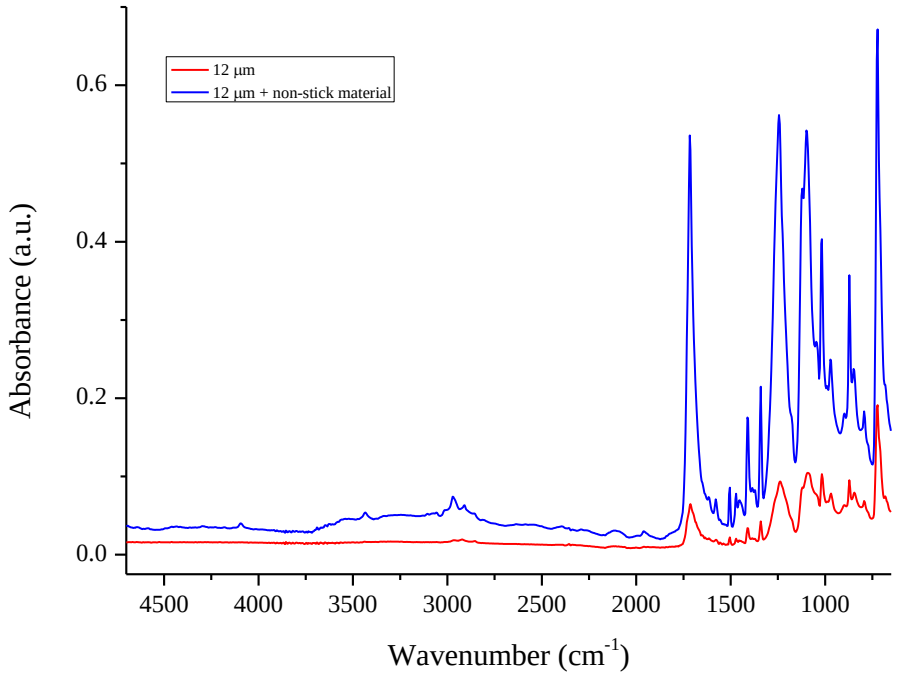

Figure 2.09: ATR FT-IR spectra of the front of a PET film sample. The red line shows a PET film and the blue line shows a PET film with the non-stick material.

2.3.2 Diffuse Reflectance Infrared Fourier Transform

2.3.2.1 Theory

Diffuse Reflectance Infrared Fourier Transform (DRIFT) is a technique that allows the bulk of the sample to be analysed, not just the surface; the instrument can penetrate about 400 µm into a sample. When light strikes a solid surface, it will be reflected regularly (specular reflection), scattered diffusely and penetrate the surface.

In DRIFT the spectrometer beam is directed into the sample where it will be reflected, scattered, and transmitted through the sample. The diffusely scattered light that is back reflected is collected and some of the light is absorbed by the sample. This light is then directed to the detector; about 28% of the diffuse IR that is reflected from the sample is collected by the detector. The light is only considered to be diffuse reflection if it is returned to the surface after being scattered within the sample.[11] *Figure 2.10* shows a representation of a textured sample that diffusely reflects IR.

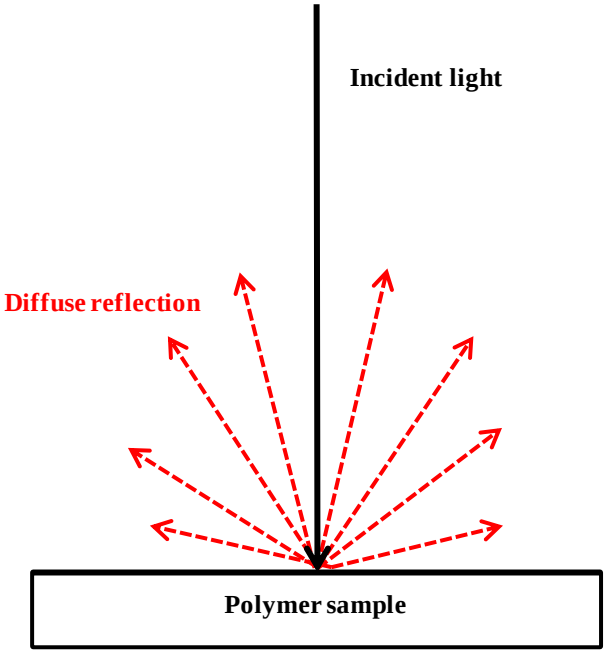

Figure 2.10: Representation of a textured sample that diffusely reflects IR.

Some factors taken into consideration to produce high quality spectra are particle size, refractive index, and homogeneity. The particle size can affect the contribution of reflection from the surface of the sample. To improve the quality of the spectrum the size of the sample particles can be reduced. Refractive index can cause effects in specular reflectance contributions, but this can be reduced by diluting the sample. Non-homogeneous samples can cause problems with reproducibility in DRIFT spectra. Therefore, it is recommended that samples prepared for analysis be uniform and well mixed.

DRIFT has several advantages including, little or no sample preparation required, and it is a non-destructive technique. DRIFT also allows chemical and physical changes in the sample to be analysed, whereas ATR only shows chemical changes; physical changes can include grain size and degree of crystallisation. A disadvantage of using DRIFT is that it can be difficult to interpret because the spectra can show chemical and physical changes and because of these physical changes a peaks wavenumber can be shifted.

2.3.2.2 Experimental conditions

An Agilent 4100 ExoScan FTIR was used to collect DRIFT spectra of the PET and PDEGT samples. The following conditions were used:

Background valid time limit:	6 minutes
Y-axis units:	Absorbance
Minimum Y Threshold:	0.1 Abs
Spectral range (cm^{-1}):	5200 to 620
Background scans:	128
Samples scans:	128
Resolution (cm^{-1}):	4
Reference cap:	Normal diffuse cap – 00239A

DRIFT was used in this research to identify any chemical changes in the film samples after exposure to UV light. The front and back sides of the samples were tested at four different points using a template so that the same point was tested each time.

Analysis of the spectra included baseline correction, averaging and normalisation to the peak at 1410 cm^{-1}, assigned to aromatic skeletal stretching. This peak has been shown by Ward *et al.* not to change on stretching or crystallisation and therefore it was used as an internal standard.[10] An example of a PET DRIFT spectra is given in *Figure 2.11*.

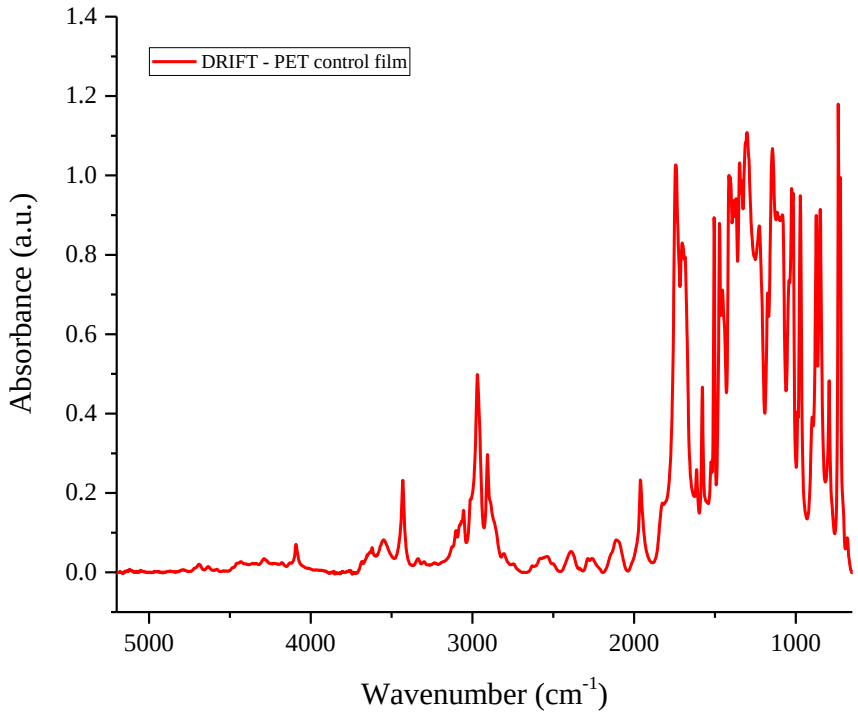

Figure 2.11: DRIFT spectra of a PET film sample.

2.4 Differential Scanning Calorimetry

2.4.1 Theory

Differential Scanning Calorimetry (DSC) is a technique that was first developed in the 1960s that allows the analysis of the thermal properties of a sample, while it is heated

or cooled. In DSC, the energy required to establish a temperature difference of zero between the sample and an inert reference, as a function of time or temperature, is recorded.[12] DSC allows the detection of physical and chemical processes occurring within the sample. Physical processes include glass transition, crystallisation, and melting, whereas chemical processes include oxidation and degradation. This technique can be used to determine the thermal properties of many materials including plastics, sealants, foods, adhesives, and lubricants.

There are two types of DSC systems utilised in research today; heat flux DSC (shown in *Figure 2.12*) and power compensation DSC. The main difference is that heat flux DSC has a single furnace whereas power compensation DSC has two independent furnaces. The heat flux DSC will be described in more detail as this was the only system used throughout this research.[13]

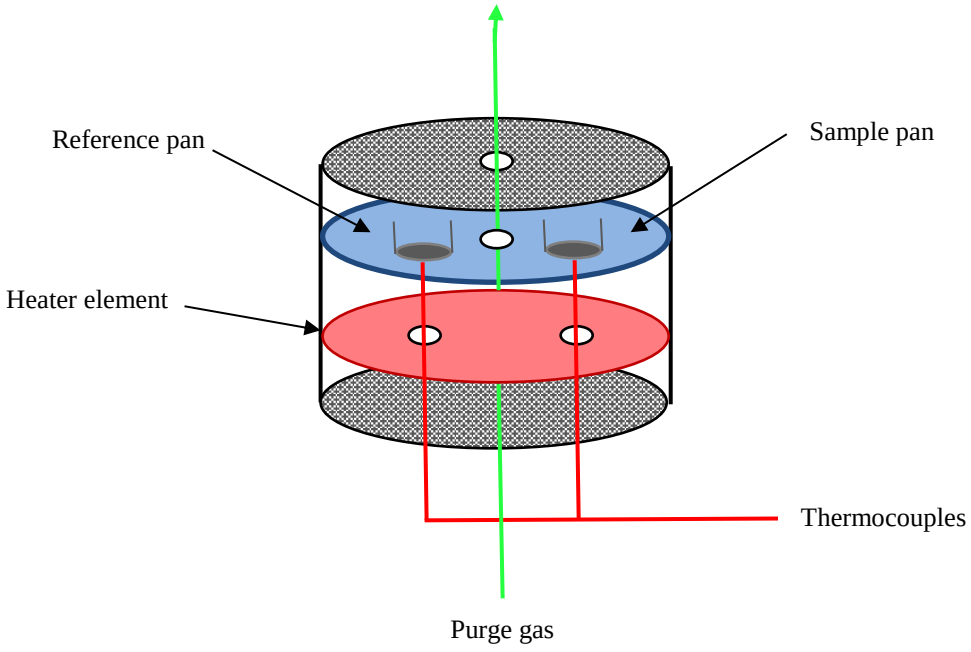

Figure: 2.12: Illustration of a DSC thermogram.

In heat-flux DSC the sample and reference pans are subjected to the same temperature programmes in a controlled atmosphere. An illustration of a heat-flux DSC is shown in *Figure 2.12*.

The calorimeter consists of a sample and reference pan holder. The sample and references pans are placed on raised stages, which heat is transferred through. The difference in temperature between the sample and reference is measured by the thermocouples as a function of temperature. This temperature difference, ΔT, is proportional to the difference in heat flow in or out of both the sample and reference pans. During exothermic or endothermic transitions, the sample temperature will be higher or lower than the reference, respectively. When the sample temperature is higher, ΔT will be positive, whereas when the sample temperature is lower, ΔT will be negative. ΔT can be converted by the software to heat capacity using *Equation 7*.

$$\Delta T = q \frac{C_p}{K} \qquad \textbf{Equation 7}$$

Where q is the heating rate, C_p is the heat capacity and K is a calibration factor.

The purge gas used in this study was nitrogen as it is useful for efficient heat transfer and for removal of volatiles. Aluminium pans were used to contain the sample and the reference sample used was simply an empty pan and lid.

The results from a typical DSC study are presented as a thermogram in *Figure 2.12,* where heat flow is plotted against temperature. The thermogram shows some of the main processes which can be observed during a heating or cooling cycle. In *Figure 2.13* the glass transition temperature (T_g) can be identified as well as exothermic and endothermic transitions.

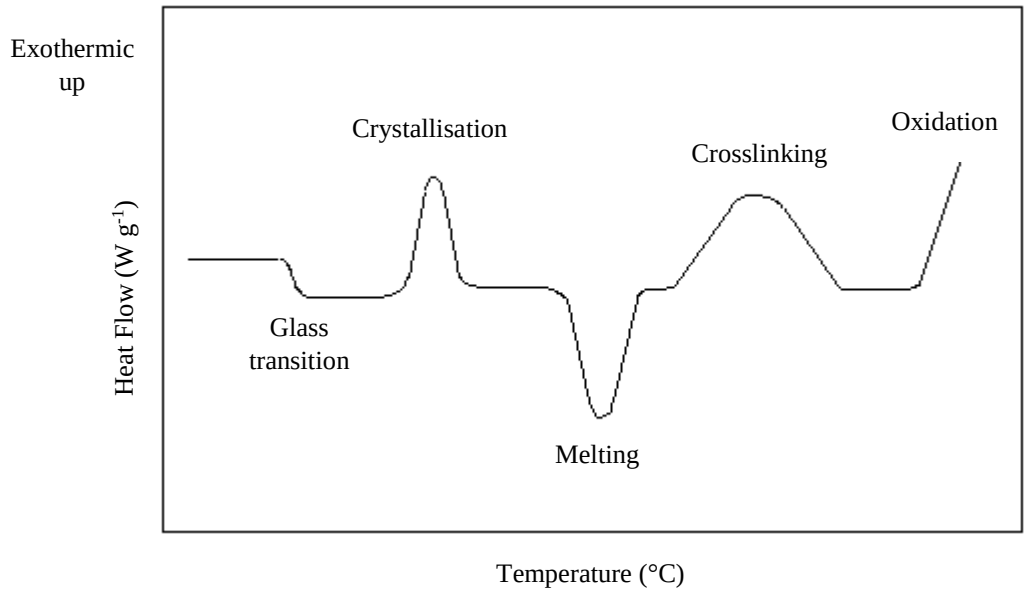

Figure: 2.13: Diagram of a heat flux DSC system.

2.4.2 Experimental conditions

A TA Instruments Q1000 DSC with an RC90 refrigerated cooling system was used to analyse the polymer films. All samples were prepared in aluminium DSC pans with lids. A heat-cool-heat method was implemented with the conditions as follows:

1. Nitrogen flow rate = 40 mL/min
2. Equilibrate at 40 °C
3. Ramp 10 °C/min to 320.00 °C
4. Isothermal for 2.00 min
5. End of Cycle 1
6. Ramp 10 °C/min to 40.00 °C
7. Isothermal for 2.00 min
8. End of Cycle 2
9. Ramp 10 °C/min to 320.00 °C
10. End of Cycle 3

All data collected was processed using TA software and all temperature values are quoted to the nearest integer value. The method used for PDEGT was altered at points 2 and 6 as follows:

1. Same as above
2. Equilibrate at 0 °C
3. 3-5. Same as above
4. Ramp 10 °C/min to 0.00 °C
5. 7-10. Same as above

Each cycle in the thermogram was then analysed using TA Universal Analysis software. The T_g, melting temperature (T_m), crystallisation temperature (T_c), enthalpy of melting (ΔH_m) and enthalpy of crystallisation (ΔH_c) were recorded for each sample.

2.5 Ultraviolet-visible Spectroscopy

2.5.1 Theory

UV-visible spectroscopy is a technique that refers to absorption spectroscopy in the UV spectral region. The absorption of UV radiation, of the correct frequency, results in transitions of valence electrons from the ground state to an excited (higher energy) state, usually an antibonding orbital. From this electronic absorption spectra are observed.[12,14] Absorption is a radiative process with a timescale of 10^{-15} seconds.

In *Figure 2.14* absorbance is depicted by the red arrow. The process of a molecule absorbing a photon of a particular energy, which results in the excitation of an electron from a lower energy level to a higher one, is known as absorbance.

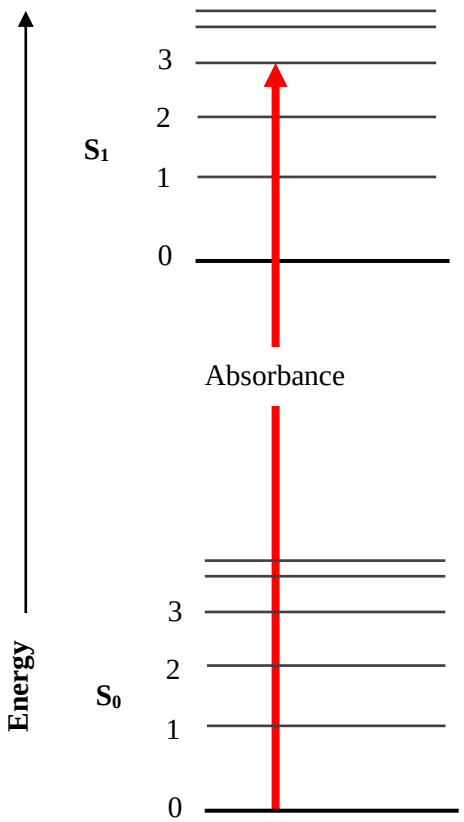

Figure 2.14: Illustration of the absorbance process, depicted by the red arrow.

The absorbance process only occurs when the specific wavelength of light has the same energy as the energy difference between the two energy states, of the particular molecule. This energy can be calculated using the Planck-Einstein relation, given in *Equation 8*.

$$E = h\upsilon = \frac{h\,c}{\lambda} \qquad \textbf{Equation 8}$$

Where E is the energy, h is Planck's constant, c is the speed of light, υ is the frequency and λ is the wavelength of the incoming photon. The electronic excitation energy is

either re-emitted as radiative energy, dissipated by a relaxation process and re-emitted as heat or converted into chemical energy.[15]

An appropriate group must be present in the polymer for the UV radiation to be absorbed and for electronic absorption spectra to result. These functional groups are known as chromophores and are responsible for electronic absorption.

Figure 2.15 shows an energy diagram with the electronic transitions that are possible. The σ - σ* transitions are of high energy and require wavelengths that do not fall in the UV-visible region, therefore they are not usually observed in UV-visible spectra. In the region between 150-250 nm, the n → σ* transitions are observed. The most commonly observed transitions in compounds with lone pairs and multiple bonds are the π - π* and n - π* transitions in the wavelength region between 200-600 nm.[16]

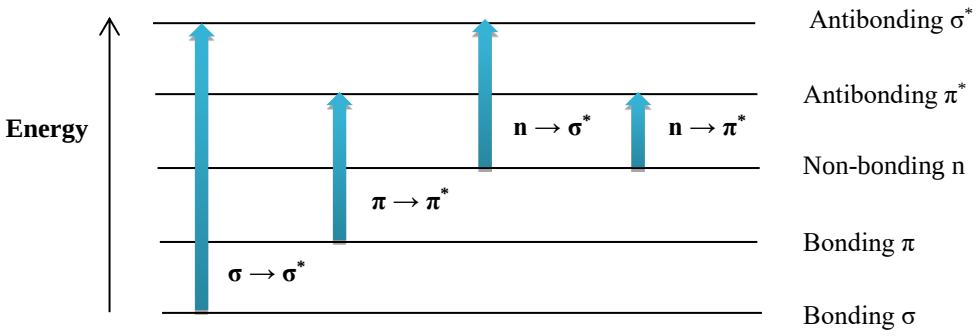

Figure 2.15: Modified schematic of possible electronic transitions.[16]

The Beer-Lambert law is given in *Equation 9* and is used for analysis in UV-visible spectroscopy.[12]

$$A = \varepsilon c l = log_{10}\left(\frac{I_o}{I}\right) \qquad \textbf{Equation 9}$$

Where A is the absorbance of the sample, Ɛ is the molar absorption coefficient, c is the concentration of the absorbing species, l is the path length of the cell, I_o is the intensity of the transmitted light, and I is the intensity of the incident light. For strongly absorbing chromophores the molar absorptivities can be very large, but if absorption is weak the molar absorptivity can be very small. The probability that a certain wavelength of light will be absorbed and the size of the chromophore are both parameters that would affect the magnitude of Ɛ; Ɛ is constant for a particular polymer at a specified wavelength.[12,17]

Transmittance can also be measured in UV-visible spectroscopy and the relationship between absorbance and transmittance is given in *Equation 10*.[12]

$$A = -log_{10} T \qquad \textbf{Equation 10}$$

The Beer-Lambert Law suggests that absorbance plotted against the concentration of the sample will be linear with a gradient of εl.

2.5.2 Experimental conditions

UV-visible spectroscopy was conducted using a UV-1800 UV-visible Spectrophotometer with a film holder from Shimadzu. The following parameters were used:

Measurement mode: absorbance

Scan range: 190 - 600 nm

Recording range: 0 – 4 A

Scan speed: slow

No of scans: 1

A graph of absorbance vs. wavelength was then plotted for each film.

2.6 Fluorescence Spectroscopy

2.6.1 Theory

Fluorescence is a radiative transition which is used in many areas of science, due to its high sensitivity and selectivity. This transition occurs from the lowest vibrational level of the first excited state to a vibrational level of the ground state.

Fluorescence is most likely to occur from the first singlet excited state to the ground singlet state because in higher energy states internal conversion and vibrational relaxation are more likely to occur. Fluorescence is an allowed transition as the electron stays in the same multiplicity.

Upon absorption of a photon, an excited molecule is typically present in the lowest excited singlet state (S_1) for approximately 10^{-8} seconds before relaxing to the ground state. The process is known as fluorescence if this relaxation is accompanied by the emission of a photon. Fluorescence is a radiative process with a timescale of 10^{-7} to 10^{-9} seconds. *Figure 2.16* shows part of the Jablonski diagram which illustrates this radiative process.

A wide range of photon energies are produced during emission due to thermal motion and closely spaced vibrational energy levels in the ground state. This results in fluorescence being observed over a band of wavelengths instead of a sharp line. Normally the quantum of radiation emitted during fluorescence is lower in energy than the quantum absorbed due to vibrational relaxation. Relaxation processes competing with fluorescence include intersystem crossing and quenching.[18]

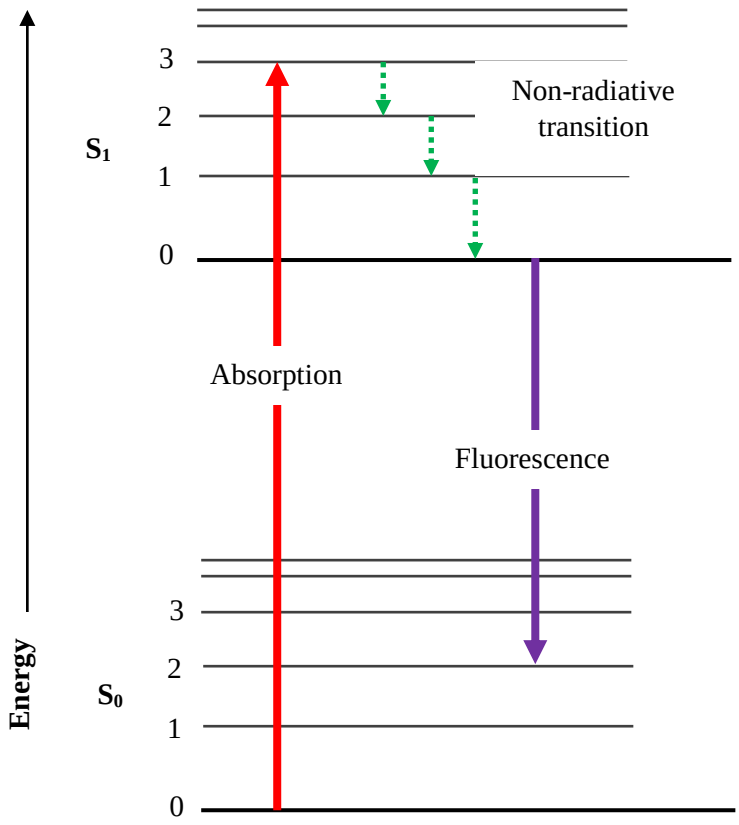

Figure 2.16: Illustration of the fluorescence process, depicted by the purple arrow.

2.6.2 Experimental conditions

A Horiba Scientific FluoroMax-4 Spectrofluorometer was used to collect fluorescence spectra. An excitation wavelength of 340 nm was chosen to monitor the fluorescence of the monohydroxy terephthalate groups, with an emission spectrum collected between 350 to 550 nm. The excitation and emission light slit widths were set to 1 and 2 nm and the samples were orientated 5° to the excitation beam. Three spectra were recorded for each sample and an average was taken.

2.7 Ultraviolet-visible-near infrared spectroscopy

2.7.1 Theory

Ultraviolet-visible-near infrared spectroscopy (UV-Vis-NIR) covers the wavelength range 200-2500 nm and is typically divided into three ranges; UV, 200-400 nm; Vis, 400-800 nm and NIR, 800-2500 nm. Electronic transitions are usually investigated in the UV-Vis region, while overtones and combination bands of vibrational transitions are found in the NIR region.[19]

UV-vis-NIR has various applications including measurement of absorption edge and band gaps, reflectance measurements on pigmented surfaces and characterisation and performance assessment for control films used in photovoltaics.

2.7.2 Experimental conditions

UV-Vis-NIR measurements were conducted at Agilent, Germany by Jan Wuelfken. An Agilent Cary 5000 UV-Vis-NIR Spectrophotometer was used. The scan range used was 250 to 2500 nm and the specular and diffuse reflection was collected. The parameters used are given in *Table 2*.

Table 2: Parameters used for UV-Vis NIR analysis.

Parameter	UV-Vis	NIR
Average time	0.1 s	0.1 s
Data interval	1.0 nm	4.0 nm
Scan rate	600 nm min^{-1}	2400 nm min^{-1}
Spectral Band Width	4.0 nm	4.0 nm
Energy level	1.0	3.0

2.8 Contact Angle

2.8.1 Theory

The angle between the intersection of the liquid-solid interface and the liquid-vapor interface when a liquid drop is placed on a solid surface is known as the contact angle (θ). This is shown in the illustration in *Figure 2.17*. The contact angle can be used as a measure of the wettability of a solid by a liquid.

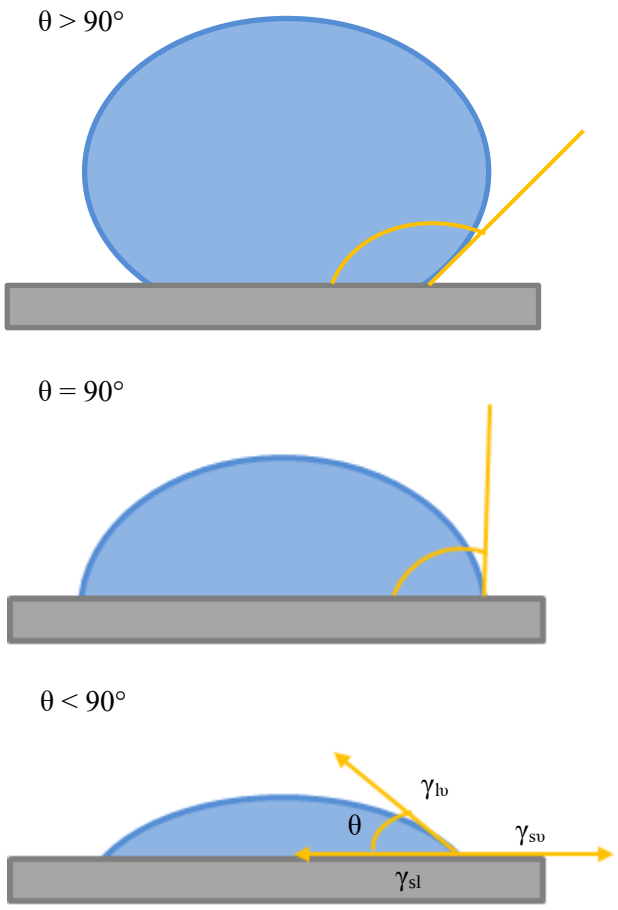

Figure 2.17: Illustration of different contact angles formed using the sessile drop method on a solid surface.

The surface tension of the liquid used determines the shape of the liquid droplet. In the bulk of the liquid droplet there is a net force of zero due to each molecule being

pulled equally in every direction by neighbouring molecules. Whereas, on the surface of the liquid droplet there are not neighbouring molecules in all directions. This means that an internal pressure is created due to the surface molecules being pulled inward. A reduction in surface area by intermolecular forces allows the liquid droplet to sustain the lowest surface free energy and is known as the surface tension.

The contact angle of a liquid droplet on a solid surface is defined by the mechanical equilibrium of the droplet under the action of three interfacial tensions. This equilibrium relation is known as Young's equation, as given in *Equation 11*.

$$\gamma_{lv} \cos \theta_{\gamma} = \gamma_{sv} + \gamma_{sl} \qquad \textbf{Equation 11}$$

Where θ_{γ} is Young's contact angle and γ_{lv}, γ_{sv} and γ_{sl} represent the liquid-vapor, solid-vapor, and solid-liquid interfacial tensions, respectively.

These three thermodynamic parameters; γ_{lv}, γ_{sv} and γ_{sl}, determine a single, unique contact angle θ_{γ}. However, contact angle phenomena are complex as several metastable states of a liquid droplet on a solid surface exist. This means that the experimental contact angle values are not usually equal to θ_{γ}.

The dynamic contact angle is the contact angle formed by expanding (advancing angle θ_a) and contracting (receding angle θ_r). The difference between these two angles is equal to the contact angle hysteresis (H), as shown by *Equation 12*.

$$H = \theta_a - \theta_r \qquad \textbf{Equation 12}$$

Contact angle hysteresis is thought to arise due to surface roughness and heterogeneity of the solid surface. Contact angle values are larger on chemically identical rough surfaces compared to smooth surfaces. Contact angles measured on rough or heterogeneous surfaces would not solely reflect surface energies as surface topography would now need to be considered. Therefore, using Young's equation for such contact angle measurements can be misleading as the equation does not consider surface topography.[20,21]

2.8.2 Experimental conditions

A Kruss Drop Shape Analyser DSA25 was used to conduct contact angle measurements. Measurements were carried out in triplicate. The Sessile Drop Technique was used for contact angle measurements with a probe liquid of water, a droplet volume of 1 µL and a resolution of 0.1°.

2.9 Scanning Electron Microscopy

2.9.1 Theory

In 1935 Knoll developed the first electron beam scanner capable of taking an image of the surface of a sample. Scanning Electron Microscope (SEM) is a type of electron microscope that scans the surface of a sample with a focused beam of electrons to produce an image.

Specimens for SEM analysis must be electrically conductive as non-conductive materials tend to charge, which causes scanning faults and image artefacts. Samples that are non-conductive must be coated with a thin layer of electrically conducting material, deposited on the film using a sputter coater. This prevents charging as electrons now have a path to ground. After samples have been coated with an electrically conducting material they are mounted on a specimen stub and placed in the specimen chamber.[22]

The main components of the SEM include a source of electrons, a column (which electrons travel down), electron detector and a sample chamber. The electron gun generates a beam of energetic electrons down the column and focuses on a spot on the specimen surface. The beam can be adjusted to control the magnification. Energetic electrons are released from the surface when incident electrons meet the sample. From the scatter patterns made by this interaction, information on size, shape, and composition of the sample can be obtained. Although there are many detectors available that can be used to attract distinct types of scattered electrons, secondary electrons are the most commonly used signal. *Figure 2.18* gives an illustration of the signals generated from a sample by incident electrons. SEM instruments produce three-dimensional, black and white images with an image magnification of up to 10 nm.[23]

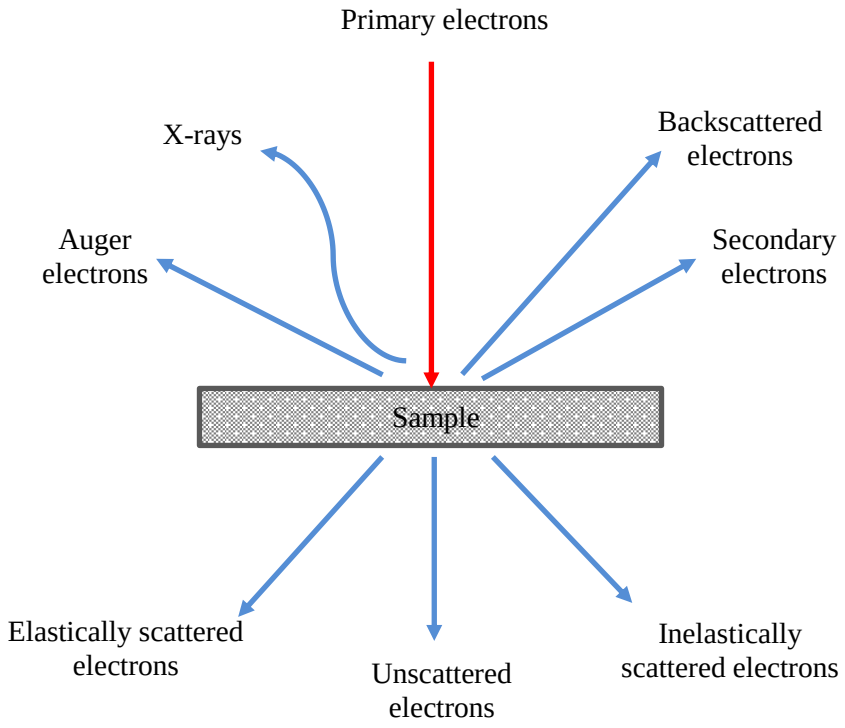

Figure 2.18: Illustration of types of signals generated by the interaction of electron beam with a specimen.

Some advantages of SEM include its wide range of applications, the detailed 3D, and topographical images, and the fact that most SEM samples require only minimal preparation. However, there are disadvantages which include samples being limited to solid samples that can handle vacuum pressure and small enough to fit inside the chamber, as well as preparation of samples usually resulting in the presence of artefacts.

2.9.2 Experimental conditions

SEM was carried out on a Cambridge Scanning Electron Microscopy Stereo scan 90. The film samples were covered with a thin layer of conductive material, in this case, silver, using a sputter coater. The sample size was 10 by 10 mm.

2.10 Calculation of errors

Error bars were calculated for the change in the area of the carbonyl peaks and peaks between 3800-2100 cm^{-1} from the ATR and DRIFT spectra. Depending on the size of the sample three or four spectra were taken during each analysis. Firstly, the spectra were baseline corrected and normalised, to the peak at 1410 cm^{-1}. The area between 3750-2160 cm^{-1} and 1880-1525 cm^{-1} were then determined from the ATR spectra and the areas between 3750-2160 cm^{-1} and 1880-1595 cm^{-1} were determined from the DRIFT spectra, for each spectrum.

The standard deviation was calculated using *Equation 13*.

$$\sigma = \sqrt{\frac{\Sigma\,(x - \bar{x})^2}{n - 1}} \qquad \textbf{Equation 13}$$

Where Σ means the sum of, x is a value in the data set, $\bar{x}$ is the mean of the data set and n is the number of data points in the set.

The standard deviation values were then used in the subtraction error equation in *Equation 14*.

$$Subtraction\ error = \sqrt{(\Delta a^2 + \Delta b^2)} \qquad \textbf{Equation 14}$$

Where Δa is the standard deviation of the exposed samples and Δb is the standard deviation of the control sample.

An example of the calculation is given for the spectra taken for the 36 µm PET sample exposed to 302 nm light for 48 hours. The standard deviation of the four areas of the carbonyl peaks is determined, followed by the error in the subtraction calculation:

$$\sigma = \sqrt{\frac{\Sigma\,(x - \bar{x})^2}{n-1}}$$

$$\sigma = \sqrt{\frac{\Sigma\,((197.93 - 198.37)^2 + (197.85 - 198.37)^2 + (200.02 - 198.37)^2 + (197.69 - 198.37)^2)}{4-1}}$$

$$\sigma = \sqrt{\frac{(0.19 + 0.28 + 2.72 + 0.47)}{3}} = \sqrt{\frac{3.66}{3}}$$

$$\sigma = 1.10$$

$$Subtraction\ error = \sqrt{(\Delta a^2 + \Delta b^2)}$$

$$Subtraction\ error = \sqrt{((1.10)^2 + (0.23)^2)}$$

$$Subtraction\ error = 1.13$$

This means that the change in the area of the carbonyl peak at 48 hours is 35.82 ± 1.13.

Error bars were also calculated for the crystallinity of the samples using the ATR FT-IR spectra using *Equation 15*.

$$Division\ error = \sqrt{\frac{a}{b}\left(\frac{\Delta a}{a}\right)^2 + \left(\frac{\Delta b}{b}\right)^2} \qquad \textbf{Equation 15}$$

For UV-visible and fluorescence data the subtraction error (*Equation 14*) was calculated, and errors bars were added to the plots of change in absorbance vs. dosage. The standard deviation (*Equation 13*) was calculated for the contact angle values and errors bars were added to the plots of contact angle vs. dosage.

2.11 References

1 Atlas Material Testing Solutions, *Weather. Test. Guideb.*, 2001, 108.

2 http://uvp.com/spectralcharts.html; Accessed March 2018

3 T. Theophanides, Ed., *Infrared Spectroscopy - Materials Science, Engineering and Technology*, InTech, 2012.

4 P. Atkins and J. de Paula, *Elements of Physical Chemistry*, Oxford University Press, Fourth Ed., 2005.

5 N. B. Colthup, L. H. Daly and S. E. Wiberley, *Introduction to Infrared and Raman Spectroscopy*, Academic Press, Third Edition., 2009.

6 Royal Society of Chemistry, *Org. Spectrosc.*, 2005, 52–106.

7 PIKE TECHNOLOGIES, *ATR - Theory and Applications*, 2011.

8 K. L. A. Chan and S. G. Kazarian, *Analyst*, 2013, **138**, 1029–1036.

9 S. G. Kazarian and K. L. A. Chan, *Analyst*, 2013, **138**, 1940–51.

10 S. R. Padibjo and I. M. Ward, 1983, **24**, 1103–1112.

11 PIKE TECHNOLOGIES, *Diffuse Reflectance – Theory and Applications*, 2011.

12 B. Stuart, *Polymer Analysis*, John Wiley and Sons, Ltd, 2003.

13 P. J. Haines, *Principles of Thermal Analysis and Calorimetry*, The Royal Society of Chemistry, 2002.

14 The Royal Society of Chemistry, *Mod. Chem. Tech.*, 92–115.

15 H. H. Jaffe and A. L. Miller, *J.Chem.Educ.*, 1966, **43**, 469–473.

16 P. Atkins and Julio de Paula, *Elements of Physical Chemistry*, Oxford University Press, Ninth Ed., 2010.

17 S. S. Fernando, P. a. Christensen, T. a. Egerton, R. Eveson, S. M. Martins-Franchetti, D. Voisin and J. R. White, *Mater. Sci. Technol.*, 2009, **25**, 549–555.

18 A. D. Hammerich, *Electronic Spectroscopy*, 2013.

19 R. A. Schoonheydt, *Chem. Soc. Rev.*, 2010, **39**, 5051.

20 A. B. D. Cassie and S. Baxter, *Trans. Faraday Soc.*, 1944, **40**, 546–551.

21 R. N. Wenzel, *Ind. Eng. Chem.*, 1936, **28**, 988–994.

22 J. Jerosch and R. Reichelt, *Biomed. Tech. (Berl).*, 1997, **42**, 358–362.

23 J. M. G. Cowie, *Polymers: Chemistry & Physics of Modern Materials*, CRC Press, Third Edition., 2007.

3 Fundamental photodegradation studies of PET

Chapter three explores the photodegradation reactions occurring when PET is exposed to broad wavelength ranges of light and narrow ranges under oxidative and non-oxidative conditions. As well as single films, stacks of films were analysed after exposure to investigate whether these could be used to study the depth profile of a single film of the same thickness, during photodegradation.

Irradiations were performed using UVP XX-series bench lamps of wavelengths 302 nm and 365 nm and a Hönle Cube 100 UV lamp of wavelength 365 nm. A weatherometer was also used to expose samples to a broad wavelength range of light, replicating outdoor exposure, between 290-800 nm. After exposure, the extent of degradation was analysed using ATR FT-IR, DRIFT, UV-visible spectroscopy, fluorescence spectroscopy, DSC, contact angle, and SEM. The instrumentation and analysis techniques used in this study have been discussed fully in *Chapter 2*.

3.1 Characterisation of PET film

The PET films investigated in this study were 12, 23 and 36 µm Melinex type S and were supplied by DuPont Teijin Films®. The films contain 0.2 wt% china clay and no UV stabilisers. The films were characterised using ATR FT-IR, DRIFT, UV-visible spectroscopy, fluorescence spectroscopy, DSC and contact angle.

The ATR and DRIFT spectra for a 36 µm control PET film are shown in *Figure 3.01 (a) and (b).* The band assignments for the peaks in these spectra are given in *Table 1*.

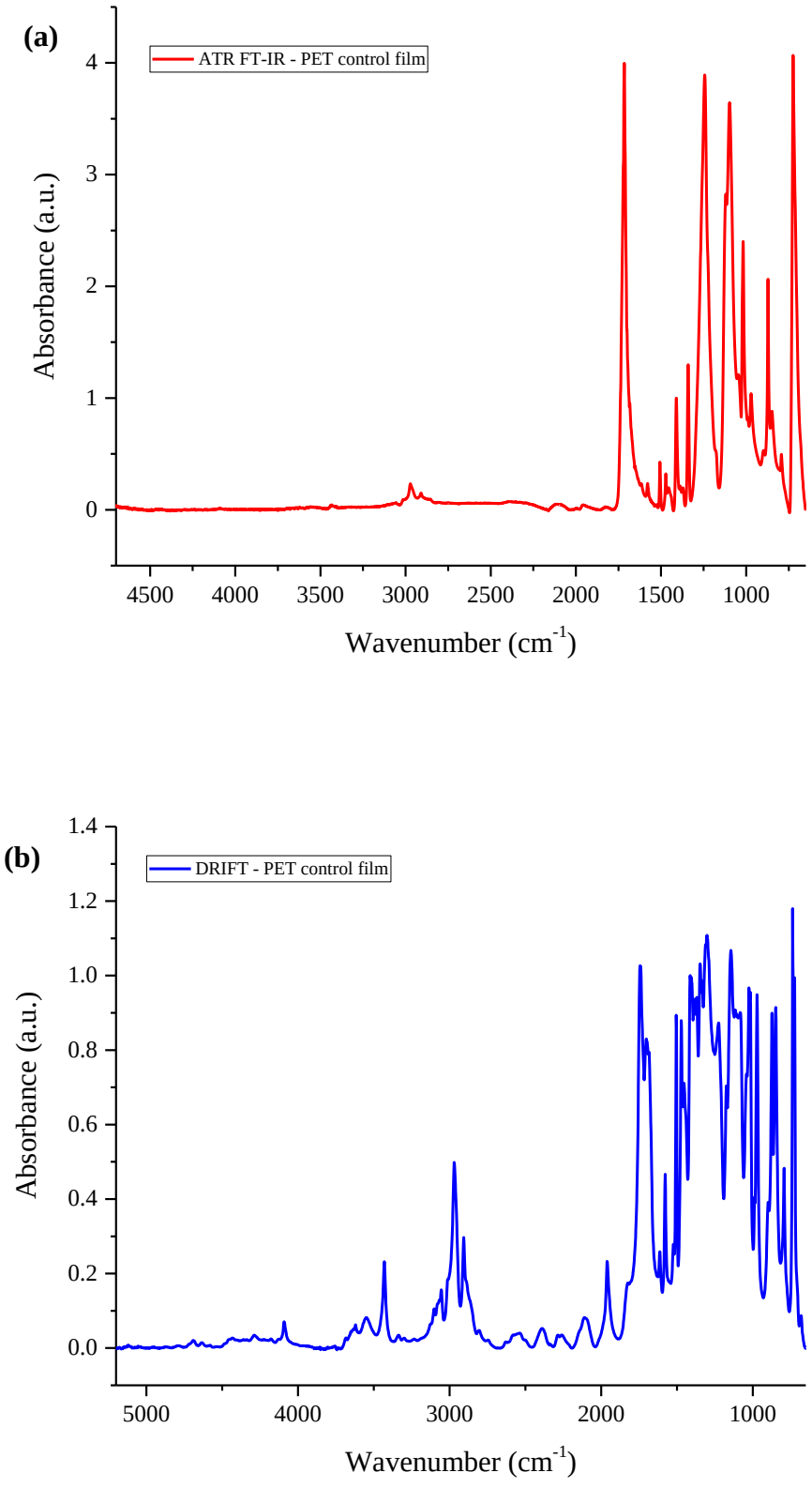

Figure 3.01: (a) ATR FT-IR and (b) DRIFT spectra of 36 µm PET film (surface *vs* bulk).

Table 1: Band assignments for the ATR FT-IR and DRIFT spectra of 36 µm PET control film.

Wavenumber (cm^{-1})		Assignment
ATR FT-IR	**DRIFT**	
3630	3625	Aqueous O-H stretching vibration[1]
3550	3540	Alcoholic O-H stretching vibration[1]
3430	3430	First overtone of the carbonyl peak[1]
3100-3060	3100, 3078, 3067, 3054	Aromatic C-H stretching[1]
3016, 2970, 2909	3015, 2970, 2908	Crystalline aliphatic CH_2 stretching[2]
2965, 2855	2963, 2855	Amorphous aliphatic CH_2 stretching[2]
1722, 1714	1743, 1731	Amorphous and crystalline carbonyl stretching[2]
1652	1654	Interaction between the hydroxy and the unsaturated ester carbonyl[3]
1578, 1506	1577, 1505	Amorphous and crystalline ring stretching[2]
1472, 1454	1470, 1453	Crystalline and amorphous glycol CH_2 bending[2]
1409	1411	Aromatic skeletal stretching[2]
1370, 1341	1370, 1345	Amorphous and crystalline glycol CH_2 wagging[2]
1244	1225	Ester group stretching[2]
1175, 1120	1173, 1115	Indicative of aromatic 1, 4-substitution pattern[2]
1097	1090	C-O stretching vibration from saturated aliphatic esters[2]
1044	1042	Amorphous CH_2 deformation[2]
1023, 1017	1025, 1017	Crystalline and amorphous in plane stretching of C-H bond[2]
989	988	O-CH_2 stretching of ethylene glycol segment[2]
970	970	Stretching of C-H bond of the trans isomer of the ethylene glycol unit.[2]
898	897	Stretching of C-H bond of the cis isomer of the ethylene glycol unit.[2]
848	849	C-H deformation of two adjacent hydrogens on the terephthalic ring[4]
870	873	Isolated hydrogen on aromatic ring[4]

The UV-visible spectrum of a 36 µm PET control film is given in *Figure 3.02*. This shows that longer wavelengths (315-400 nm) are absorbed weakly whereas shorter wavelengths (300-315 nm) are absorbed strongly, which has been reported previously.[5,6] This absorbance is due to the n – π* transitions from the ester carbonyl chromophoric groups, present in polyesters.[7]

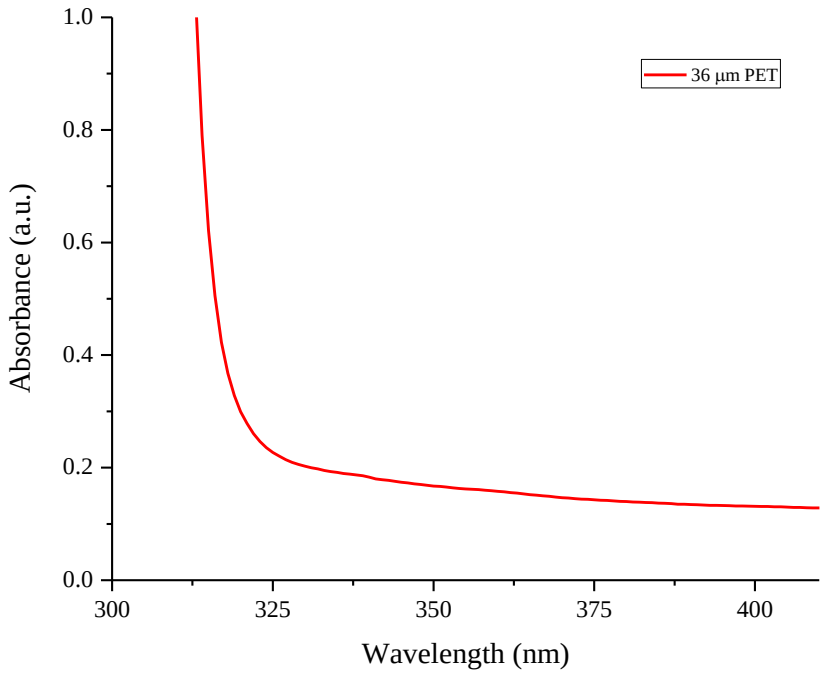

Figure 3.02: UV-visible spectrum of 36 µm PET film between 300-410 nm.

Figure 3.03 shows the fluorescence emission spectrum for a control sample of 36 µm PET film, with peaks at 370, 385 and 410 nm. The excitation wavelength used was 340 nm. The peak at 370 nm has been assigned to an excimer and peaks at 385 and 410 nm have been assigned to the presence of a ground state dimer.[8]

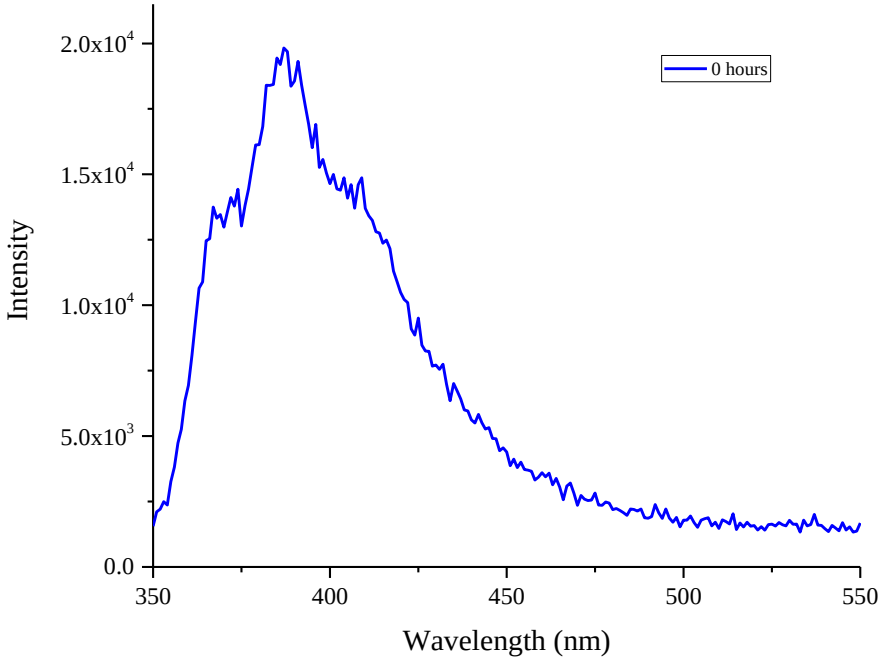

Figure 3.03: Fluorescence emission spectrum of 36 µm PET film between 350-550 nm, with an excitation wavelength of 340 nm.

Figure 3.04 shows the DSC thermogram for a control sample of 36 µm PET film. The thermogram shows a melt endotherm with a maximum of 255°C on the first heating cycle and a crystallisation peak on the cooling cycle with a maximum of 209°C. During the second heating cycle, two melting endotherms occur at 247°C and 254°C corresponding to two different crystalline forms of the polymer.

Table 2 shows the melting and crystallisation temperatures, with corresponding ΔH values for control samples of 23 and 36 µm PET films. All samples were analysed under nitrogen at a ramp rate of 10 $^{\circ}$C min^{-1}.

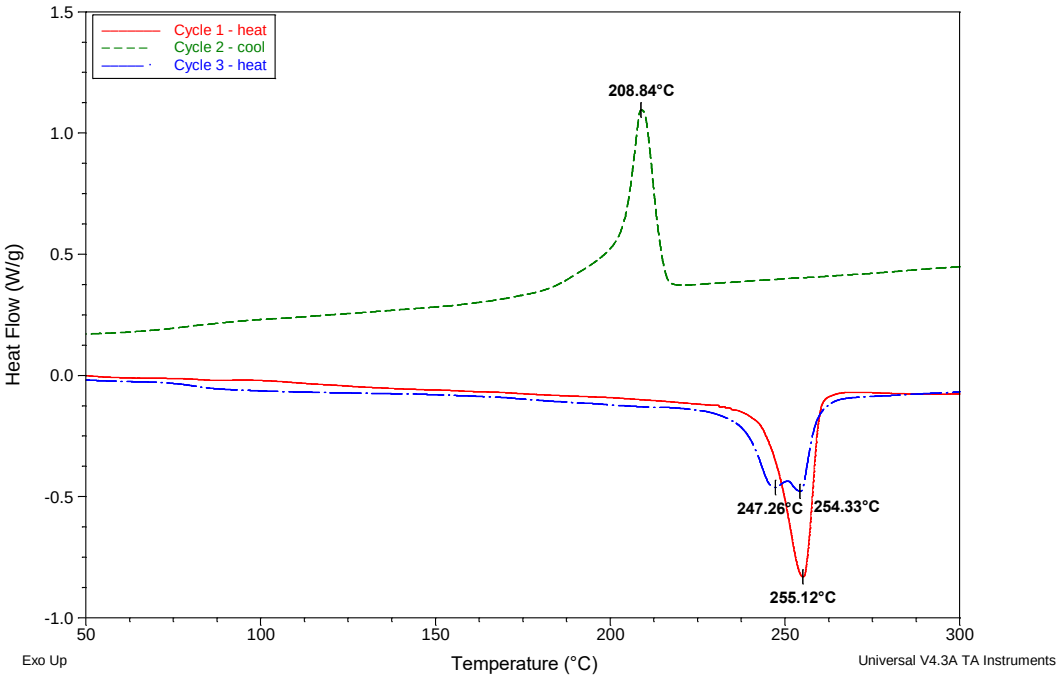

Figure 3.04: DSC thermogram of the heat-cool-heat cycle for 36 µm PET film.

Table 2: Melt and crystallisation temperatures and corresponding ΔH values.

Thickness (µm)	Cycle 1		Cycle 2		Cycle 3	
	T_m	ΔH	T_c	ΔH	T_m	ΔH
23	255	65	203	48	254	64
	255	62	201	47	254	60
36	255	65	208	52	254	61
	255	63	209	51	254	58

Contact angle measurements were carried out in triplicate on four separate 36 µm PET control films. From these twelve values the average was calculated to be 86.90 ± 2.76 for the 36 µm films. The same experiment was undertaken for the 23 µm PET control films and the average was calculated to be 76.36 ± 1.88. *Figure 3.05* shows the twelve

contact angle values for the 23 and 36 µm PET control films. A high contact angle value indicates that the films have a hydrophobic surface.

The average contact angle values of 23 and 36 µm PET film differ by approximately 11°. The effect of film thickness on the contact angle has been studied by Li *et al.* The authors reported that the contact angle value decreased with decreasing film thickness, but this was only true for samples with a thickness equal too, or less than 0.05 µm.[9] Therefore, it is believed that the thickness of the films does not affect the contact angle values, shown in *Figure 3.05*. It is thought that this difference is due to heterogeneity of the surface or surface roughness; contact angle values measured on a rough surface would be larger compared to a smooth surface.[10] This will be discussed fully in *Section 3.3.6*.

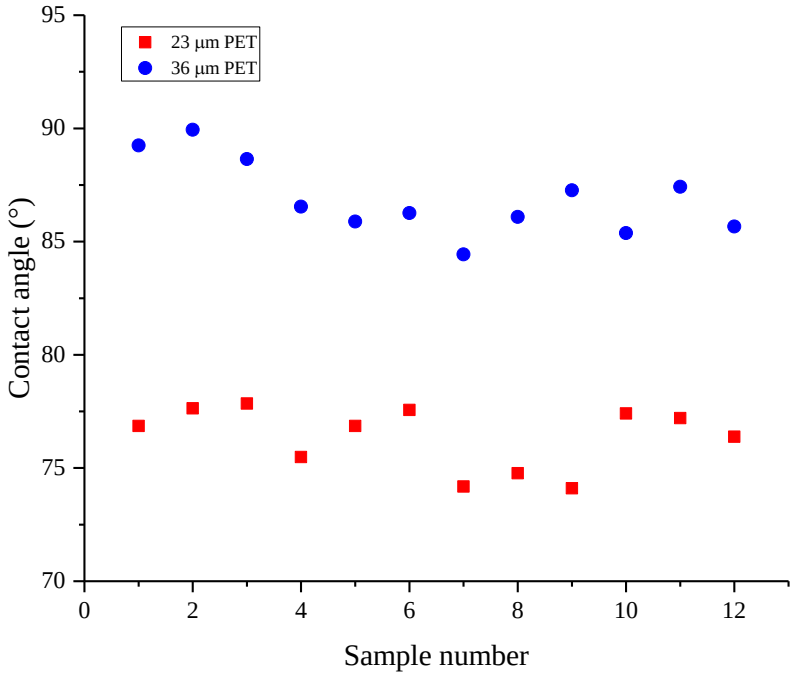

Figure 3.05: Contact angle measurements of 23 and 36 µm films.

3.2 Stacked films

This study uses stacks of 12, 23 and 36 µm PET films to understand if a stack of films degrades in the same way as a single film of the same thickness, when exposed to UV light. If these samples were to degrade in the same way this would mean that a stack of thin films could be used to study the depth profile of a thicker single film during photodegradation. For example, if a single 36 µm film degrades in the same way as a stack of three 12 µm films, then stacks of films could be used for depth profiling of thicker films.

3.2.1 Intensity Measurements

An intensity meter was used to measure the intensity of the 302 nm and 365 nm UV lamps. The intensity meter was placed the same distance from the lamp as the PET samples during exposure. A zero point was established, and stacks of film were then placed on the meter, which allowed the absorbance to be calculated. *Figure 3.06* shows the intensity measured through stacks of 12, 23 and 36 µm PET films.

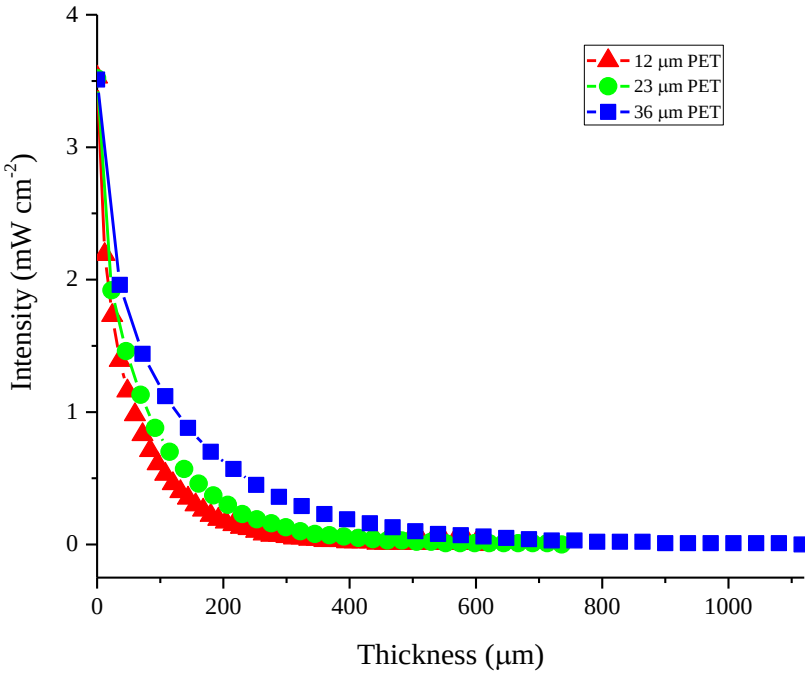

Figure 3.06: Measured intensity vs. thickness of stack for all thicknesses of film under 302 nm light.

As expected, fewer 36 µm films were needed than 12 µm film to reach the same value of intensity. Interestingly, whilst a 3 x 12 µm stack may have been expected to be the same as a single 36 µm film, this is not the case. This indicates that scattering is occurring between the layers of the stacks.

Figure 3.06 shows that the intensity of the transmitted light through the 12 µm films is lower at any given thickness than the 36 µm films. For example, the intensity value through three pieces of 12 µm film is lower than through one piece of 36 µm film. This is due to additional layers being present in the 12 µm stack; therefore, more scattering occurs due to a higher number of interfaces.

Table 3: Absorbance values for 12, 23 and 36 µm PET films under 302 nm light.

No. of films	Absorbance of 12 µm	Absorbance of 23 µm	Absorbance of 36 µm
1	0.207	0.263	0.253
2	0.310	0.382	0.387
3	0.405	0.493	0.496
4	0.483	0.602	0.600
5	0.557	0.701	0.700

The data presented in *Table 3* shows that a single piece of 12 µm film absorbed the least light. This was expected as the thinnest film in the study should absorb the least, however, absorbance was expected to scale with thickness, but this was not the case. For example, the table shows that one piece of 36 µm film did not absorb three times as much as a single piece of 12 µm film.

None of the absorbances for the single or stacks of film scale with thickness. This could be because the intensity meter used to obtain this data measures a broad spectrum of UV radiation, not single wavelengths of light. The Beer-Lambert Law, given in *Chapter 2 Equation 9*, shows that there should be a linear relationship between intensity and thickness but this is only true for single wavelengths.[11] Therefore, as the

meter does not measure the intensity of a single wavelength of light the absorbance results are unreliable.

3.2.2 Scattering Model

Due to the complicated nature of measuring the scattered light, a scattering model was created at DuPont Teijin Films. Light Tools was used to create the model, assuming the PET was homogeneous with a constant refractive index of 1.54. The source output was set at 100 lumens. The light source spectral charts were provided for the creation of the model, shown in *Chapter 2, Figure 2.04*.

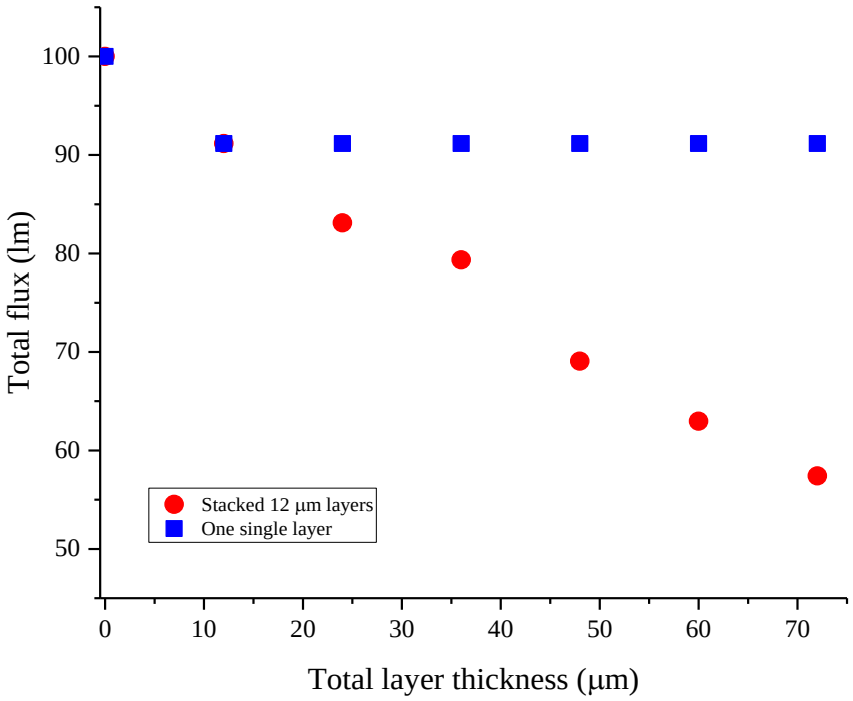

Figure 3.07: The total flux of stacked layers vs. single layers.

The model was created to investigate the behaviour of light incident upon PET film at a given thickness, made up of layers of 12 μm film versus one single layer of film. The model showed that each time light hits the interface of a piece of PET film only 91.165% of the light passes through the film, regardless of thickness. *Figure 3.07*

shows the total flux, in lumens, of stacked layers compared to single layers of film. These results show that the total flux for one single film does not change as the thickness of the film increases, whereas stacked layers of 12 µm film show a decrease in total flux as the number of film layers increases. This is shown schematically in *Figure 3.08.*

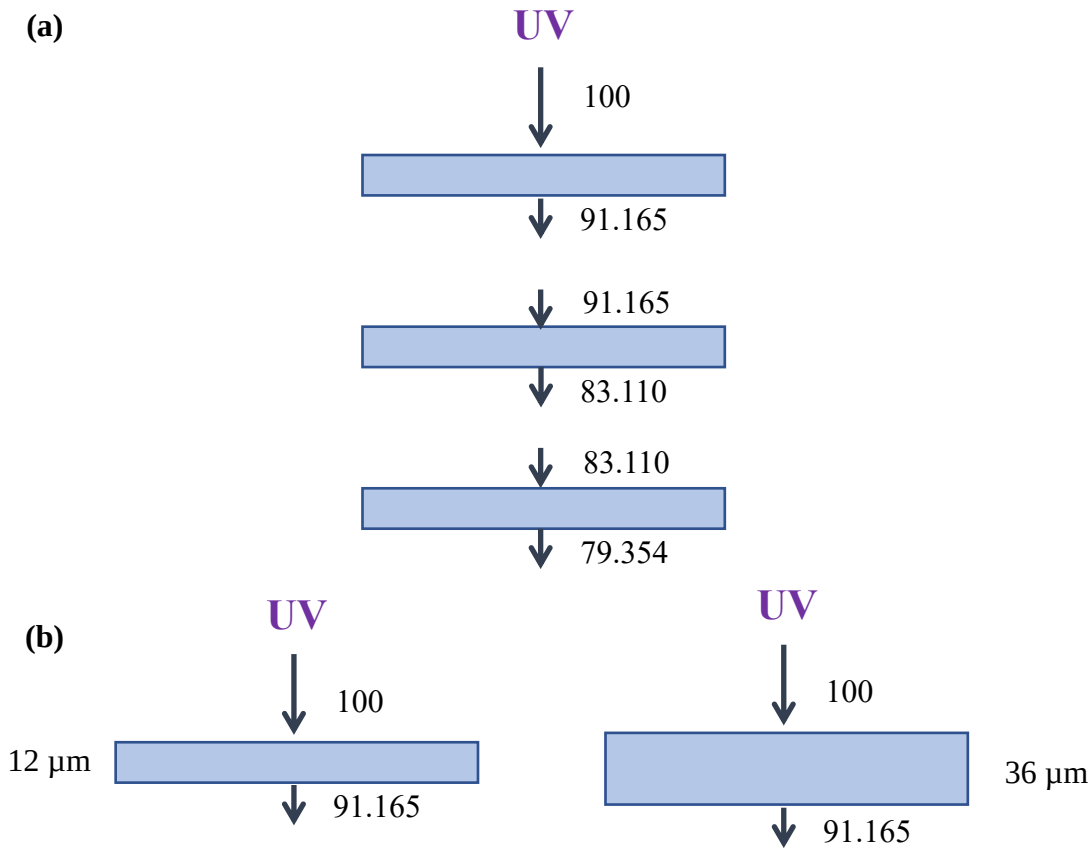

Figure 3.08: Illustration of light passing through (a) a stack of films and (b) a single piece of 12 and 36 µm film.

The total flux does not change when the thickness of a single film is increased. The light hits the surface of the film and travels through in the same direction before exiting. This is because it is assumed, in the model, that the film has a constant refractive index and there are no filler particles present. Therefore, there is nothing to

change the direction of the light or cause it to scatter, resulting in the same result of 91.165 lumens at all modelled thicknesses.

The fact that the total flux decreases with increasing number of film layers can be explained by the physical laws of reflectivity. Each time light hits the film surfaces a certain amount of light is lost due to reflectivity. This happens at each interface in the stack of films which explains why the total flux decreases with increasing number of layers in the stack, as the number of interfaces has also increased.

The reflectivity can be calculated using the refractive index and incidence angle of the light. For normal incidence values, the percentage reflectivity can be calculated using the Fresnel equation, given in *Equation 1*.

$$R_0 = \left[\frac{n_1 - n_2}{n_1 + n_2}\right]^2 \qquad \textbf{Equation 1}$$

Where n_1 is the refractive index of air and n_2 is the refractive index of the material. In this case, the material studied is a PET film and has a refractive index of 1.54. From this, the reflectivity was calculated to be approximately 4.5%.

Tables 4 and 5 show the experimental results, the theoretical results according to the scattering model and the accuracy of the model's predictions for the 365 nm and 302 nm lamps, respectively. From analysing the results, it is apparent that the model predicts the intensity of light transmitted through a stack of 12 μm films better under 365 nm light than 302 nm light. PET has a strong absorption at 302 nm and only a weak absorption at 365 nm. The scattering model only accounts for scatter and not absorbance. This explains why the model is not as accurate for the 302 nm lamp, and why there is still some error in the 365 nm lamp results.

Therefore, it was thought that stacks of film would not degrade in the same way as a single film of the same thickness, due to scattering that takes place at each interface.

Table 4: Experimental values, model values and accuracy when modelled applied to 365 nm light.

	Experimental values ($mW\ cm^{-2}$)	Model results		Accuracy (%)
		In ($mW\ cm^{-2}$)	Out ($mW\ cm^{-2}$)	
Layer 1	3.56	3.56		94.29
	3.06		3.24546	
Layer 2		3.24546		89.57
	2.65		2.95871	
Layer 3		2.95871		86.01
	2.32		2.6973	
Layer 4		2.6973		82.96
	2.04		2.45899	
Layer 5		2.45899		79.85
	1.79		2.24173	

Table 5: Experimental values, model values and accuracy when modelled applied to 302 nm light.

	Experimental values ($mW\ cm^{-2}$)	Model results		Accuracy (%)
		In ($mW\ cm^{-2}$)	Out ($mW\ cm^{-2}$)	
Layer 1	3.53	3.53		68.05
	2.19		3.21811	
Layer 2		3.21811		58.97
	1.73		2.93378	
Layer 3		2.93378		51.97
	1.39		2.67457	
Layer 4		2.67457		47.57
	1.16		2.43827	
Layer 5		2.43827		44.09
	0.98		2.22284	

3.2.3 Conclusions

Intensity measurements and a scattering model have been used to evaluate if using stacks of thin films is a reliable way to study the depth profile of a single film of the same thickness, during degradation. Both studies showed that scattering was occurring at the interface of each layer in a stack of films. Therefore, a stack of films will not degrade in the same way as a single film of the same thickness. Consequently, stacks of thin films were not used to study the depth profile of thicker films.

3.3 Weatherometer irradiations

Samples of 23 and 36 µm PET films were irradiated in an Atlas Suntest XLS+ Weatherometer at a set irradiance of (365 ± 35) W m^{-2}, measured between 290-800 nm, and a temperature of (37.5 ± 2.5)°C. The weatherometer was used to simulate outdoor exposure.

Samples were placed in the weatherometer for 10 weeks (equivalent to a dosage of approximately 6.1 x 10^5 W m^{-2} hr^{-1}) and analysed every week (equivalent to a dosage of approximately 6.1 x 10^4 W m^{-2} hr^{-1}) using ATR FT-IR, DRIFT, UV-visible spectroscopy, fluorescence spectroscopy, DSC, contact angle and SEM.

3.3.1 ATR FT-IR

Samples of 23 and 36 µm PET films were irradiated in the weatherometer for 10 weeks (equivalent to a dosage of approximately 6.1 x 10^5 W m^{-2} hr^{-1}) and analysed using ATR FT-IR every week (equivalent to a dosage of approximately 6.1 x 10^4 W m^{-2} hr^{-1}). One week of irradiation in the weatherometer is approximately 7.5 weeks outdoors; this has been previously calculated and is shown in *Chapter 2, Section 2.2.1*. *Figure 3.09* shows the ATR spectra for the front of the 36 µm PET films after every week of exposure. After only 1 week of exposure there are significant changes in the spectra, in the region from 3800-2100 cm^{-1}, as well as the carbonyl and fingerprint regions. The rear surface of the samples showed no notable change with exposure time.

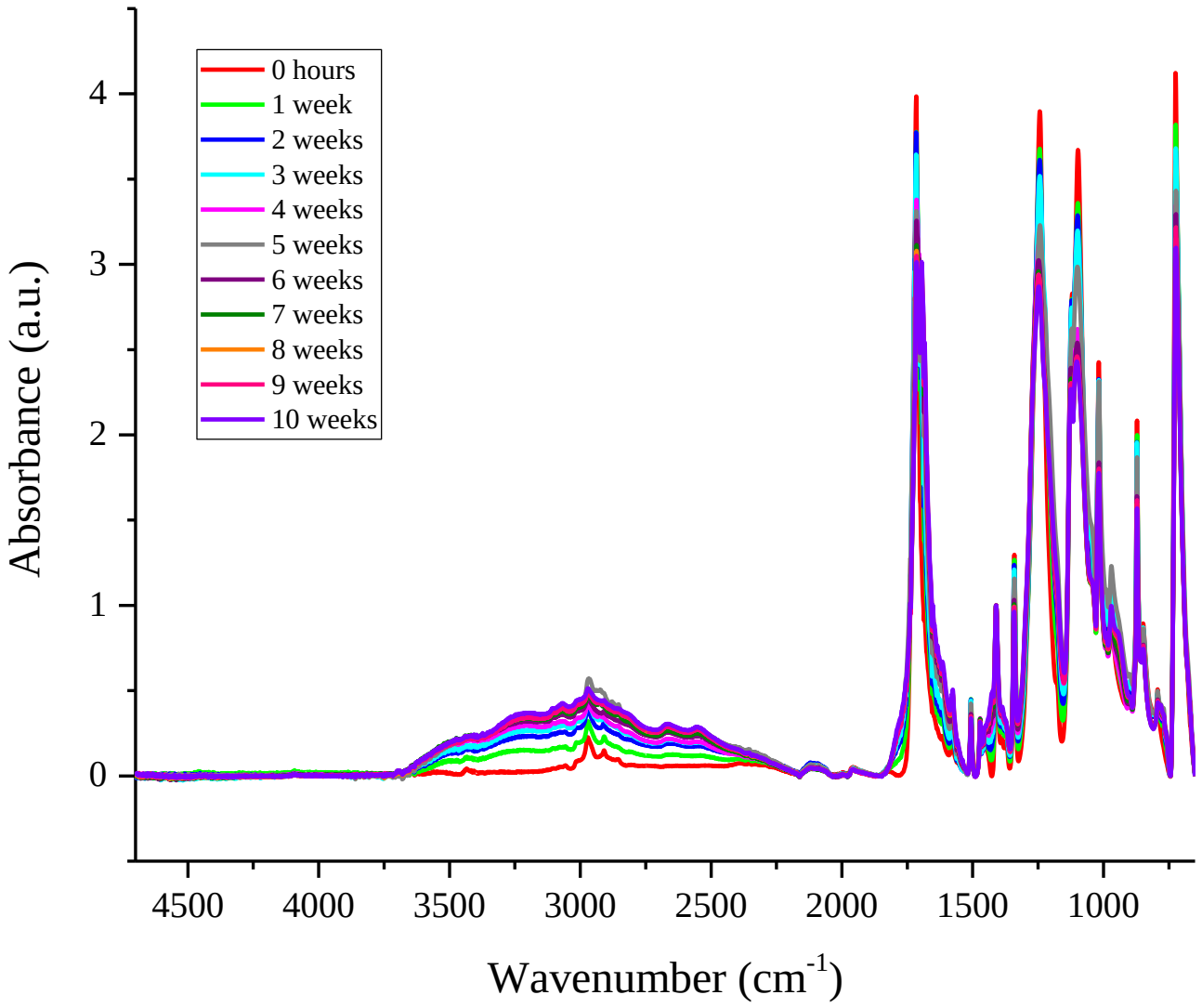

Figure 3.09: ATR FT-IR spectra of 36 µm PET films irradiated in the weatherometer for 10 weeks in 1 week increments.

Figure 3.10 shows the region from 3800-2100 cm^{-1} of the control spectra of 36 µm PET and after 10 weeks of irradiation in the weatherometer; equivalent of approximately a year and a half outdoors. The assignments for the peaks contained within this region are given in *Table 6*.

The peak at 3290 cm^{-1} has developed upon irradiation and has been assigned to the hydroxy of a carboxylic acid group. This indicates that carboxylic acid end groups are produced during exposure. A mechanistic pathway has been proposed by Fechine *et al.* for the formation of these groups, under oxidative conditions, shown in *Chapter 1, Figure 1.29*.[8] The concentration of these groups is now used as a way to indirectly measure the extent of degradation,[12–16] and they can act as a catalyst for additional degradation.[17]

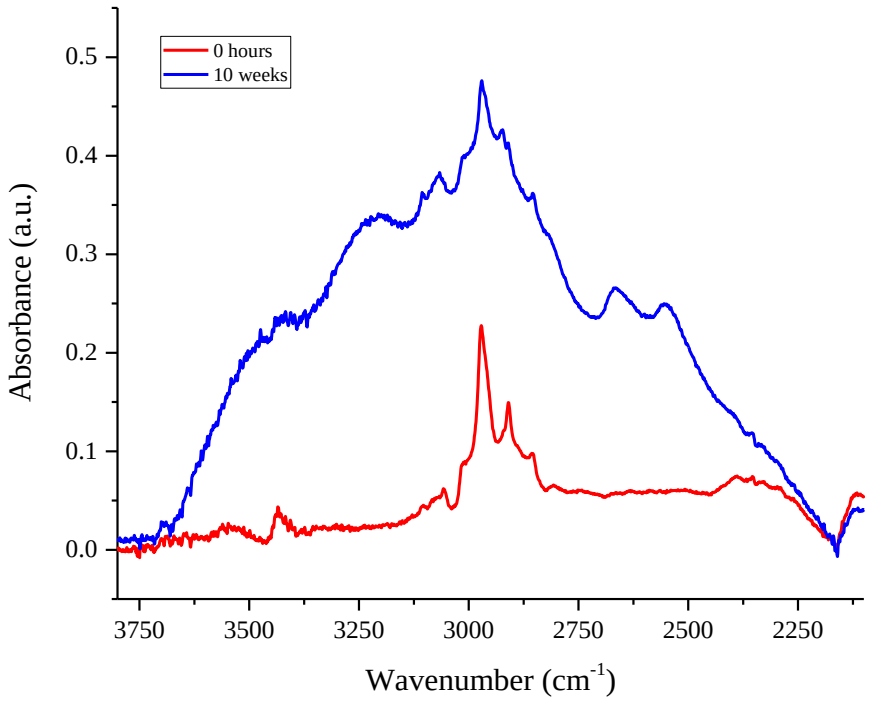

Figure 3.10: ATR FT-IR spectra of 36 µm PET, irradiated in the weatherometer, in the region between 3800-2100 cm^{-1}.

Table 6: Band assignments for the region between 3800-2100 cm^{-1} of the ATR FT-IR spectrum of PET.

Peak (cm^{-1})	Assignment
3630	Aqueous O-H stretching vibration[1]
3550	Alcoholic O-H stretching vibration[1]
3430	First overtone of the carbonyl peak[1]
3290	Carboxylic acid end groups[1]
3100 – 3060	Aromatic C-H stretching[2]
3016, 2970, 2909	Crystalline aliphatic CH_2 stretching[2]
2928	C-H symmetric stretching vibration associated with the Ar-CH_3 group.
2965, 2855	Amorphous aliphatic CH_2 stretching[2]
2640, 2540	Characteristic of the carboxylic acid dimer[18]

A further two peaks have developed upon irradiation at 2640 and 2540 cm^{-1} and are thought to be characteristic of the carboxylic acid dimer.[18] The formation of these groups has been reported in the literature when changes have been identified in the carbonyl peak.[19] It is believed that the peaks at 2640 and 2540 cm^{-1} have not yet been attributed to the dimer form of carboxylic acids in the photodegradation of PET materials.

From *Table 6*, the peaks between 3100 and 3060 cm^{-1} have been attributed to the stretching modes of the four aromatic C-H bonds of the terephthalate ring.[2] After exposure in the weatherometer there is an increase in absorbance and area of this group of peaks. This is thought to be due to the production of mono-substituted aromatic rings, thus resulting in another aromatic C-H bond on the terephthalate ring. Phenyl radicals have been reported to be produced during the photodegradation of PET.[13,20] These phenyl radicals can combine with a hydrogen radical to produce mono-substituted aromatic rings. The increase in absorbance of these peaks could also be due to the peaks being overlapped with the growing hydroxy.

Peaks assigned to the crystalline and amorphous aliphatic CH_2 stretching vibrations have decreased in height with exposure time. In particular, the amorphous peaks are

barely identifiable. It has been reported that the crystalline phase of polymers that do no undergo scission by direct absorption are less affected by degradation, due to this region being less permeable to oxygen. Thus, it has been concluded that initial degradation is limited to the amorphous phase. However, the ester carbonyl that is part of the main chain in PET can absorb UV light directly, causing bond breakage. Therefore, it has been suggested that chain scission may also take place within the crystalline phase.[5] This is in agreement with the reduction in the size of both the crystalline and amorphous CH_2 stretching peaks. It could also be the case that the apparent decrease in the size of these peaks is due to the peaks being overlapped with the growing hydroxy peak.

After exposure, a new peak at 2928 cm^{-1} has developed and has been assigned to the C-H symmetric stretching vibration associated with the Ar-CH_3 group. Stephenson *et al.* suggested a pathway for the photolysis of PET, as given in *Chapter 2, Figure 1.13*, which shows the production of phenyl and methyl radicals.[21] It is thought that these radicals could combine together to produce an Ar-CH_3 group, confirmed by the production of the peak at 2928 cm^{-1} during exposure.

Figure 3.11 shows the change in the carbonyl peak after irradiation in the weatherometer for 10 weeks. This is equivalent of approximately a year and a half outdoors. The various peaks contained within the carbonyl peak before and after exposure are given in *Table 7*.

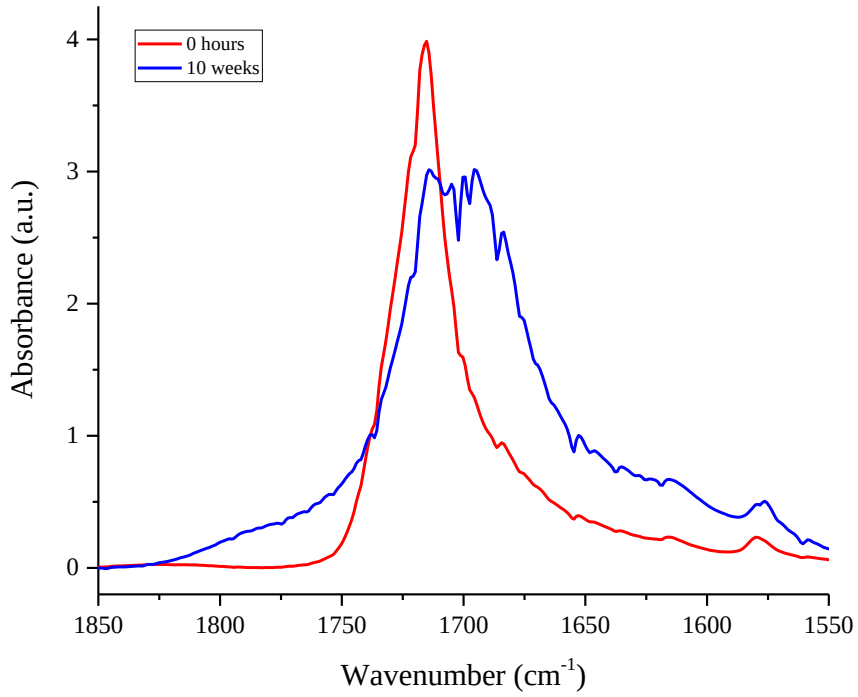

Figure 3.11: ATR FT-IR spectra of 36 µm PET, irradiated in the weatherometer, in the carbonyl region between 1850-1550 cm^{-1}.

Figure 3.11 shows that after exposure there is general broadening of the carbonyl peak, indicating the production of new carbonyl species. The broadening at longer wavenumbers is thought to be due to the formation of anhydride groups. Scheirs and Gardette reported the development of a peak assigned to anhydrides during the photo-oxidation of PEN but not PET, due to the differences in segmental mobility between the two polymers at the irradiation temperature. They explained that this would result in PEN having a lower molecular mobility which would inhibit the radicals from diffusing apart as PEN was irradiated below its T_g. This provides the environment for the pathway for anhydride production to occur.[22] However, it is proposed that anhydrides could be produced during the exposure of PET, in this study, as irradiations were performed at lower temperatures compared to the study reported by Scheirs and Gardette. This means that PET was irradiated below its T_g and therefore would inhibit radicals from diffusing apart and provide the environment for anhydride production.

Table 7: Band assignments for the carbonyl region of the ATR FT-IR spectrum of PET.

Peak (cm^{-1})	Assignment
1785	Carbonyl stretch from anhydride carbonyl[22,23]
1738	Carbonyl stretch from aliphatic aldehyde[24]
1722	Amorphous carbonyl stretch from ester[2]
1714	Crystalline carbonyl stretch from ester[2]
1705	Carbonyl stretch from carboxylic acid dimer[19,23,24]
1700	Carbonyl stretch from carboxylic acid end groups[26]
1695	Carbonyl stretch from quinone groups[27,28]
1685	Carbonyl stretch from terephthalic acid

At longer wavenumbers, there is also the development of another peak at 1738 cm^{-1} which has been assigned to the carbonyl stretch from an aliphatic aldehyde. Aldehydes have been reported to be produced during the photodegradation of PET.[29]

Peaks at 1722 and 1714 cm^{-1} assigned to the amorphous and crystalline carbonyl stretch from the ester group have shown a decrease in absorbance after exposure.[2] This was expected as chain scission occurs at the ester group during exposure and so the decrease in absorbance of these peaks indicates the breakdown of the ester.

Analysis of the carbonyl region also shows the development of additional peaks at 1705, 1700, 1695 and 1685 cm^{-1} attributed to the carboxylic acid dimer, end groups, quinone species and the terephthalic acid monomer. The increase in concentration of these groups after exposure has caused the broadening of the carbonyl at shorter wavenumbers.

A peak assigned to the dimer form of the carboxylic acid has been reported in the literature by Delprat *et al.* during the photodegradation of an ethylene-propylene copolymer,[19] but has not been described for PET materials. The production of carboxylic acid end groups has been reported by a number of authors and has been used as a way to measure the extent of degradation.[1,29,30] Fechine *et al.* has proposed a pathway for the production of these groups under oxidative conditions.[8]

The production of quinone groups has been identified using UV-visible spectroscopy and Fechine *et al.* have proposed mechanistic pathways for their production.[31,27] Edge *et al.* reported changes in IR spectra, of thermally degraded PET, which signify the production of aromatic ketones.[27] This could suggest the formation of quinone groups at 1695 cm^{-1}.

The peak at 1685 cm^{-1} has been assigned to the carbonyl stretch from terephthalic acid; the monomer unit used in the production of PET. A spectrum of terephthalic acid and irradiated PET were overlaid to identify this peak. The development of the peak at 1685 cm^{-1} indicates the breakdown of the polymer into its monomer units.

In this study, the extent of photodegradation, using ATR spectra, was measured by the change in area of the region between 3800-2100 cm^{-1} and the carbonyl peak, with dosage or exposure time. The area was taken for peaks between 3750 and 2160 cm^{-1} and the area of the carbonyl peak between 1880 and 1525 cm^{-1}.

Figure 3.12 (a) and (b) show the change in area of the region between 3800-2100 cm^{-1} and the carbonyl peak with dosage, for 23 and 36 µm PET film. Both graphs show a sharp increase initially, followed by a more moderate increase and some fluctuation in the change in area. This fluctuation is thought to be due to the fact that the intensity the film is exposed to, in the weatherometer, is dependant upon its position on the sample tray.

At the start of the exposure, the sharp increase is thought to be due to chain scission reactions of weak links. Wang *et al.* reported that the photodegradation process of PET takes place in two steps. Initially, a very rapid step occurs due to the number of scissions of weak links, followed by the degradation of normal links (weak links are more easily and readily broken than normal links). The author reported that the rate constants of degradation for weak links were higher than that for normal links, as the weak links are more easily broken.[32]

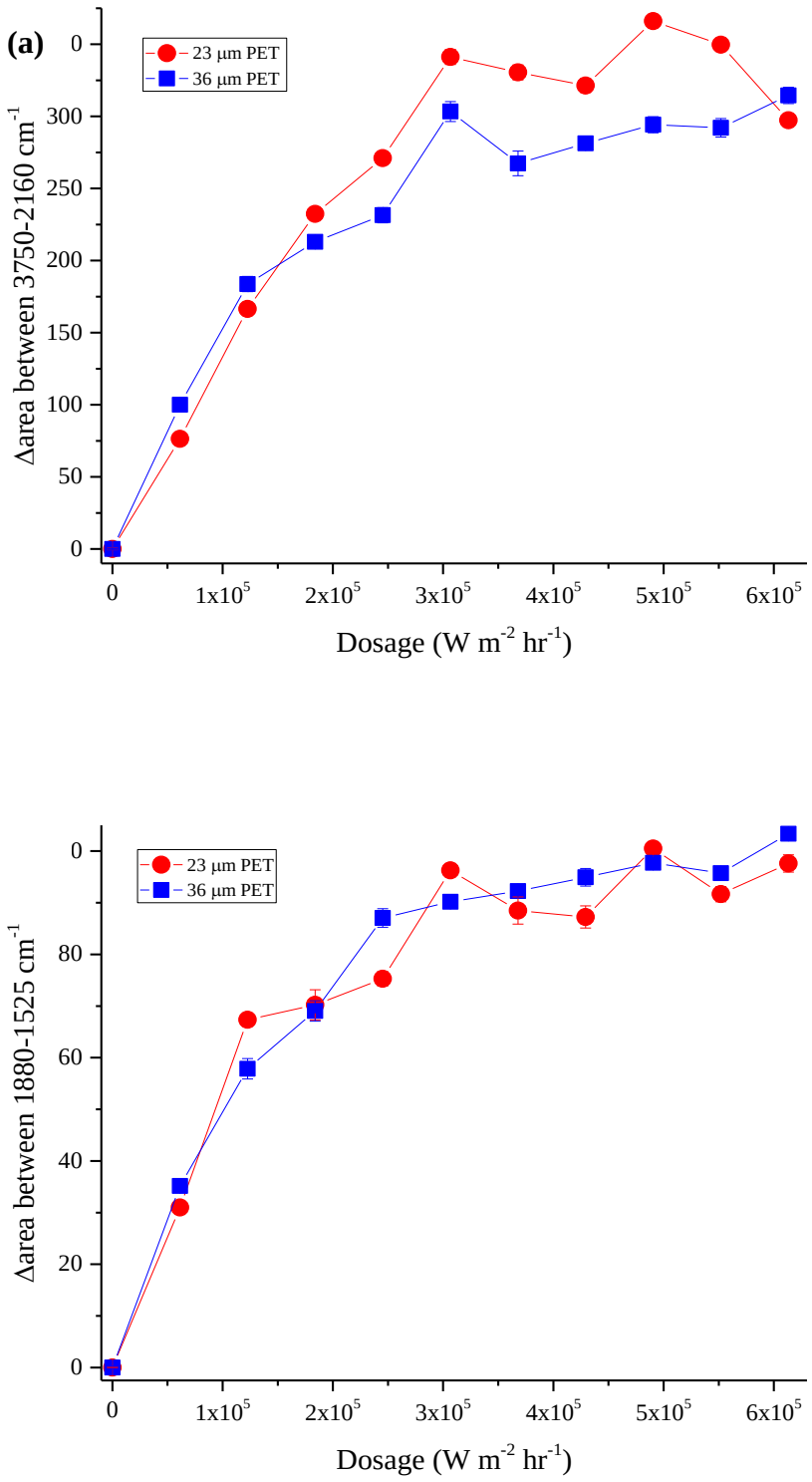

Figure 3.12: Extent of photodegradation of 23 and 36 µm PET measured by the change in area of peaks between (a) 3750-2160 cm^{-1} and (b) 1880-1525 cm^{-1}(carbonyl).

The weak links in this specific sample are believed to be the diethylene glycol segment. During thermal degradation, DEG is known to be a weak link in PET.[33] The photodegradation of DEG units has not been reported in the literature, however, the photodegradation of PDEGT homopolymer has been investigated in this study and will be discussed in detail in *Chapter 5*.

From analysing the extent of degradation graphs, shown in *Figure 3.12 (a) and (b)*, the results agree with those reported by Wang *et al*. This suggests that the PET film used in this study degrades through a two step process when exposed to light in the range 290-800 nm, replicating outdoor exposure.

Figure 3.13 shows the fingerprint region of a control and a film irradiated in the weatherometer for 10 weeks. Peaks that have changed or developed in the spectra after exposure have been assigned in *Table 8*.

Peaks at 1430 and 1220 cm^{-1} have been assigned to the combination band due to C-O stretching and O-H deformation and C-O stretching, respectively. These peaks are associated with the carboxylic dimer and have developed upon exposure. As far as is known these peaks have not yet been reported in the literature.

Figure 3.13 shows a reduction in the size of the peaks at 970 and 898 cm^{-1}, assigned to the trans and cis isomer of the C-H stretching of the ethylene glycol unit, respectively.[2] The reductions are related to the scission of ester links in the polymer chain during photodegradation of PET.

A peak at 940 cm^{-1} has developed during exposure in the weatherometer and has been assigned to the C-H vibration associated with vinyl groups.[34] Grassie and Scott proposed a pathway for an alternative chain scission reaction producing vinyl groups. This pathway is shown in *Chapter 1*, *Figure 1.21*.

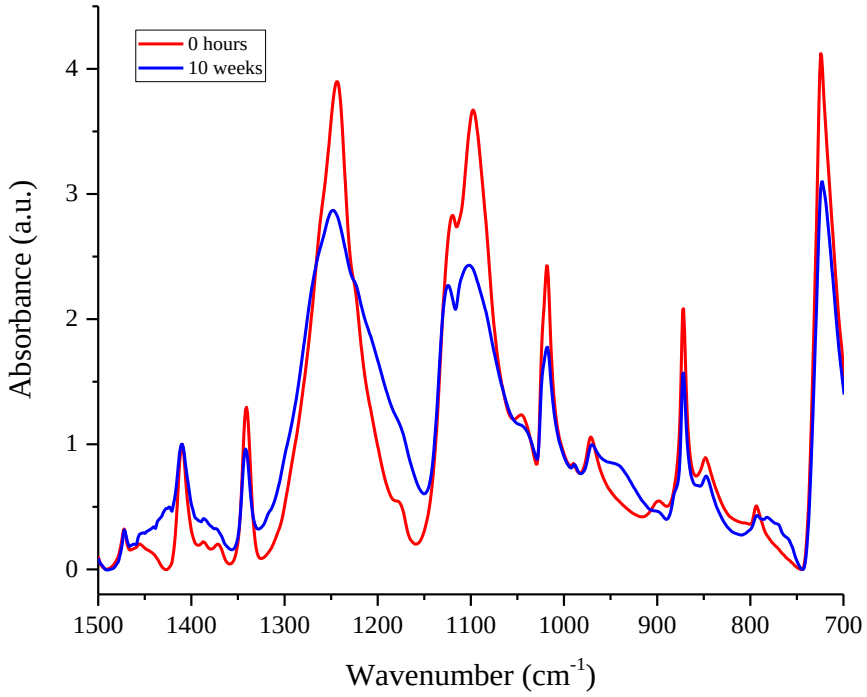

Figure 3.13: ATR FT-IR spectra of 36 µm PET, irradiated in the weatherometer, in the fingerprint region between 1500-650 cm^{-1}.

The region between 850-750 cm^{-1} is sensitive to changes in the substitution pattern of the terephthalic ring. After exposure, there has been a change in the peak at 848 cm^{-1} and the development of peaks at 778, 769 and 758 cm^{-1}.

There is a minor reduction in the size of the peak at 848 cm^{-1} assigned to the C-H deformation of two adjacent hydrogens on the terephthalic ring, suggesting that substitution has occurred on the ring.[35,4] The development of peaks at 769 and 758 cm^{-1} assigned to the 1, 2, 3-substituted and 1, 2, 4-substituted rings further supports the suggestion that substitution has occurred on the terephthalic ring.

The evolution of the peak at 778 cm^{-1}, in *Figure 3.13*, has never been assigned in the literature, during the photodegradation of PET, but is thought to be due to mono-substituted rings. The phenyl radical produced during the photodegradation of PET, shown in *Chapter 1*, *Figure 1.26*, can abstract a hydrogen atom from the backbone of the polymer chain to form a mono-substituted ring.

Table 8: Band assignments for the fingerprint region of the ATR FT-IR spectrum of PET.

Peak (cm^{-1})	Assignment
1430	Combination band due to C-O stretching and O-H deformation vibration, associated with carboxylic acid dimer.[24]
1220	C-O stretching vibration, associated with carboxylic acid dimer.[24]
970	Stretching of C-H bond of the trans isomer of the ethylene glycol unit.[2]
940	C-H vibration associated with vinyl groups.[34]
898	Stretching of C-H bond of the cis isomer of the ethylene glycol unit.[2]
848	C-H deformation of two adjacent hydrogens on the terephthalic ring (indicates 1, 4 substitution)[4]
778	Out-of-plane deformation vibrations of mono-substituted rings[24]
769	Out-of-plane deformation vibrations of 1, 2, 3-substituted rings[24]
758	Out of plane deformation vibrations of 1, 2, 4-substituted rings[24]

From the ATR data, it is clear that PET degrades to a greater extent when exposed to 302 nm light compared to 365 nm light of the same intensity, on the surface of the sample. During exposure degradation products are formed including, carboxylic acid end groups, dimers, and mono-substituted rings.

3.3.2 DRIFT

The DRIFT spectra of 36 µm PET film samples irradiated in the weatherometer for 10 weeks (equivalent to a dosage of approximately 6.1 x 10^5 W m^{-2} hr^{-1}) in 1 week increments (equivalent to a dosage of approximately 6.1 x 10^4 W m^{-2} hr^{-1}) are shown in *Figure 3.14*. The 23 µm PET samples show the same general trends. One week of irradiation in the weatherometer is equal to approximately 7.5 weeks outdoors. *Figure 3.14* shows noticeable changes in the DRIFT spectra, after irradiation, in the region between 3800-2100 cm^{-1} and the carbonyl region. DRIFT spectra differ from ATR spectra as DRIFT analyses the whole thickness of the film, whereas ATR only analyses the surface of the film samples.

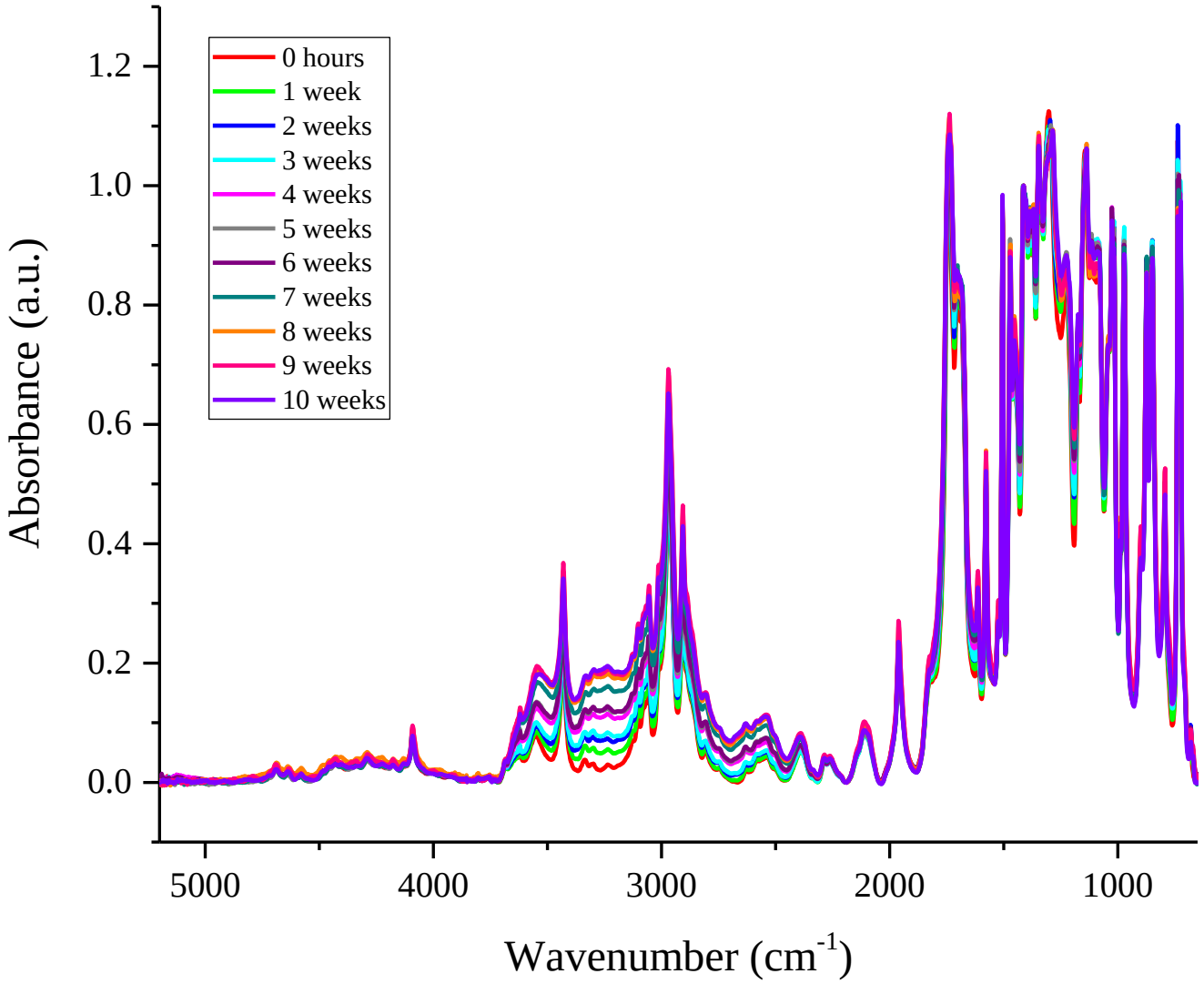

Figure 3.14: DRIFT spectra of PET films irradiated in the weatherometer for 10 weeks, in 1 week increments.

Figure 3.15 shows the region of the spectra between 3800-2100 cm^{-1} for the control sample and PET irradiated in the weatherometer for 10 weeks. The assignments for the peaks in this region are given in *Table 9*.

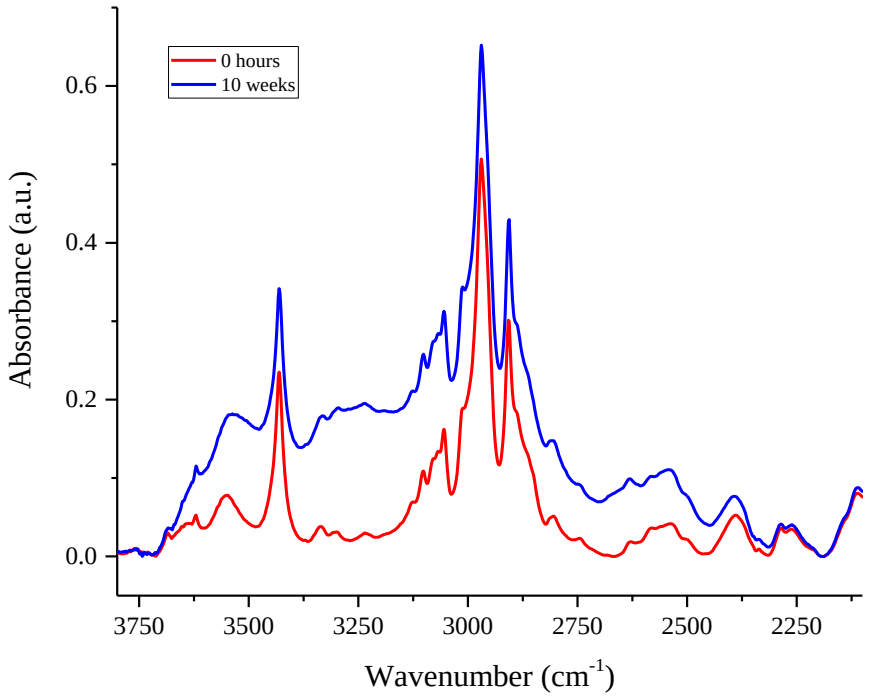

Figure 3.15: DRIFT spectra of 36 µm PET, irradiated in the weatherometer, in the region between 3800-2100 cm^{-1}.

Peaks at 3620, 3550 and 3290 cm^{-1} have been assigned to the aqueous, alcoholic and carboxylic acid hydroxy stretches, respectively. From *Figure 3.15* these peaks have increased in absorbance with exposure time. This indicates the production of new hydroxy groups, including carboxylic acid end groups, which are known to be produced during the photodegradation of PET. The peaks at 3430 and 3335 cm^{-1} due to the overtones of the carbonyl peak have also increased in absorbance with exposure time, this is thought to be due to the overlap with the growing hydroxy peaks.

Peaks assigned in *Table 9*, associated with the aromatic and aliphatic C-H stretching vibrations, have shown no meaningful change in size, after exposure. This could indicate that in the bulk of the film there has been no substitution on the ring or change

in the environment of aliphatic C-H stretches, or that changes have occurred, but they are below the sensitivity range of the DRIFT instrument.

Table 9: Band assignments for the region between 3800-2100 cm^{-1} of the DRIFT spectrum of PET.

Peak (cm^{-1})	Assignment
3620	Aqueous O-H stretching vibration[1]
3550	Alcoholic O-H stretching vibration[1]
3430	First overtone of the carbonyl group in ester[1]
3335	First overtone of carbonyl group in carboxylic acid end group[36]
3290	Carboxylic acid end groups[1]
3100, 3078, 3067, 3054	Aromatic C-H stretching[2]
3015, 2970, 2908	Crystalline aliphatic CH_2 stretching[2]
2963, 2855	Amorphous aliphatic CH_2 stretching[2]

The carbonyl region of the spectra, between 1900-1550 cm^{-1}, for a control film and a sample exposed in the weatherometer for 10 weeks, are shown in *Figure 3.16*. The assignments for the various peaks contained within the carbonyl peak are given in *Table 10*.

From *Figure 3.16* it is apparent that there is general broadening of the carbonyl peak, with irradiation time. This indicates the production of new carbonyl species during the photodegradation reactions. At higher wavenumbers, this broadening is due to the production of anhydride groups.[37] As explained in *Section 3.3.1* anhydrides can be produced, in this study, as irradiations were performed at a temperature that provides an ideal environment for anhydride formation to occur.

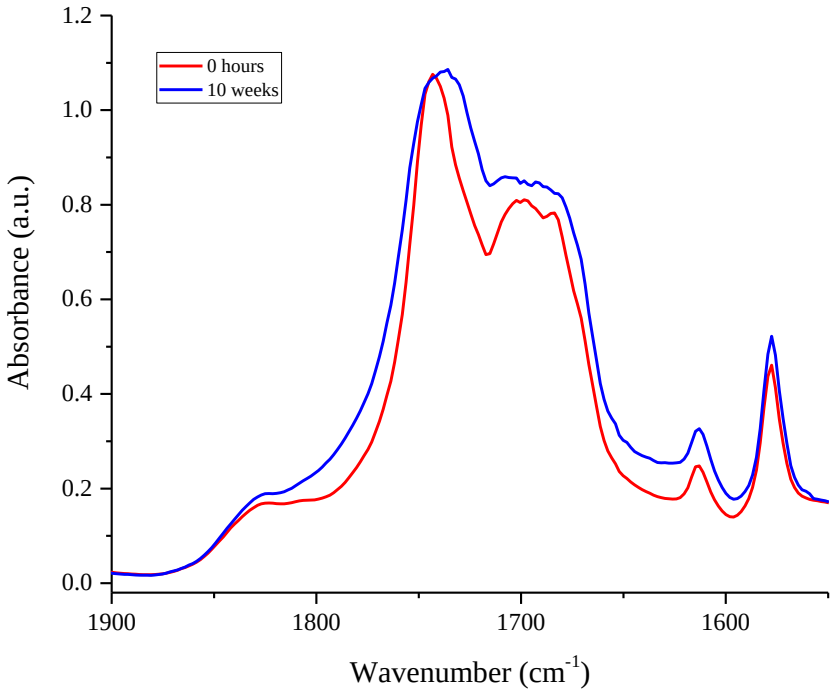

Figure 3.16: DRIFT spectra of 36 µm PET, irradiated in the weatherometer, in the carbonyl region between 1900-1550 cm^{-1}.

The broadening of the peak at lower wavenumbers is due to the formation of other degradation products. These degradation products include carboxylic acid end groups, which are known to be produced during the photodegradation of PET. Pathways have been proposed for their production and are shown in *Chapter 1, Figure 1.29.*

The peak at 1683 cm^{-1} was first reported by Donato *et al.* and assigned to the carbonyl stretch of benzoic acids, characteristic of the terminal acid groups in the polymer.[36] Carboxylic acid end groups are known to be produced during the photodegradation of PET.

There is also another peak present in this region at 1702 cm^{-1}. This peak has been reported to be present in DRIFT spectra of PET but has never been assigned.[36] It is thought that this peak could be due to carboxylic acid dimers due to the increase in absorbance of this peak after exposure.

Table 10: Band assignments for the carbonyl region of the DRIFT spectrum of PET.

Peak (cm^{-1})	Assignment
1785	Carbonyl stretch from anhydride carbonyl[22]
1743	Carbonyl stretching vibration of an ester[36]
1683	Carbonyl stretch from terminal acid end groups[36]

In this study, the extent of photodegradation, using DRIFT spectra, was measured by the change in area of the peaks between 3750-2160 cm^{-1} and the area of the carbonyl peaks, between 1880-1595 cm^{-1}. *Figure 3.17 (a) and (b)* shows the change in area of these peaks, for 23 and 36 µm PET, with dosage.

Figure 3.17 (a) shows that both thicknesses of film initially show a steady increase in change in area. At higher dosages, differences become apparent between the two different thicknesses of films, with the 23 µm film displaying a greater extent of degradation. This difference between the 23 and 36 µm films is also shown by the change in area of the carbonyl peak, given in *Figure 3.17 (b).* The 23 µm film degrading to a greater extent is plausible as a thinner film has less bulk and therefore should theoretically degrade quicker; specifically, oxygen will diffuse more readily through a thin film rather than a thick film. DRIFT is a technique which analyses the whole of the film, so differences between the 23 and 36 µm PET films are understandable as they are of different thicknesses. This difference in the extent of degradation could also be due to the differences in intensity depending on where the films were placed on the sample tray in the weatherometer. It is thought that at prolonged hours of exposure/higher dosages these differences would become more apparent.

The data point at approximately $5x10^5$ W m^{-2} hr^{-1}, in *Figures 3.17 (a) and (b),* is suspected to be an outlier, due to the differences in intensity on the sample tray.

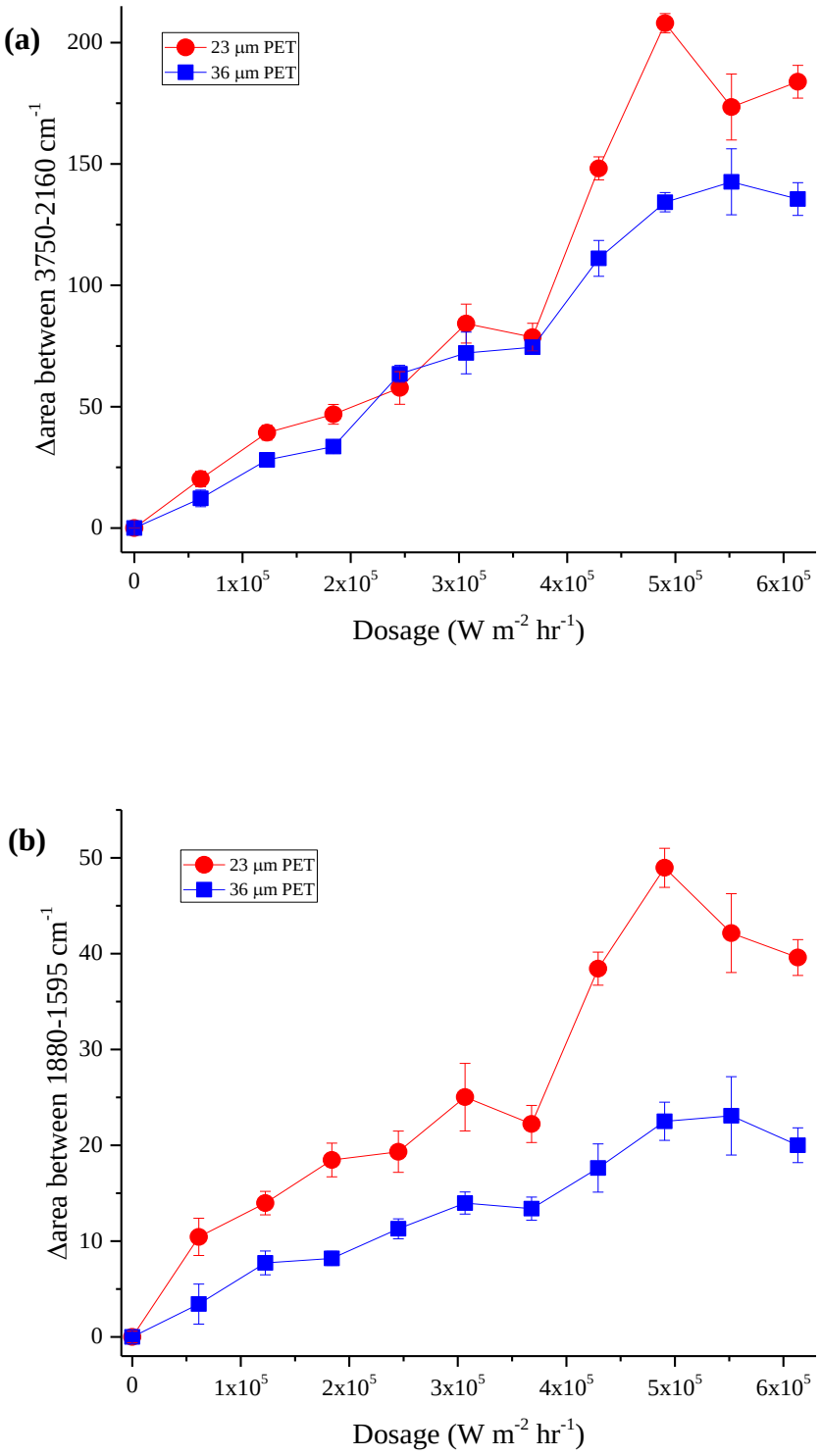

Figure 3.17: Extent of photodegradation of 23 and 36 µm PET measured by the change in area of peaks between (a) 3750-2160 cm^{-1} and (b) 1880-1595 cm^{-1}(carbonyl).

These results are in contrast with the ATR data which shows an initial sharp increase, followed by a more moderate increase, and has been previously attributed to a two-step process. Considering this, the DRIFT results indicate a one step process in the bulk of the film, due to the steady increase in change in area of the peaks.

3.3.3 UV-visible spectroscopy

The UV-visible spectra of samples irradiated in the weatherometer for 10 weeks and analysed every week are given in *Figure 3.18*. The UV-visible spectra show an increase in absorbance at 340 nm and a minor increase at 400 nm. The increase at longer wavelengths, after exposure, has been reported by Fechine *et al.*[31] and is indicative of the production of new chromophores.

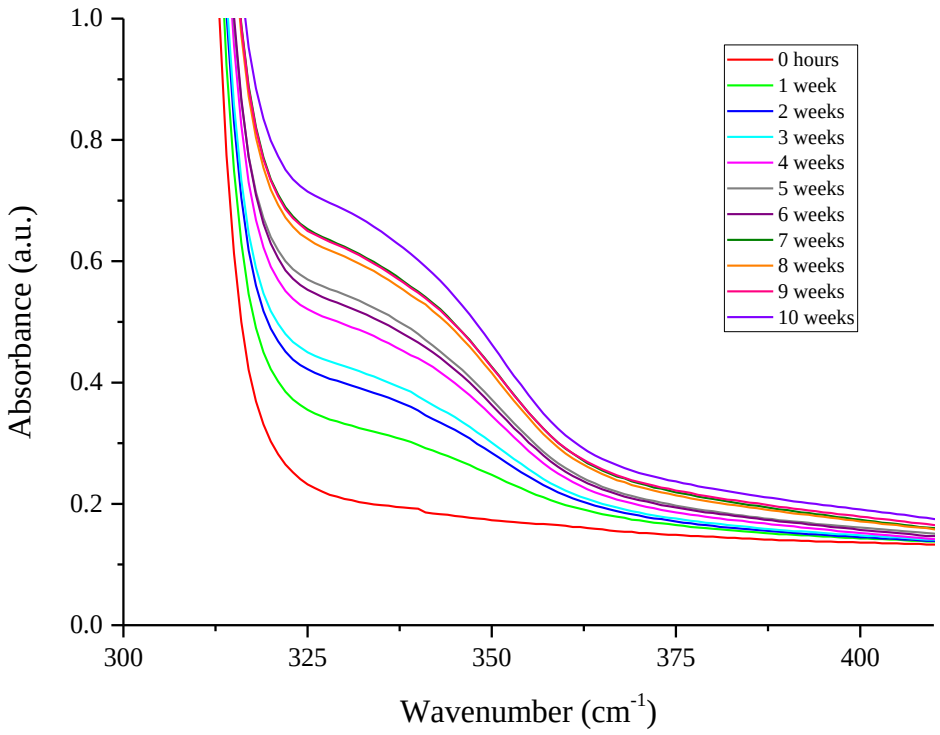

Figure 3.18: UV-visible spectra of 36 µm PET irradiated in the weatherometer for 10 weeks, in 1 week increments.

The increase at 340 nm has been attributed to monohydroxy terephthalate groups. These species were first identified by Pacifici and Straley,[38] and a mechanism was proposed for their formation by Day and Wiles.[13] The authors reported that the hydroxy groups, produced during the photodegradation of PET, are capable of substituting in the phenylene ring to form monohydroxy terephthalate groups.[13] This mechanism proposed by Day and Wiles is given in *Chapter 1*, *Figure 1.28.*

Figure 3.18 also shows a small increase in absorbance at 400 nm. This is mainly due to the formation of quinone and diquinone groups during the photodegradation of PET. Edge *et al.* have proposed a mechanistic pathway for the production of these groups, during thermal degradation, suggesting that there is an equilibrium between the hydroxylated species and their corresponding quinones.[39] Possible reactions leading to the formation of quinone and diquinone groups, during exposure to UV light, have been proposed by Fechine *et al.*, shown in *Chapter 1*, *Figure 1.31*[31]

Figure 3.19 shows the change in absorbance of the peak at 340 nm, for the 23 and 36 µm PET films, with dosage. Both the 23 and 36 µm films similarly increase with dosage. However, at higher dosages the 340 nm peak beings to fluctuate in absorbance due to the attack of the new chromophoric groups. The new chromophoric groups are produced during exposure and in addition, are subsequently attacked.

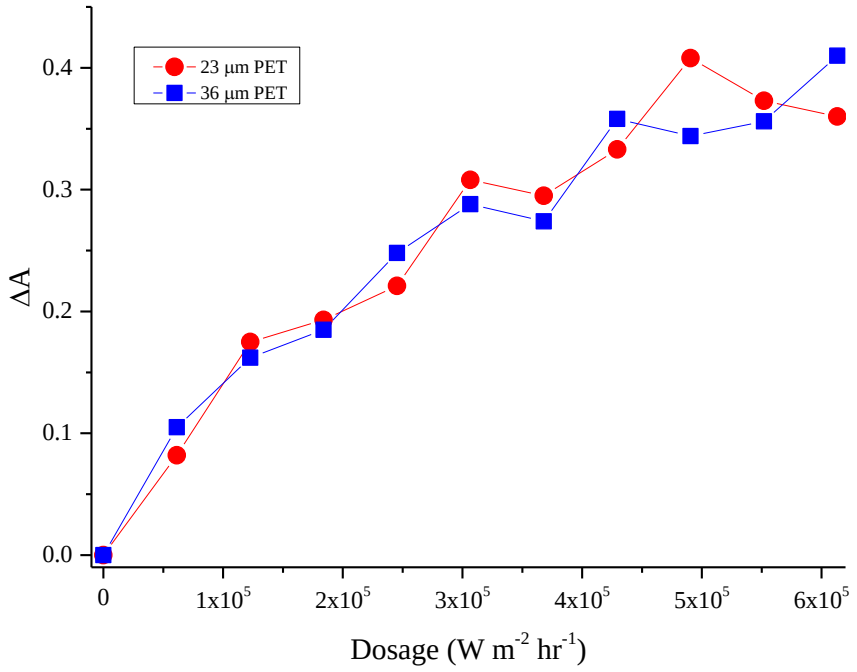

Figure 3.19: Change in absorbance at 340 nm for 23 and 36 µm PET films irradiated in the weatherometer (graph contains error bars).

Figure 3.20 shows a proposed reaction pathway for the attack of the monohydroxy terephthalate groups by hydroxyl radicals, which are known to be produced during the photodegradation of PET. Subsequent attacks on molecule A will continue until the fragments are all converted into small and stable molecules.

Both the ATR (*Figure 3.09)* and DRIFT *(Figure 3.14)* spectra show an increase in absorbance of the peak assigned to the aqueous O-H stretching vibration.[1] This supports the reaction pathway in *Figure 3.20* as water is produced as a by product of the reaction scheme. This pathway has been reported in the literature, but not in relation to photodegradation reactions taking place in PET.[40,41]

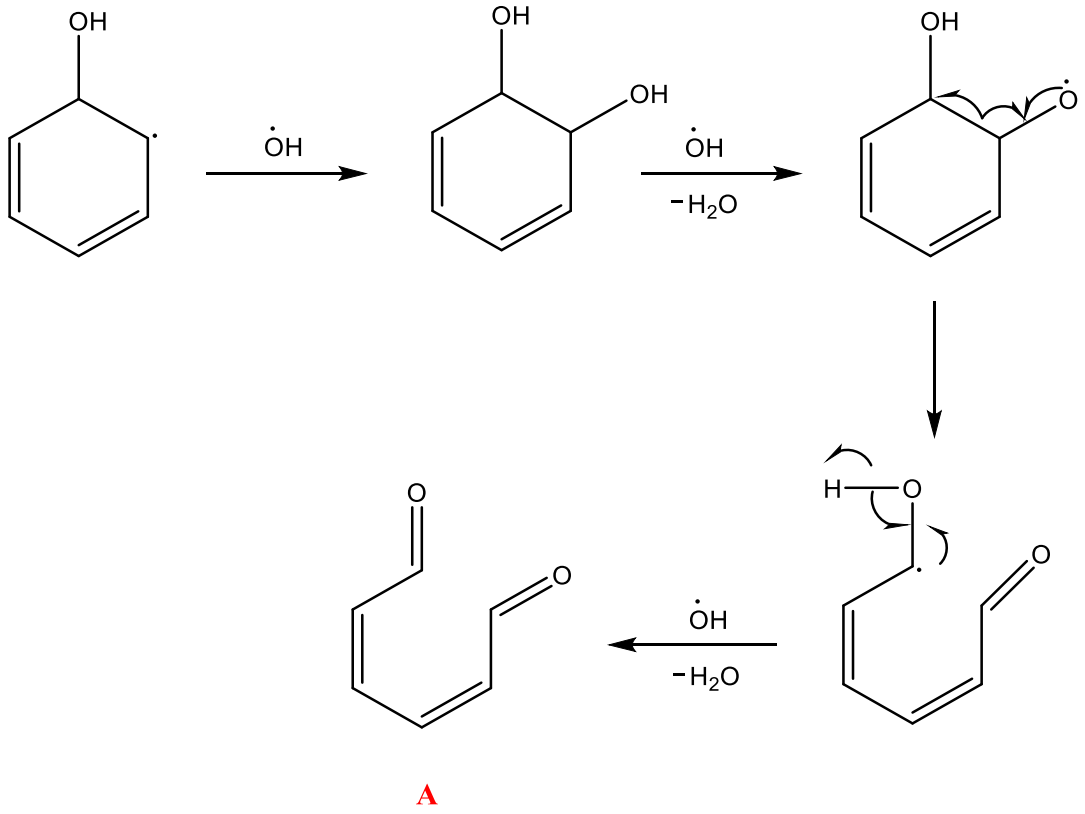

Figure 3.20: Proposed mechanistic pathway for the attack of monohydroxy terephthalate groups during exposure.

This fluctuation in absorbance at the 340 nm peak could also be due to the photodegraded polymer simply being more hygroscopic than the control sample.

3.3.4 Fluorescence spectroscopy

Figure 3.21 shows the initial natural fluorescence spectrum of PET, depicted by the black line on the graph. The control spectrum shows peaks at 370, 385 and a shoulder at 410 nm. The peak at 370 nm was first reported when PET was excited by 290 nm light, whereas the peak at 385 nm with a shoulder at 410 nm was reported after excitation by 340 nm.

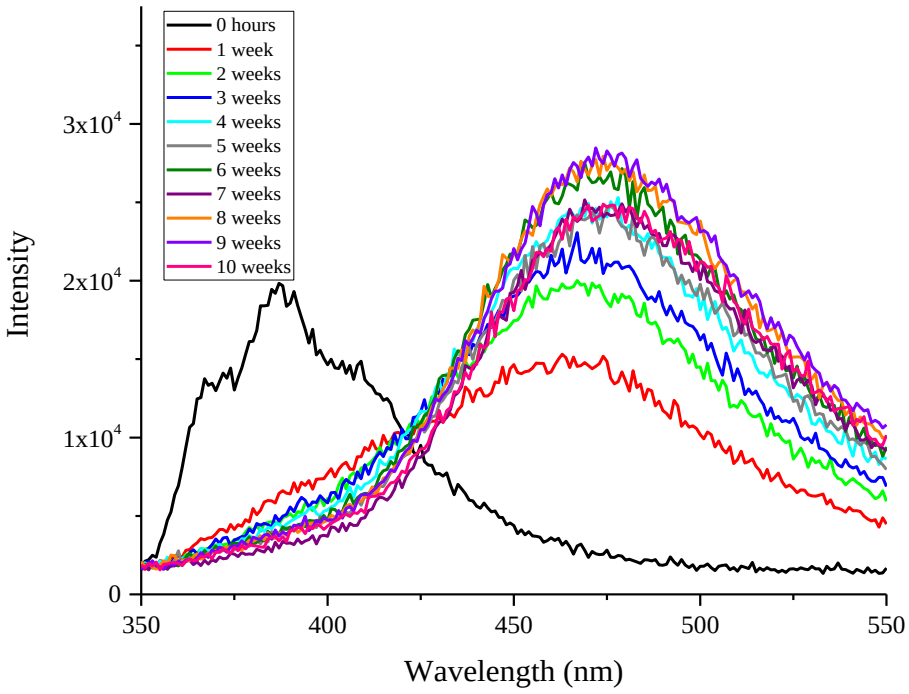

Figure 3.21: Fluorescence spectra of 36 µm PET irradiated in the weatherometer for 10 weeks, in 1 week increments.

Various groups have studied the emission band at 370 nm, but at present, this is known as the excimer band. Initially, Philips and Shug assigned this peak to either the formation of a PET excimer or triplet-state emission, with Takai *et al.* in agreement that the 370 nm peak was due to the excimer. However, Allen and McKellar proposed that this peak could be associated with a ground state dimer,[42] which was later supported by modelling studies from Hemker *et al.*[43] and Lafemina *et al.*.[44] Lafemina *et al.* also reported that this peak must originate in the amorphous regions of the polymer from results of molecular dynamic simulations in crystalline PET.[45] Currently, Chen *et al.*, Fukazawa *et al.* and Fechine *et al.* have all attributed the peak at 370 nm to an excimer.[8,46,47]

There have also been considerable amounts of research into the assignments for the peak at 385 nm. The 385 nm peak along with the shoulder at 410 nm were initially reported by Day and Wiles in addition to the peak at 370 nm.[1] Allen and McKellar

proposed that the peak at 385 nm could be due to a ground state dimer,[42] which was later reinforced by Hemker *et al.*.[43] Model systems were studied by Chen *et al.* and it was suggested that the emissions at 385 and 410 nm were related to the carbonyl groups in the main chain of PET. The authors explained that at least one of the carbonyl groups is not coplanar with the phenylene ring which enables the $n \rightarrow \pi^*$ transition. This transition is enhanced due to the interaction of the carbonyl and the π electrons on the ring, which most likely leads to less coplanarity. This enhanced $n \rightarrow \pi^*$ transition of the non-coplanar carbonyl, results in emission at 385 nm with a shoulder at 410 nm.[46] This is in agreement with previous studies. At present, emission at 385 and 410 nm are known to be associated with a ground state dimer.[8]

After exposure, the intensity of the initial emission peaks decreases. This has been reported as being due to a loss of interaction between chromophores, caused by chain scission.[8] Irradiation in the weatherometer causes the development of a peak centered at 475 nm. Pacifici and Straley suggested this emission was due to photolytic degradation products,[38] which was further supported by Day and Wiles.[1] From studying model systems Chen *et al.* suggested that the emission at 475 nm is an exciplex from the interaction between the excited carbonyl group and the phenylene π-electrons.[46]

The evolution of the emission at 475 nm has therefore been assigned to the production of monohydroxy terephthalate groups. A mechanistic pathway for their production was proposed by Day and Wiles and is given in *Chapter 1, Figure 1.28.*[29] This species was initially identified by Pacifici and Straley.[38]

Figure 3.22 shows the change in intensity of the peak at 475 nm, for the 23 and 36 µm PET films, with dosage. This shows that both samples show an increase with dosage, due to the production of monohydroxy terephthalate chromophoric groups. From the graph, it is apparent that at higher dosages there is some fluctuation in the change in intensity of the 475 nm peak. This is due to the production and subsequent attack of the new chromophores. A reaction pathway for the breakdown of these groups has been discussed in *Section 3.3.3* and is given in *Figure 3.20.*

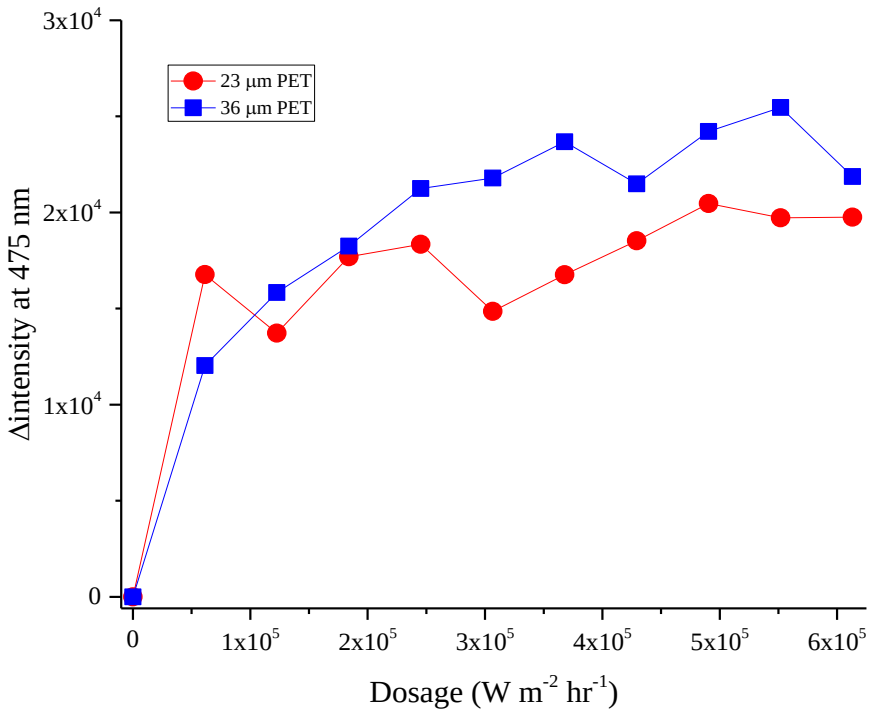

Figure 3.22: Change in intensity at 475 nm, with dosage, for 23 and 36 µm PET.

3.3.5 DSC

3.3.5.1 Heating cycle

The first heating cycles for samples irradiated in the weatherometer are shown in *Figure 3.23*, in 2 week increments. A decrease in T_m is evident from *Figure 3.23* which could be explained by two different mechanisms. Firstly, this could indicate that branched chains are produced during exposure. Branching reduces the packing efficiency of the polymer; crystalline content is lowered and hence the T_m decreases.[26]

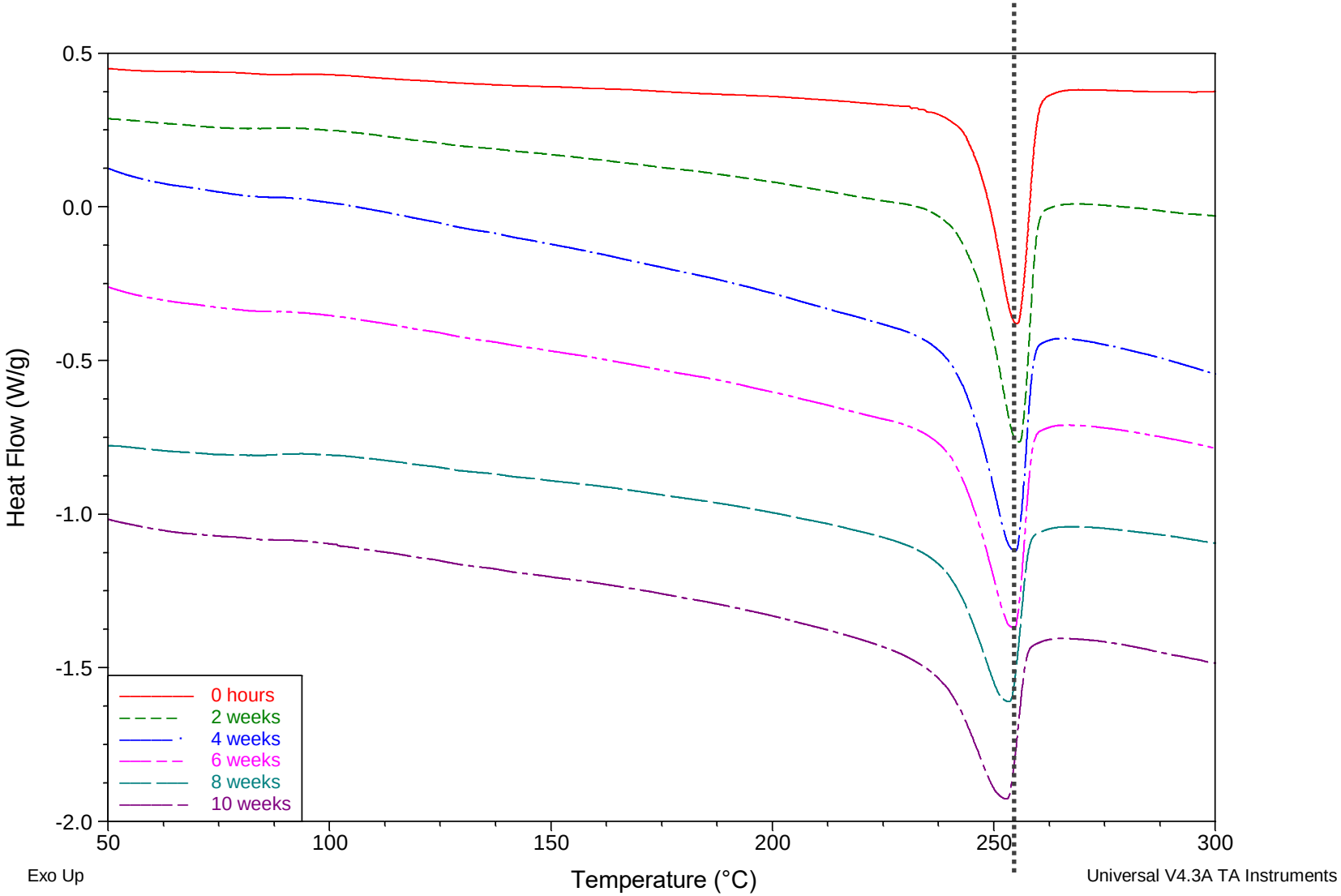

Figure 3.23: Heating cycle of DSC thermogram for 36 µm PET irradiated in the weatherometer.

Similarly, crosslinking could also cause a decrease in Tm. Another theory is that crosslinking has occurred in the polymer film which would be depicted in a DSC thermogram by a broader melting peak and a lower onset temperature, compared to a control sample. Samples with a higher degree of crosslinking cause non-uniformity of the crystal lattices which cause them to melt at a different temperature.[48]

The onset temperature of the melting peak also decreased with exposure time indicating the production of crystals with reduced size, thickness, and lower melting temperatures.[26]

3.3.5.2 Cooling cycle

Figure 3.24 shows the cooling cycle of samples irradiated in the weatherometer for 10 weeks. From *Figure 3.24* it is clear there was an initial increase in T_c after 2 weeks of exposure. An increase in T_c indicates that chain scission has occurred, which is consistent with the mechanisms of photodegradation that have been proposed.[1,31] Chain scission reactions lead to the production of shorter chain fragments which can easily crystallise upon cooling. Therefore, the T_c increases due to the exposed polymer being able to crystallise more easily than the control sample during the cooling cycle.[49–52]

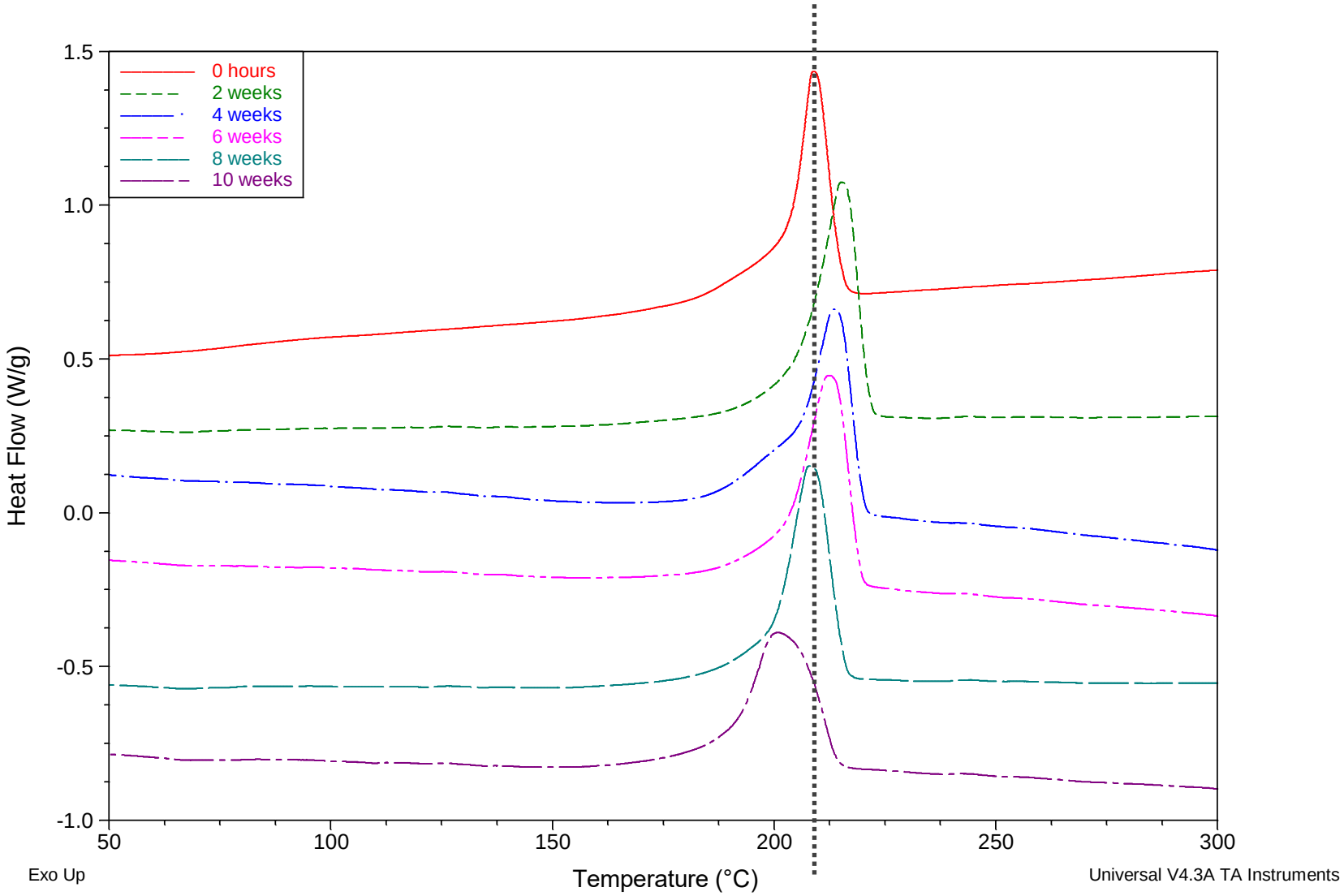

Figure 3.24: Cooling cycle of DSC thermogram for 36 µm PET irradiated in the weatherometer.

After this initial increase, the T_c starts to decrease with exposure time. A decrease in T_c indicates that branched chains could be produced during exposure. Branched chains make it more difficult for the polymer to crystallise during cooling, therefore the T_c decreases due to the undegraded polymer being able to crystallise quicker than the exposed sample during the cooling cycle. A decrease in T_c is in agreement with Jayakannan and co-workers,[53] but not in agreement with the study reported by Li *et al.*[54] Jayakannan *et al.* studied the effect of branching on the crystallisation behaviour of PET. They reported that branched PET showed a lower T_c than that of linear PET at different cooling rates.[53] This also agrees with the decrease in T_m.

Another reason for this decrease in T_c could be crosslinking of the polymer chains during exposure. Much the same as branching, crosslinking makes it more difficult for the polymer chains to pack during the cooling cycle. This means that the T_c will decrease due to the uncrosslinked polymer being able to pack more easily and crystallise quicker than the exposed sample.[55]

3.3.5.3 Reheat cycle

On the reheat cycle, shown in *Figure 3.25*, two melting endotherms occur at 247°C and 254°C, corresponding to two different crystalline forms of the polymer. The peak at 247°C originates from the melting of the crystallites formed at the T_c, and the peak at 254°C corresponds to the melting of the original crystallites reorganised during the DSC scan.[56]

It is evident from *Figure 3.25* that the peak at 247°C gradually diminishes with exposure time. It is thought that this could be because the crystallinity of the PET has already increased during exposure, meaning that there will be fewer crystallites formed at the crystallisation temperature. It could also be the case that the peak at 247°C is not reducing, but the peak at 254°C is expanding and dominating the region. The crystallinity of the PET films has increased with exposure time and these original crystals have already shown a decrease in melt temperature (*Figure 3.23*). Therefore, due to the production of more original crystallites, the peak expands and decreases in melt temperature due to branching or crosslinking.

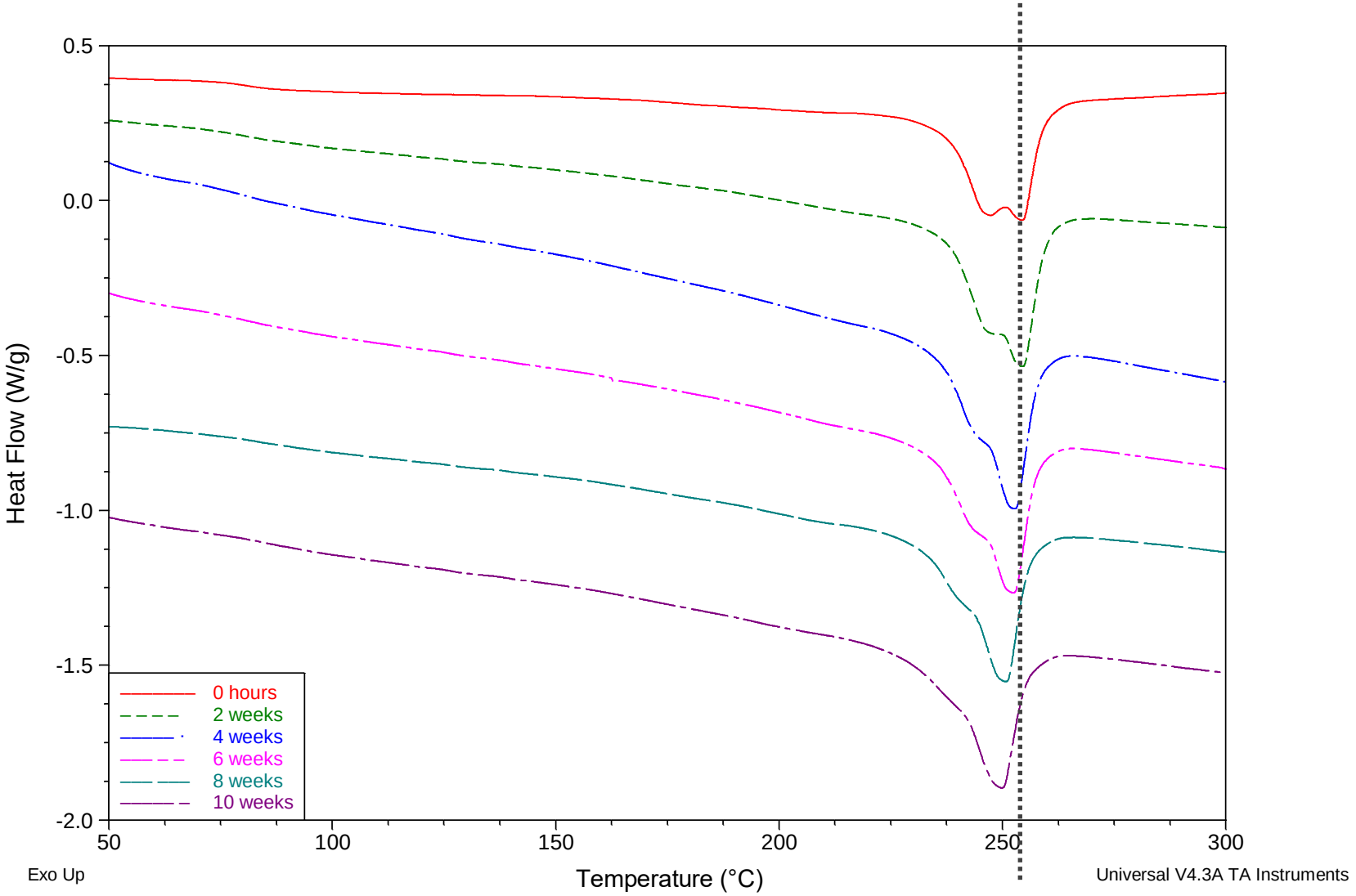

Figure 3.25: Reheat cycle of DSC thermogram for 36 µm PET irradiated in the weatherometer.

The melting peak at 254°C in the control sample, decreases with exposure time due to the crystals produced during the cooling cycle containing smaller, more imperfect molecules.[57,58]

3.3.6 Contact angle

Figure 3.26 shows the average contact angle values for 23 and 36 μm PET irradiated in the weatherometer. This shows that there is an initial decrease in contact angle with dosage for both the 23 and 36 μm PET.

A decrease suggests that the surface of the films have become more hydrophilic upon irradiation. This agrees with the production of carboxylic acid end groups, which are known to be produced during the photodegradation of PET, as shown by the mechanistic pathway in *Chapter 1, Figure 1.29.*

This decrease is then followed by an increase in contact angle, which could be explained by contact angle hysteresis. Contact angle hysteresis is known as the difference between the advancing angle, θ_a, and the receding angle, θ_r, as shown in *Equation 2*.[59]

$$\Delta\theta = \theta_a - \theta_r \qquad \textbf{Equation 2}$$

When a droplet decreases in volume, either through evaporation or withdrawing water from the droplet, the contact angle also decreases. The same contact area is maintained until the droplet begins to recede, with a constant contact angle, θ_r. On the other hand, when a droplet increases in volume, either through condensation or adding water to the droplet, the contact angle also increases. Again, the same contact area is maintained, until the droplet begins to advance, at a constant contact angle, θ_a. The receding and advancing angles are both characteristic of topography and surface chemistry. Any angle between the advancing and receding contact angles is known as the metastable form of the droplet.[60]

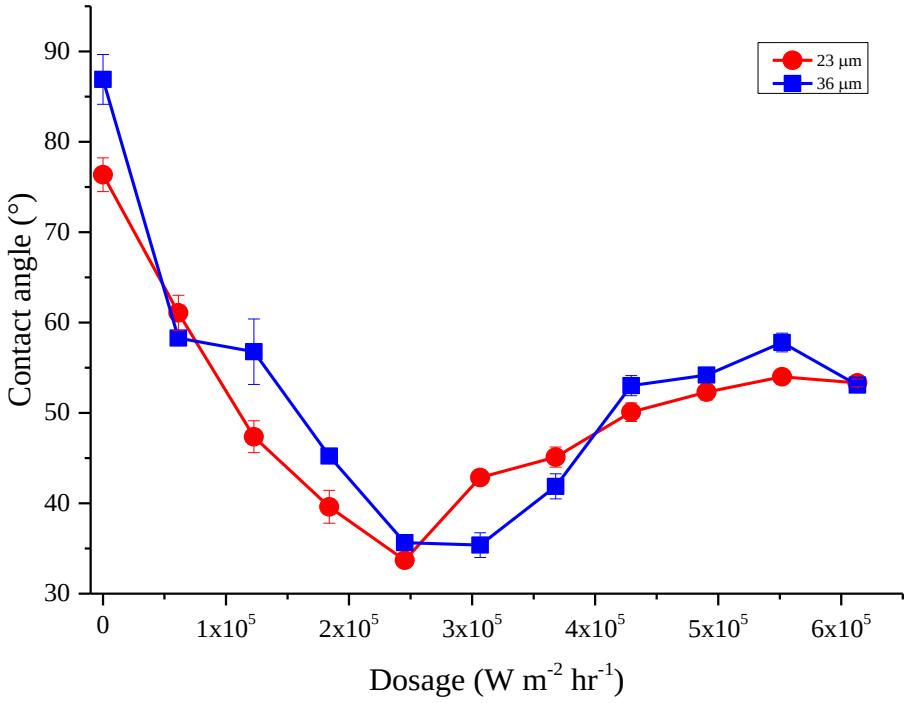

Figure 3.26: Contact angles of front and back side of 23 and 36 µm PET irradiated in the weatherometer for 10 weeks.

This indicates that an increase in contact angle, at higher dosages, could be due to water condensing on the droplet at different rates for each sample of film. This could be possible as the contact angle values for each film were taken on separate occasions, which could mean the laboratory was at a different temperature each time.

In the literature, the general conclusion seems to be that contact angle hysteresis arises from surface roughness and/or heterogeneity. It is therefore thought that this increase in contact angle could also be due to the heterogeneity of the surface or surface roughness. Contact angles measured on heterogeneous or rough surfaces would not solely reflect surface energies as surface topography would now need to be considered. Contact angles on rough and heterogeneous surfaces were initially studied by Wenzel[61] and Cassie and Baxter,[62] respectively.

According to the Wenzel model water penetrates the surface grooves of a rough surface, resulting in higher surface wettability due to an increase in contact area. This means that there would be a decrease in the contact angle value.

In contrast, the Cassie-Baxter model shows that water does not penetrate the surface grooves and lies on top of these grooves instead. This means that air bubbles are trapped in the grooves, resulting in an increase in the contact angle.[10] A transition between the Cassie-Baxter State to the Wenzel state has been observed.[10] Illustrations of these models are given in *Figure 3.27*.

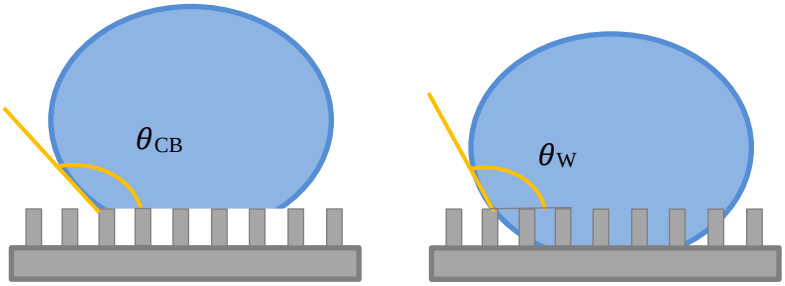

Figure 3.27: Illustration of Cassie-Baxter and Wenzel states.

3.3.7 Scanning Electron Microscopy

SEM images of 23 and 36 µm PET films irradiated in the weatherometer in 1 week increments for 10 weeks are shown in *Figures 3.28 and 3.29*, respectively. The images show that there is no meaningful change on the surface of the films until 7 weeks of exposure. After 7 weeks surface cracks are visible and by 9 weeks of exposure fractures are now apparent. Seven weeks of irradiation in the weatherometer is approximately equivalent to 1 year outdoors. This means that after only 1 year outdoors these PET films would show surface cracking, which could lead to the failure of physical properties. These images indicate that there are physical changes occurring during exposure, as well as the chemical changes.

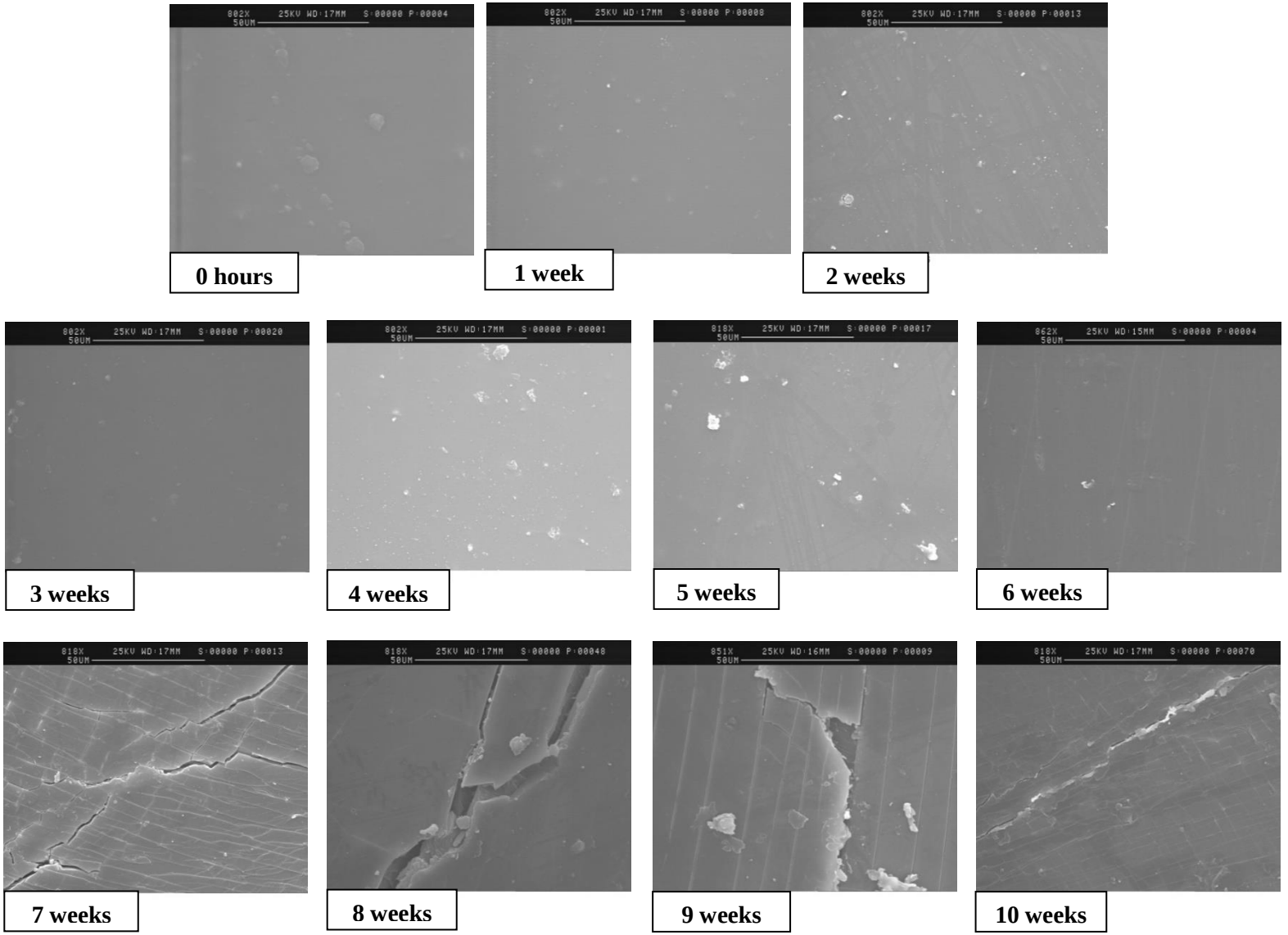

Figure 3.28: SEM images of 23 µm PET film irradiated in the weatherometer for 10 weeks, in 1 week increments.

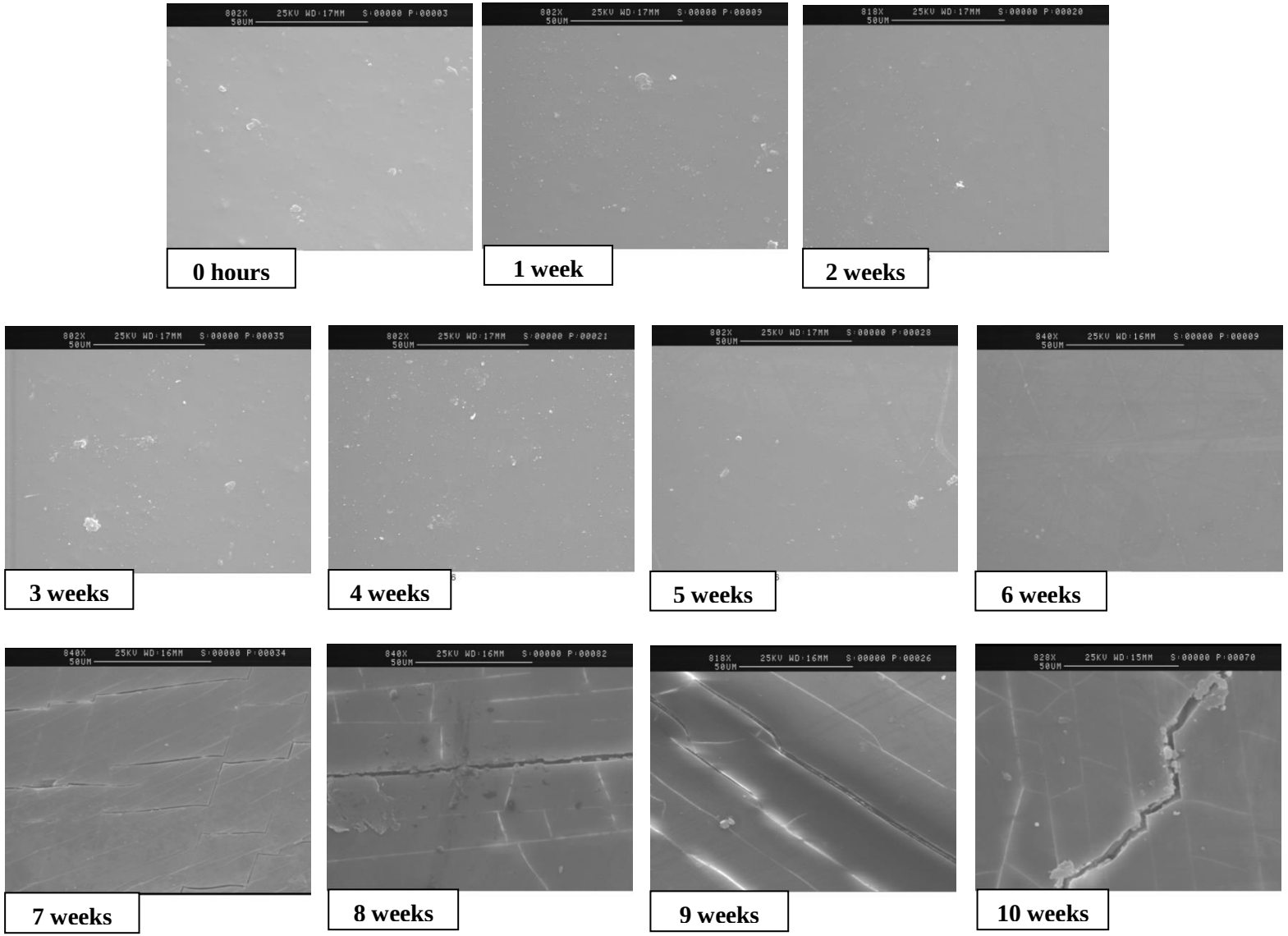

Figure 3.29: SEM images of 36 µm PET film irradiated in the weatherometer for 10 weeks, in 1 week increments.

3.3.8 General Conclusions

The photodegradation reactions occurring in PET, during exposure to conditions simulating outdoors, were investigated. Results show the production of various degradation products, including carboxylic acid end groups, dimers, anhydrides, aldehydes, quinones and monohydroxy terephthalate groups. ATR spectra also show the production of mono-substituted rings, which has never been reported before in literature during the degradation of PET materials. In addition, there was evidence of substitution, chain scission, branching and crosslinking reactions. A more hydrophilic surface, as well as surface cracks, were also reported after exposure. After only 1 week of exposure, this is approximately equal to 7.5 weeks outdoors, the PET films were already showing signs of degradation.

It is thought that PET degrades under a broad wavelength range of light due to its high absorbance at shorter wavelengths, initially. The degradation products formed, from the absorbance of short wavelengths, can absorb light of longer wavelengths which subsequently causes another scheme of reaction sequences to occur. This being said, it is near impossible to determine the role of each wavelength in the degradation when exposing PET to a broad wavelength range of light. For this reason, narrow wavelength ranges of light were used to study the role of different wavelengths in the photodegradation of PET.

3.4 Effect of specific wavelengths on the photodegradation of PET

PET films of 23 and 36 μm thickness were exposed to two wavelengths of light; UV-A (365 nm) and UV-B (302 nm). As discussed in *Chapter 2*, the lamps used are wavelength bands centered on 302 nm and 365 nm but are referred to as the 302 nm and 365 lamps throughout this study. Irradiations were carried out at room temperature under oxidative conditions. This allowed for the analysis of the effect of different wavelengths of light on the photodegradation of PET. Samples were analysed using ATR FT-IR, DRIFT, UV-visible spectroscopy, DSC, and SEM.

3.4.1 ATR FT-IR

The ATR spectra of PET exposed to 302 nm or 365 nm light, for 1 week (equivalent to a dosage of approximately 4.2 x 10^3 W m^{-2} hr^{-1} or 4.8 x 10^3 W m^{-2} hr^{-1}) in 24 hour increments (equivalent to a dosage of approximately 6.1 x 10^2 W m^{-2} hr^{-1} or 8.3 x 10^2 W m^{-2} hr^{-1}), are given in *Figures 3.30 and 3.31*, respectively. *Figure 3.30* shows change in the spectra in the region between 3800-2100 cm^{-1}, as well as the carbonyl and fingerprint regions. However, PET exposed to 365 nm light, shown in *Figure 3.31*, show only minor changes in the ATR spectra as PET only weakly absorbs this wavelength of light. The rear surface of the samples showed no notable change with exposure time.

Figures 3.32 shows the region of the ATR spectra of samples exposed to 302 nm light, between 3800-2100 cm^{-1}, containing the hydroxy peaks as well as the aromatic and aliphatic C-H stretching peaks. A summary of the assigned peaks in this region are given in *Table 11*.

Peaks associated with carboxylic acid end groups, dimers and the Ar-CH_3 group have developed in the spectra upon exposure to 302 nm light. There has been change in other peaks in this region, including the size of the peaks associated with aromatic C-H stretching due to the production of mono-substituted rings which results in another aromatic C-H bond on the ring. There has also been a decrease in height of the peaks assigned to the crystalline and amorphous aliphatic CH_2 stretching vibrations, associated with chain scission reactions taking place during degradation. These peaks have been discussed in detail in *Section 3.3.1*.

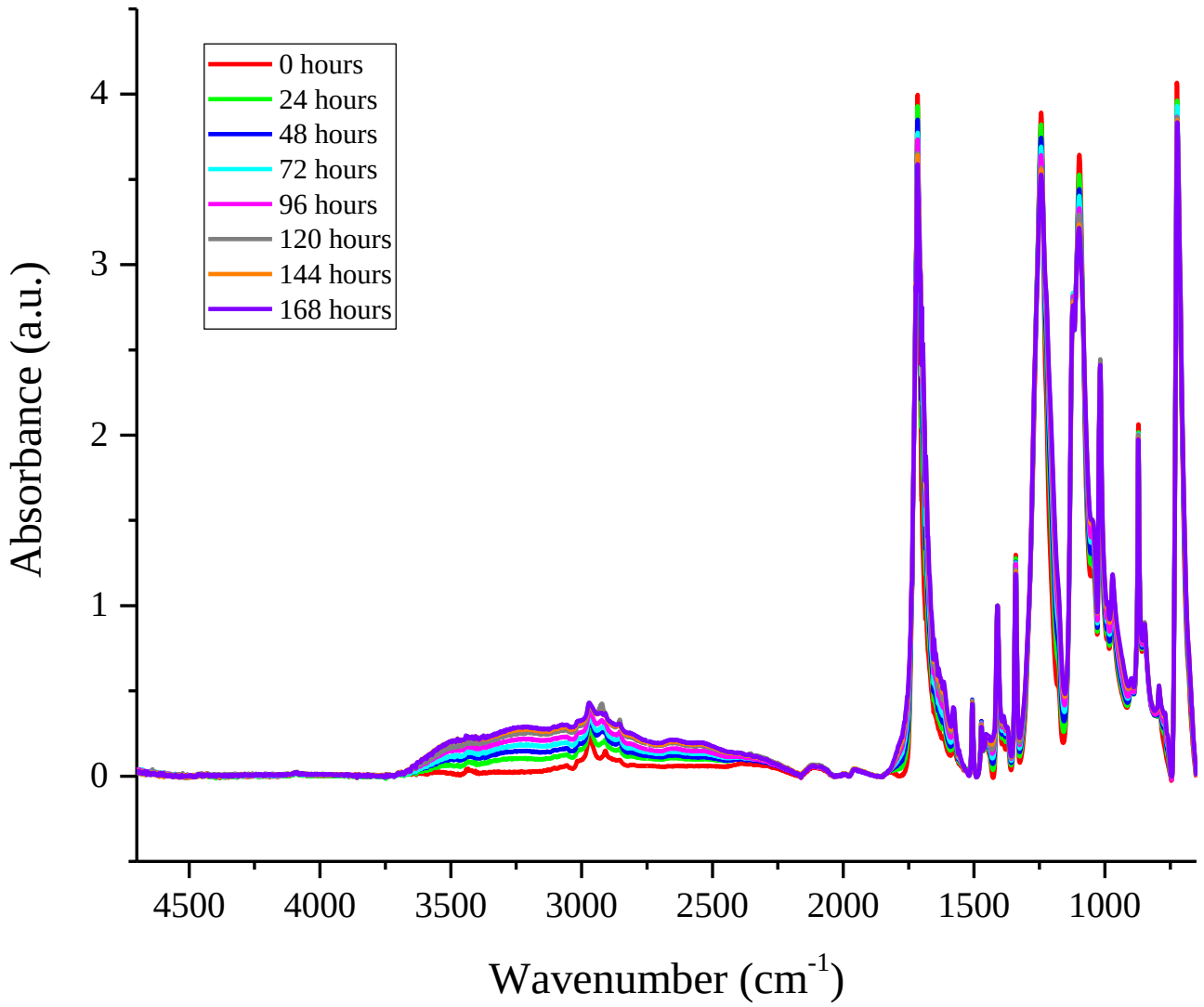

Figure 3.30: ATR FT-IR spectra of 36 µm PET films exposed to 302 nm light for 1 week, in 24 hour increments.

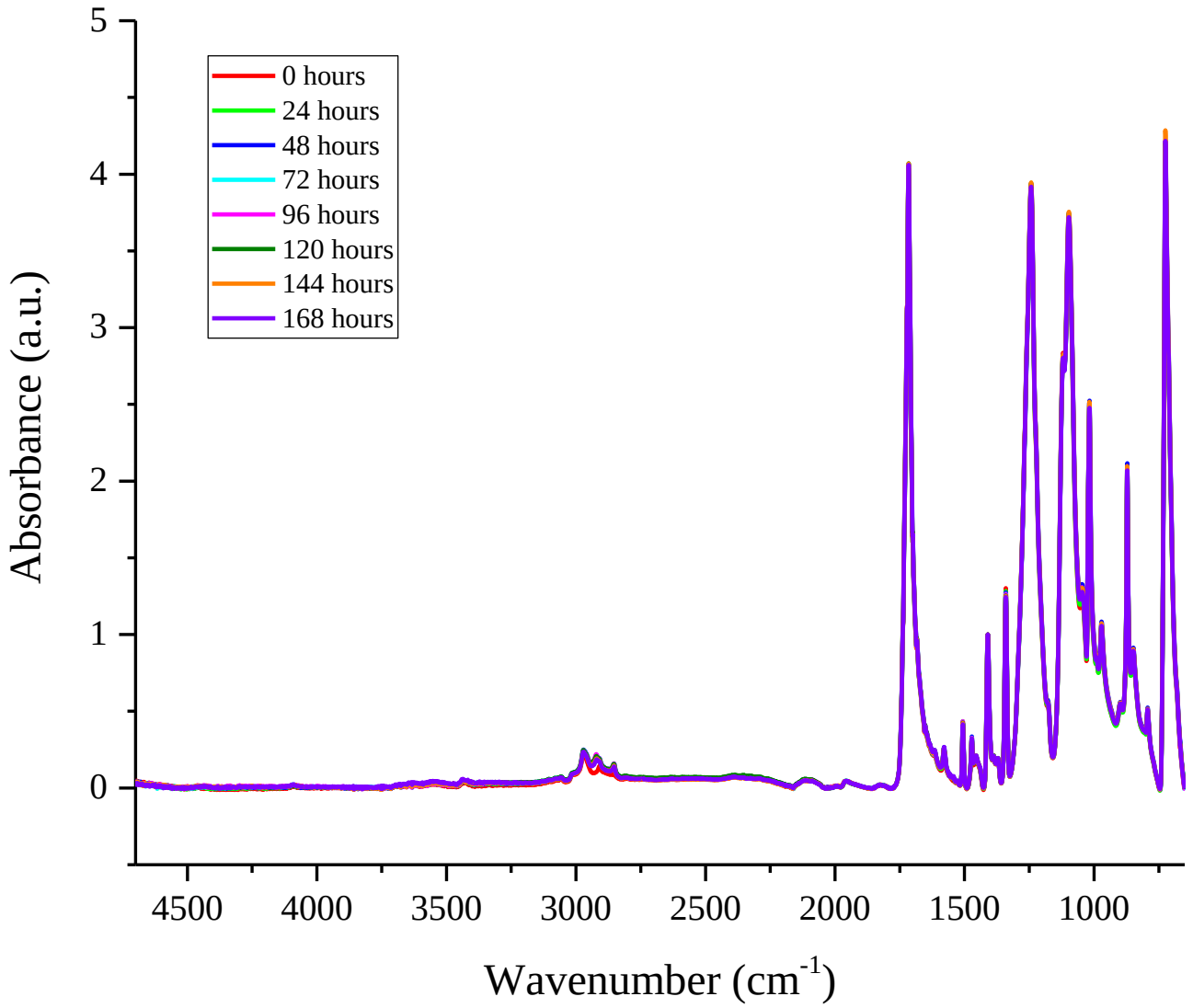

Figure 3.31: ATR FT-IR spectra of 36 µm PET films exposed to 365 nm light for 1 week, in 24 hour increments.

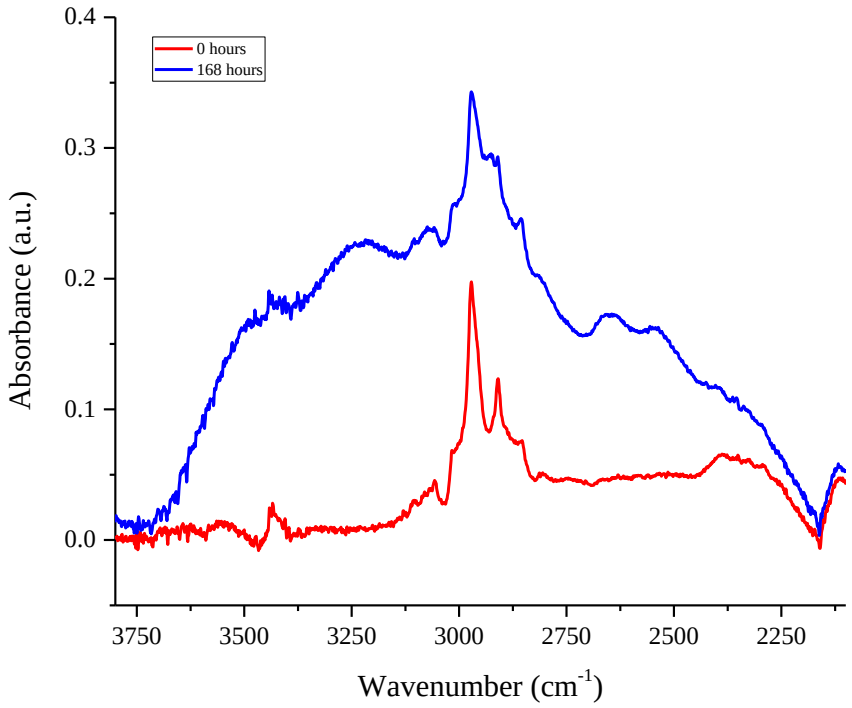

Figure 3.32: ATR FT-IR spectra of 36 µm PET films, exposed to 302 nm light, in the region between 3800-2100 cm^{-1}.

Table 11: Band assignments for the region between 3800-2100 cm^{-1} of the ATR FT-IR spectrum of PET.

Peak (cm^{-1})	Assignment
3630	Aqueous O-H stretching vibration[1]
3550	Alcoholic O-H stretching vibration[1]
3430	First overtone of the carbonyl peak[1]
3290	Carboxylic acid end groups[1]
3100 – 3060	Aromatic C-H stretching[2]
3016, 2970, 2909	Crystalline aliphatic CH_2 stretching[2]
2928	C-H symmetric stretching vibration associated with the Ar-CH_3 group.
2965, 2855	Amorphous aliphatic CH_2 stretching[2]
2640, 2540	Characteristic of the carboxylic acid dimer[18]

*Figure 3.33 s*hows the carbonyl peak broadening with exposure which indicates that new carbonyl groups have formed during exposure to 302 nm light. The various peaks contained within the carbonyl in the ATR spectra have been assigned and are given in *Table 12*.

During the photodegradation of PET, the production of anhydride and aliphatic aldehyde groups cause the carbonyl peak to broaden to higher wavenumbers with irradiation time. Peaks assigned to carboxylic acid dimers, carboxylic acid end groups, terephthalic acid and quinone species all increase in intensity with exposure time and cause the broadening of the carbonyl peak at lower wavenumbers. Simultaneously, there is a decrease in the peaks associated with the carbonyl stretch from the ester group, due to chain scission reactions occurring during exposure. All peaks contained within the carbonyl have been discussed in detail in *Section 3.3.2*.

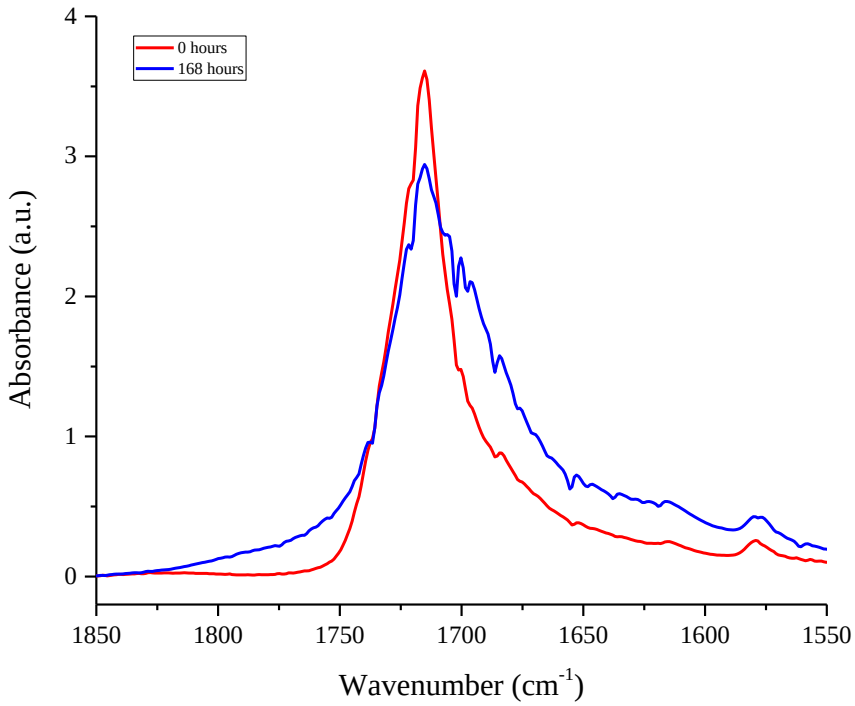

Figure 3.33: ATR FT-IR spectra of 36 µm PET, exposed to 302 nm light, in the carbonyl region between 1850-1550 cm^{-1}.

Table 12: Band assignments for the carbonyl region of the ATR FT-IR spectrum of PET.

Peak (cm^{-1})	Assignment
1785	Carbonyl stretch from anhydride carbonyl[22,23]
1738	Carbonyl stretch from aliphatic aldehyde[24]
1722	Amorphous carbonyl stretch from ester[2]
1714	Crystalline carbonyl stretch from ester[2]
1705	Carbonyl stretch from carboxylic acid dimer[19,23,24]
1700	Carbonyl stretch from carboxylic acid end groups[26]
1695	Carbonyl stretch from quinone groups[27,28]
1685	Carbonyl stretch from terephthalic acid

As previously stated, the extent of photodegradation was measured by the change in area of peaks between 3800-2100 cm^{-1} and the carbonyl peak, with dosage. *Figure 3.34 (a) and (b)* shows the change in area of these peaks against dosage for 23 and 36 µm PET films exposed to 302 nm and 365 nm light. The graphs show that samples exposed to 302 nm light show an increase in change in area with dosage, whereas samples exposed to 365 nm light show only minor changes. This is because short wavelengths of light are absorbed strongly, whereas longer wavelengths are absorbed weakly by PET.

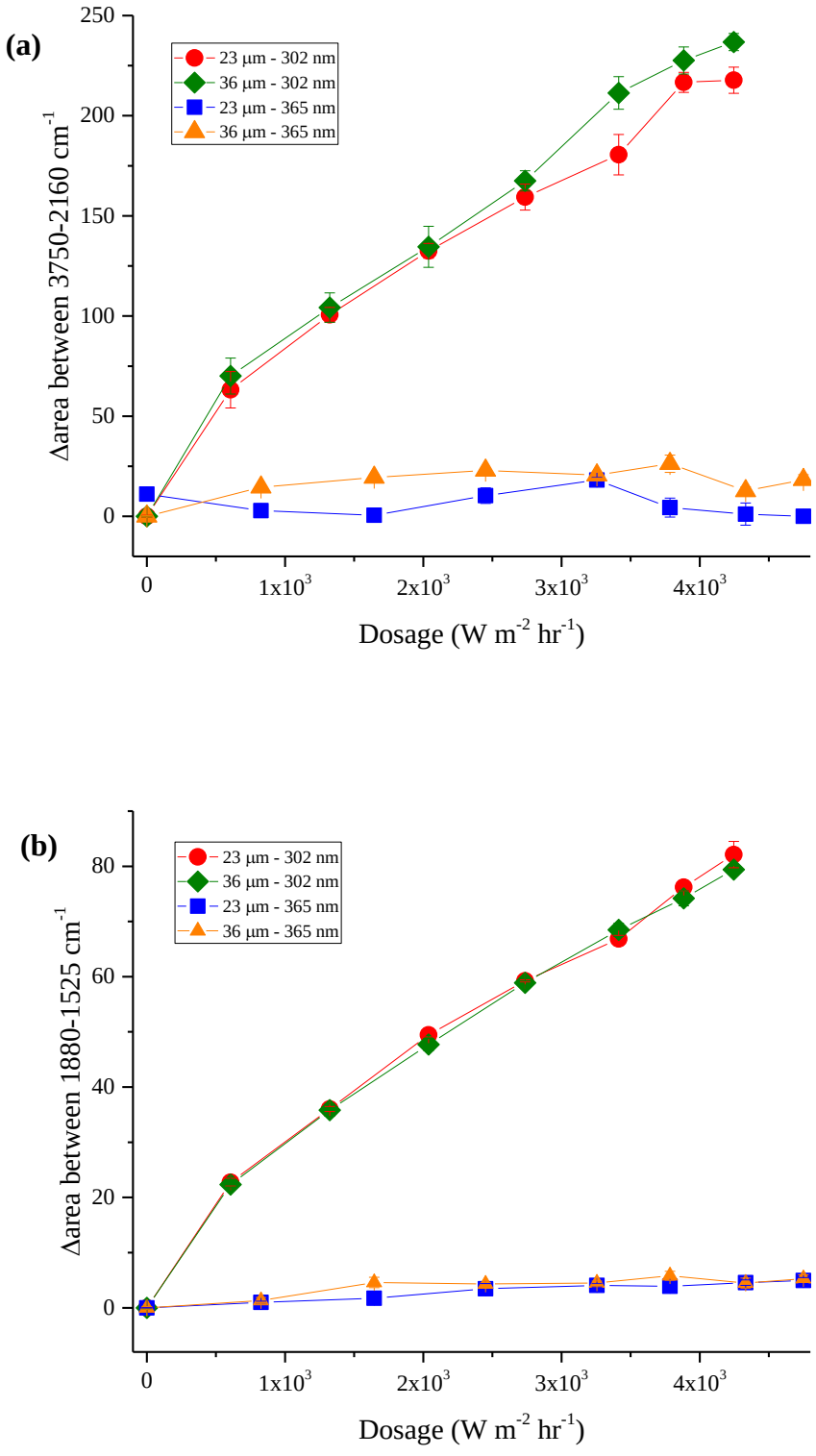

Figure 3.34: Extent of photodegradation of 23 and 36 µm PET measured by the change in area of peaks between (a) 3750-2160 cm^{-1} and (b) 1880-1525 cm^{-1}(carbonyl).

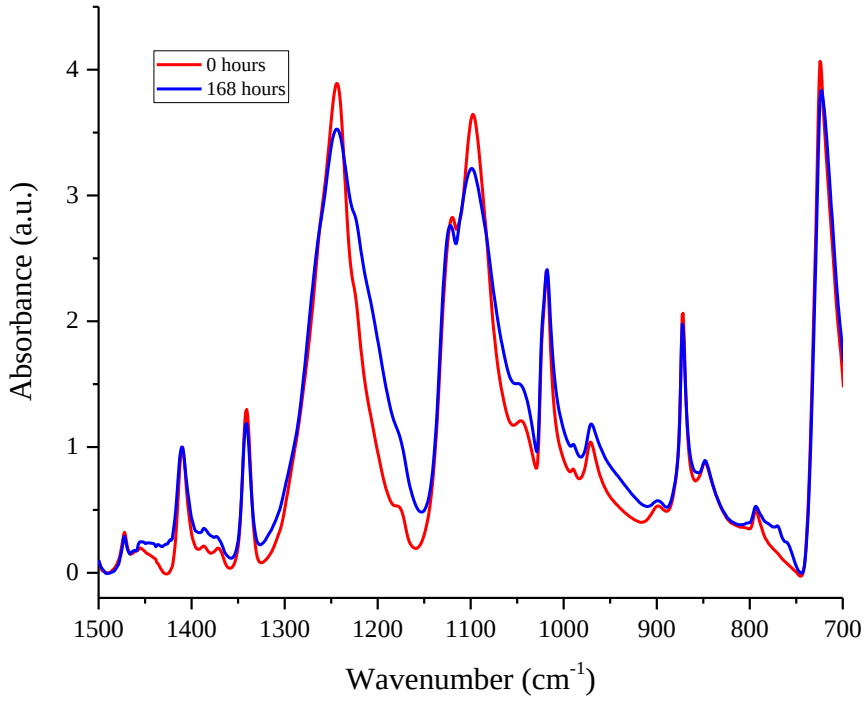

Figure 3.35: ATR FT-IR spectra of 36 µm PET, exposed to 302 nm light, in the fingerprint region between 1500-650 cm^{-1}.

The fingerprint region of the control film and a film exposed to 302 nm light for 168 hours (equivalent to a dosage of approximately 4 x 10^3 W m^{-2} hr^{-1}) are shown in *Figure 3.35*. Assignments for peaks that have changed or developed in this region are given in *Table 13*.

After exposure, peaks have developed at 1430 and 1220 cm^{-1} and have been assigned to the carboxylic acid dimer, as well as the evolution of a peak at 940 cm^{-1} related to the production of vinyl groups. Peaks associated with the trans and cis isomers of the ethylene glycol segment have shown a reduction in size, linked to the scission of the ester links during photodegradation. There has also been changes in the peak at 848 cm^{-1} and the development of two new peaks at 769 and 758 cm^{-1}, which indicate change in the substitution pattern of the terephthalic ring.

Interestingly, there has been no development of a peak at 778 cm^{-1} when samples were exposed to 302 nm or 365 nm light. This is in contrast to the results for samples irradiated in the weatherometer, shown in *Figure 3.13*. The peak at 778 cm^{-1} is believed to be associated with the production of mono-substituted rings. These results indicate that for this peak to evolve a broad wavelength range must be used during exposure instead of narrow wavelength ranges. It is thought that more than one wavelength of light is playing a part in the production of these mono-substituted rings. This peak will be discussed further in *Chapter 4*, where PET has been pre-exposed to one wavelength of light before being exposed to another wavelength of light.

Table 13: Band assignments for the fingerprint region of the ATR FT-IR spectrum of PET.

Peak (cm^{-1})	Assignment
1430	Combination band due to C-O stretching and O-H deformation vibration, associated with carboxylic acid dimer.[24]
1220	C-O stretching vibration, associated with carboxylic acid dimer.[24]
970	Stretching of C-H bond of the trans isomer of the ethylene glycol unit.[2]
940	C-H vibration associated with vinyl groups.[34]
898	Stretching of C-H bond of the cis isomer of the ethylene glycol unit.[2]
848	C-H deformation of two adjacent hydrogens on the terephthalic ring (indicates 1, 4 substitution)[4]
769	Out-of-plane deformation vibrations of 1, 2, 3-substituted rings[24]
758	Out of plane deformation vibrations of 1, 2, 4-substituted rings[24]

From the ATR spectra, it can be concluded that PET is more susceptible to 302 nm light than 365 nm light, on the surface.

The crystallinity of the film samples was calculated using the area of the crystalline (1472 cm^{-1}) and amorphous (1453 cm^{-1}) CH_2 glycol peaks in the ATR spectra.[2] The percentage crystallinity for PET films was calculated using *Equation 3*.

$$\%\ crystallinity = \frac{A_{1472}}{A_{1472} + A_{1453}}\ x\ 100\% \qquad \textbf{Equation 3}$$

Where A_{1472} is the area of the crystalline peak and A_{1453} is the area of the amorphous peak. *Figure 3.36* shows the percentage crystallinity values for 23 and 36 µm films exposed to 302 and 365 nm light, independently.

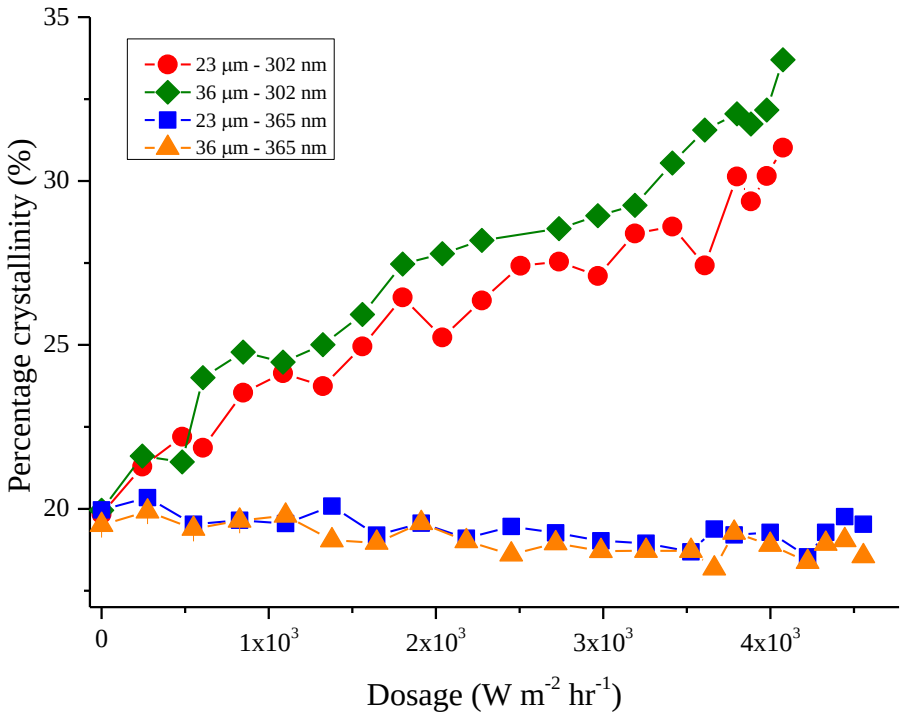

Figure 3.36: Percentage crystallinity for 23 and 36 µm PET film exposed to 365 nm and 302 nm light against dosage.

Figure 3.36 shows that samples exposed to 302 nm light show an increase in crystallinity with exposure time, on the surface of the sample. However, films exposed to 365 nm light show no meaningful change in crystallinity on the surface.

An increase in crystallinity was expected in film samples exposed to 302 nm light due to a process known as chemicrystallisation. This process has been reported to occur during hydrolytic degradation of PET and during photo-oxidation in other polymers.[63] During this study, PET films were exposed below their T_g and it has been noted that polymers are unable to exhibit chemicrystallisation when they are irradiated at a temperature below their T_g. However, chemicrystallisation can occur in PET, below the T_g, if the samples are exposed in an environment that contains significant amounts of moisture. This is because water can act as a plasticiser, promoting molecular mobility and therefore chemicrystallisation can occur.[5,64]

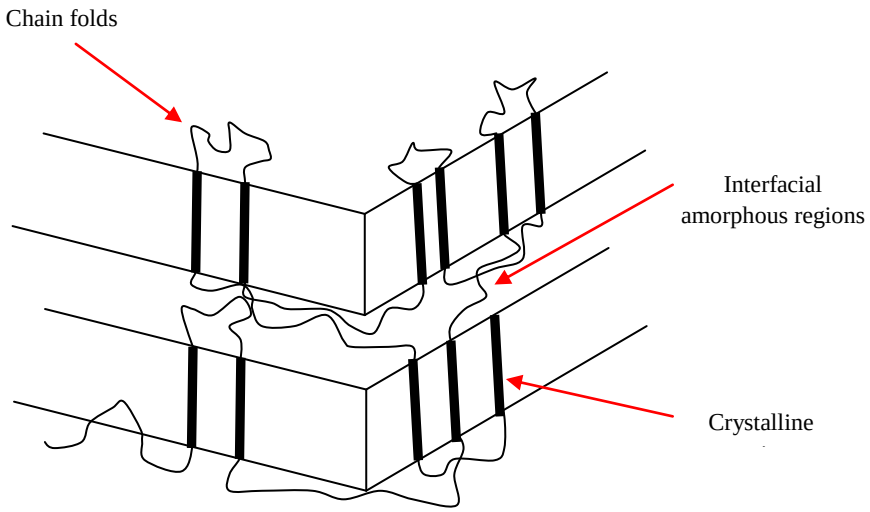

Figure 3.37: Illustration of crystalline regions, amorphous regions and chain folds in a semi-crystalline polymer.[65]

Chemicrystallisation involves chain scission only taking place in the amorphous regions and chain folds of the polymer, during initial degradation, due to the inaccessibility of the crystalline regions. *Figure 3.37* shows an illustration of the crystalline and amorphous regions in the polymer, as well as the chain folds present. Chain scission leads to the production of small chain fragments which have sufficient mobility to realign in the polymer media, resulting in an increase in the polymers crystallinity.[49–51]

During this study the method by Ma *et al.* for the determination of end groups in PET, using NMR, was trialled. It was however, noted that the increase in percentage crystallinity that we see from the IR data, in *Figure 3.36*, meant it was no longer possible to use this method as the films would no longer dissolve in the solvent.

3.4.2 DRIFT

The DRIFT spectra of samples exposed to 302 nm light, for 1 week (equivalent to a dosage of approximately 4.2 x 10^3 W m^{-2} hr^{-1}) in 24 hour increments (equivalent to a dosage of approximately 6.1 x 10^2 W m^{-2} hr^{-1}), are shown in *Figure 3.38*. This shows that there has been change in the region between 3800-2100 cm^{-1} and the carbonyl region. This indicates that 302 nm light effects both the bulk and the surface. The DRIFT spectra for samples exposed to 365 nm light, for 1 week (equivalent to a dosage of approximately 4.8 x 10^3 W m^{-2} hr^{-1}) in 24 hour increments (equivalent to a dosage of approximately 8.3 x 10^2 W m^{-2} hr^{-1}), are shown in *Figure 3.39* and show that only minor changes have occurred with exposure time.

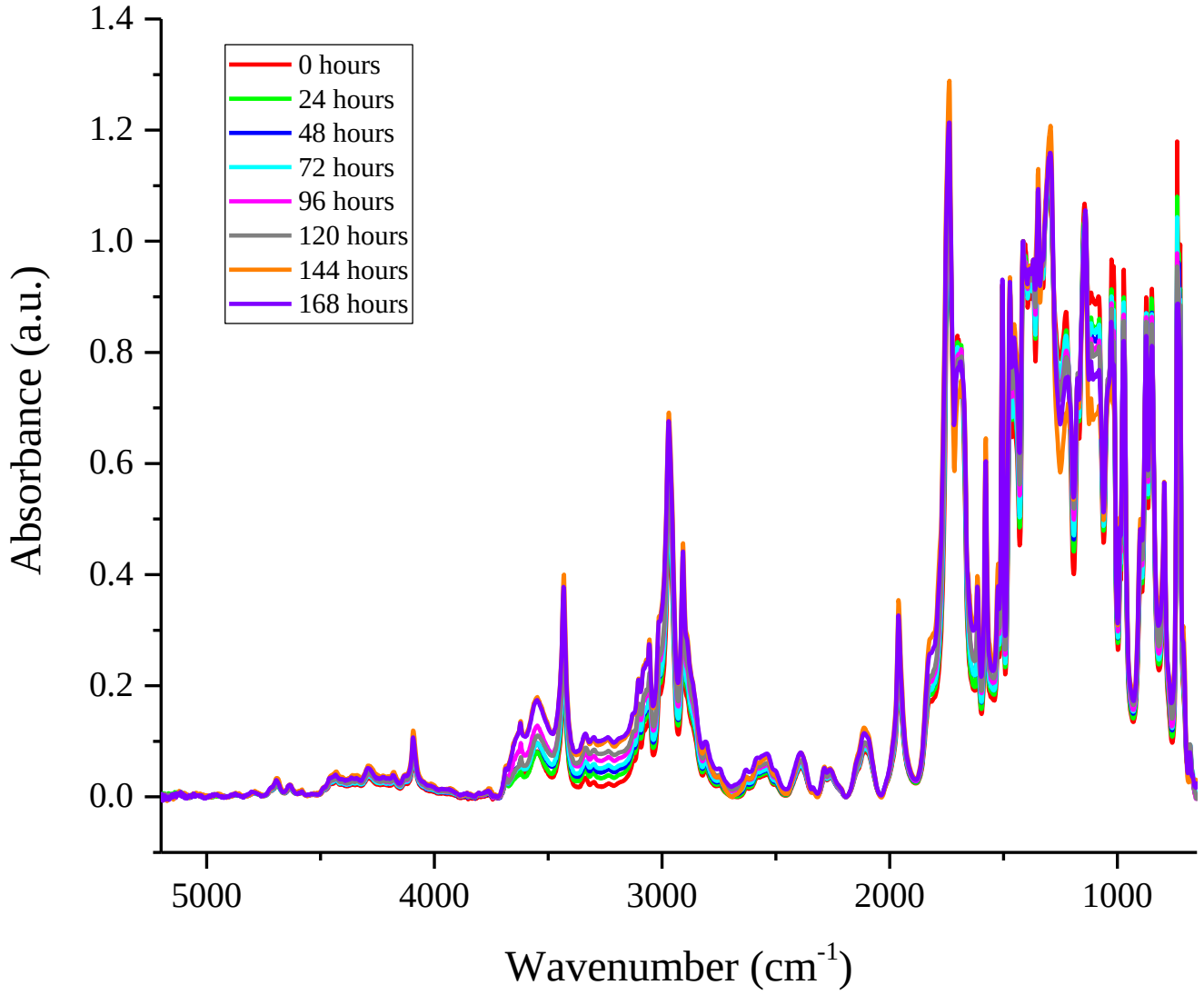

Figure 3.38: DRIFT spectra of 36 µm PET film exposed to 302 nm light for 1 week, in 24 hour increments.

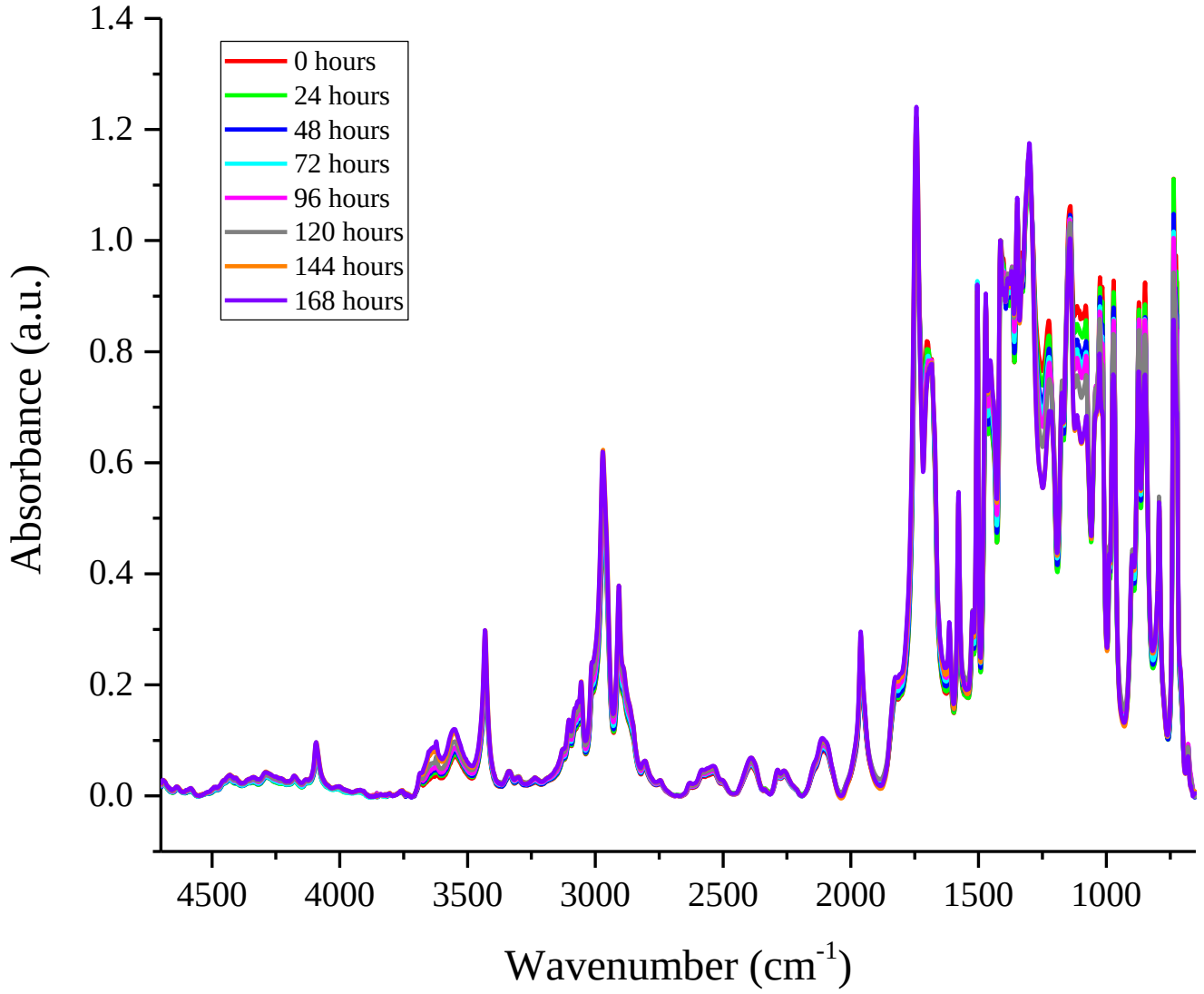

Figure 3.39: DRIFT spectra of 36 µm PET film exposed to 365 nm light for 1 week, in 24 hour increments.

Table 14 gives the assignments for the peaks present in the region between 3800-2100 cm^{-1} for samples exposed to 302 nm light. The main change in this region is the increase in absorbance of the peaks assigned to the aqueous, alcoholic and carboxylic acid hydroxy stretches. This indicates the production of new hydroxy groups during exposure, including carboxylic acid end groups. This region has been discussed in detail in *Section 3.3.2*.

Table 14: Band assignments for the region between 3800-2100 cm^{-1} of the DRIFT spectrum of PET.

Peak (cm^{-1})	Assignment
3620	Aqueous O-H stretching vibration[1]
3550	Alcoholic O-H stretching vibration[1]
3430	First overtone of the carbonyl group in ester[1]
3335	First overtone of carbonyl group in carboxylic acid end group[36]
3290	Carboxylic acid end groups[1]
3100, 3078, 3067, 3054	Aromatic C-H stretching[2]
3015, 2970, 2908	Crystalline aliphatic CH_2 stretching[2]
2963, 2855	Amorphous aliphatic CH_2 stretching[2]

The peaks in the carbonyl region of the DRIFT spectra (*Figure 3.38*) have been assigned and are given in *Table 15*. Carbonyl peaks present in the control film include those assigned to the carbonyl stretch of the ester and those of the terminal acid end groups. After exposure, a shoulder has developed at higher wavenumbers which has been assigned to the carbonyl stretch of the anhydride group. These peaks have been discussed in further detail in *Section 3.3.2*.

Table 15: Band assignments for the carbonyl region of the DRIFT spectrum of PET.

Peak (cm^{-1})	Assignment
1785	Carbonyl stretch from anhydride carbonyl[22]
1743	Carbonyl stretching vibration of an ester[36]
1683	Carbonyl stretch from terminal acid end groups[36]

As discussed previously, the extent of photodegradation was measured by the change in area of peaks between 3800-2100 cm^{-1} and the carbonyl peak. The change in area of these peaks was plotted against dosage for 23 and 36 µm PET films, exposed to 302 nm and 365 nm light, and are given in *Figure 3.40 (a) and (b).* Both graphs show that the PET exposed to 302 nm light increases in change in area with dosage. However, if you compare the samples exposed to 302 nm light with those exposed to 365 nm light the difference in the extent of degradation is smaller than those reported from the ATR spectra (*Figure 3.34*). This indicates that 302 nm light predominately affects the surface of the sample, whereas 365 nm light primarily affects the bulk of the film.

At longer hours of exposure/higher dosages differences between the different thicknesses of films, exposed to the same wavelength of light, are starting to become apparent. This is understandable as DRIFT analyses the whole of the film and different thicknesses of film will degrade to different extents.

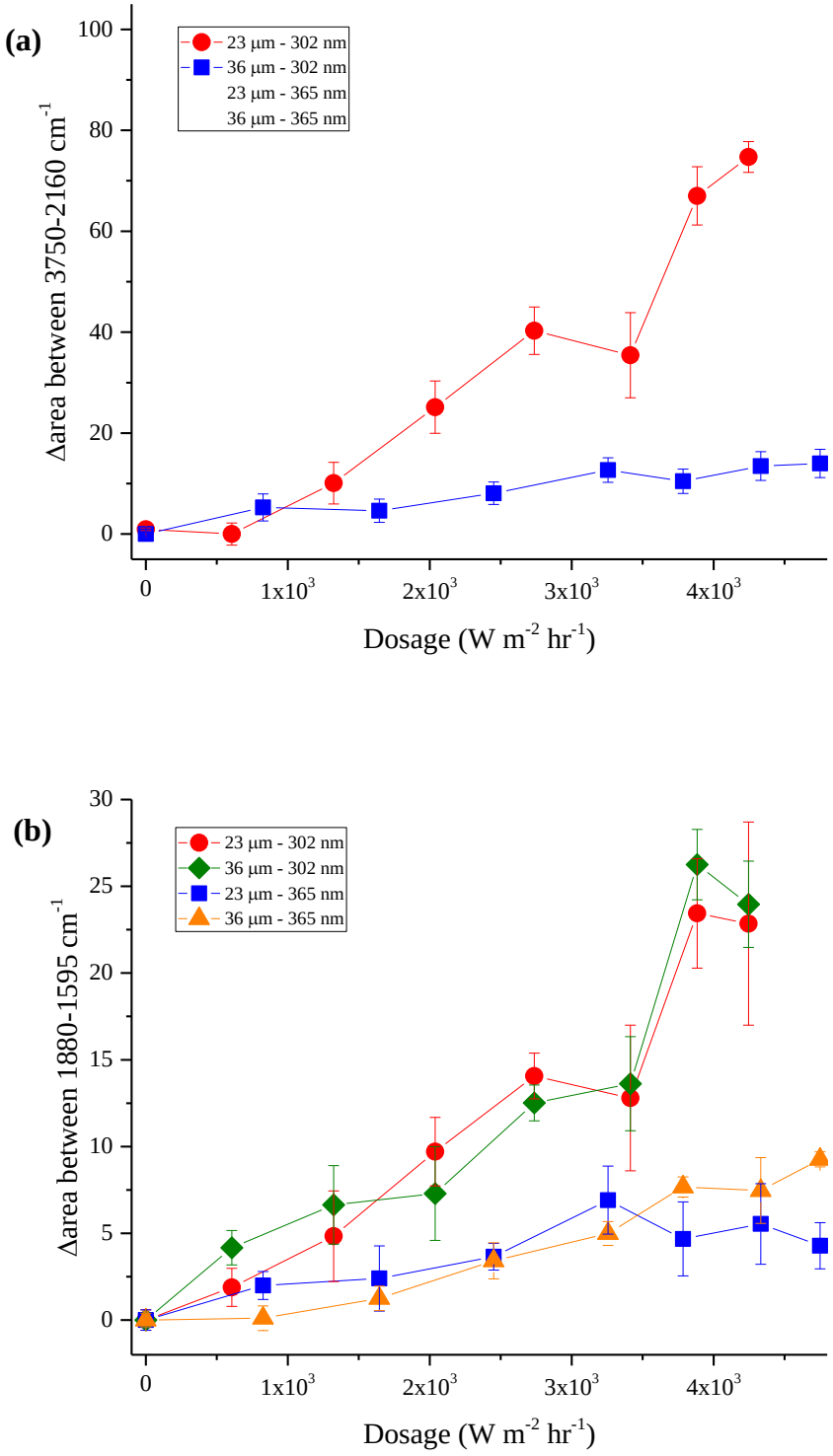

Figure 3.40: Extent of photodegradation of 23 and 36 µm PET measured by the change in area of peaks between (a) 3750-2160 cm^{-1} and (b) 1880-1595 cm^{-1}(carbonyl).

3.4.3 UV-visible spectroscopy

Figure 3.41 (a) shows the UV-visible spectra for samples exposed to 302 nm light for 1 week, analysed every 24 hours. From the UV-visible spectra, it is apparent that there has been an increase in absorbance at 340 nm and a minor increase at 400 nm, with exposure time. This indicates that new chromophores have been produced during exposure.

The increase in absorbance at 340 nm has been previously discussed in *Section 3.3.3* and attributed to monohydroxy terephthalate groups. These species were identified by Pacifici and Straley,[38] and a pathway for their production was proposed by Day and Wiles,[38] which is given in *Chapter 1, Figure 1.28*. The minor increase in absorbance at 400 nm has also been discussed in *Section 3.3.3* and has been attributed to the production of quinone groups. Mechanisms for the formation of these groups have been proposed by and Fechine *et al.,* shown in *Chapter 1, Figure 1.31*.[31]

On the other hand, exposing PET films to 365 nm light shows only minor changes in the region form 340-400 nm. UV-visible spectra were taken every 24 hours of exposure and are shown in *Figure 3.41 (b).* The spectra show minor increases in absorbance at 340 nm and 400 nm with exposure time, indicating that new chromophores are produced, but to a lesser extent. This is comparable to the IR spectra previously discussed in *Section 3.4.1*.

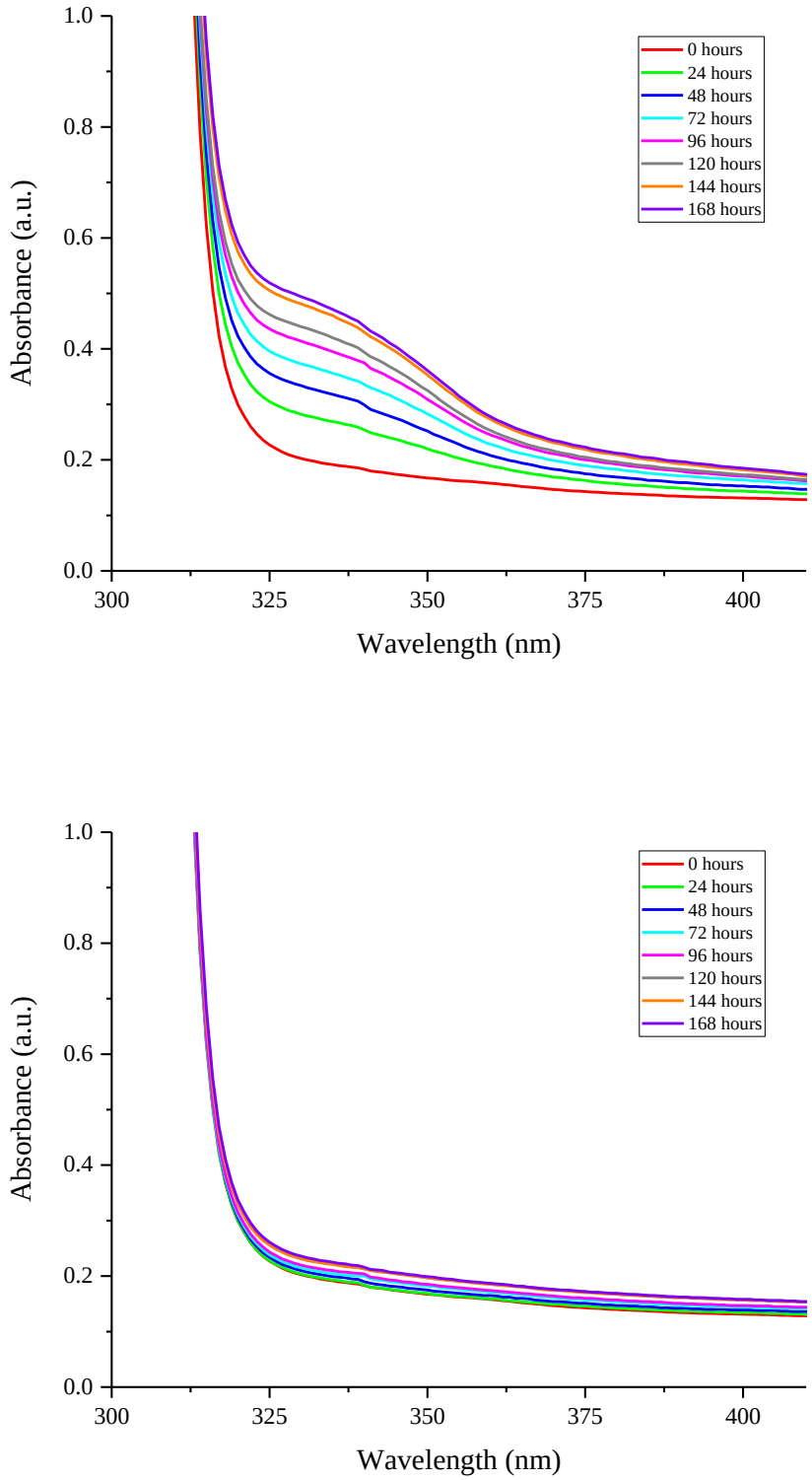

Figure 3.41: UV-visible spectra of 36 µm PET exposed to (a) 302 nm light and (b) 365 nm light for 1 week, in 24 hour increments.

The extent of photodegradation was measured by the change in absorbance, of the UV-visible spectra, at 340 nm. *Figure 3.42* shows the change in absorbance with dosage for 23 and 36 µm PET exposed to 302 nm and 365 nm light, independently. This shows that samples exposed to 302 nm light show a much greater extent of degradation compared to those exposed to 365 nm light. Samples exposed to 365 nm light still show some minor increases with dosage. The UV-visible spectrum for PET shows a high absorbance value at 302 nm light and low absorbance at 365 nm light. The results indicate that even although 365 nm light is only absorbed weakly, this low absorbance is still significant as there are increases in absorbance after exposure. It is expected that 365 nm light would show further degradation if a more intense light source was used or if the samples were exposed for longer.

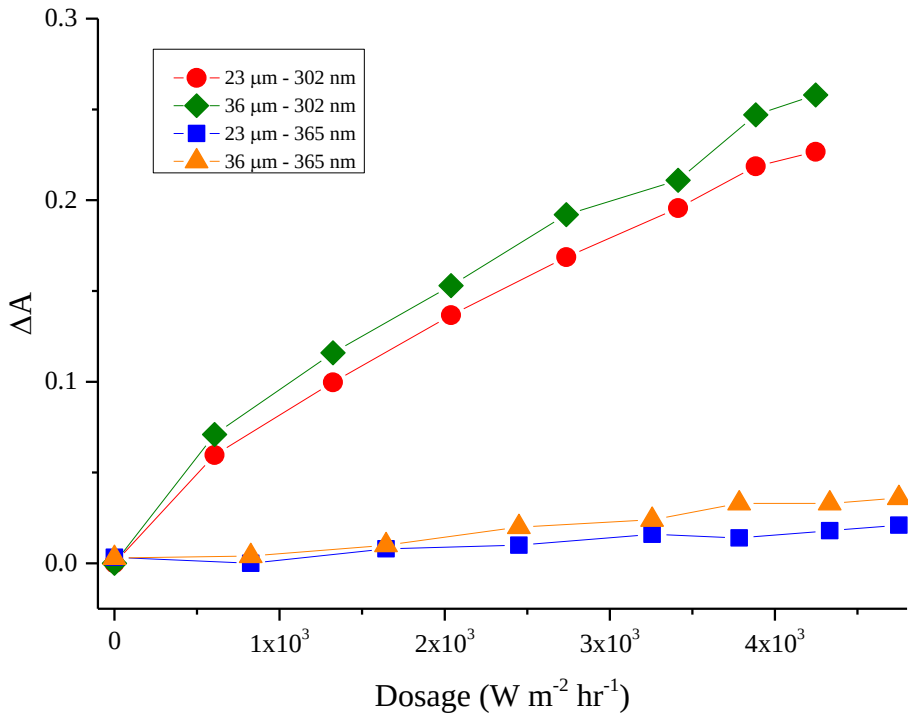

Figure 3.42: Change in absorbance at 340 nm for 23 µm and 36 µm PET films exposed to 365 nm and 302 nm light.

3.4.4 DSC

The thermal properties of the PET film samples before and after exposure were determined using DSC.

3.4.3.1 Heating cycle

Figure 3.43 (a) shows the first heating cycle for samples exposed to 302 nm light for 1 week in 24 hour increments. The melting temperature does not change significantly with exposure time. The melt endotherm shows broadening and thus a small decrease in onset temperature. This indicates that crystals with reduced size, thickness, and lower melting temperatures were produced by chain scission reactions during exposure.[26] This also suggests that at prolonged hours of exposure/higher dosages a decrease in melting temperature may occur.

Figure 3.43 (b) shows the first heating cycles for samples exposed to 365 nm light, respectively. The thermogram shows that there was no significant change in the melting peak after exposure.

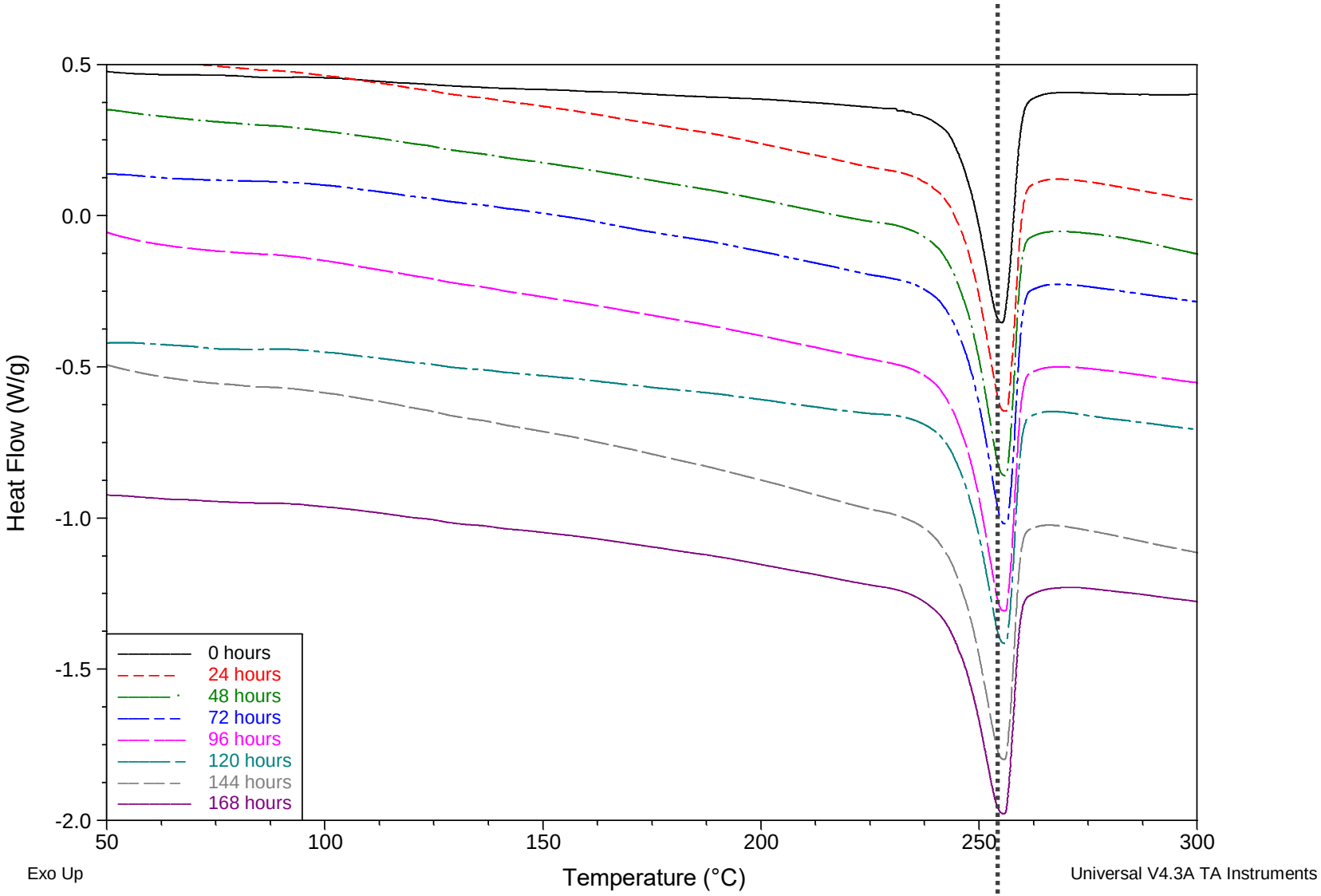

Figure 3.43(a): Heating cycle of DSC thermograms for 36 µm PET exposed to 302 nm light.

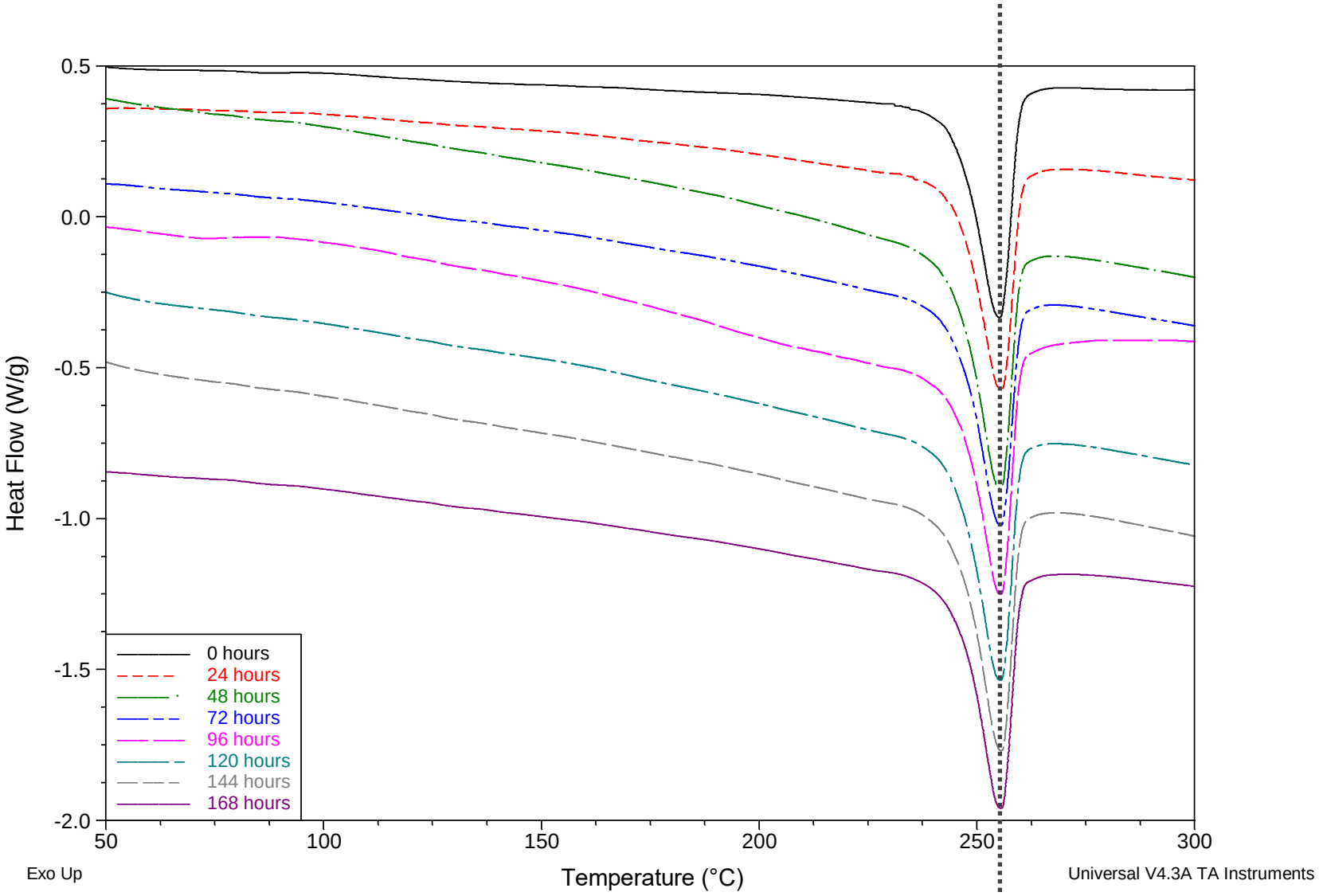

Figure 3.43(b): Heating cycle of DSC thermograms for 36 µm PET exposed to 365 nm light.

3.4.3.2 Cooling cycle

The cooling cycles for 36 µm PET exposed to 302 nm light, in 24 hour increments, are shown in *Figure 3.44 (a)*. The thermograms show that the T_c increases with exposure time, indicating that chain scission has occurred. Chain scission reactions lead to the formation of short chain fragments, which can then easily crystallise during cooling as they have sufficient mobility to realign in the polymer media.[49–51] This means that during the cooling cycle the exposed polymer can crystallise more easily than the control sample which means an increase in T_c.[13–15,] Chain scission reactions have been reported to occur during the photodegradation of PET. [1,31] Grassie and Scott observed that initial chain scission could occur in the ester group at any one of three points, an illustration of this has been given in *Chapter 1, Figure 1.20*.[34]

After the increase in crystallisation temperature there is no subsequent decrease, as seen with samples irradiated in the weatherometer (*Figure 3.24*). Again, this indicates that a broad wavelength range of light is required for chain scission, branching and crosslinking to occur. This data supports the theory that short wavelength light causes chain scission reactions to occur, whereas long wavelength light primarily causes branching and crosslinking to occur during exposure. This will be discussed further in *Chapter 4*, where PET samples are exposed to one wavelength of light followed by another wavelength of light.

Figure 3.44 (b) shows the cooling cycles for samples exposed to 365 nm light in 24 hour increments. The crystallisation temperature does not change significantly with exposure time. However, the cooling cycle for the sample exposed for 120 hours, depicted by the teal line on the graph in *Figure 3.44 (b)*, shows a small decrease in T_c. This is thought to be an outlier as each DSC scan was carried out on a separate piece of PET film each time.

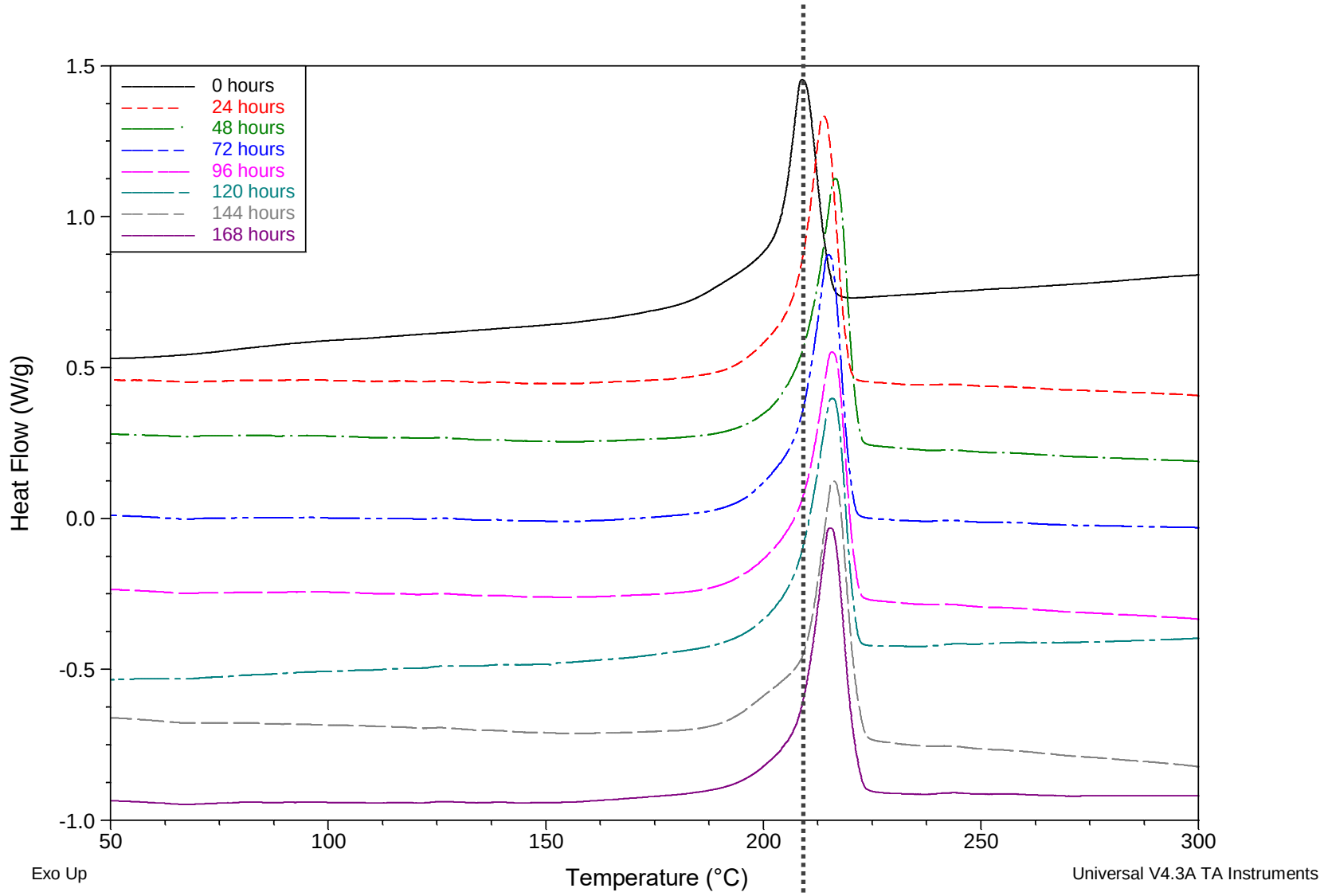

Figure 3.44(a): Cooling cycle of DSC thermograms for 36 µm PET exposed to 302 nm light.

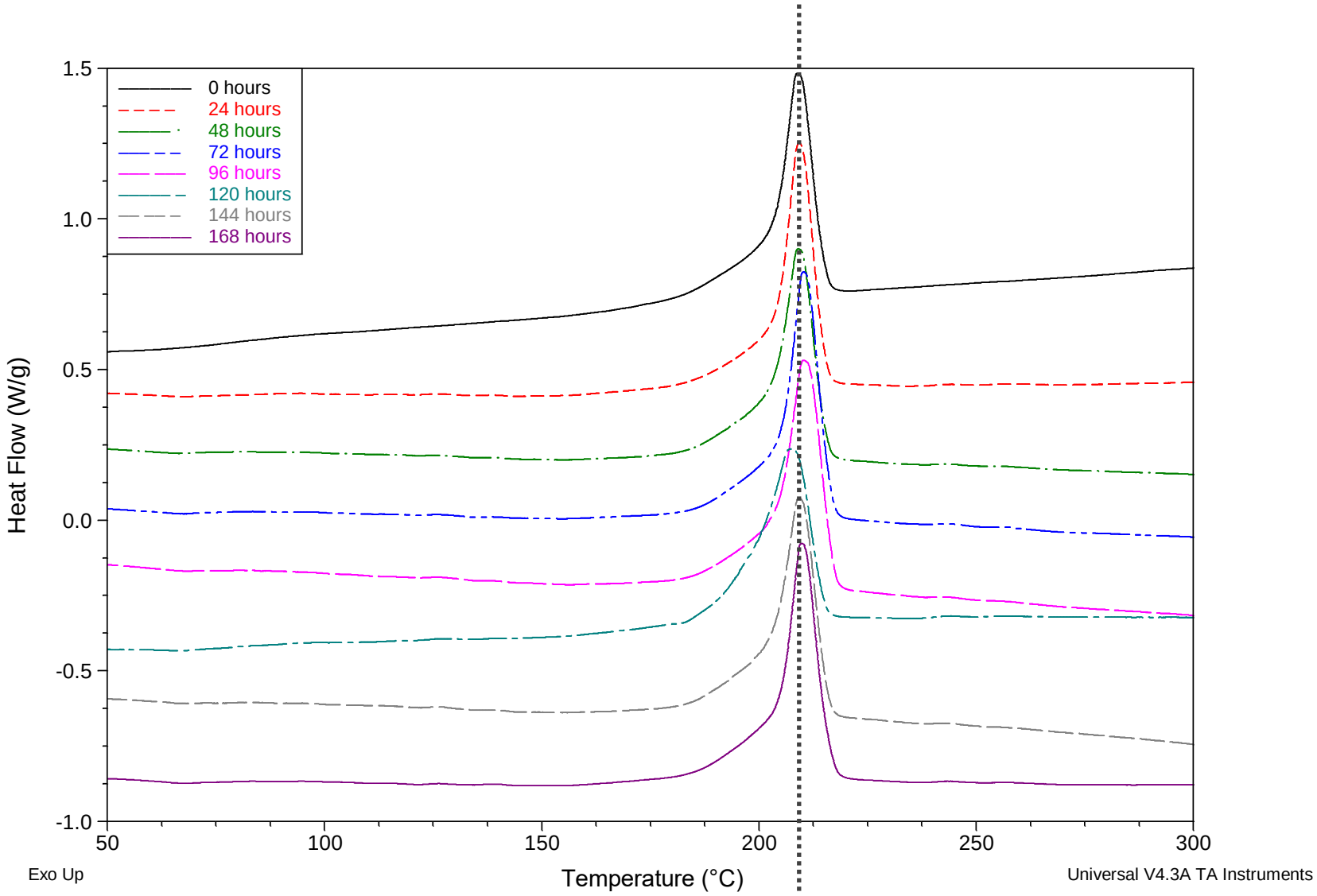

Figure 3.44(b): Cooling cycle of DSC thermograms for 36 µm PET exposed to 365 nm light.

3.4.3.3 Reheat cycle

During the second heating cycle, shown in *Figure 3.45 (a)*, two melting endotherms occur at 247°C and 254°C, corresponding to two different crystalline forms of the polymer. The peak at 247°C originates from the melting of the crystallites formed at the T_c, and the peak at 254°C corresponds to the melting of the original crystallites reorganised during the DSC scan.[56]

From *Figure 3.45 (a)* it is apparent that the peak at 247°C gradually diminishes with exposure time. The fact that the crystallinity of the PET has already increased, as shown in *Figure 3.36*, means that there will be fewer crystallites formed at the crystallisation temperature. It could also be the case that the peak at 247°C is not reducing, but the peak at 254°C is expanding and dominating the region. Due to the increase in crystallinity of the films during exposure, there are more original crystallites, and therefore the peak expands. However, there is no decrease in melt temperature of the peak at 254°C, as seen previously with PET samples irradiated in the weatherometer. This indicates that for crosslinking or branching to occur and cause a decrease in melt temperature, PET must be exposed to a broad wavelength range of light rather than a narrow wavelength range. It is thought that short wavelengths of light cause chain scission in the polymer, whereas long wavelengths of light cause crosslinking or branching reactions to take place during exposure.

Figure 3.45 (b) shows the second heating cycles for samples exposed to 365 nm light, respectively. The thermogram shows that there was no significant change in the melting peak after exposure.

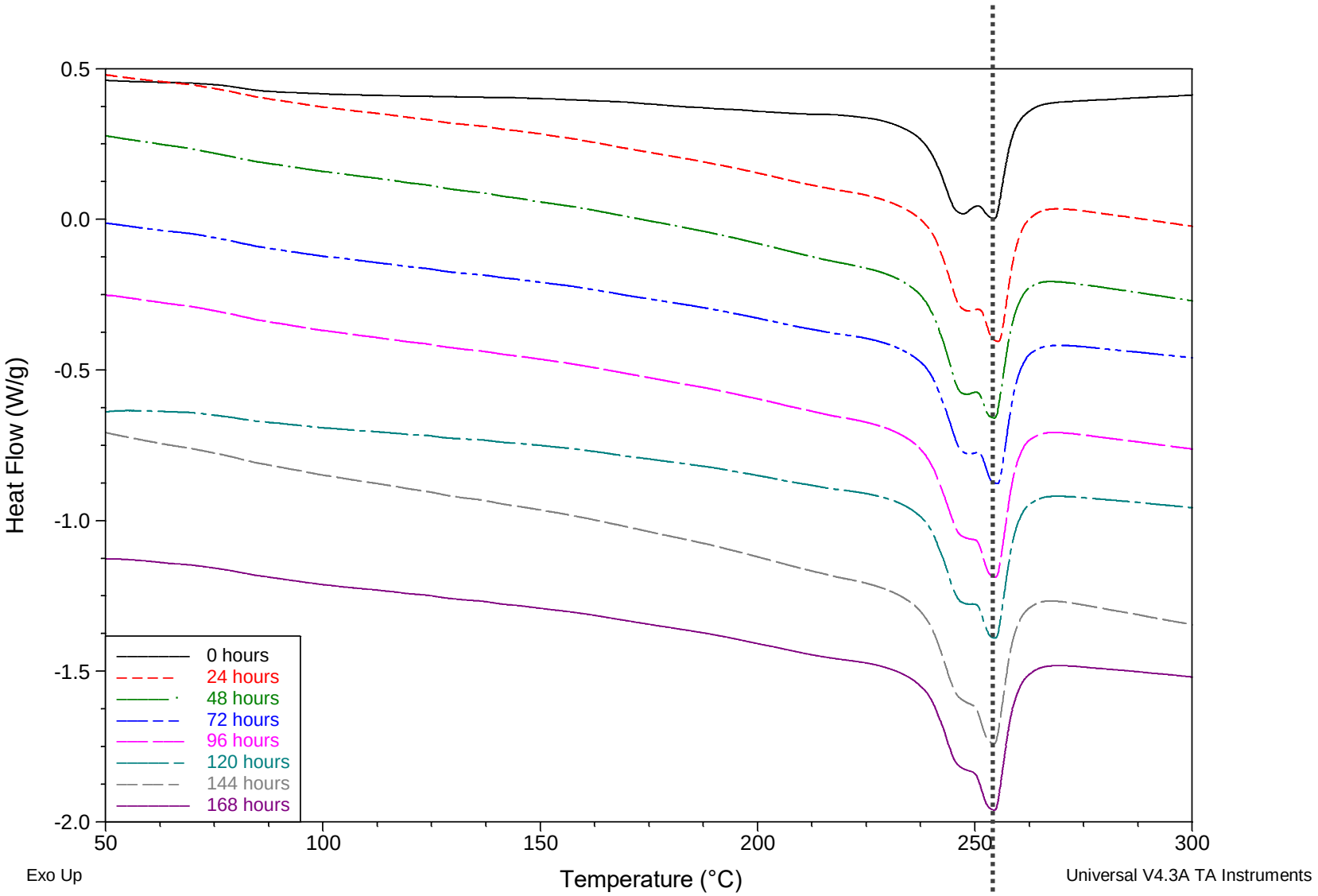

Figure 3.45(a): Reheat cycle of DSC thermograms for 36 µm PET exposed to 302 nm light.

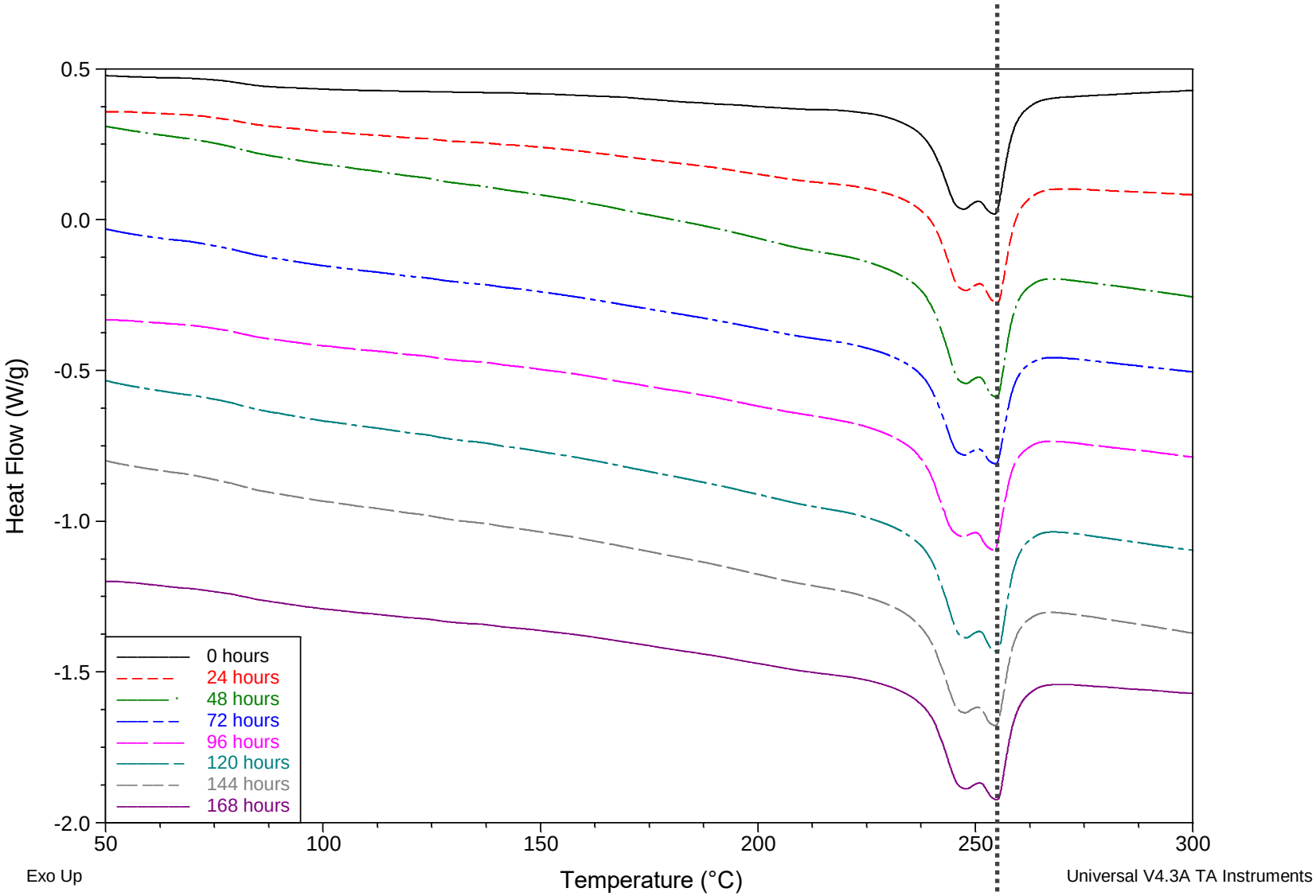

Figure 3.45(b): Reheat cycle of DSC thermograms for 36 µm PET exposed to 365 nm light.

3.4.5 Scanning Electron Microscopy

SEM images of 36 µm PET films exposed to 302 nm light for 1 week in 24 hour increments are shown in *Figure 3.46*. The images show significant changes on the surface after only 72 hours of exposure. At 72 hours surface cracking is visible, which appears to get progressively worse with exposure. Surface cracks can lead to fractures, which will affect the physical properties of the polymer.

3.4.6 General Conclusions

The effect of wavelength on the photodegradation reactions taking place in PET during exposure was studied, using 302 nm and 365 nm light. PET films were shown to degrade faster when exposed to 302 nm light compared to 365 nm light of the same intensity. Films exposed to 302 nm light showed production of carboxylic acid end groups, dimers, anhydrides, aldehydes, quinones and monohydroxy terephthalate groups. Furthermore, results indicated substitution and chain scission reactions, as well as surface cracks, occurring in the samples exposed to 302 nm light, while samples at 365 nm light showed only minor changes. Comparing results from this study to those analysed in the weatherometer study, it is thought that short wavelength light causes chain scission reactions to occur, whereas long wavelength light primarily causes branching and crosslinking reactions during exposure. Upon exposure to light PET appears to degrade more rapidly when exposed to short wavelength light compared to long wavelength light of the same intensity.

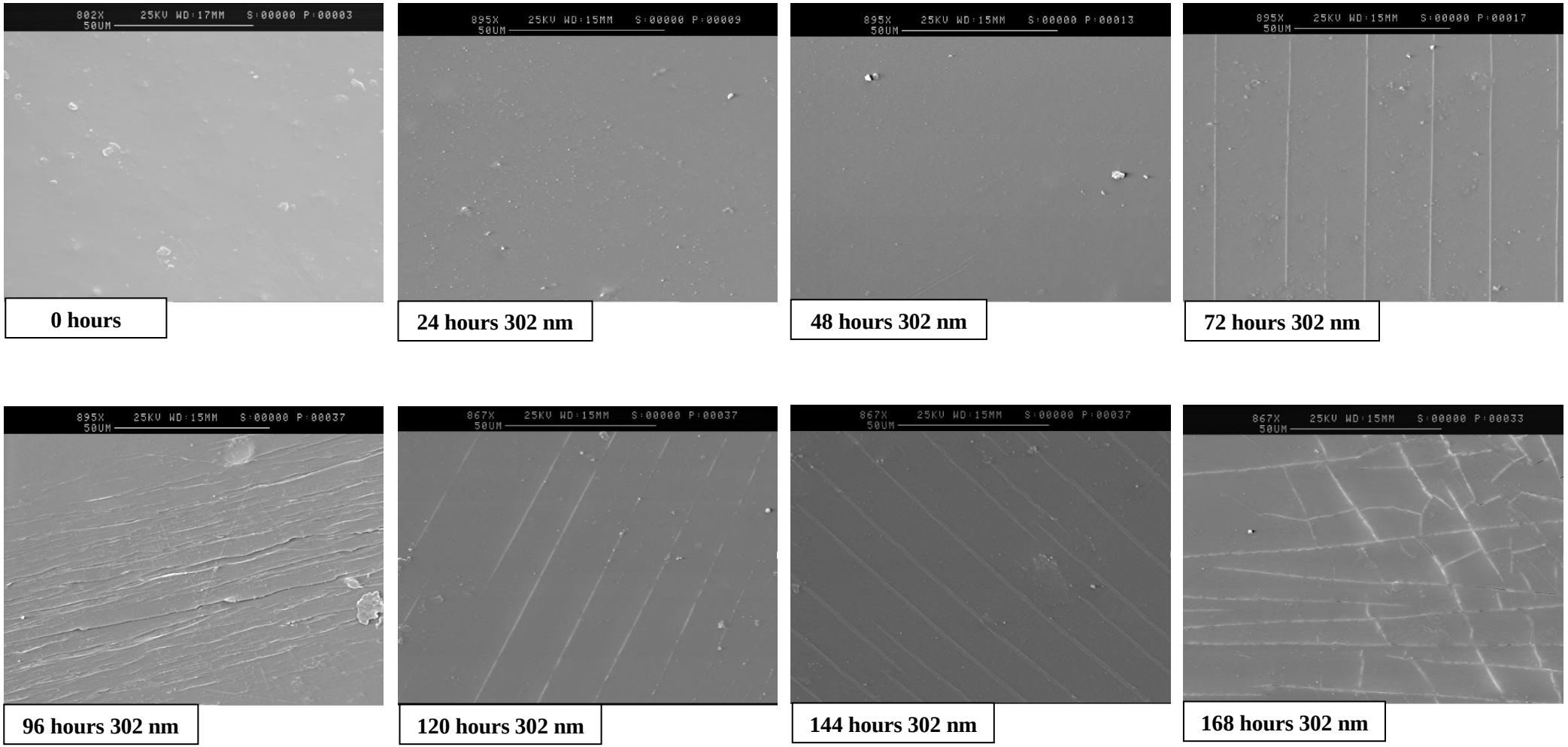

Figure 3.46: SEM images of 36 µm PET film exposed to 302 nm light for 1 week, in 24 hour increments.

3.5 Exposing PET to high intensity 365 nm light

PET films of 36 µm thickness were exposed to high intensity 365 nm light. The lamp used in this study is approximately 26 times more intense than the previous 365 nm lamp. Irradiation was carried out at approximately 43°C under oxidative conditions. As minor changes were identified when PET films were exposed to 365 nm light a more intense lamp was used to allow for any minimal changes to be accentuated. Samples were analysed using ATR FT-IR, DRIFT and UV-visible spectroscopy.

3.5.1 Infrared

Figure 3.47 shows the ATR spectra for samples of PET exposed to high intensity 365 nm light for 6 weeks (equivalent to a dosage of approximately 8.3 x 10^5 W m^{-2} hr^{-1}), in 1 week increments (equivalent to a dosage of approximately 1.4 x 10^5 W m^{-2} hr^{-1}). Peak assignments for the ATR of PET have already been discussed in detail in *Section 3.3.1*. *Figure 3.47* shows only minor changes in the region between 3800-2100 cm^{-1} and the carbonyl region. This agrees with results reported in *Section 3.3.1* and indicates that 365 nm light does not have a significant effect on the surface of the film during exposure. Any minor changes in the spectra could also be due to the fact that a separate piece of film was analysed after each week of exposure.

However, the DRIFT spectra, shown in *Figure 3.48*, shows that significant changes have developed during exposure in the region between 3800-2100 cm^{-1} and at the carbonyl peak. For peak assignments for the DRIFT spectra of PET please refer to *Section 3.3.2*, where they have been discussed in detail. The changes in the spectra follow the same trends as those seen in *Section 3.3.2*.

Exposing PET film to high intensity 365 nm light shows change in the bulk of the film but not the surface. Degradation is preferentially taking place in the bulk of the film rather than the surface. This is understandable when the fact that 365 nm light is weakly absorbed is considered.

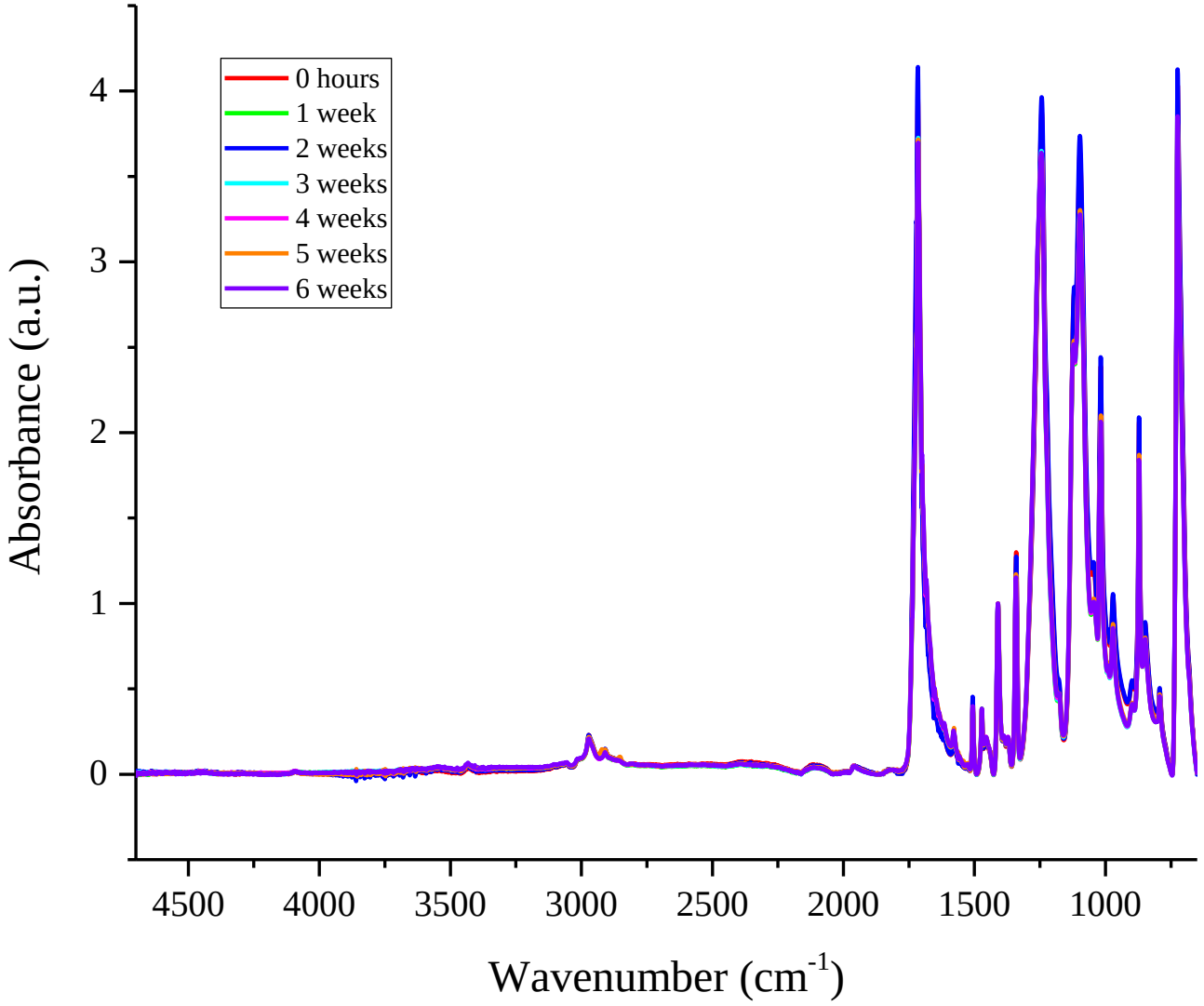

Figure 3.47: ATR FT-IR spectra of 36 µm PET film exposed to high intensity 365 nm light for 6 weeks, in 1 week increments.

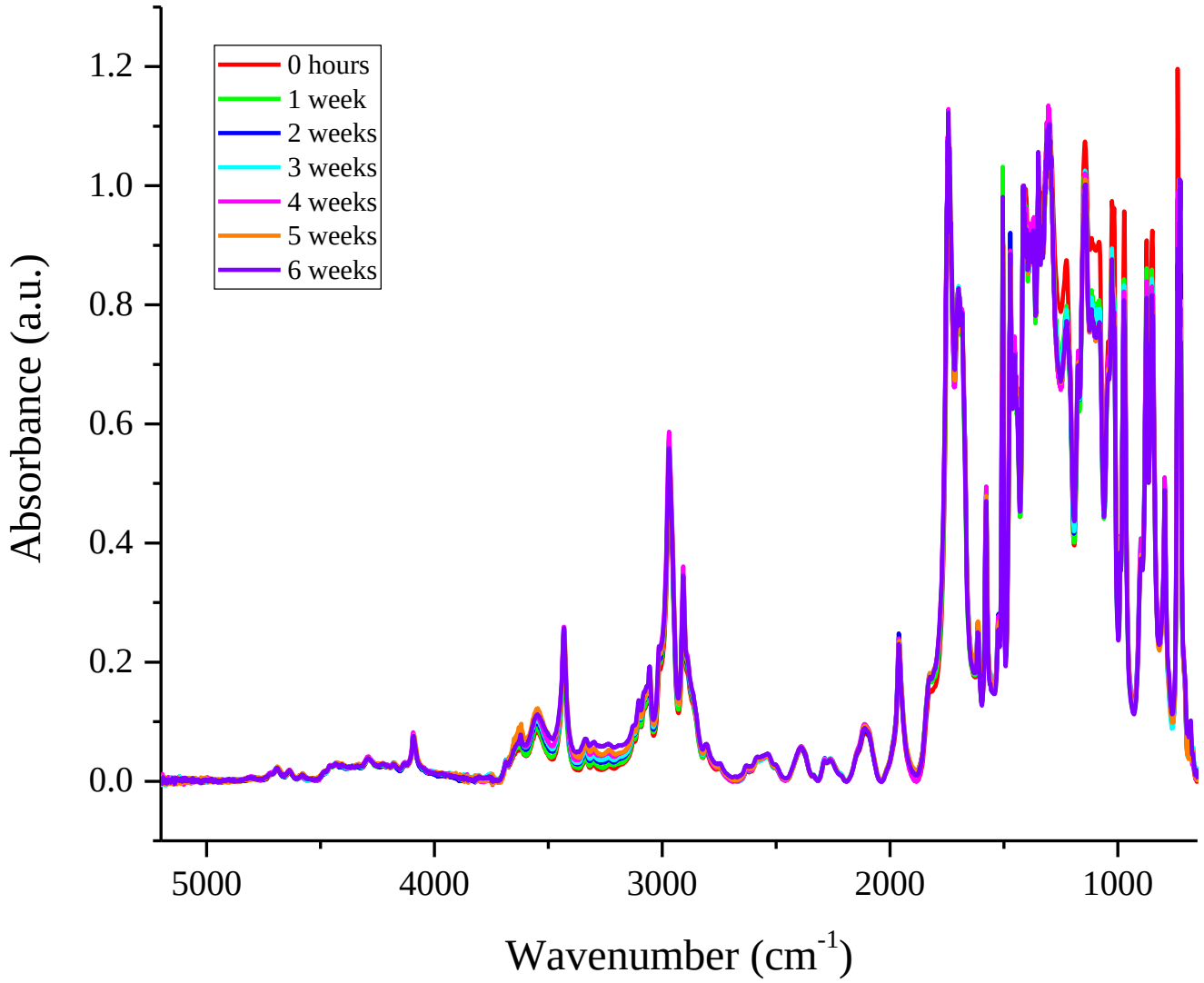

Figure 3.48: DRIFT spectra of 36 µm PET film exposed to high intensity 365 nm light for 6 weeks, in 1 week increments

3.5.2 UV-visible spectroscopy

The UV-visible spectra of samples exposed to high intensity 365 nm light for 6 weeks in 1 week increments are shown in *Figure 3.49*. The spectra show an increase in absorbance at 340 nm and a minor increase at 400 nm. The increase at 340 nm has been attributed to monohydroxy terephthalate groups, while the minor increase at 400 nm is due to the formation of quinone species. The origin of this increase in absorbance has been discussed in *Section 3.3.3*.

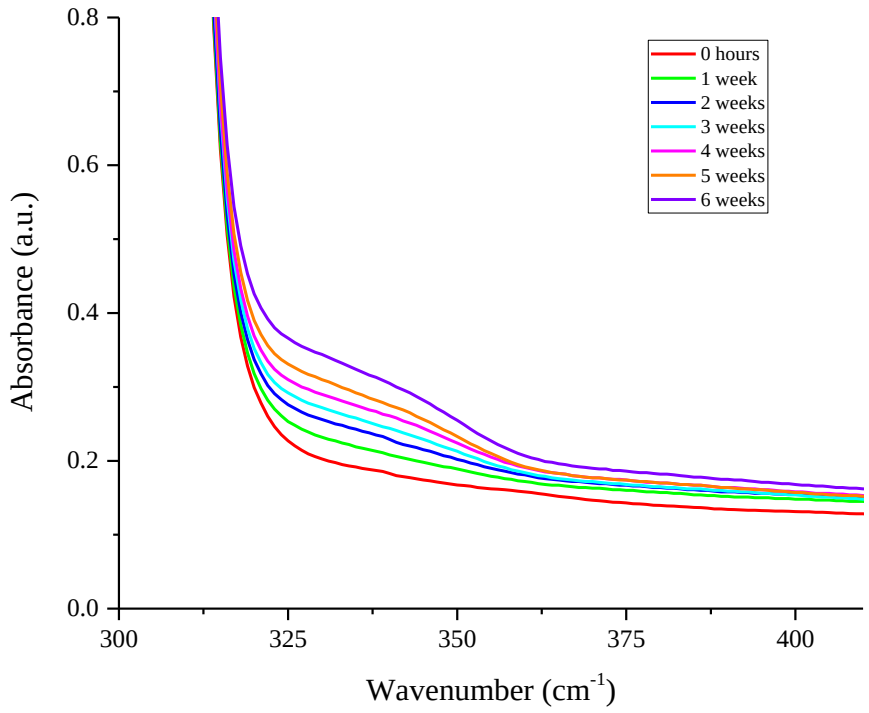

Figure 3.49: UV-visible spectra of 36 µm PET film exposed to high intensity 365 nm light for 6 weeks, in 1 week increments.

UV-visible spectroscopy analyses the whole thickness of the film, and as changes were already identified in the DRIFT spectra (which also analyses the whole thickness of the film), changes were expected in the UV-visible spectra. This, again, indicates that 365 nm light is affecting the bulk of the film.

3.5.3 General Conclusions

High intensity 365 nm light was used to allow for any minimal changes in the PET films to be highlighted during exposure. Long wavelength light has been reported to make no meaningful change during the degradation of PET but reports in the literature have only focused on the surface of the films. DRIFT was used here to allow for the bulk of the film to be analysed. Results showed that the surface of the films showed only minimal change, whereas the bulk of the film showed significant changes in the spectra after exposure. This indicates that 365 nm light is preferentially affecting the bulk of the film rather than the surface.

3.6 Effect of degradation atmosphere on the photodegradation of PET

This short study explored the effect of degradation atmosphere on the photodegradation of 36 μm PET films. The photodegradation cell, shown in *Chapter 2, Figure 2.06,* was used to run exposures under nitrogen. Samples of PET were exposed to 302 nm light, under nitrogen and analysed using ATR FT-IR and DRIFT.

3.6.1 Exposing PET to 302 nm light under nitrogen

3.6.1.1 ATR FT-IR

The ATR spectra of PET exposed to 302 nm light under nitrogen are shown in *Figure 3.50*. PET was exposed for 1 week (equivalent to a dosage of approximately 1.0 x 10^3 W m^{-2} hr^{-1}) and analysed every 24 hours (equivalent to a dosage of approximately 1.4 x 10^2 W m^{-2} hr^{-1}). There are some minor changes in the region between 3800-2100 cm^{-1} and in the carbonyl region. These show the same trends as seen with samples exposed to 302 nm light in an oxidative atmosphere (*discussed in Section 3.4.1*), but from the ATR spectra (*Figure 3.50*) it appears that these changes are occurring to a lesser extent. Peak assignments for the ATR spectra are given in *Section 3.3.1 and* have also been discussed in detail in this section.

Figure 3.51 shows the region of the spectra between 1100-650 cm^{-1} to highlight the development of peaks in this region. Peaks have evolved at 820 and 805 cm^{-1}, but these peaks have not been reported, in this study, when PET was exposed under oxidative conditions. These peaks have been reported to be associated with changes in substitution patterns of the ring and the build-up of conjugated aromatic structures.[4]

Conjugated aromatic structures have been previously reported by Marcotte *et al.* during photolysis of PET. If a hydrogen abstraction reaction was to take place on the ring from a neighbouring molecule, this would cause the formation of free radicals which could be responsible for crosslinking in the polymer.[20] Crosslinking would cause the production of highly conjugated aromatic structures. A pathway for the production of these groups is shown in *Chapter 1, Figure 1.15.*

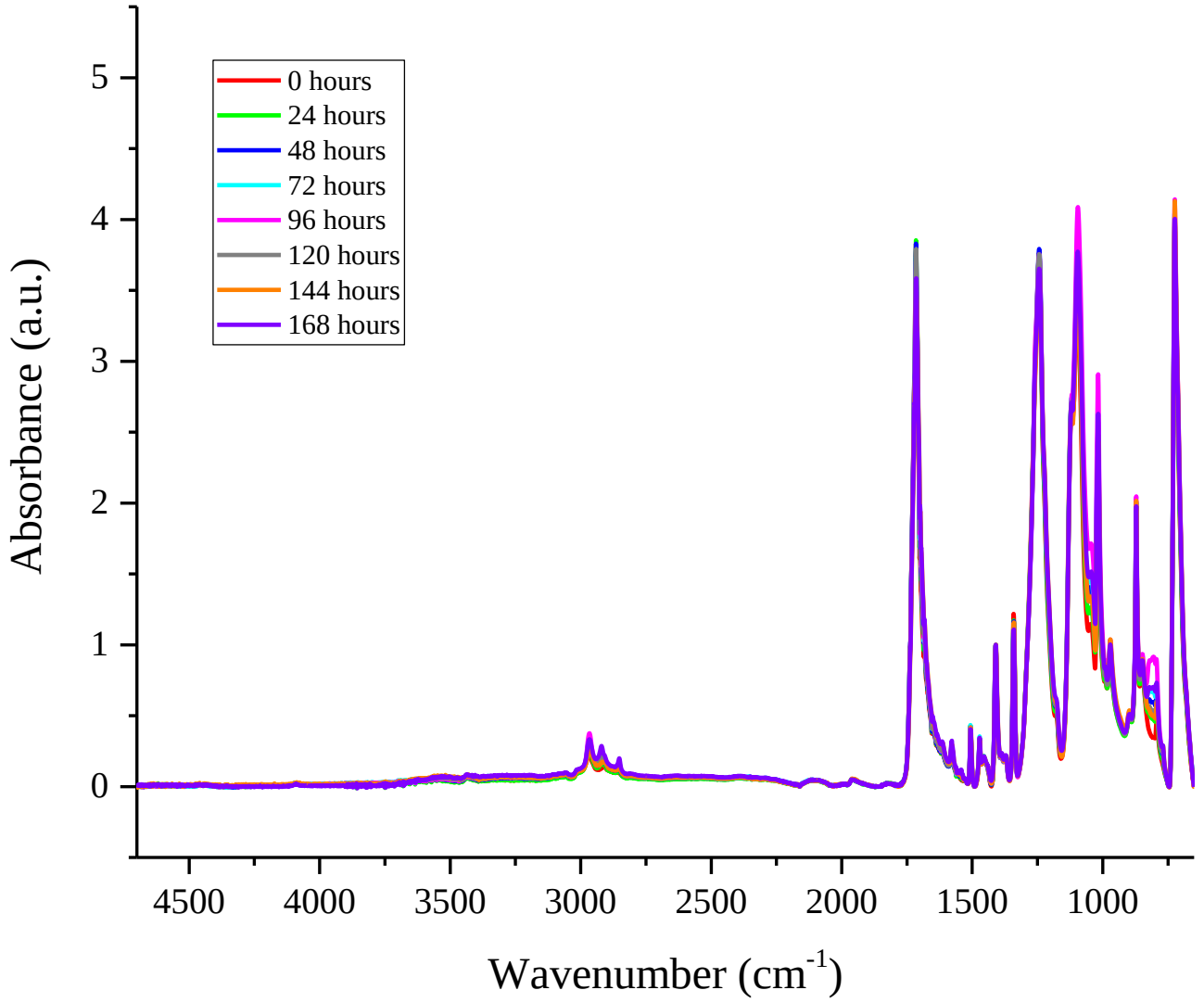

Figure 3.50: ATR FT-IR spectra of 36 µm PET films exposed to 302 nm light for 1 week, in 24 hour increments, under nitrogen.

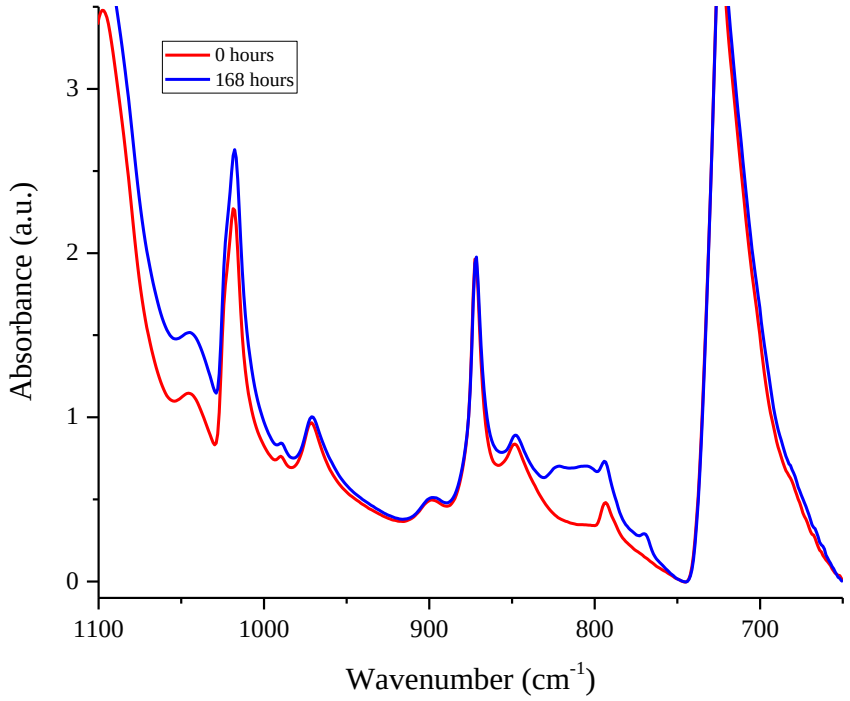

Figure 3.51: ATR FT-IR spectra of 36 µm PET exposed to 302 nm light under nitrogen, in the region between 1100-650 cm^{-1}.

Another peak has developed at 769 cm^{-1} which has been previously assigned to the 1, 2, 3-substituted ring due to the formation of monohydroxy terephthalate groups. These groups can only be produced in an oxidative atmosphere, so it is thought that the cell was not flushed with nitrogen prior to exposure for long enough and therefore oxygen was still present.

The extent of photodegradation of samples exposed to 302 nm and 365 nm light under air and those exposed to 302 nm light under nitrogen, are shown in *Figure 3.52.* Again, the extent of degradation was calculated using the change in area of the peaks between 3750-2160 cm^{-1} and the carbonyl peak between 1880-1525 cm^{-1}. The graphs show that the sample exposed under nitrogen degrades to a lower extent than those exposed under oxidative conditions, to 302 nm light.

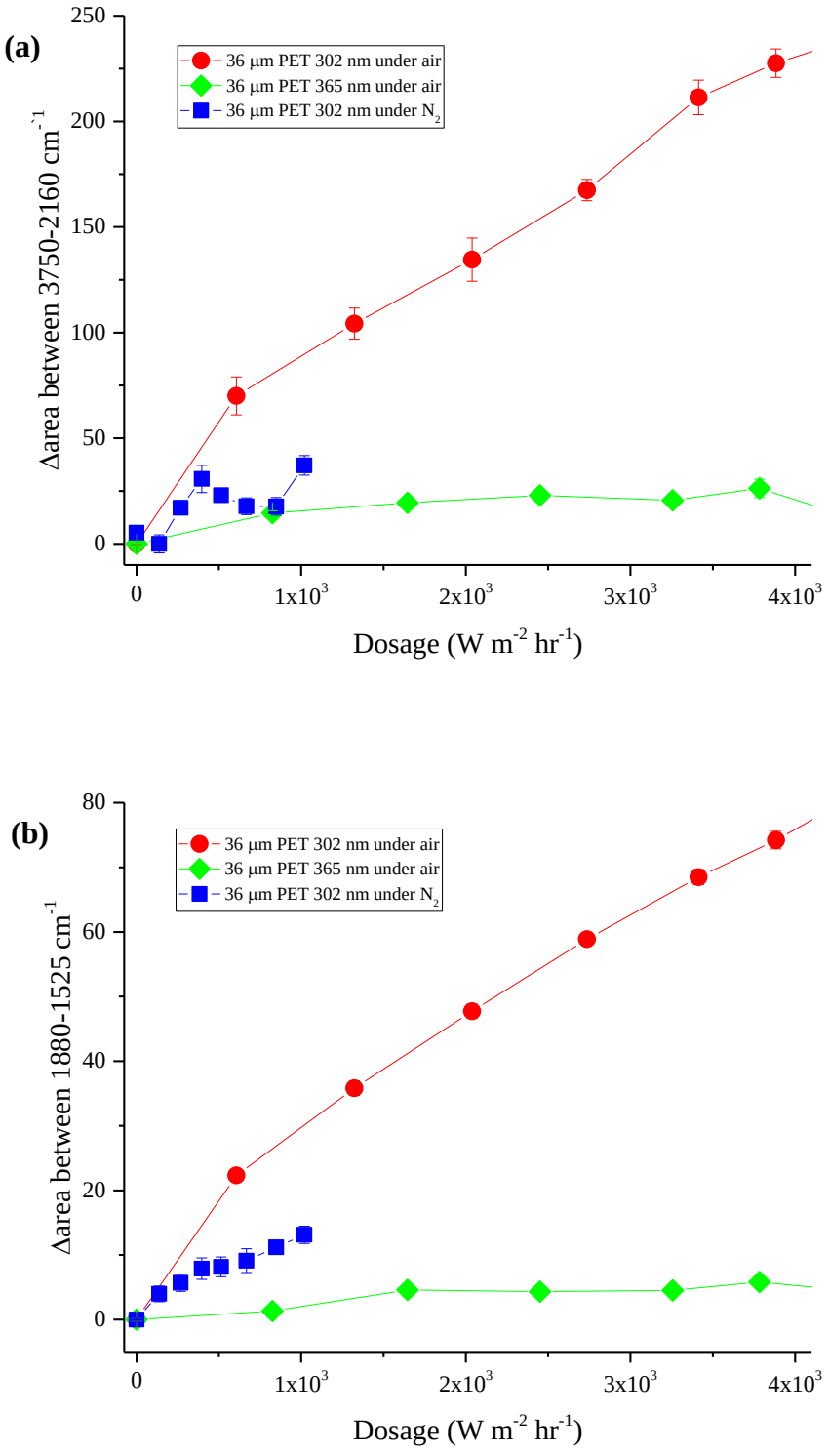

Figure 3.52: Extent of photodegradation of 36 µm PET, exposed under air and nitrogen, measured by the change in area of peaks between (a) 3750-2160 cm^{-1} and (b) 1880-1525 cm^{-1}(carbonyl).

Photodegradation of PET in an oxidative atmosphere combines effects of both photolysis and oxidative reactions. The photolysis process is important in a non-oxidative environment but in the presence of oxygen, photo-oxidation is thought to be the most important degradation process. Therefore, in this case, the samples exposed under nitrogen degrade to a lesser extent due to the absence of oxygen.

Marcotte *et al.* and Day and Wiles have proposed mechanistic pathways for the photodegradation of PET under non-oxidative conditions, as shown in *Chapter 1, Figure 1.14 and 1.18*, respectively.

3.6.1.2 DRIFT

The DRIFT spectra of samples exposed to 302 nm light under nitrogen, for 1 week (equivalent to a dosage of approximately 1.0 x 10^3 W m^{-2} hr^{-1}) in 24 hour increments (equivalent to a dosage of approximately 1.4 x 10^2 W m^{-2} hr^{-1}), are shown in *Figure 3.53*. The spectra show some minor changes in the region between 3800-2100 cm^{-1} and in the carbonyl region. The peak assignments for the DRIFT spectra of PET are given in *Section 3.3.2*, where they have also been discussed in detail. The changes in the spectra follow the same trends as those seen in *Section 3.4.2*, but from the spectra in *Figure 3.53*, it appears that the changes occur to a lesser extent. However, the cell used to hold the film had to be placed further away from the UV lamp and therefore the intensity of light that the film was exposed to was lower than those exposed in *Section 3.4.2*. Therefore, it is necessary to analyse the rates against dosage.

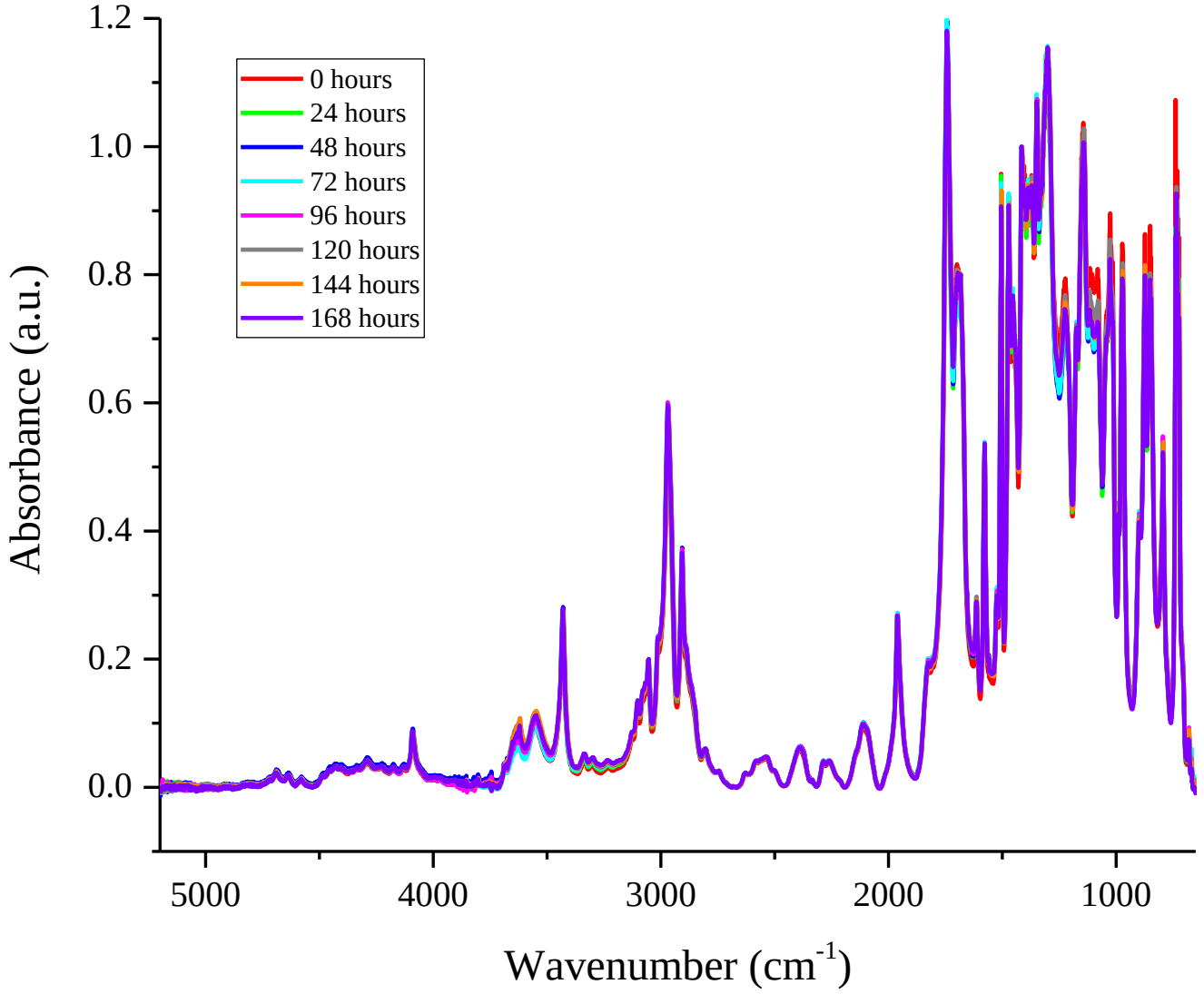

Figure 3.53: DRIFT spectra of 36 µm PET films exposed to 302 nm light for 1 week, in 24 hour increments, under nitrogen.

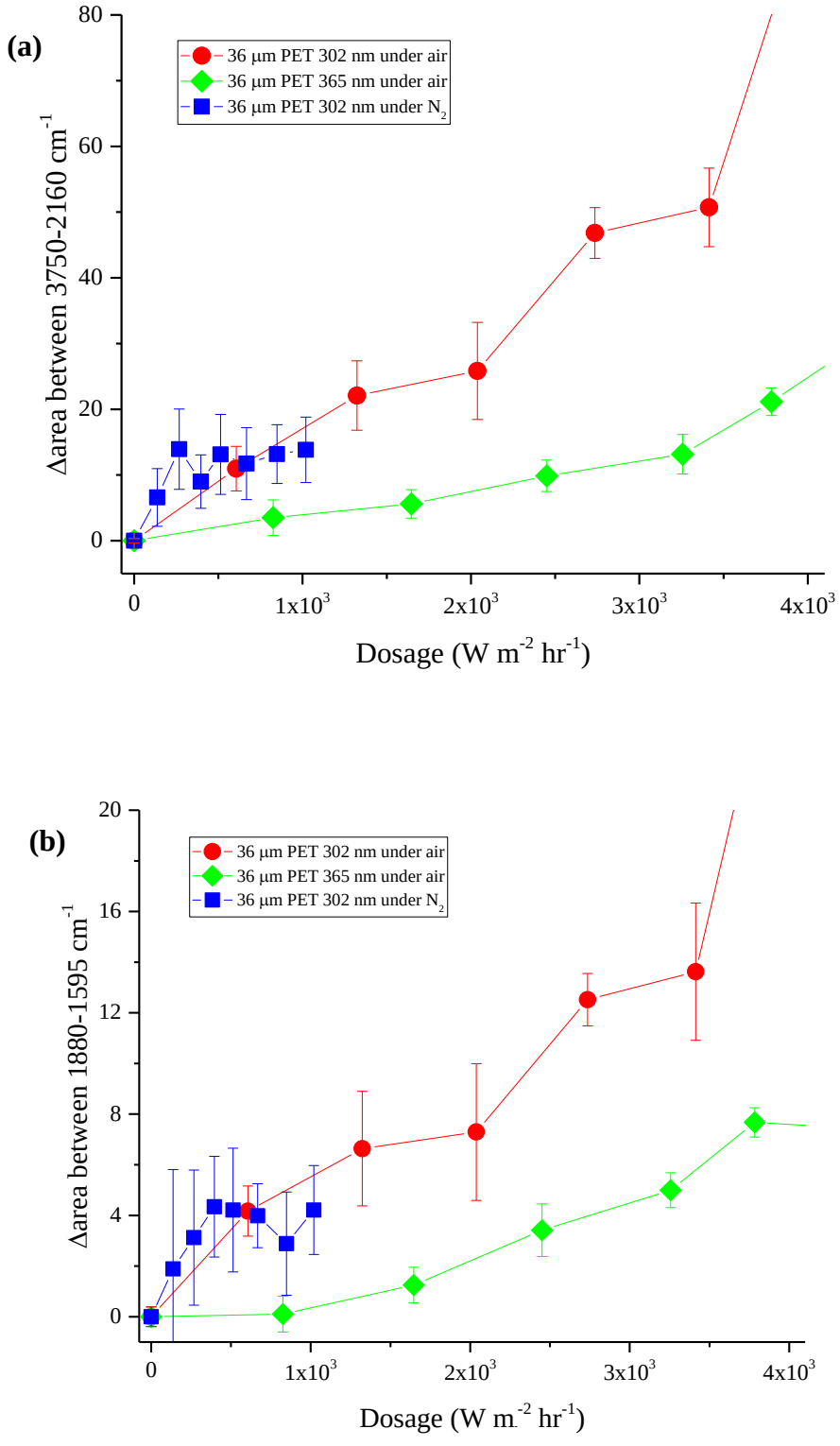

Figure 3.54: Extent of photodegradation of 36 µm PET, exposed under air and nitrogen, measured by the change in area of peaks between (a) 3750-2160 cm^{-1} and (b) 1880-1595 cm^{-1}(carbonyl).

Figure 3.54 shows the extent of photodegradation of samples exposed to 302 nm and 365 nm light under air and those exposed to 302 nm light under nitrogen, calculated from the DRIFT spectra in *Figure 3.53.* The extent of degradation was calculated as the change in area of the peaks between 3750-2160 cm^{-1} and those in the carbonyl region between 1880-1595 cm^{-1}. The sample exposed to 302 nm light under nitrogen and those exposed to 302 nm light under air show a similar extent of degradation. This contrasts with the extent of degradation calculated from the ATR data (*Figure 3.52*), which show samples exposed under nitrogen displaying degradation to a lesser extent. It is thought that nitrogen was not allowed to flush through the cell for long enough, leading to trapped air in deeper positions of the film. Considering this, it is possible that the surface would degrade to a lesser extent, but the bulk would degrade to the same extent as those exposed under air, due to oxygen in the deeper positions of the film.

With the knowledge that oxygen was still present in the film before exposure, under nitrogen, the samples were first placed in the vacuum oven for 24 hours and then the experiment was repeated. *Figure 3.55* shows the extent of degradation, calculated from DRIFT spectra, of samples exposed to 302 nm light under nitrogen and those placed under vacuum before being exposed to 302 nm light under nitrogen. Both graphs show that samples placed under vacuum before exposure show degradation to a lesser extent. This confirms that oxygen was present in the deeper positions of the film during the original experiment. Therefore, the extent of photodegradation also decreases in the bulk of the film when exposed in a non-oxidative atmosphere, compared to an oxidative atmosphere, due to the absence of oxygen.

Considering the error bars from the graphs in *Figure 3.54 and 3.55*, for the samples exposed under nitrogen and those placed under vacuum before irradiation, it is apparent that the errors in the data are rather large. It is thought that the cell could be leaking or that the cell was not allowed to pump down under nitrogen for long enough. It would, therefore, be beneficial to explore a more efficient way to expose samples under a non-oxidative environment.

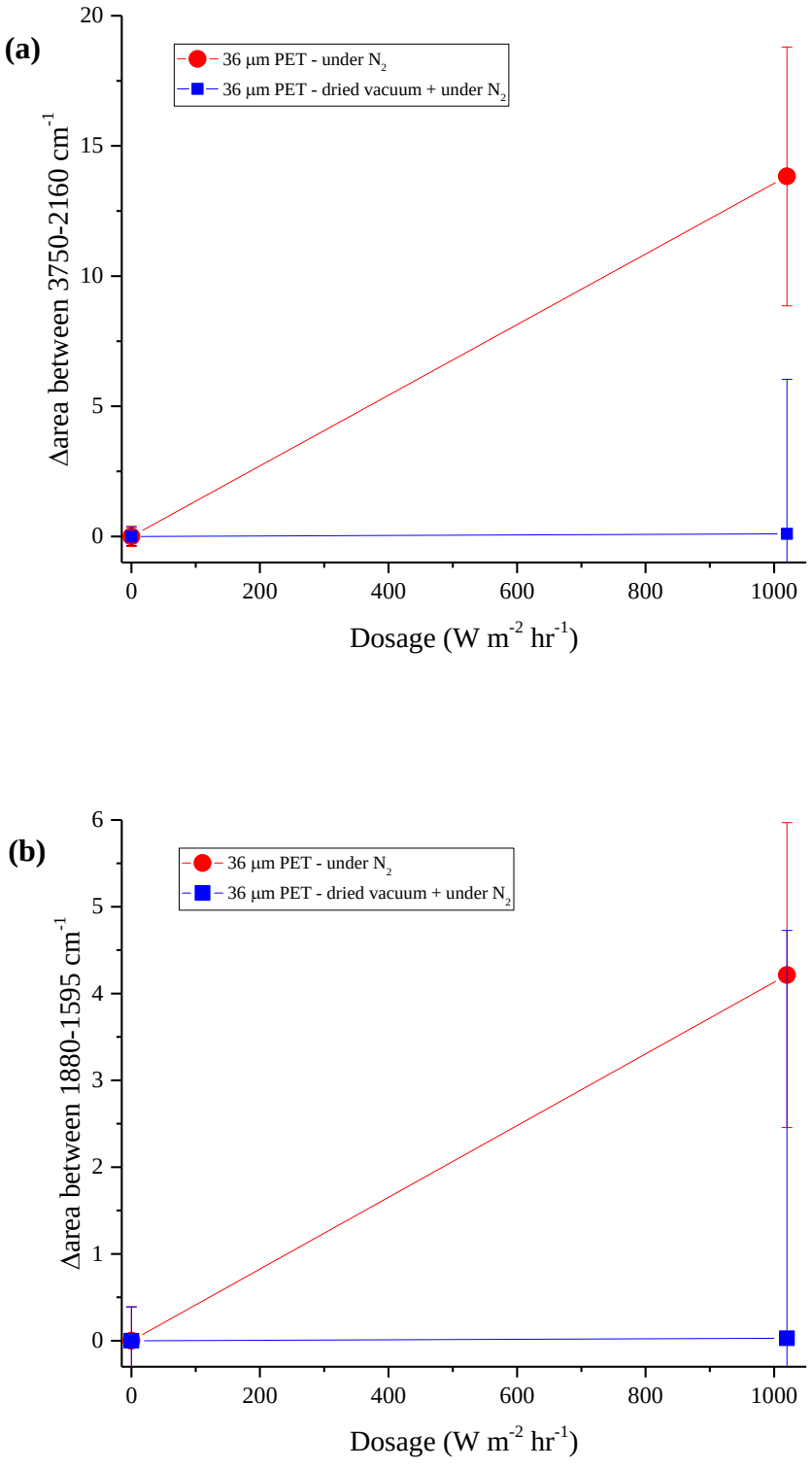

Figure 3.55: Extent of photodegradation of 36 µm PET, exposed under nitrogen, measured by the change in area of peaks between (a) 3750-2160 cm^{-1} and (b) 1880-1595 cm^{-1}(carbonyl).

3.6.2 General Conclusions

The effect of degradation atmosphere during irradiation of 36 μm PET was investigated using ATR FT-IR and DRIFT. Results show that samples exposed to 302 nm light under nitrogen show degradation to a lesser extent compared with samples exposed in air. In the presence of oxygen, photo-oxidation is considered the most important degradation process. Consequently, the samples in this study exposed under nitrogen degrade to a lesser extent due to the absence of oxygen in the system.

3.7 References

1 M. Day and D. M. Wiles, *J. Appl. Polym. Sci.*, 1972, **16**, 175–189.

2 Z. Chen, J. N. Hay and M. J. Jenkins, *Eur. Polym. J.*, 2012, **48**, 1586–1610.

3 C. F. L. Ciolacu, N. Roy Choudhury and N. K. Dutta, *Polym. Degrad. Stab.*, 2006, **91**, 875–885.

4 C. F. Ladasiu Ciolacu, N. Roy Choudhury and N. K. Dutta, *Polym. Degrad. Stab.*, 2006, **91**, 875–885.

5 G. J. M. Fechine, R. M. Souto-Maior and M. S. Rabello, *J. Mater. Sci.*, 2002, **37**, 4979–4984.

6 S. Wunscher, S. Stumpf, A. Teichler, O. Pabst, J. Perelaer, E. Beckert and U. S. Schubert, *J. Mater. Chem.*, 2012.

7 P. Atkins and J. de Paula, *Elements of Physical Chemistry*, Oxford University Press, Fourth Ed., 2005.

8 G. J. M. Fechine, M. S. Rabello, R. M. Souto Maior and L. H. Catalani, *Polymer*, 2004, **45**, 2303–2308.

9 Y. Li, J. Q. Pham, K. P. Johnston and P. F. Green, *Langmuir*, 2007, **23**, 9785–9793.

10 D. Murakami, H. Jinnai and A. Takahara, *Langmuir*, 2014, **30**, 2061–2067.

11 P. Gijsman, G. Meijers and G. Vitarelli, *Polym. Degrad. Stab.*, 1999, **65**, 433–441.

12 N. S. Allen, M. Edge, M. Mohammadian and K. Jones, *Polym. Degrad. Stab.*, 1994, **43**, 229–37.

13 M. Day and D. M. Wiles, *J. Appl. Polym. Sci.*, 1972, **16**, 203–215.

14 J. R. White and A. Turnbull, *J. Mater. Sci.*, 1994, **29**, 584–613.

15 P. Blais, M. Day and D. M. Wiles, *J. Appl. Polym. Sci.*, 1973, **17**, 1895–1907.

16 Y. Nakayama, K. Takahashi and T. Sasamoto, *Surf. Interface Anal.*, 1996, **24**,

711–717.

17 D. M. Bikiaris and G. P. Karayannidis, *Polym. Degrad. Stab.*, 1999, **63**, 213–218.

18 A. K. Crane, E. Y. L. Wong and M. J. MacLachlan, *CrystEngComm*, 2013, **15**, 9811.

19 P. Delprat and X. Duteurtreb, *Polym. Degrad. Stab.*, 1995, **50**, 1–12.

20 F. B. Marcotte, D. Campbell, J. A. Cleaveland and D. T. Turner, *J. Appl. Polym. Sci. Part A-1*, 1967, **5**, 481–501.

21 C. V Stephenson, C. Lacey and W. S. Wilcox, *J. Polym. Sci.*, 1961, **55**, 477–488.

22 J. Scheirs and J. L. Gardette, *Polym. Degrad. Stab.*, 1997, **56**, 339–350.

23 A. Rivaton, J. L. Gardette, C. E. Hoyle, M. Ziemer and D. R. Fagerburg, 2000, **41**, 3541–3554.

24 N. B. Colthup, L. H. Daly and S. E. Wiberley, *Introduction to Infrared and Raman Spectroscopy*, Academic Press, Third Edition., 2009.

25 J. V. Gulmine, P. R. Janissek, H. M. Heise and L. Akcelrud, *Polym. Degrad. Stab.*, 2003, **79**, 385–397.

26 M. Edge, R. Wiles, N. S. Allen, W. A. McDonald and S. V Mortlock, *Polym. Degrad. Stab.*, 1996, **53**, 141–151.

27 G. A. Cordell, *The Alkaloids*, Academic Press, 1997.

28 M. Day and D. M. Wiles, *J. Appl. Polym. Sci.*, 1972, **16**, 191–202.

29 N. S. Allen, M. Edge, M. Mohammadian and K. Jones, *Polym. Degrad. Stab.*, 1994, **43**, 229–237.

30 G. J. M. Fechine, M. S. Rabello and R. M. Souto-Maior, *Polym. Degrad. Stab.*, 2002, **75**, 153–159.

31 W. E. I. Wang, A. Taniguchi, M. Fukuhara and T. Okada, *J. Appl. Polym. Sci.*,

1998, **74**, 306–310.

32 H. A. Pohl, *J. Am. Chem. Soc.*, 1951, **73**, 5660–5661.

33 N. Grassie and G. Scott, *Polymer Degradation and Stabilisation*, Cambridge University Press, 1985.

34 B. J. Holland and J. N. Hay, *Polymer*, 2002, **43**, 1835–1847.

35 P. de Donato, J. M. Cases, B. Humbert, P. Lutgen and G. Feyder, *J. Polym. Sci. Part B Polym. Phys.*, 1992, **30**, 1305–1310.

36 J. Scheirs and J. Gardette, *Polym. Degrad. Stab.*, 1997, **56**, 339.

37 J. G. Pacifici and J. M. Straley, *Polym. Lett.*, 1969, **7**, 7–9.

38 M. Edge, N. S. Allen, R. Wiles, W. McDonald and S. V. Mortlock, *Polymer*, 1995, **36**, 227–234.

39 J. F. Rabck, *Polymer photodegradation. Mechanims and experimental methods.*, London: Chapman and Hall, 1995.

40 T. Berndt and O. Boge, *Phys. Chem. Chem. Phys.*, 2001, **3**, 4946–4956.

41 N. S. Allen and J. F. Mckellar, *Makromol. Chem.*, 1978, **179**, 523–526.

42 D. j. Hemker, C. W. Frank and J. W. Thomas, *Polymer*, 1988, **29**, 437–447.

43 J. P. LaFemina and G. Arjavalingam, *J. Phys. Chem.*, 1991, **95**, 984–988.

44 J. P. LaFemina, D. R. Carter and M. B. Bass, *J. Phys. Chem.*, 1992, **96**, 2767–2772.

45 L. Chen, X. Jin, J. Du and R. Qian, *Makromol. Chem.*, 1991, **192**, 1399–1408.

46 N. Fukazawa, K. Yoshioka, H. Fukumura and H. Masuhara, *J. Phys. Chem.*, 1993, **97**, 6753–6759.

47 T. Kijchavengkul, R. Auras and M. Rubino, *Polym. Test.*, 2008, **27**, 55–60.

48 S. S. Hosseini, S. Taheri, A. Zadhoush and A. Mehrabani-Zeinabad, *J. Appl. Polym. Sci.*, 2007, **103**, 2304–2309.

49 C. Sammon, J. Yarwood and N. Everall, *Polym. Degrad. Stab.*, 2000, **67**, 149–158.

50 D. Kint and S. Munoz-Guerra, *Polym. Int.*, 1999, **48**, 346–352.

51 F. Khabbaz, A.-C. Albertsson and S. Karlsson, *Polym. Degrad. Stab.*, 1999, **63**, 127–138.

52 M. Jayakannan and S. Ramakrishnan, *J. Appl. Polym. Sci.*, 1998, **74**, 59–66.

53 G. Li, S. L. Yang, J. M. Jiang and C. X. Wu, *Polymer*, 2005, **46**, 11142–11148.

54 Q. Baojun and Q. Xin, *J. Photopolym. Sci. Technol. Vol.*, 1997, **2**, 2–353.

55 G. Groeninckx and H. Reynaers, *J. Polym. Sci.*, 1980, **18**, 1311–1324.

56 M. S. Rabello and J. R. White, *Polym. Compos.*, 1996, **17**, 691–704.

57 W. K. Fisher and J. C. Corelli, *J. Polym. Sci. Polym. Chem. Ed.*, 1981, **19**, 2465–2493.

58 C. W. Extrand, *Langmuir*, 2004, **20**, 4017–4021.

59 L. Gao and T. J. Mccarthy, *Langmuir*, 2006, **22**, 6234–6237.

60 R. N. Wenzel, *Ind. Eng. Chem.*, 1936, **28**, 988–994.

61 A. B. D. Cassie and S. Baxter, *Trans. Faraday Soc.*, 1944, **40**, 546–551.

62 B. Fayolle, E. Richaud, X. Colin and J. Verdu, *J. Mater. Sci.*, 2008, **43**, 6999–7012.

63 N. S. Allen, M. Edge, M. Mohammadian and K. Jones, *Polym. Degrad. Stab.*, 1994, 43, 229–237.

64 J. M. G. Cowie, *Polymers: Chemistry & Physics of Modern Materials*, CRC Press, Third Edition., 2007.

4 The effect of UV light pre-treatment on the photo-oxidation of PET

PET films were exposed to 302 nm light followed by 365 nm light and vice versa, under oxidative conditions. Films were irradiated in a UVP XX-series UV bench lamp and a Hönle Cube 100 UV lamp. The extent of degradation was monitored using ATR FT-IR, DRIFT, UV-visible spectroscopy, fluorescence spectroscopy, DSC, contact angle, and SEM. All experimental techniques used in this study have been explained in detail in *Chapter 2.*

Photodegradation of PET has been studied by several groups under a range of UV wavelength ranges. However, the effect of exposing a sample to one wavelength of light followed by another wavelength of light has yet to be considered. Exposing samples to the full spectrum of light means that photodegradation reactions taking place as a consequence of short and long wavelengths of light, happen simultaneously, as seen in weatherometer experiments in *Chapter 3*. As discussed in *Chapter 3*, it is near impossible to determine the role of each wavelength in the degradation when exposing PET to a broad wavelength range of light. Whereas, if samples were exposed to different wavelengths of light consecutively, the reactions that happen simultaneously outdoors could be studied. This chapter centers on understanding the effect of exposing PET to different wavelengths of light sequentially, under oxidative conditions.

4.1 Exposure to 302 nm followed by 365 nm

4.1.1 ATR FT-IR

The films were exposed to 302 nm light with an average intensity of (31.7 ± 4.0) W m^{-2} and a temperature of (22.5 ± 2.5)°C, followed by 365 nm light at an average intensity of (825.5 ± 20) W m^{-2} and a temperature of (43 ± 2.5)°C. The spectral charts for these lamps are

Films exposed to 302 nm light for 1 week (equivalent to a dosage of approximately 4.3 x 10^3 W m^{-2} hr^{-1}) show spectral change on the front surface, predominately in the region between 3800-2100 cm^{-1} and the carbonyl and fingerprint regions, as shown in *Figure 4.01*. The rear surface of the films showed no notable change after exposure.

After further exposure to 365 nm light for 6 weeks in 1 week increments, there were only minor changes identified. The spectra of samples exposed to 302 nm followed by 365 nm light are shown in *Figure 4.01*.

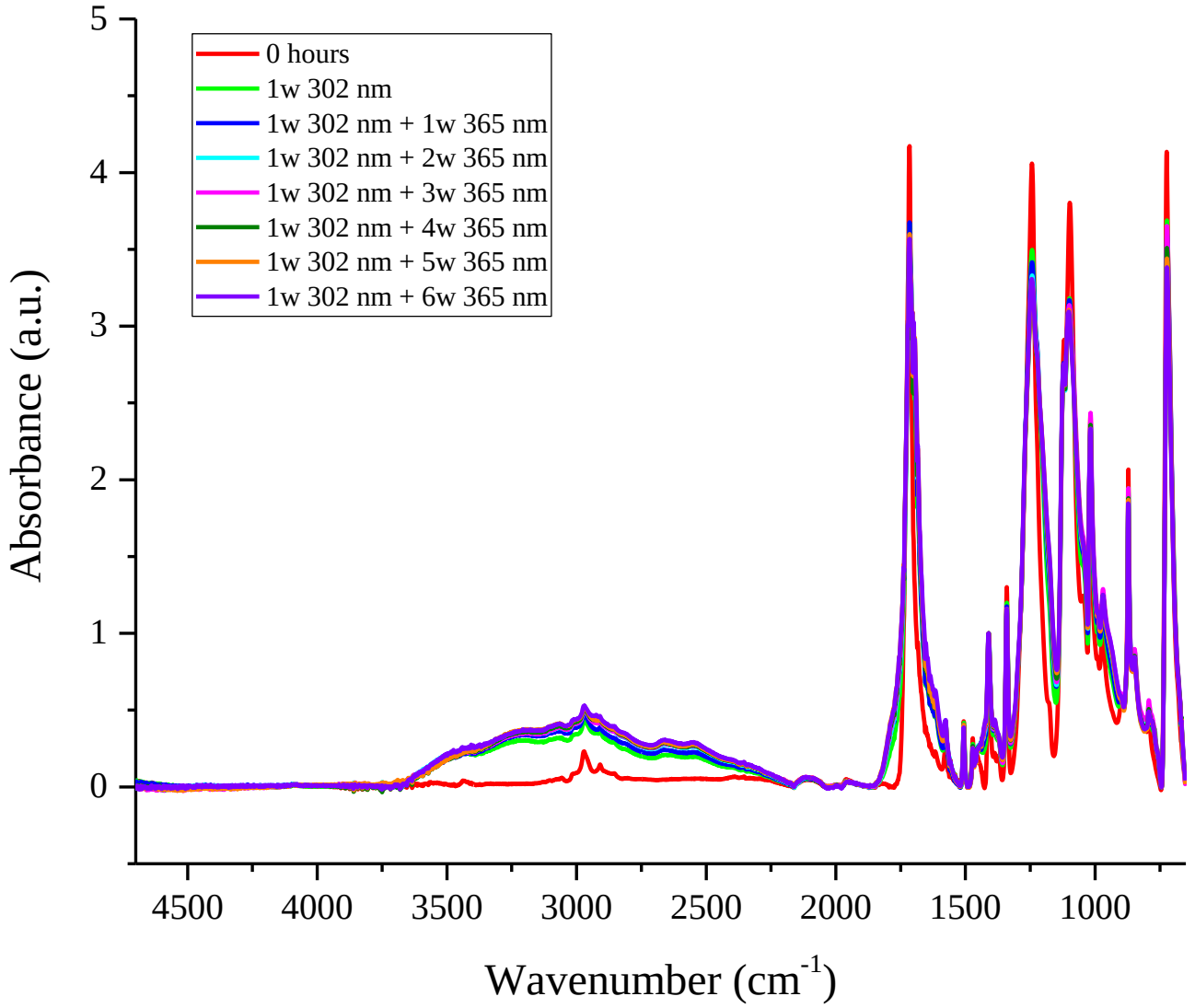

Figure 4.01: ATR FT-IR spectra of PET film samples exposed to 302 nm light for 1 week followed by exposure to 365 nm light for 6 weeks in 1 week increments.

Figure 4.02 shows the region from 3800-2100 cm^{-1} of the control spectrum of 36 µm PET, as well as the samples exposed to 302 nm light for 1 week and further exposed to 365 nm light for 6 weeks. *Table 1* shows the assignment of the peaks present in this region.

The carboxylic acid hydroxy peak, identified at 3290 cm^{-1}, increases in absorbance with exposure time, which indicates that carboxylic acid end groups are produced during exposure. Mechanistic pathways have been proposed, by Day and Wiles and Fechine *et al.*, for the production of these groups during the photo-oxidation of PET, as shown in *Chapter 1, Figure 1.26*.[1,2]

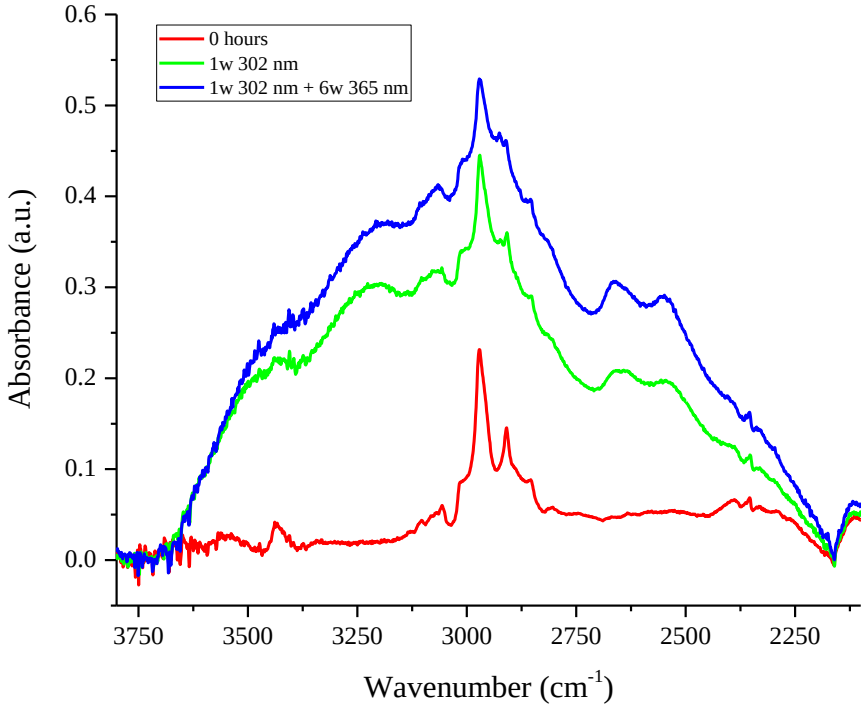

Figure 4.02: ATR spectra of 36 µm PET exposed to 302 nm light, in the hydroxy region from 3800 to 2100 cm^{-1}.

Two additional peaks have developed upon irradiation at 2640 and 2540 cm^{-1}, which are thought to be characteristic of the carboxylic acid dimer.[3] The formation of the carboxylic acid dimer groups has been reported in literature when changes in the

carbonyl peak have been identified.[4] As far as is known the peaks at 2640 and 2540 cm^{-1} have never been attributed to the carboxylic acid dimer species.

Table 1: Band assignments for the hydroxy region of the ATR spectrum of PET.

Peak (cm^{-1})	Assignment
3630	Aqueous O-H stretching vibration[7]
3550	Alcoholic O-H stretching vibration[7]
3430	First overtone of the carbonyl peak[7]
3290	Carboxylic acid end groups[7]
3100 – 3060	Aromatic C-H stretching[8]
3016, 2970, 2909	Crystalline aliphatic CH_2 stretching[8]
2928	C-H symmetric stretching vibration associated with the Ar-CH_3 group.
2965, 2855	Amorphous aliphatic CH_2 stretching[8]
2640, 2540	Characteristic of the carboxylic acid dimer[9]

The group of peaks assigned to the stretching modes of the four aromatic C-H bonds of the terephthalate ring between 3100 and 3060 cm^{-1} show an increase in absorbance and area with exposure time. This is thought to be due to the formation of mono-substituted aromatic rings, therefore resulting in another aromatic C-H bond on the ring. It is thought that the phenyl radicals can combine with a hydrogen radical to produce these mono-substituted aromatic rings. These radicals are produced during the photodegradation of PET.[2,5] It could also be the case that this increase in absorbance could be due to the peaks overlapping with the growing hydroxy.

The crystalline and amorphous aliphatic CH_2 stretching vibration peaks, assigned in *Table 1*, have shown a decrease in area with exposure time. This has been described in *Chapter 3*, as being due to the fact that the ester carbonyl in PETs main chain can absorb UV light directly, which results in chain scission not only taking place in the amorphous regions but also within the crystalline phase. This agrees with the reduction in the size of both the crystalline and amorphous CH_2 stretching peaks with

exposure time. The decrease in size of these peaks could also be due to the peaks being overlapped with the growing hydroxy group.

The evolution of the peak at 2928 cm^{-1} has been assigned to the C-H symmetric stretching vibration associated with the Ar-CH_3 group. The production of phenyl and methyl radicals have been reported in the literature by Stephenson *et al.*, during exposure of PET. It is believed that these radicals could combine to produce the Ar-CH_3 group, confirmed by the development of the peak at 2928 cm^{-1}.[6]

Figure 4.03 shows the carbonyl peak for samples exposed to 302 nm for 1 week and those exposed to 302 nm light followed by 365 nm light for 6 weeks, compared to a control spectrum. The various peaks contained within the carbonyl in the spectra of exposed samples have been summarised in *Table 2*. These peaks have been discussed in further detail in *Chapter 3*.

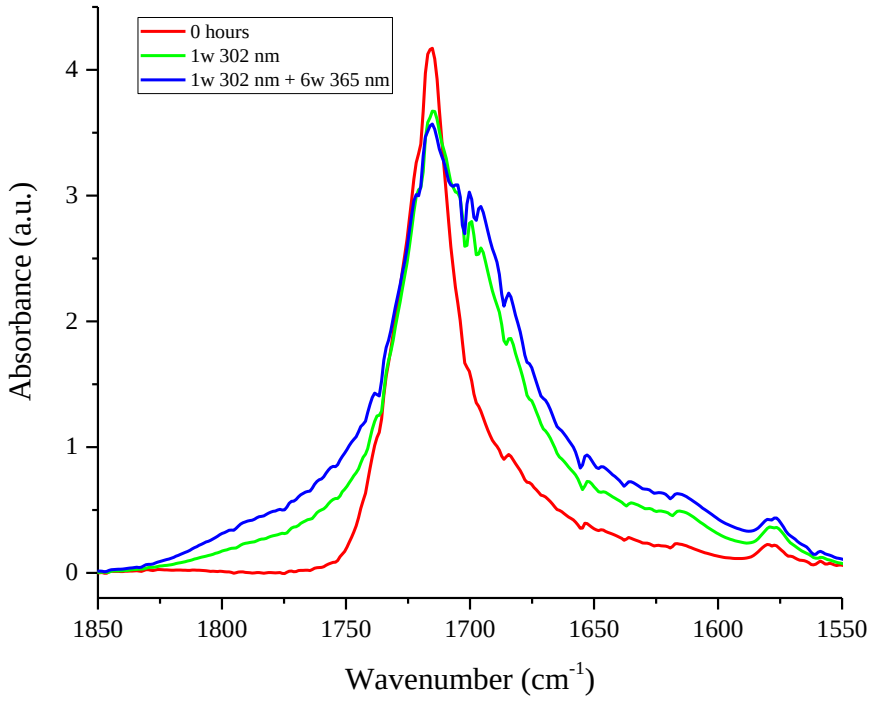

Figure 4.03: ATR spectra of 36 µm PET exposed to 302 nm light, in the carbonyl region from 1850 to 1550 cm^{-1}.

After 1 week under 302 nm light there is general broadening of the carbonyl peak, which continues with further exposure to 365 nm light. This indicates the production of new carbonyl species. The broadening of the peak at long wavenumbers indicates the formation of anhydrides. In *Chapter 3*, it was explained that anhydrides could be produced during the exposure of PET as well as PEN due to the temperature at which the irradiations were performed. PET was exposed at a temperature that would inhibit the radicals from diffusing apart and consequently providing the environment for anhydride formation.[10]

The peaks at 1722 and 1714 cm^{-1}, assigned to the amorphous and crystalline stretch from the ester, decrease in absorbance with a simultaneous increase in peaks assigned to groups produced during the photodegradation process. This indicates the break down of the ester group and the formation of new carbonyl groups during exposure. Peaks assigned to aliphatic aldehydes, carboxylic acid end groups and dimers, as well as quinone groups, have developed upon irradiation after 1 week under 302 nm light. After further exposure to 365 nm light, the absorbance of these groups increases, indicating an increase in the production of these degradation products.

Delprat *et al.* have reported the development of a peak assigned to carboxylic acid dimers during studies of the photodegradation of an ethylene-propylene copolymer. However, the presence of this peak has not been reported during the photodegradation of PET materials. Several authors have reported the production of carboxylic acid end groups, with Fechine *et al.* proposing a pathway for their formation under oxidative conditions.

Fechine *et al.* proposed mechanistic pathways for the production of the quinone species. These groups have been identified using UV-visible spectroscopy and changes in IR spectra have been reported, during thermal degradation, as being due to the production of these species.[1,11] This indicates that quinones could also cause a change in the IR spectra, at 1695 cm^{-1}, during photodegradation.

The peak identified at 1685 cm^{-1} has been assigned to the carbonyl stretch from terephthalic acid. Terephthalic acid is the monomer unit used in the production of PET. To identify this peak an ATR FT-IR spectrum of terephthalic acid was taken and

overlaid with a spectrum of irradiated PET film. The development of this peak after exposure indicates the breakdown of the polymer into its monomer units.

Table 2: Band assignments for carbonyl region of the ATR spectrum of PET.

Peak (cm^{-1})	Assignment
1785	Carbonyl stretch from anhydride carbonyl[12,13]
1738	Carbonyl stretch from aliphatic aldehyde[3]
1722	Amorphous carbonyl stretch from ester[8]
1714	Crystalline carbonyl stretch from ester[8]
1705	Carbonyl stretch from carboxylic acid dimer[4,13,14]
1700	Carbonyl stretch from carboxylic acid end groups[15]
1695	Carbonyl stretch from quinone groups[11,16]
1685	Carbonyl stretch from terephthalic acid

As previously explained in *Chapter 3*, the rate of photodegradation was measured by the change in area of the hydroxy peak, between 3740 and 2160 cm^{-1}, and the carbonyl peak, between 1880 and 1525 cm^{-1}.

Figure 4.04 (a) and (b) show the change in area of the region between 3800-2100 cm^{-1} and the carbonyl peak with exposure time, under 365 nm light. Both graphs show the rate of photodegradation for a control sample only exposed to 365 nm light versus a sample exposed to 302 nm light before being exposed to 365 nm light. The red line on each of the graphs, depicting the sample that has been pre-exposed to 302 nm light, degrades to a greater extent than the sample that was only exposed to 365 nm light (the blue line). *Figure 4.04*, therefore, shows that pre-exposing samples to 302 nm light does influence the effect of subsequent exposure to 365 nm light. This was expected as short wavelength light causes the production of new chromophores which can then absorb light at longer wavelengths. This was shown by Fechine *et al.* and is also proven in the UV-visible spectra that will be reported later in this chapter.[1]

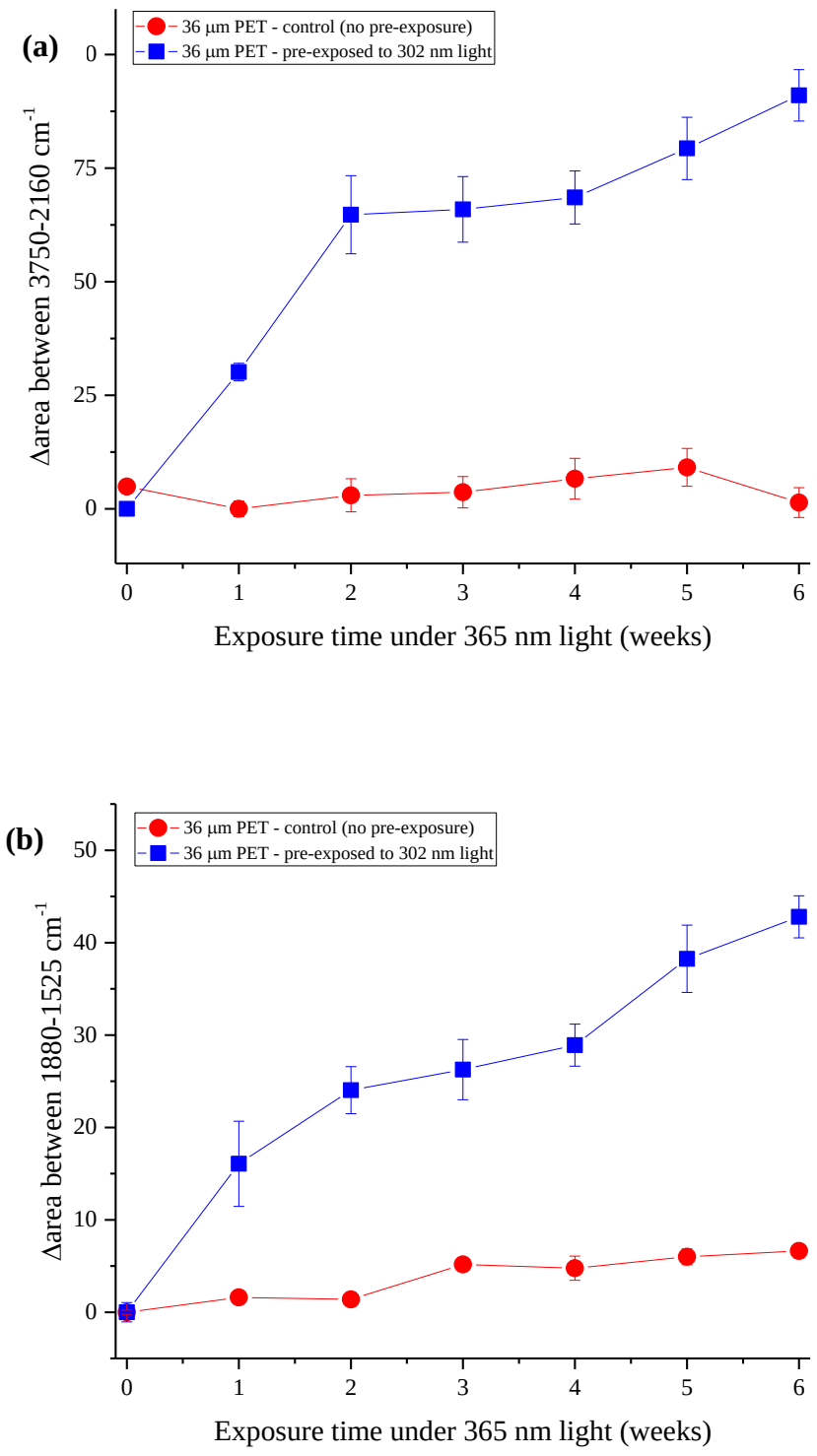

Figure 4.04: Extent of photodegradation measured by the change in area of the peaks between (a) 3750-2160 cm^{-1} and (b) 1880-1525 cm^{-1}, from the ATR spectra.

The fingerprint region of the ATR FT-IR spectra is shown in *Figure 4.05*, for samples exposed to 302 nm light, for 1 week, followed by 365 nm light, for 6 weeks. The peaks that have changed or developed in the spectra, during exposure, have been assigned in *Table 3*.

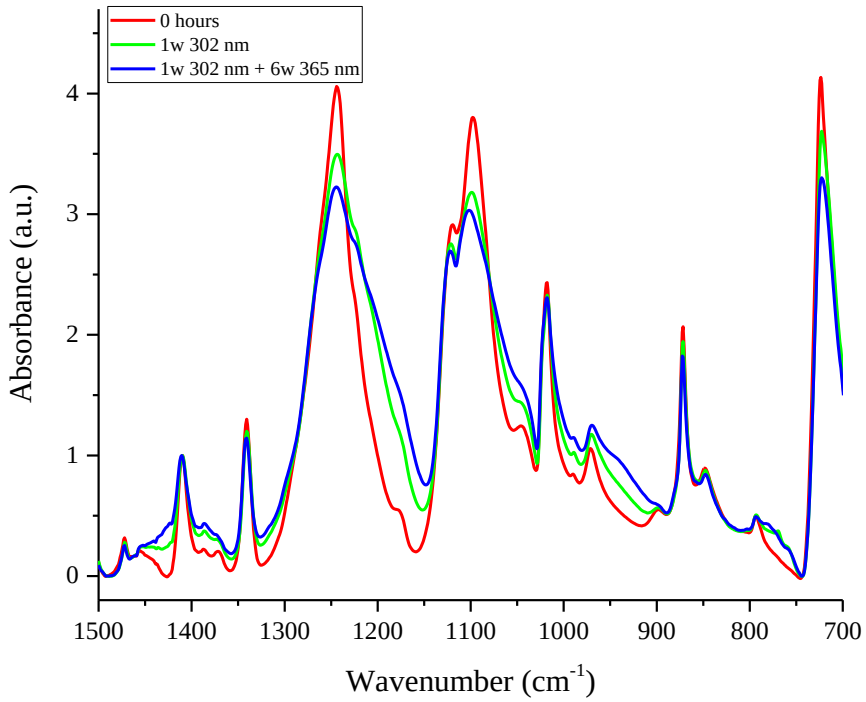

Figure 4.05: ATR spectra of 36 µm PET exposed to 302 nm light, in the fingerprint region from 1500 to 650 cm^{-1}.

The development of peaks at 1430 and 1220 cm^{-1} have been assigned to the combination band due to the C-O stretching and O-H deformation and C-O stretching, respectively. As far as is known, these peaks have not been reported in the literature, but are believed to be associated with the carboxylic acid dimer.

The peaks at 970 and 898 cm^{-1}, assigned to the trans and cis isomer of the C-H stretching of the ethylene glycol unit, respectively, have shown a decrease in size after exposure.[8] This reduction in size is likely to be associated with the scission of ester links in the polymer chain during irradiation.

Table 3: Band assignments in the fingerprint region of the ATR spectrum of PET.

Peak (cm^{-1})	Assignment
1430	Combination band due to C-O stretching and O-H deformation vibration, associated with carboxylic acid dimer.[3]
1220	C-O stretching vibration, associated with carboxylic acid dimer.[3]
970	Stretching of C-H bond of the trans isomer of the ethylene glycol unit.[8]
940	C-H vibration associated with vinyl groups.[17]
898	Stretching of C-H bond of the cis isomer of the ethylene glycol unit.[8]
848	C-H deformation of two adjacent hydrogens on the terephthalic ring (indicates 1, 4 substitution)[18]
778	Out-of-plane deformation vibrations of mono-substituted rings[3]
769	Out-of-plane deformation vibrations of 1, 2, 3-substituted rings[3]
758	Out of plane deformation vibrations of 1, 2, 4-substituted rings[3]

Figure 4.05 shows the development of a peak at 940 cm^{-1} after exposure, which has been assigned to the C-H vibration associated with vinyl groups. Vinyl groups have been shown to be produced during the photodegradation of PET; Grassie and Scott have proposed an alternative chain scission pathway, shown in *Chapter 1, Figure 1.21*.

The region of the spectra between 850-750 cm^{-1} is known to be sensitive to changes in the substitution pattern on the terephthalic ring. There have been changes in the peak at 848 cm^{-1} and development of peaks at 778, 769 and 758 cm^{-1} after exposure to UV light.

The peak at 848 cm^{-1}, assigned to the C-H deformation of two adjacent hydrogens on the terephthalic ring, has shown a minor reduction in size. This indicates that substitution has occurred on the ring.[18,19] This is further supported by the development of peaks at 769 and 758 cm^{-1}, assigned to the 1, 2, 3-substituted and 1, 2 4-substituted rings.

The evolution of the peak at 778 cm^{-1}, has never been reported in literature during the photodegradation of PET materials. It is believed that this peak is due to the production of mono-substituted rings. *Chapter 1, Figure 1.11* shows a reaction

pathway that shows the production of phenyl radicals, which can abstract a hydrogen from the backbone of the polymer chain to form a mono-substituted ring.

Interestingly, in this set of spectra, a peak at 778 cm^{-1} develops in the film upon exposure to 365 nm light after first being exposed to 302 nm light. This peak has been assigned to mono-substituted aromatic rings and has not been reported in the literature during the irradiation of PET materials.

This peak has been identified in samples exposed in the weatherometer and samples exposed to 302 nm light followed by 365 nm light. Samples exposed to 302 nm and 365 nm light, independently, and those exposed to 365 nm followed by 302 nm light (*shown in Section 4.2*) show no development of this peak at 778 cm^{-1}. This indicates that exposure to more than one wavelength of light is required for the formation of these mono-substituted rings to take place.

Referring to *Chapter 1, Figure 1.26*, it was initially thought that 302 nm light could be responsible for steps 3 and 4, while 365 nm light could be responsible for the reaction in step 5. This is because samples that are exposed to 302 nm light independently produce carboxylic acid end groups, which mean that the samples have completed steps 3 and 4. However, no peak associated with mono-substituted rings develops in the spectra after exposure to 302 nm light, so it can be assumed that the sample has not undertaken step 5.

Step 3 includes the breaking of the hydroperoxide group, which are transparent at wavelengths above 340 nm and have a low molar absorptivity coefficient at 340 nm.[20] Step 4 shows chain cleavage of the C-O bond, which can be caused by exposing the polymer to approximately 334 nm light. The spectral chart for the 302 nm light used is shown in *Chapter 2, Figure 2.04,* and shows that 340 nm and 334 nm light are contained within this narrow range of wavelengths.

Step 5 of the reaction (*Chapter 1, Figure 1.26)* shows the cleavage of a C-C bond, which can be accomplished by exposing the polymer to approximately 307 nm light. Considering the spectral chart of the 365 nm light, (*Chapter 2, Figure 2.05)* contradicts

the theory that 365 nm light could be initiating step 5 of the reaction as this light only covers the approximate range between 330-400 nm.

This also suggests that only exposing samples of PET to 302 nm light should result in the formation of mono-substituted rings. Studying the spectra closely there is an increase in absorbance at 778 cm^{-1} and some minor change in the slope of the spectra in this area, indicating what could be the introduction of the development of a peak. However, this increase in absorbance could also be due to the growth of other peaks around the peak at 778 cm^{-1}.

Considering the results obtained when samples are exposed to 302 nm light followed by 365 nm light, another reason for the production of this peak at 778 cm^{-1} could be due to the production of new chromophores which are subsequently attacked. Exposing PET to 302 nm light causes the formation of new chromophoric groups, such as monohydroxy terephthalate groups and quinone species. These groups are shown to absorb longer wavelengths of light, shown later in this chapter in *Section 4.1.3*. This means that after these new chromophores are produced and exposed to 365 nm light, further degradation may take place which could result in the production of mono-substituted rings.

The production of mono-substituted rings could be caused by various reasons, however, at the moment, further research is required to discover the reason behind the formation of these groups.

When PET is exposed to 302 nm light new chromophores are produced which can absorb at 365 nm light. The fact that there are only minor changes occurring in the spectra when the samples are exposed to 365 nm light, is consistent when it is considered that it is weakly absorbed and the fact that ATR is a surface technique. This indicates that there could be further change occurring in the bulk of the films that cannot be analysed using the ATR.

4.1.2 DRIFT

Figure 4.06 shows the DRIFT spectra of 36 µm PET films exposed to 302 nm light, for 1 week (equivalent to a dosage of approximately 4.3×10^3 W m^{-2} hr^{-1}), followed by 365 nm light, for 6 weeks, in 1 week increments. The spectra show significant changes, after exposure to 302 nm light, in the region between 3800-2100 cm^{-1} and the carbonyl region. Additional exposure to 365 nm light shows continues significant changes in these regions. This indicates that 365 nm light is primarily affecting the bulk rather than the surface, considering DRIFT analyses the whole of the film compared to ATR which only studies the surface.

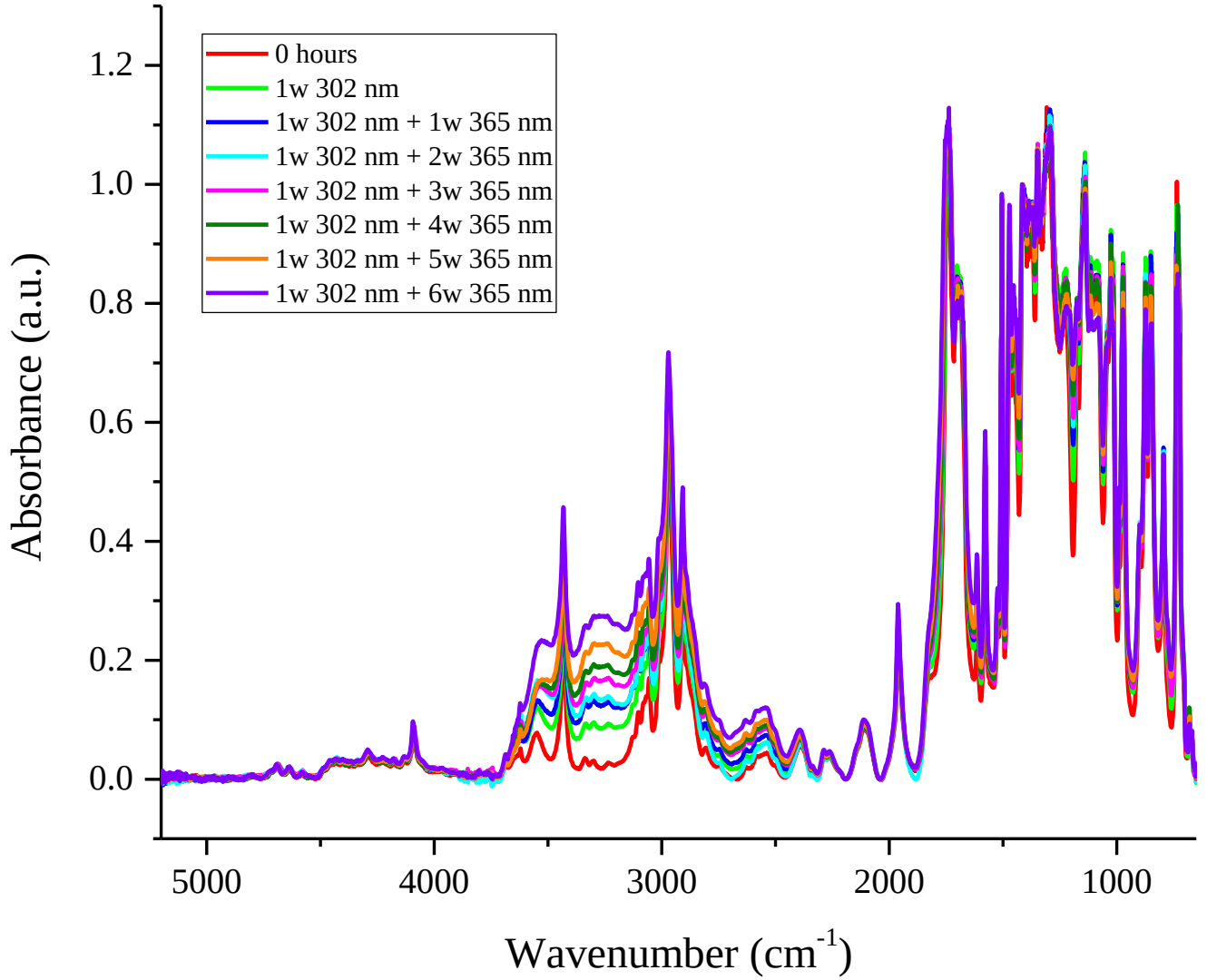

Figure 4.06: DRIFT spectra of PET film samples exposed to 302 nm light for 1 week followed by exposure to 365 nm light for 6 weeks in 1 week increments.

Table 4 shows the assignments for the region between 3800-2100 cm^{-1} of the DRIFT spectra shown in *Figure 4.07*.

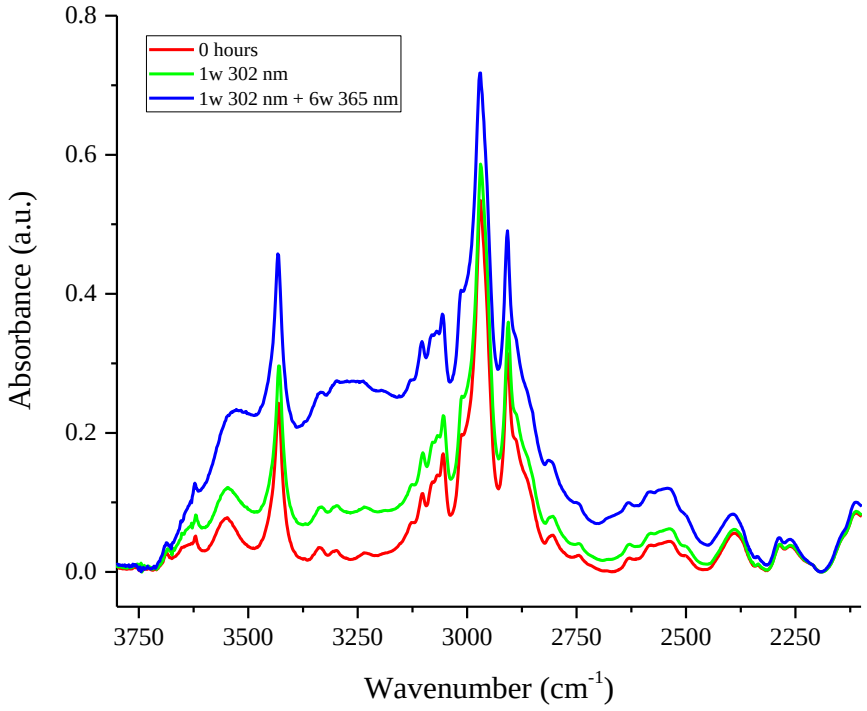

Figure 4.07: ATR spectra of 36 µm PET exposed to 302 nm light, in the hydroxy region from 3800 to 2100 cm^{-1}.

As seen with the ATR spectra, the peaks at 3620, 3550 and 3290 cm^{-1} have been assigned to the aqueous, alcoholic and carboxylic acid hydroxy stretches, respectively. After exposure, it is evident, from *Figure 4.07* that the peaks have increased in absorbance with exposure time. This suggests that new hydroxy groups have formed during irradiation, including carboxylic acid end groups, which are known to be produced during the photodegradation of PET. The peaks at 3430 and 3335 cm^{-1} have also increased in absorbance, after exposure and have been assigned to the overtones of the carbonyl peak. This increase is thought to be due to the overlap with the growing hydroxy peaks.

Table 4: Band assignments for the hydroxy region of the DRIFT spectrum of PET.

Peak (cm^{-1})	Assignment
3625	Aqueous O-H stretching vibration[7]
3540	Alcoholic O-H stretching vibration[7]
3430	First overtone of the carbonyl group in ester[7]
3335	First overtone of carbonyl group in carboxylic acid end group[21]
3290	Carboxylic acid end groups[7]
3100, 3078, 3067, 3054	Aromatic C-H stretching[8]
3015, 2970, 2908	Crystalline aliphatic CH_2 stretching[8]
2963, 2855	Amorphous aliphatic CH_2 stretching[8]

Peaks associated with the aromatic and aliphatic C-H stretching vibrations, assigned in *Table 4*, have shown no meaningful change after irradiation. This could indicate that there has been no substitution on the ring or change in the environment of aliphatic C-H stretches in the bulk of the film, or changes have occurred, but they are below the sensitivity range of the DRIFT instrument.

Figure 4.08 shows the carbonyl region of the DRIFT spectra, between 1900-1550 cm^{-1}, for a control film and a sample exposed to 302 nm light followed by 365 nm light. The assignments for the various peaks contained within the carbonyl peak are given in *Table 5*.

There is general broadening of the carbonyl peak, with irradiation time. This indicates that new carbonyl species are formed during the photodegradation of PET, which has been reported in the literature.

The broadening at higher wavenumbers is due to the production of anhydride groups.[10] As discussed in *Chapter 3*, anhydrides can be produced, during this exposure, as irradiations were performed at a temperature that provides an ideal environment for anhydride formation to occur.

At lower wavenumbers, this broadening is due to the formation of other degradation products, including carboxylic acid end groups. These groups are known to be produced and pathways have been proposed for their formation. The peak at 1683 cm^{-1}, has been assigned to the carbonyl stretch from terminal acid end groups by Donato *et al.*[21]

Another peak in this region at 1702 cm^{-1} has been reported to be present in DRIFT spectra of PET but has never been assigned.[21] It is believed that this peak could be due to carboxylic acid dimers due to its increase in absorbance after exposure to 302 nm light.

Broadening at lower wavenumbers is due to the production of degradation products, whereas broadening of the peak at higher wavenumbers is thought to be due to the production of anhydride groups.[10]

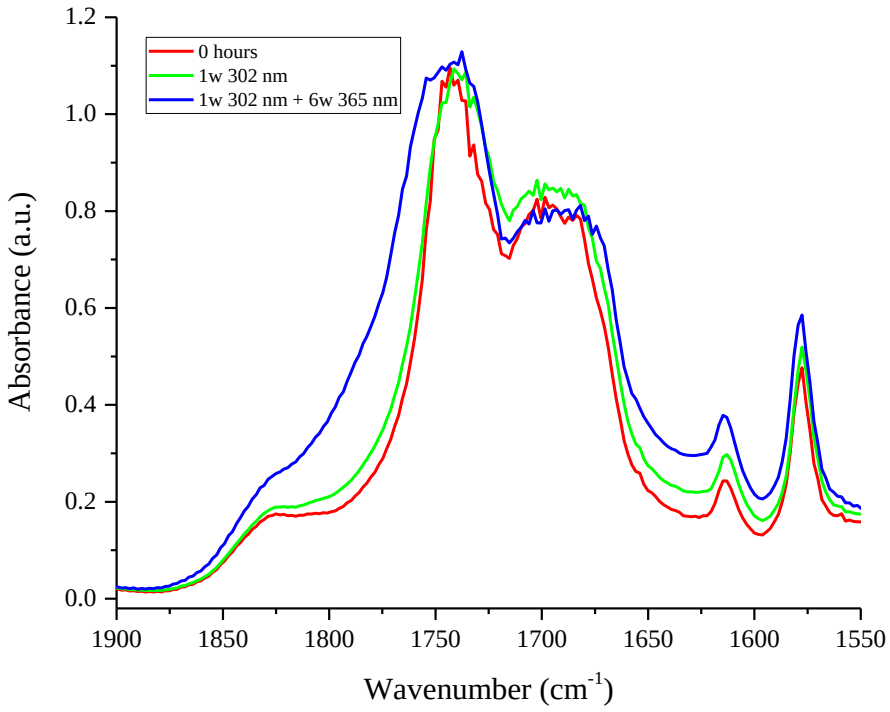

Figure 4.08: ATR spectra of 36 µm PET exposed to 302 nm light, in the carbonyl region from 1900 to 1550 cm^{-1}.

Table 5: Band assignments for carbonyl region of the DRIFT spectrum of PET.

Peak (cm^{-1})	Assignment
1785	Carbonyl stretch from anhydride carbonyl[12]
1743	Carbonyl stretching vibration of an ester[21]
1683	Carbonyl stretch from terminal acid end groups[21]

The extent of photodegradation, measured by the change in area between 3750-2160 cm^{-1} and the carbonyl peak, are shown in *Figure 4.09 (a) and (b)*, respectively. The graphs, in *Figure 4.09 (a) and (b)*, show the same trends as seen with the ATR data; the sample exposed to 365 nm light shows lesser degradation than the sample that was pre-exposed to 302 nm light before being exposed to 365 nm light. However, the extent of photodegradation determined from the DRIFT data show larger changes compared to the ATR data. This shows that 365 nm light has a predominant effect in the bulk of the film, although it is weakly absorbed. The control sample exposed only to 365 nm light also shows larger changes in the DRIFT spectra, compared to the ATR spectra, again confirming the effect of 365 nm light on the bulk of the film.

Pre-exposure with 302 nm light primarily causes degradation reactions on the surface of the film, but from analysing the spectra there is also some degradation in the bulk of the film. This means that new chromophores have been produced in the bulk as well as the surface, that absorb at longer wavelengths, allowing for the absorption of 365 nm light.

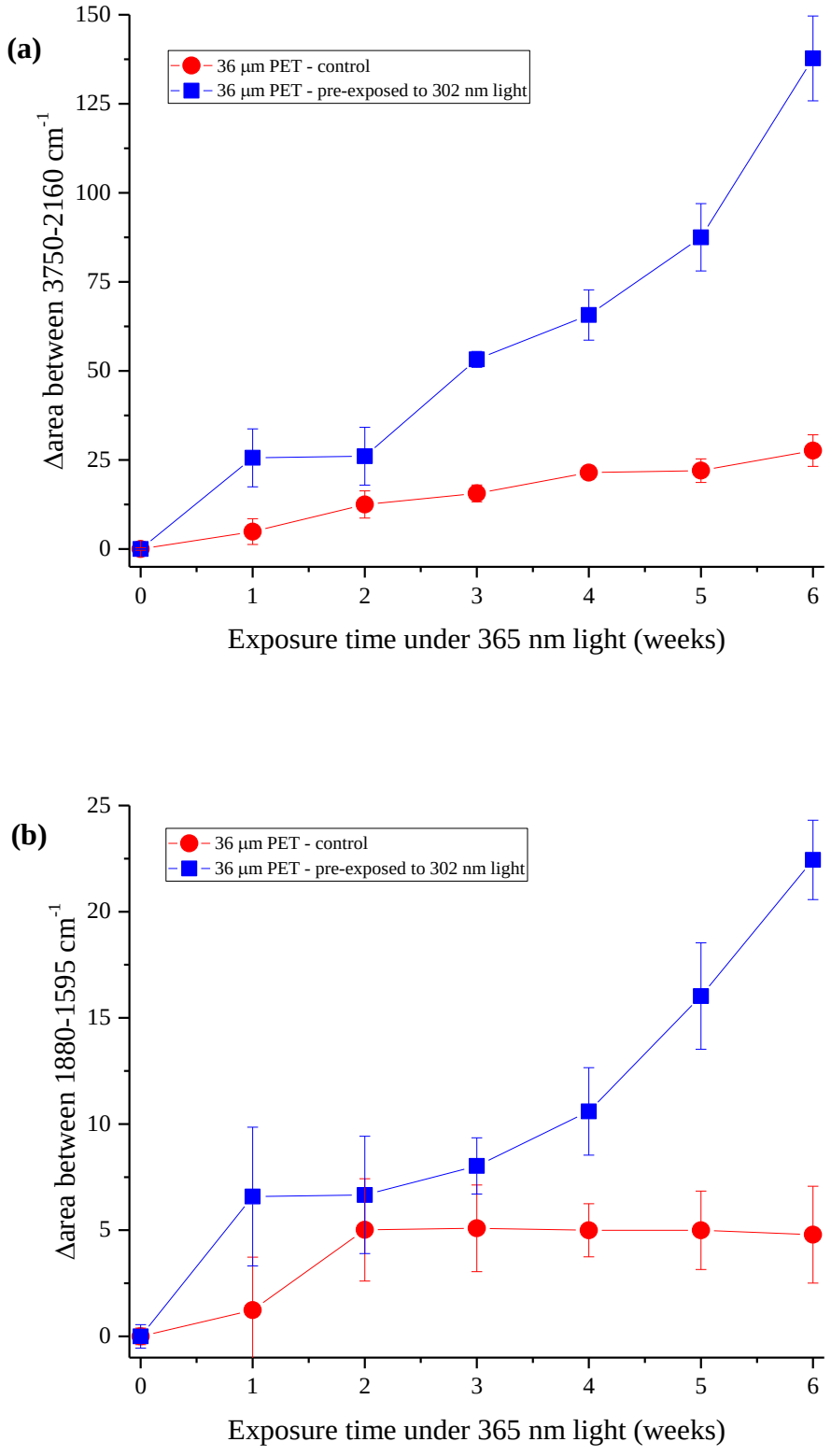

Figure 4.09: Rates of photodegradation measured by the change in area of the peaks between (a) 3750-2160 cm^{-1} and (b) 1880-1595 cm^{-1}, from the ATR spectra.

4.1.3 UV-visible spectroscopy

The UV-visible spectra of samples exposed to 302 nm light followed by 365 nm light are given in *Figure 4.13*. When PET is exposed to 302 nm light for 1 week an increase in absorbance at 340 nm and a slight increase at 400 nm are observed, shown in *Figure 4.13*. This increase in absorbance at longer wavelengths, when exposed to short wavelength light, has been reported by Fechine *et al.*[1] and is indicative of the production of new chromophores during exposure.

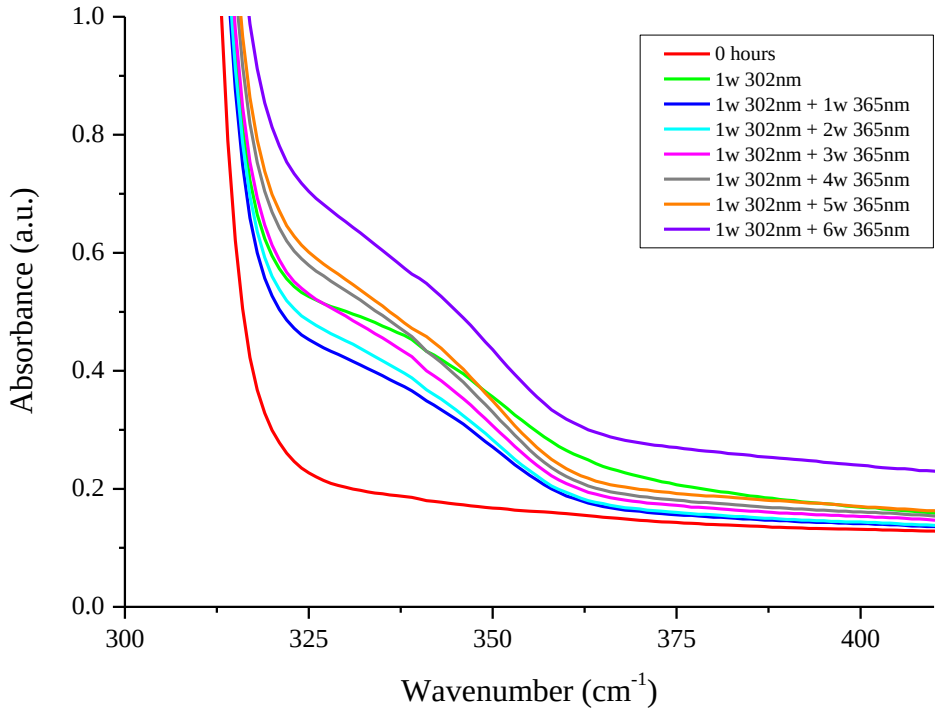

Figure 4.13: UV-visible spectra of 36 µm PET film samples exposed to 302 nm light followed by 365 nm light.

The increase at 340 nm is associated with monohydroxy terephthalate groups, which were first identified by Pacifici and Straley. Day and Wiles reported that the hydroxy groups, produced during exposure of PET, are capable of substituting in the phenylene ring to form monohydroxy terephthalate groups. The authors proposed a mechanism for their formation, shown in *Chapter 1, Figure 1.27*.

The small increase in absorbance at 400 nm, shown in *Figure 4.13*, has been attributed to the formation of quinone and diquinone groups during irradiation. Fechine *et al.* have proposed possible reaction schemes leading to the formation of quinone and diquinone groups, during exposure to UV light, given in *Chapter 1*, *Figure 1.31*.[1]

After the PET films were exposed to 365 nm light, the peak at 340 nm begins to fluctuate in absorbance due to the attack of the new chromophoric group. The new chromophoric groups are produced during irradiation and in addition, it is thought that they are subsequently attacked.

A reaction pathway for this subsequent attack has been proposed and is given in *Chapter 3, Figure 3.20*. This shows the attack of the monohydroxy terephthalate groups by hydroxy radicals; known to be produced during the photodegradation of PET. This pathway has been reported in the literature, but not in relation to the photodegradation of PET.[22,23] It could also be the case that this fluctuation in absorbance of the 340 nm peak is due to the photodegraded polymer being more hygroscopic than the control sample.

4.1.4 Fluorescence spectroscopy

Initial natural fluorescence of a control sample of PET, depicted by the black line in *Figure 4.14*, shows peaks at 370 and 385 nm and a shoulder at 410 nm. The peak at 370 nm was first reported when PET was excited by 290 nm light, whereas the peak at 385 nm with a shoulder at 410 nm was reported after excitation by 340 nm.

The emission band at 370 nm has been studied by various groups over the years and has been reported to be attributed to a ground state dimer and an excimer band. This has been discussed further in *Chapter 3, Section 3.3.4*. At present, Chen *et al.*, Fukazawa *et al.* and Fechine *et al.* have all attributed the peak at 370 nm to an excimer.[24–26]

There has also been a significant amount of research into the assignment for the peak at 385 nm, which has been discussed further in *Chapter 3, Section 3.3.4*. There seems to be more agreement between authors that the peak at 385 nm is known to be associated with a ground state dimer.[24]

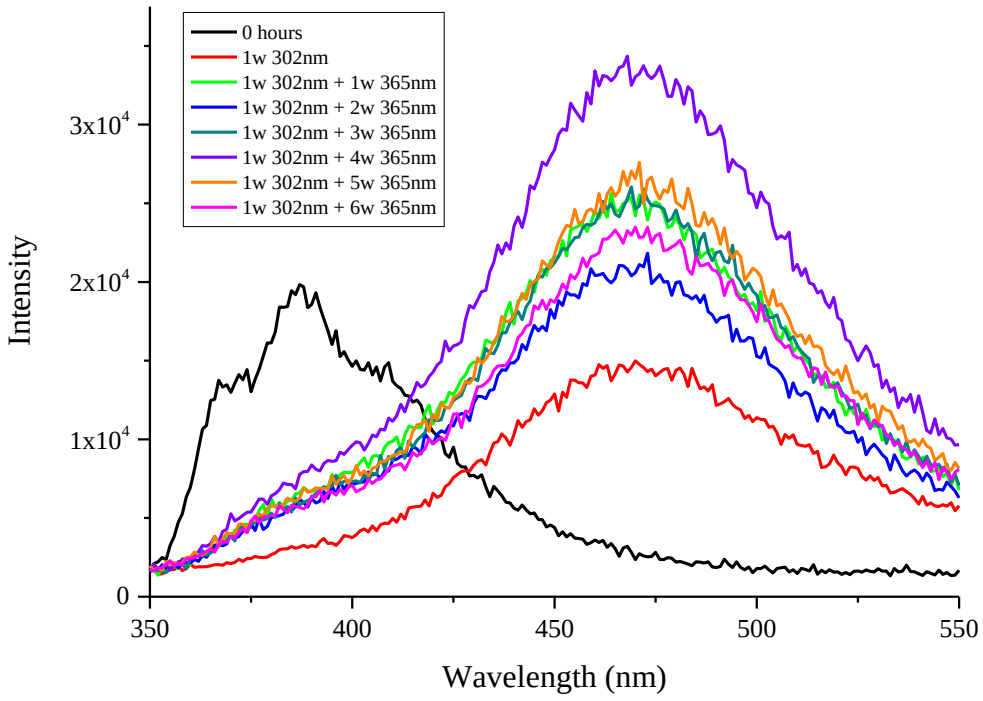

Figure 4.14: Fluorescence spectra of 36 µm PET film samples exposed to 302 nm light followed by 365 nm light.

After exposure to 302 nm light for 1 week, the intensity of the initial emission peak decreases. This has been reported as being due to a loss of interaction between chromophores, caused by chain scission.[24] There is also the evolution of a peak centered at 475 nm, after irradiation. It was suggested, by Pacifici and Straley, and further supported by Day and Wiles that this emission was due to photolytic degradation products.[27 7] Chen *et al.* used model systems in his study to propose that this emission is due to an exciplex from the interaction between the excited carbonyl group and the phenylene π-electrons.[25] Therefore the emission peak at 475 nm has been assigned to the formation of monohydroxy terephthalate groups. A mechanistic pathway for their production has been proposed by Day and Wiles, shown in *Chapter 1, Figure 1.27.*[28] This species was initially identified by Pacifici and Straley.[27]

Samples exposed to 302 nm light followed by 365 nm light show some fluctuation in intensity of the 475 nm peak. This is thought to be due to the production and

subsequent attack of the new chromophoric groups. A reaction pathway for the breakdown of these groups has been discussed in *Chapter 3, Section 3.3.3* and is given in *Figure 3.20*. The spectra for the sample exposed to 302 nm light for 1 week followed by 365 nm light for 4 weeks, represented by the purple line in *Figure 4.14*, is suspected to be an outlier.

4.1.5 DSC

4.1.5.1 Heating cycle

Figure 4.10 shows the first heating cycle for samples exposed to 302 nm light followed by 365 nm light. The melting temperature does not change significantly, after exposure to 302 nm light for 1 week. The melt endotherm shows broadening and thus a small decrease in onset temperature. This indicates that crystals with reduced size, thickness, and lower melting temperatures were produced by chain scission reactions during exposure.[15] This also suggests that at prolonged hours of exposure/higher dosages a decrease in melting temperature may occur.

After further exposure to 365 nm light, a decrease in T_m is observed which could be explained by two different mechanisms. Firstly, this could indicate that branched chains are produced during exposure. Branching reduces the packing efficiency of the polymer; crystalline content is lowered and hence the T_m decreases.[15] Similarly, crosslinking could also cause a decrease in Tm. Another theory is that crosslinking has occurred in the polymer film which would be depicted in a DSC thermogram by a broader melting peak and a lower onset temperature, compared to a control sample. Samples with a higher degree of crosslinking cause non-uniformity of the crystal lattices which cause them to melt at a different temperature.[29]

The onset temperature of the melting peak also decreased with exposure time indicating the production of crystals with reduced size, thickness, and lower melting temperatures.[15]

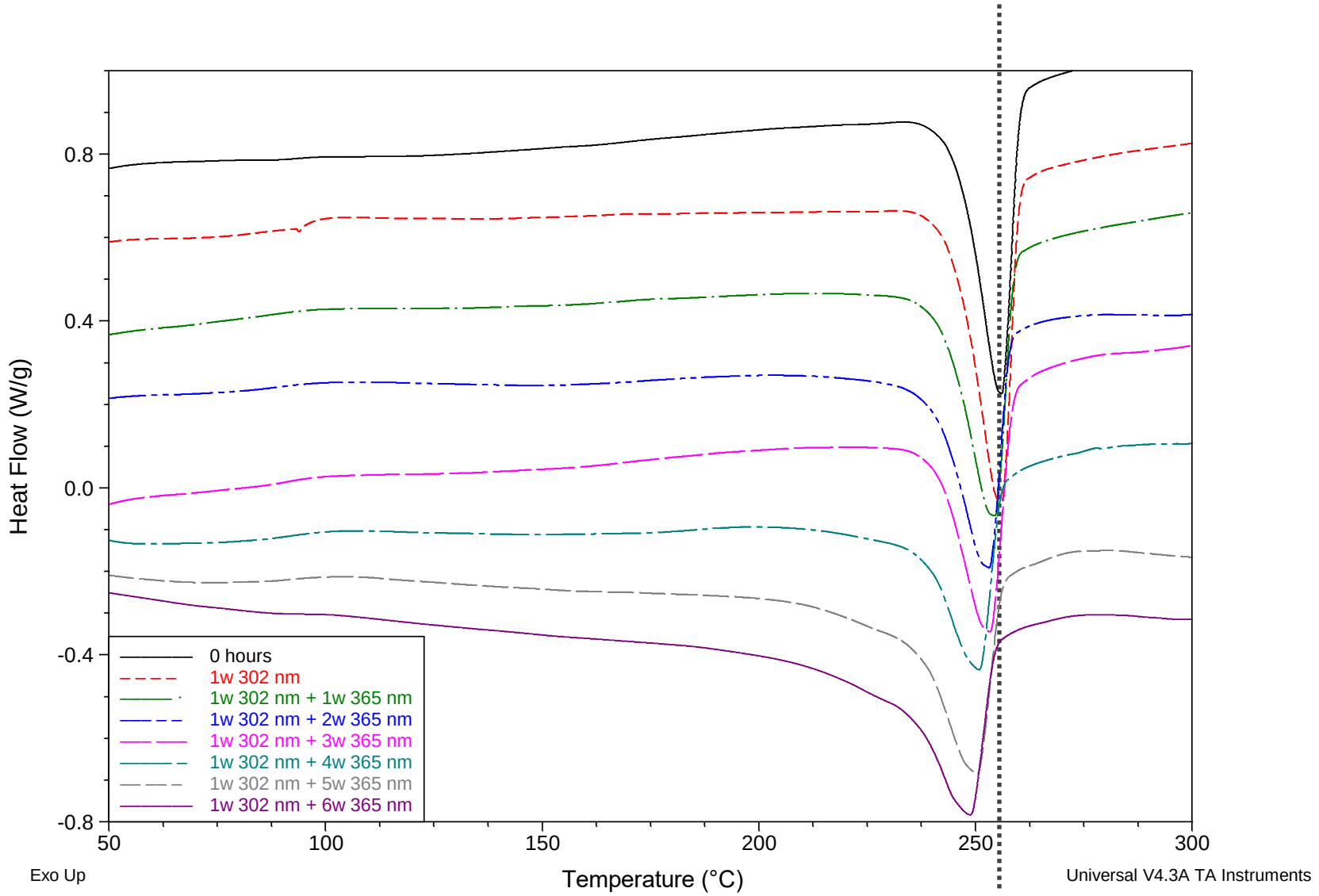

Figure 4.10: First heating cycle of DSC thermogram for PET film exposed to 302 nm light followed by 365 nm light.

4.1.5.2 Cooling cycle

Figure 4.11 shows the cooling cycles for samples exposed to 302 nm light followed by 365 nm light. The data shows that the T_c of the films initially increased with time when exposed to 302 nm light for 1 week. An increase in T_c indicates that chain scission has occurred, which is consistent with the mechanisms of photodegradation that have been proposed.[7,1] Chain scission reactions lead to the production of shorter chain fragments which can easily crystallise upon cooling. Therefore, the T_c increases due to the exposed polymer being able to crystallise quicker than the control sample during the cooling cycle.[30–33]

However, after exposure to 365 nm light, the T_c decreased with exposure time. A decrease in T_c indicates that branched or crosslinked chains could be produced during exposure. Branched or crosslinked chains make it more difficult for the polymer to crystallise during cooling, therefore the T_c decreases due to the undegraded polymer being able to crystallise quicker than the exposed sample during the cooling cycle. A decrease in T_c is in agreement with Jayakannan and co-workers,[34] but not agreeable with the study reported by Li *et al*.[35] Jayakannan *et* al studied the effect of branching on the crystallisation behaviour of PET. They reported that branched PET showed a lower T_c than that of linear PET at different cooling rates.[34] This also agrees with the decrease in T_m.

Exposing PET film to 302 nm light before exposing to 365 nm light influences the T_c of the sample. When exposed to 302 nm light, PET shows an increase in T_c and no meaningful change when exposed separately to 365 nm light, discussed in *Chapter 3, Section 3.4.3.*

The results from the DSC thermograms agree with the theory, proposed in *Chapter 3*, that short wavelength light causes chain scission to occur, whereas long wavelength light primarily causes branching and crosslinking to occur.

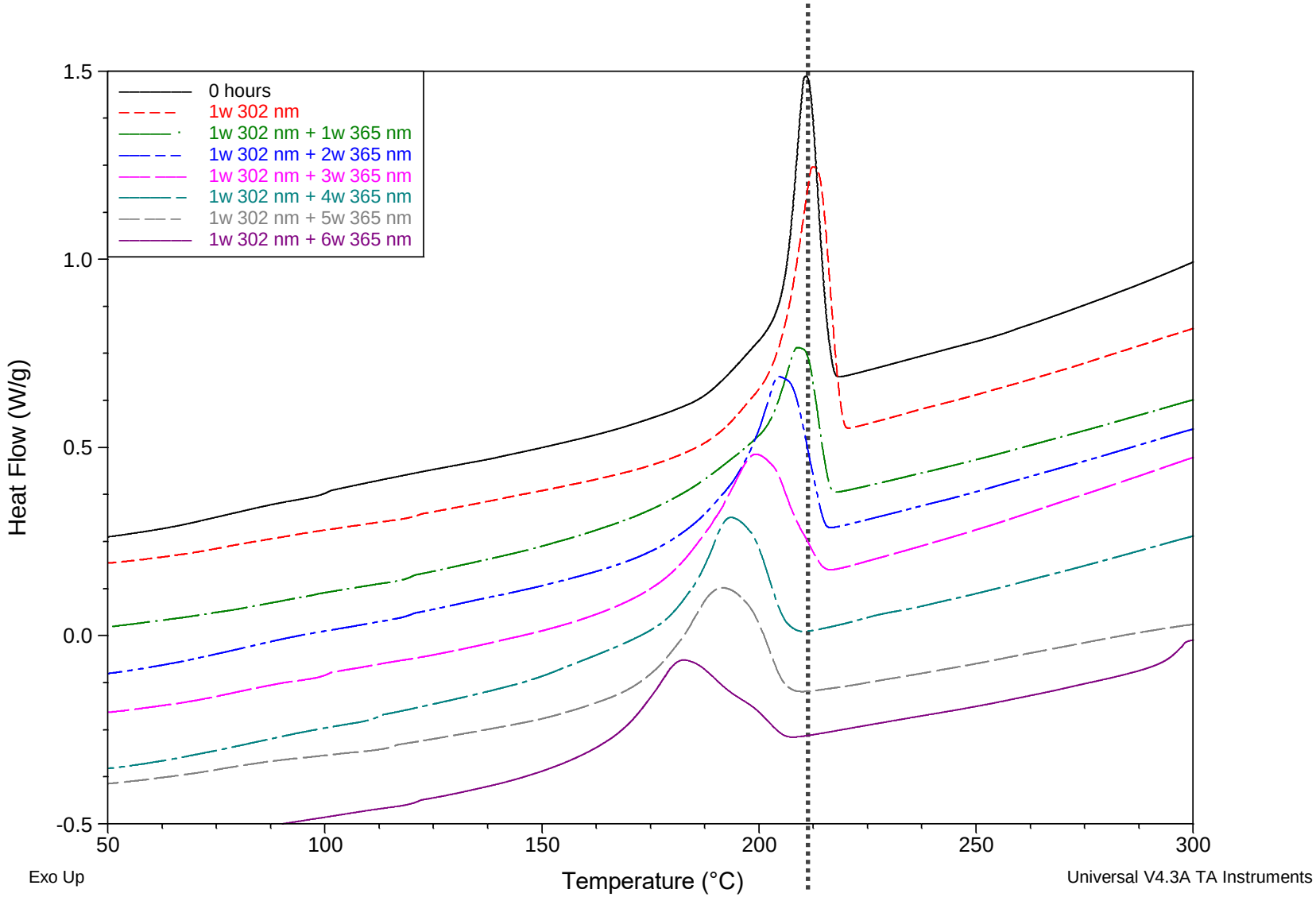

Figure 4.11: Cooling cycle of DSC thermogram for PET film exposed to 302 nm light followed by 365 nm light.

4.1.5.3 Reheat cycle

On the second heating cycle, shown in *Figure 4.12*, the melting temperature decreases with exposure time due to the crystals produced during the cooling cycle containing smaller, more imperfect molecules.[36,37]

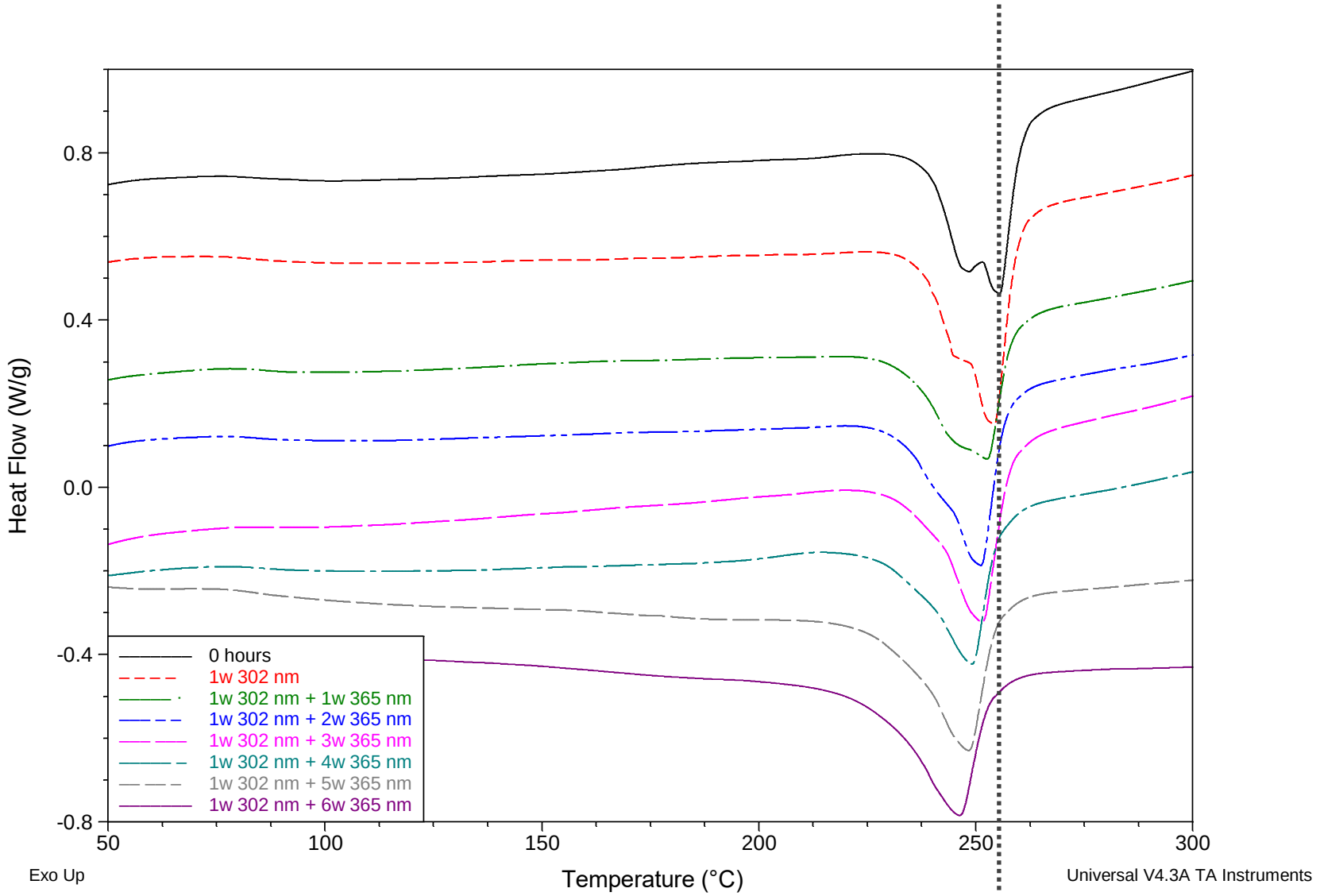

Figure 4.12: Second heating cycle of DSC thermogram for PET film exposed to 302 nm light followed by 365 nm light.

4.1.6 Contact Angle

Figure 4.15 shows the contact angle values for the front and back of each PET sample. A description of the sample names used on the x-axis of the graph in *Figure 4.15* are given in *Table 6*. Sample 'b' has been exposed to 302 nm light for 1 week and shows a decrease in contact angle on its front surface. This was expected as 302 nm light causes degradation primarily at the surface, which can be seen from the IR data reported in *Section 4.1.1*. On the rear face of the sample, there was no change in the contact angle. This is thought to be because 302 nm light is strongly absorbed at the surface, and therefore does not cause chemical change on the rear surface of the films.

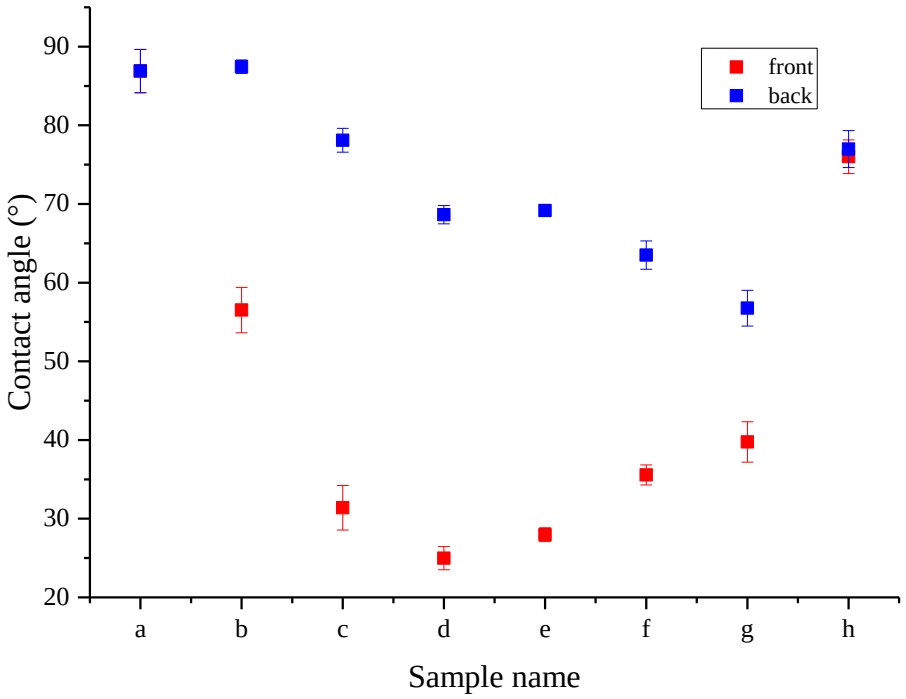

Figure 4.15: Contact angles of front and back side of 36 µm PET films exposed to 302 nm light followed by 365 nm light.

When the samples were then exposed to 365 nm light there was a further decrease in the contact angle on the front side and a decrease on the rear side of the film. The decrease on the rear side of the film can be explained due to the fact that 365 nm light is weakly absorbed by the film. The decrease on the front side of the films is thought

to be due to oxidation reactions which can occur under 302 nm or 365 nm light. It could also be the case that as 365 nm light can now be absorbed by the sample, due to the production of new chromophores (after exposure to 302 nm light), causing the formation of new hydrophilic groups.

Table 6: Description of the sample name on the x-axis of the graph in Figure 4.15.

Sample name	Sample description
a	0 hrs
b	1w 302 nm
c	1w 302 nm + 1w 365 nm
d	1w 302 nm + 2w 365 nm
e	1w 302 nm + 3w 365 nm
f	1w 302 nm + 4w 365 nm
g	1w 302 nm + 5w 365 nm
h	1w 302 nm + 6w 365 nm

A decrease in contact angle suggests that the surfaces of the films have become more hydrophilic upon exposure to UV light. This correlates with the fact that carboxylic acid groups are believed to be produced during the photodegradation of PET.

After exposure to 302 nm light for 1 week and a further 3 weeks of exposure to 365 nm light, the contact angle starts to increase with exposure time, on the front side of the films.

The decrease in contact angle followed by an increase, shown in *Figure 4.15*, could be explained by contact angle hysteresis. Contact angle hysteresis is known as the difference between the advancing angle, θ_a, and the receding angle, θ_r, as shown in *Equation 2*.[38]

$$\Delta\theta = \theta_a - \theta_r \qquad \textbf{Equation 2}$$

The receding and advancing angles are both characteristic of topography and surface chemistry.[39] An increase in contact angle, as shown in *Figure 4.15*, could be due to water condensing on the droplet at different rates for each sample of film. This could be possible as the contact angle values for each film were taken on separate occasions, which could mean the laboratory was at a different temperature each time.

The general conclusion, in the literature, seems to be that contact angle hysteresis arises from surface roughness and/or heterogeneity. It is therefore thought that this increase in contact angle could also be due to the heterogeneity of the surface or surface roughness. Contact angles measured on heterogeneous or rough surfaces would not solely reflect surface energies as surface topography would now need to be considered.

Contact angle values measured on a rough surface would be larger compared to a smooth surface. According to the Wenzel model water penetrates the surface grooves of a rough surface, resulting in higher surface wettability due to an increase in contact area, resulting in a decrease in the contact angle value.

In contrast, the Cassie-Baxter model water does not penetrate the surface grooves, on a rough surface, and lies on top of these grooves instead. This means that air bubbles are trapped in the grooves, resulting in an increase in the contact angle.[40] An illustration of these models is given in *Figure 4.16.*

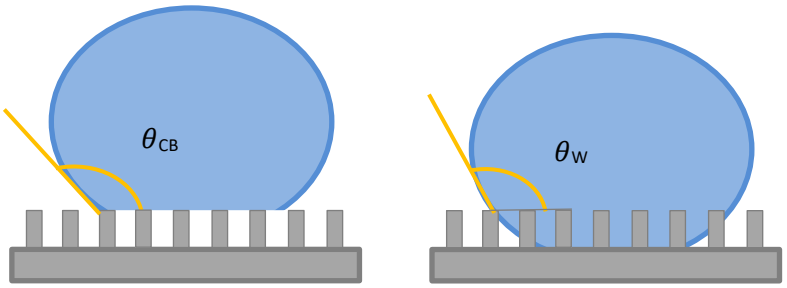

Figure 4.16: Illustration of Cassie-Baxter and Wenzel states.

4.1.7 Scanning Electron Microscopy

The SEM images taken before and after exposure to 302 nm for 1 week and further exposed to 365 nm light for 6 weeks are shown in *Figure 4.17*. After 1 week under 302 nm light surface cracks are visible, which can cause the initiation of fractures. This shows that not only is their chemical change during exposure, physical changes are also occurring. After further exposure to 365 nm light, there are no notable changes on the surface of the PET films. This confirms that 302 nm light is predominately causing degradation on the surface, while 365 nm light causes change in the bulk of the film.

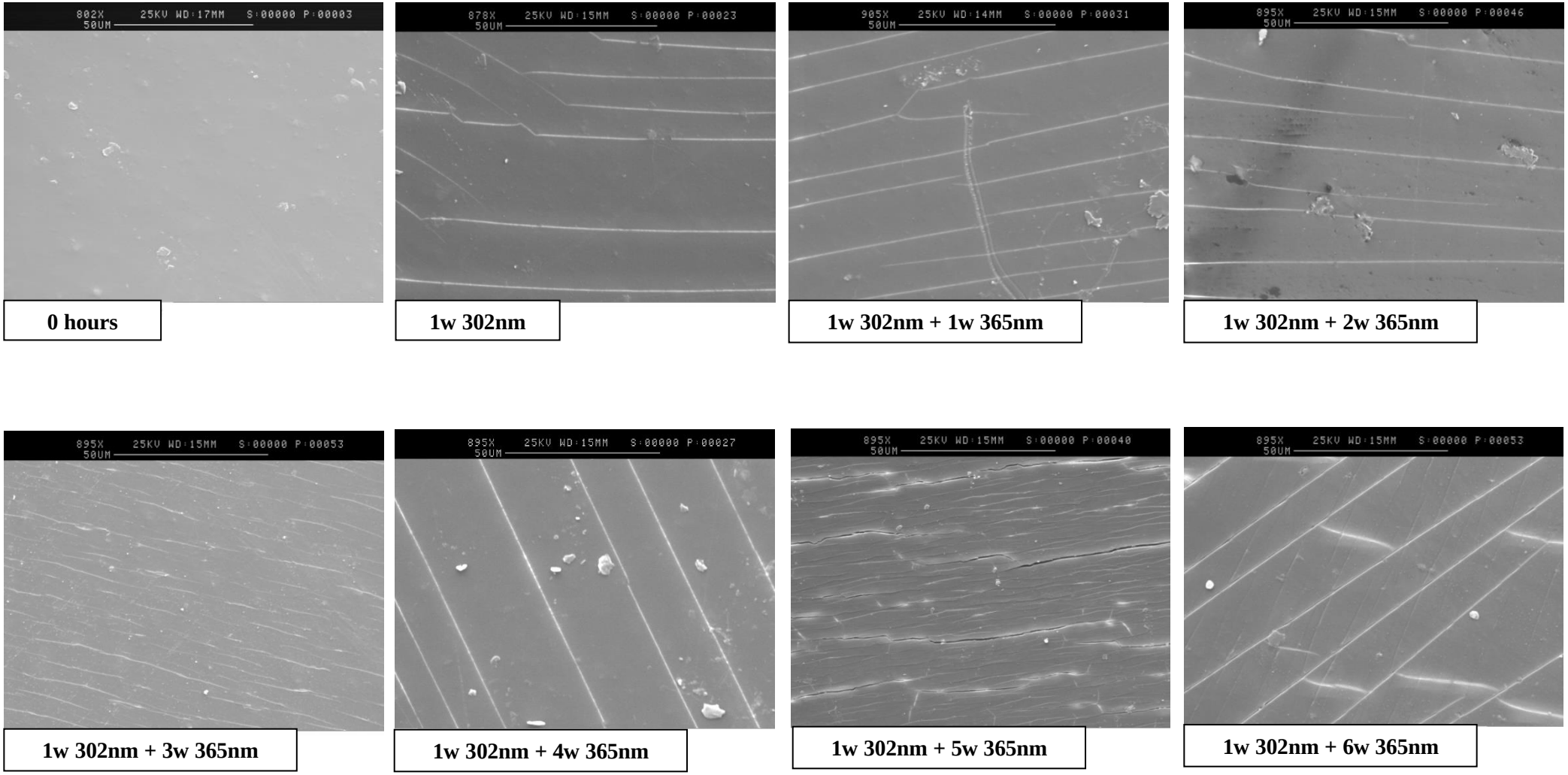

Figure 4.17: SEM images of PET samples exposed to 302 nm light for 1 week followed by 365 nm light for 6 weeks in 1 week increments.

4.1.8 Conclusions

The effect of pre-exposing PET films with 302 nm light followed by 365 nm light was analysed using various techniques. Exposing samples to 302 nm light produces new chromophoric groups, which allow the polymer to absorb light of longer wavelengths; 365 nm light. Results show the production of numerous degradation products including, carboxylic acid end groups, dimers, anhydrides, aldehydes and monohydroxy terephthalate groups. ATR spectra also show the formation of mono-substituted rings, after exposure to 365 nm light, which has never been reported before in literature during the photodegradation of PET films. Furthermore, results indicate that 302 nm light is causing chain scission, whereas 365 nm light is primarily causing branching and crosslinking reactions to occur, which supports results reported in *Chapter 3*. It is a reasonable assumption to conclude that exposure to 302 nm light does influence the effect of subsequent exposure to 365 nm light.

4.2 Exposure to 365 nm followed by 302 nm

4.2.1 ATR FT-IR

The films were exposed to 365 nm light with an average intensity of (825.5 ± 20) W m^{-2} and a temperature of (43 ± 2.5)°C, followed by 302 nm light at an average intensity of (31.7 ± 4.0) W m^{-2} and a temperature of (22.5 ± 2.5)°C.

The ATR spectra of PET exposed to 365 nm light followed by 302 nm light are given in *Figure 4.18*. *Figure 4.18* shows that after 1 week of exposure to 365 nm light (equivalent to a dosage of approximately 1.4 x 10^5 W m^{-2} hr^{-1}) there is no meaningful change in the spectra. However, after subsequent exposure to 302 nm light, changes are now present in the spectra of the front surface of the films. Spectral changes have been identified in the region between 3800-2100 cm^{-1} and the carbonyl and fingerprint regions, as reported before when samples were exposed only to 302 nm light (*Chapter 3, Section 3.4.1*). Changes in the spectra were only present on the front side of the films, with no notable change on the rear side.

Figure 4.19 shows the region of the ATR spectra of samples exposed to 365 nm light followed by 302 nm light, between 3800-2100 cm^{-1}, containing the hydroxy peaks as well as the aromatic and aliphatic C-H stretching peaks. The assigned peaks in this region are summarised in *Table 7.*

The development of peaks in this region, after exposure to 302 nm light, have been assigned to carboxylic acid end groups and dimers. There has also been a decrease in height of the peaks assigned to the crystalline and amorphous aliphatic CH_2 stretching vibrations, associated with chain scission reactions taking place during irradiation. Changes have been identified in other peaks in this region, including the size of the peaks associated with aromatic C-H stretching. The increase in size of these peaks is due to the production of mono-substituted rings, which results in another aromatic C-H bond on the ring. These peaks have been discussed in detail in *Section 4.1.1*.

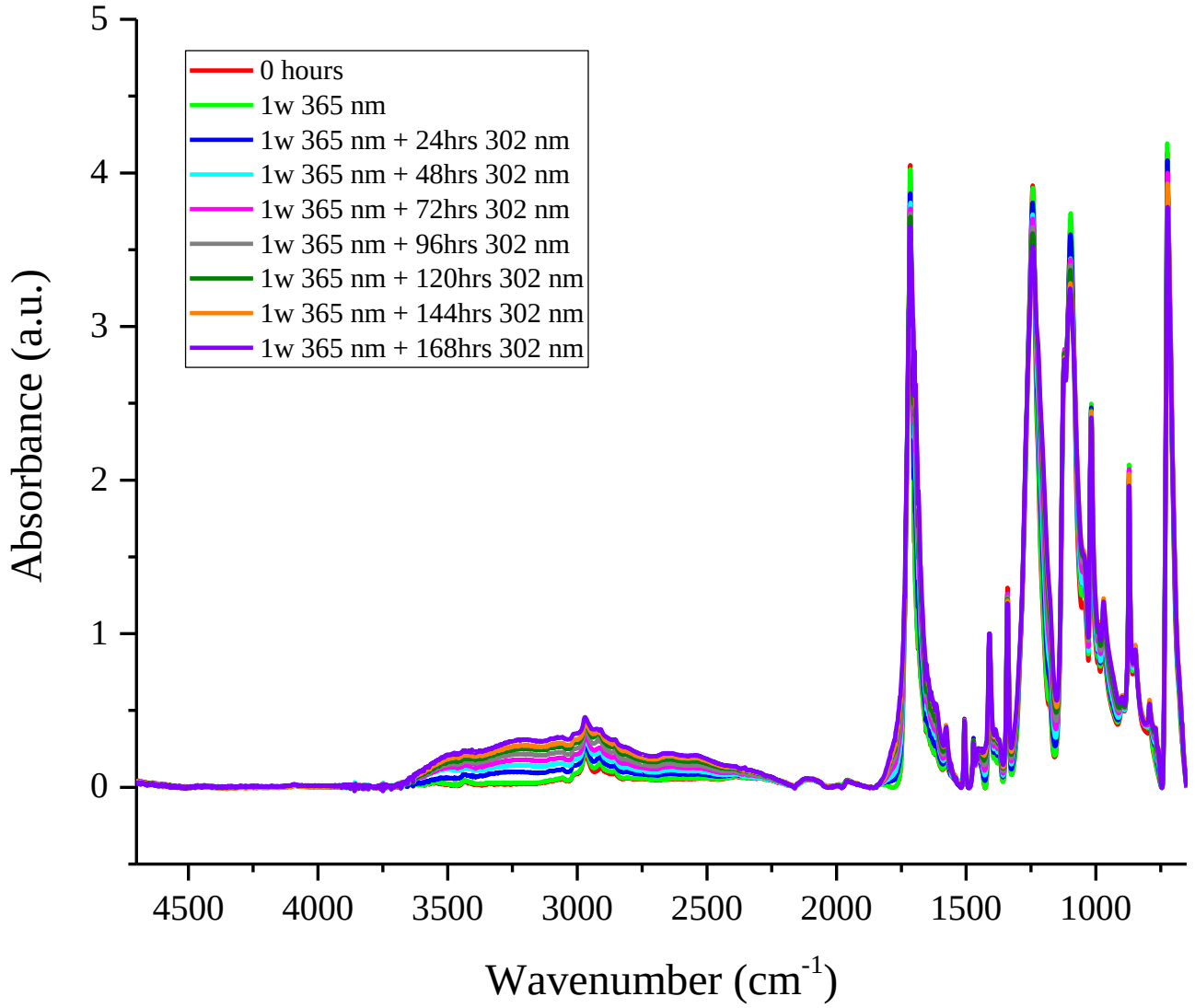

Figure 4.18: ATR FT-IR spectra of PET film samples exposed to 365 nm light for 1 week followed by exposure to 302 nm light for 1 week in 24 hour increments.

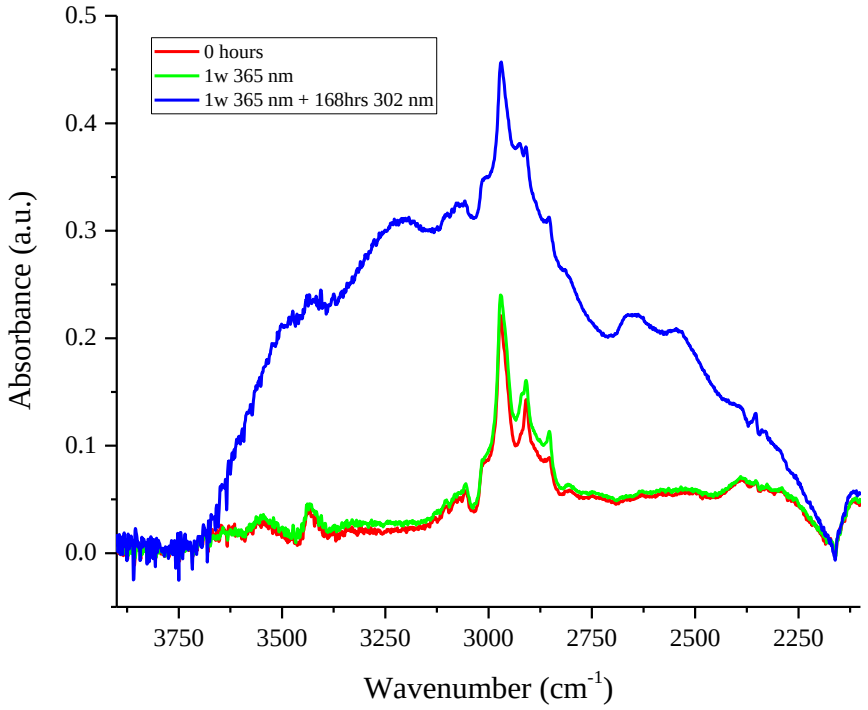

Figure 4.19: ATR spectra of 36 µm PET exposed to 365 nm light followed by 302 nm light, in the region between 3800-2100 cm^{-1}.

Table 7: Band assignments for the hydroxy region of the ATR spectrum of PET.

Peak (cm^{-1})	Assignment
3630	Aqueous O-H stretching vibration[7]
3550	Alcoholic O-H stretching vibration[7]
3430	First overtone of the carbonyl peak[7]
3290	Carboxylic acid end groups[7]
3100 – 3060	Aromatic C-H stretching[8]
3016, 2970, 2909	Crystalline aliphatic CH_2 stretching[8]
2928	C-H symmetric stretching vibration associated with the Ar-CH_3 group.
2965, 2855	Amorphous aliphatic CH_2 stretching[8]
2640, 2540	Characteristic of the carboxylic acid dimer[9]

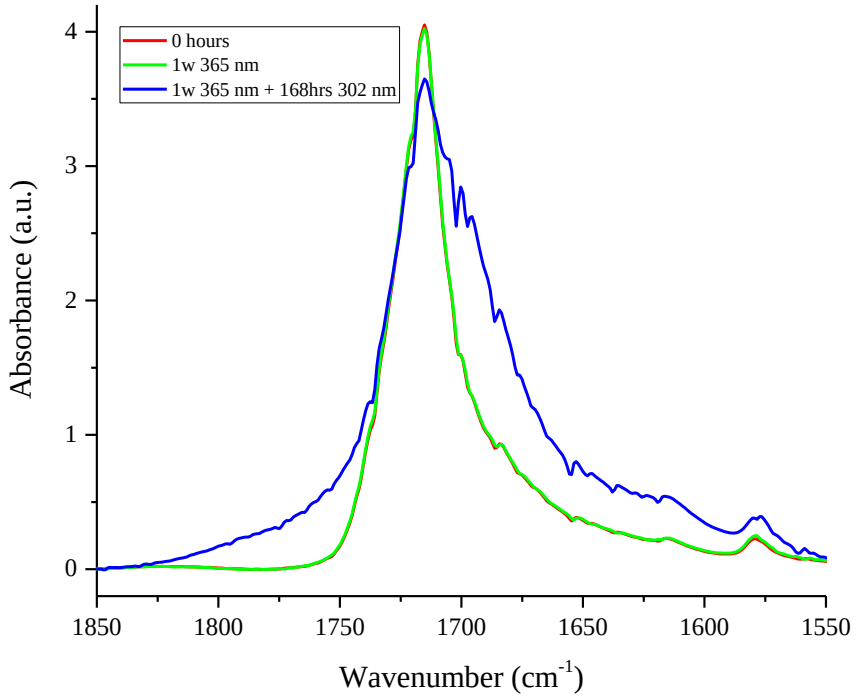

Figure 4.20: ATR spectra of 36 µm PET exposed to 365 nm light followed by 302 nm light, in the carbonyl region.

Table 8: Band assignments for carbonyl region of the ATR spectrum of PET.

Peak (cm^{-1})	Assignment
1785	Carbonyl stretch from anhydride carbonyl[12,13]
1738	Carbonyl stretch from aliphatic aldehyde[3]
1722	Amorphous carbonyl stretch from ester[8]
1714	Crystalline carbonyl stretch from ester[8]
1705	Carbonyl stretch from carboxylic acid dimer[4,13,14]
1700	Carbonyl stretch from carboxylic acid end groups[15]
1695	Carbonyl stretch from quinone groups[11,16]
1685	Carbonyl stretch from terephthalic acid

Figure 4.20 shows the carbonyl region, of the ATR spectra, for PET exposed to 365 nm light followed by 302 nm light. After exposure to 365 nm light, there is no meaningful change in the spectra, whereas, after further exposure to 302 nm light changes are now identifiable. The various peaks contained within the carbonyl region have been assigned and are given in *Table 8.*

At higher wavenumbers the carbonyl peak is shown to broaden, after exposure to 302 nm light, indicating the production of anhydride and aliphatic aldehyde groups. While at lower wavenumbers, peaks assigned to carboxylic acid dimers, carboxylic acid end groups, terephthalic acid and quinone species all increase in intensity with exposure time and cause the broadening of the peak. At the same time, there is a decrease in the peaks associated with the carbonyl stretch from the ester group, due to chain scission reactions occurring during irradiation. All peaks contained within the carbonyl region have been discussed in detail in *Section 4.1.1*.

As previously stated, the extent of photodegradation was measured by the change in area of the hydroxy peak and the carbonyl peak, shown in *Figure 4.21 (a) and (b)*, respectively. The graphs show the rate of photodegradation for a sample only exposed to 302 nm light and a sample exposed to 365 nm light before being exposed to 302 nm light. The red line, on both graphs, representing the control sample that was only exposed to 302 nm light, shows an extent of degradation similar to that of the sample pre-exposed to 365 nm light (the blue line). This shows that the changes in the hydroxy and carbonyl peaks are very similar for samples only exposed to 302 nm light compared to those pre-exposed to 365 nm light before being exposed to 302 nm light. This indicates that 365 nm light does not significantly influence the effect of subsequent exposure to 302 nm light. This was expected as PET does not have a strong absorbance at longer wavelengths of light, as shown in the UV-visible spectra in *Chapter 3, Section 3.3.3*.

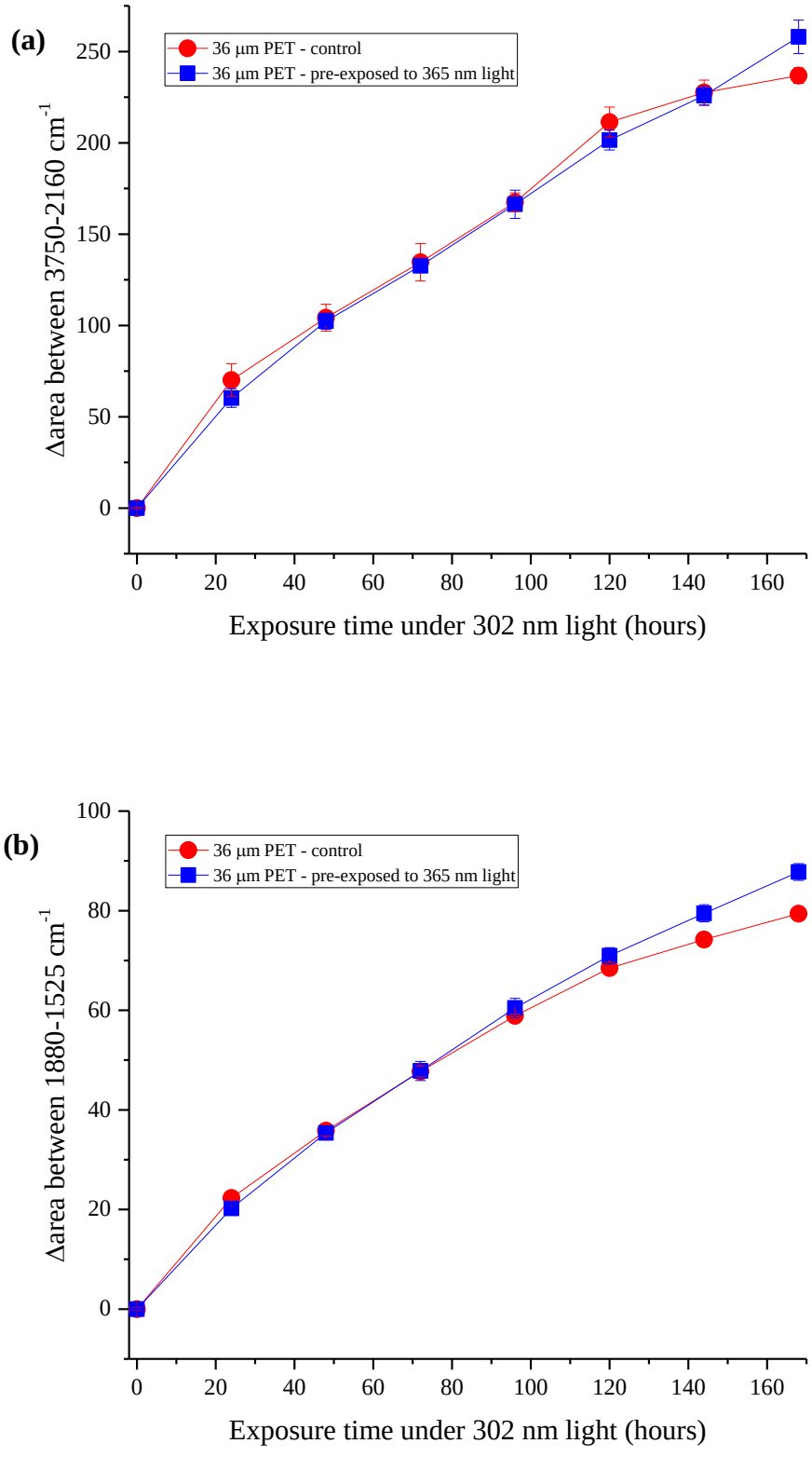

Figure 4.21: Extent of photodegradation measured by the change in area of the peaks between (a) 3750-2160 cm^{-1} and (b) 1880-1525 cm^{-1}, from the DRIFT spectra.

The fingerprint region of the control film and films exposed to 365 nm light followed by 302 nm light are shown in *Figure 4.22.* Assignments for peaks that have changed or developed in this region are given in *Table 9.*

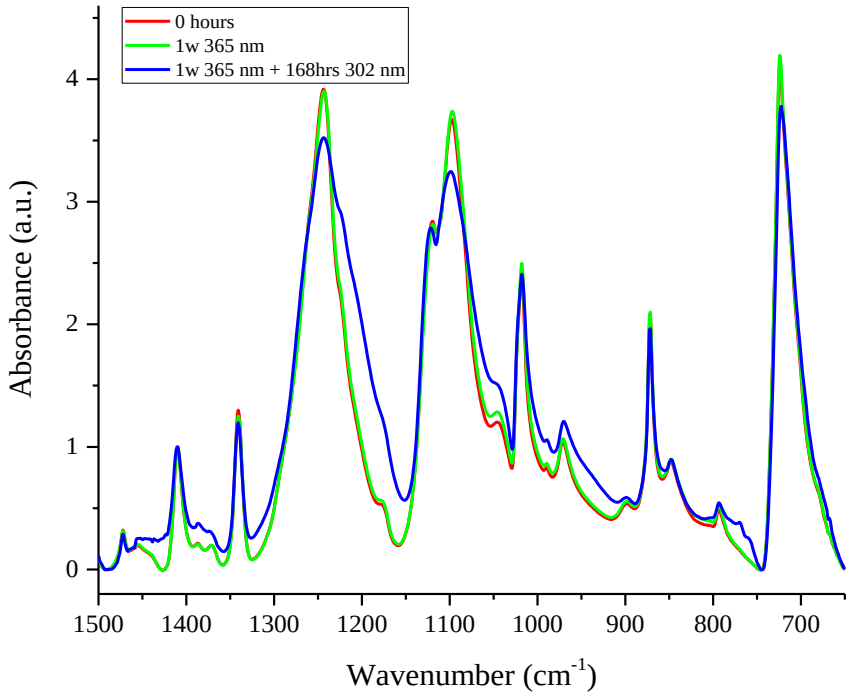

Figure 4.22: ATR spectra of 36 µm PET exposed to 365 nm light followed by 302 nm light, in the fingerprint region.

Peaks have developed in the spectra, after exposure, at 1430 and 1220 cm^{-1}, which are believed to be associated with the carboxylic acid dimer group. There has also been the evolution of a peak at 940 cm^{-1} which is related to the production of vinyl groups. Peaks associated with the trans and cis isomers of the ethylene glycol segment have shown a reduction in size, linked to the scission of the ester links during photodegradation. Spectral changes have also been identified in the peak at 848 cm^{-1} and in the development of two new peaks at 769 and 758 cm^{-1}, which indicate a change in the substitution pattern of the terephthalic ring.

Table 9: Band assignments for the fingerprint region of the ATR FT-IR spectrum of PET.

Peak (cm^{-1})	Assignment
1430	Combination band due to C-O stretching and O-H deformation vibration, associated with carboxylic acid dimer.[3]
1220	C-O stretching vibration, associated with carboxylic acid dimer.[3]
970	Stretching of C-H bond of the trans isomer of the ethylene glycol unit.[8]
940	C-H vibration associated with vinyl groups.[17]
898	Stretching of C-H bond of the cis isomer of the ethylene glycol unit.[8]
848	C-H deformation of two adjacent hydrogens on the terephthalic ring (indicates 1, 4 substitution)[18]
769	Out-of-plane deformation vibrations of 1, 2, 3-substituted rings[3]
758	Out of plane deformation vibrations of 1, 2, 4-substituted rings[3]

ATR spectra show that exposing PET to 365 nm light does not appear to have any significant difference to further exposure to 302 nm light on the ATR spectra, shown in *Figure 4.18*. This could be because the absorbance of light at 365 nm is very low for PET, so no new chromophores will be produced on the surface of the film. When the samples are then exposed to 302 nm light, changes are due to the strong absorbance in this wavelength range and cause the production of new chromophoric groups.

4.2.2 DRIFT

DRIFT spectra of samples exposed to 365 nm light for 1 week (equivalent to a dosage of approximately 1.4×10^5 W m^{-2} hr^{-1}) followed by 302 nm light for 1 week, in 24 hour increments, are shown in *Figure 4.23*.

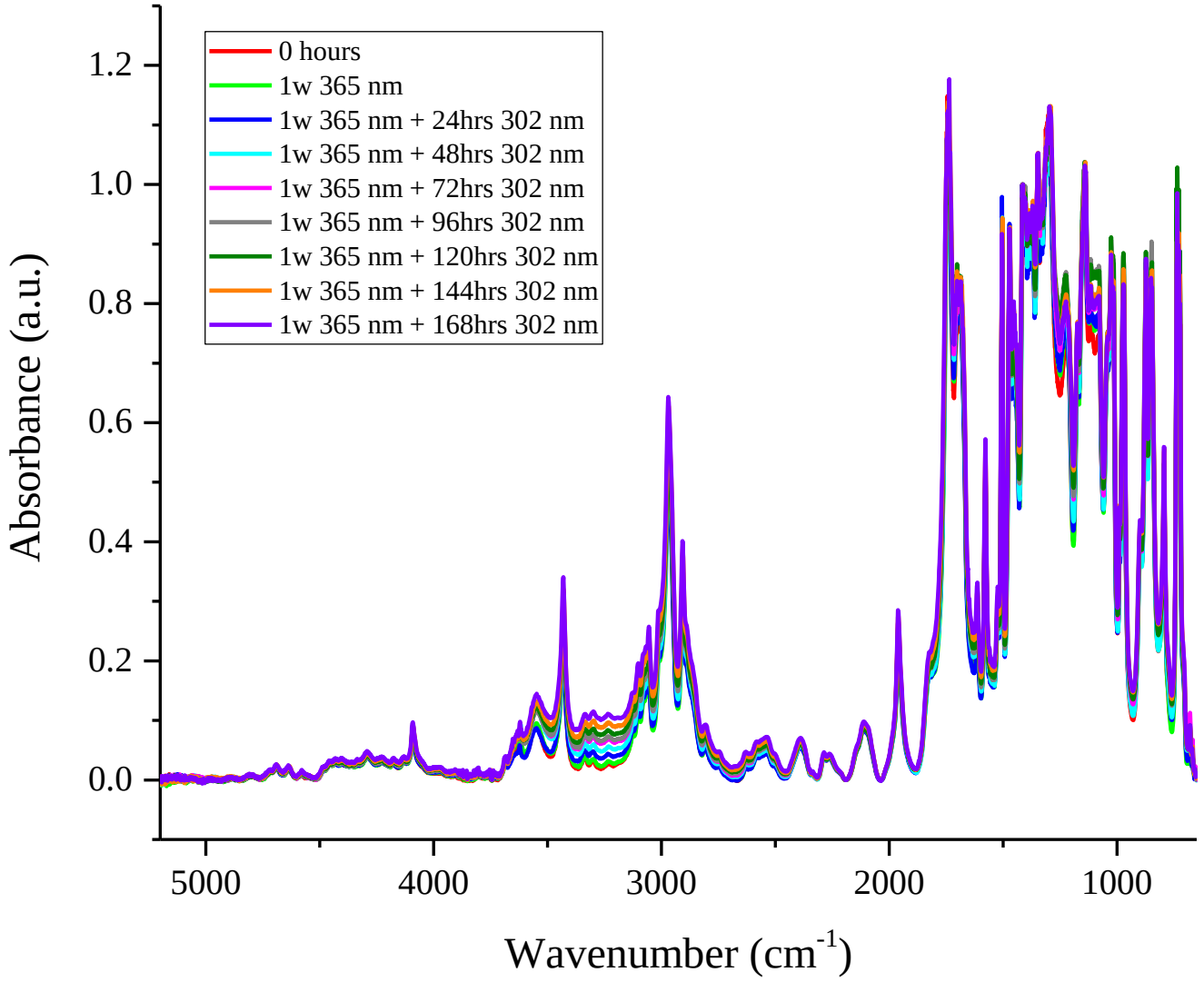

Figure 4.23: DRIFT spectra of PET film samples exposed to 302 nm light for 1 week followed by exposure to 365 nm light for 6 weeks in 1 week increments.

Exposure to 365 nm light for 1 week shows only very minor changes in the DRIFT spectra. However, after prolonged exposure, 365 nm light causes major changes in the spectra, as shown in *Chapter 3*, indicating that these minor changes after 1 week of exposure are significant. Therefore, exposing PET to 365 nm light primarily effects the bulk of the film and not the surface, as no changes were identified in the ATR spectra. Although absorbance at 365 nm is low for PET, a high intensity lamp was used in this study.

After further exposure to 302 nm light, spectral changes are primarily observed in the region between 3800-2100 cm^{-1} and the carbonyl region. The assignments for peaks present in the region between 3800-2100 cm^{-1} for samples exposed to 365 nm light followed by 302 nm light are given in *Table 10*. The key change in this region is the increase in absorbance of the peaks assigned to the aqueous, alcoholic and carboxylic acid hydroxy stretches. This suggests that new hydroxy groups have been produced during exposure, including carboxylic acid end groups. This region has been discussed in detail in *Section 4.1.2*.

Table 10: Band assignments for the region between 3800-2100 cm^{-1} of the DRIFT spectrum of PET.

Peak (cm^{-1})	Assignment
3620	Aqueous O-H stretching vibration[7]
3550	Alcoholic O-H stretching vibration[7]
3430	First overtone of the carbonyl group in ester[7]
3335	First overtone of carbonyl group in carboxylic acid end group[21]
3290	Carboxylic acid end groups[7]
3100, 3078, 3067, 3054	Aromatic C-H stretching[8]
3015, 2970, 2908	Crystalline aliphatic CH_2 stretching[8]
2963, 2855	Amorphous aliphatic CH_2 stretching[8]

The peaks in the carbonyl region of the DRIFT spectra, shown in *Figure 4.23*, have been assigned and are given in *Table 11*. In the control film, the peaks present include those assigned to the carbonyl stretch of the ester and those of the terminal acid end groups. After irradiation, a shoulder has developed at higher wavenumbers which has been assigned to the carbonyl stretch of the anhydride group. These peaks have been discussed in further detail in *Section 4.1.2*.

Table 11: Band assignments for the carbonyl region of the DRIFT spectrum of PET.

Peak (cm^{-1})	Assignment
1785	Carbonyl stretch from anhydride carbonyl[12]
1743	Carbonyl stretching vibration of an ester[21]
1683	Carbonyl stretch from terminal acid end groups[21]

Plots of the extent of photodegradation, determined as the change in area of the hydroxy and carbonyl peaks, are shown in *Figure 4.24 (a) and (b).* Both graphs show the rate for samples exposed to 365 nm light followed by 302 nm light as well as samples only exposed to 302 nm light. The graphs show that both sets of samples show similar extents of degradation. However, after 120 hours of exposure the sample only exposed to 302 nm light appears to degrade to a greater extent than the sample exposed to 365 nm light followed by 302 nm light. This indicates that pre-exposing samples to 365 nm light could have an effect after prolonged exposure to 302 nm light. This wavelength of light (365 nm) is absorbed weakly, confirming why the bulk of the film would be affected and not the surface, as seen from the ATR spectra. Although PET only shows a very small absorbance at 365 nm light, a very intense light source is used in this study.

The fact that both trends on the graph are quite similar, indicates that exposing samples to 365 nm light has no major effect on further exposure to 302 nm light, at short exposure times. Prolonged exposure could highlight differences in samples pre-exposed to 365 nm light.

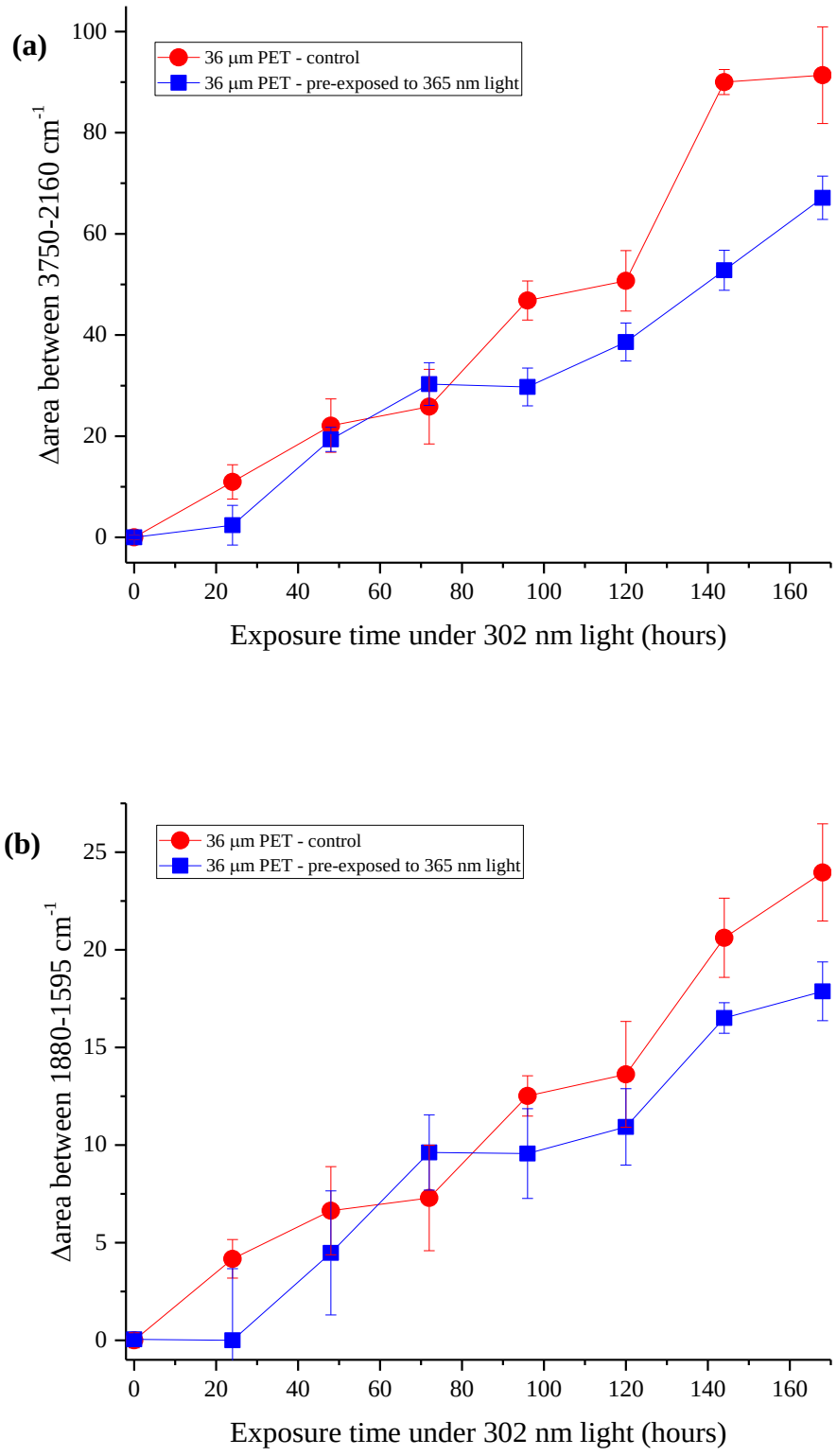

Figure 4.24: Extent of photodegradation measured by the change in area of the peaks between (a) 3750-2160 cm^{-1} and (b) 1880-1595 cm^{-1}, from the DRIFT spectra.

4.2.3 UV-visible spectroscopy

Figure 4.28 shows the UV-visible spectra for samples exposed to 365 nm light followed by 302 nm light. From this, it is apparent that only minor spectral changes can be identified in the spectrum associated with the PET exposed to 365 nm light after 1 week. After further exposure to 302 nm light, an increase in absorbance at 340 nm and a minor increase at 400 nm are observed. This increase in absorbance at longer wavelengths is indicative of the production of new chromophores with irradiation time.

As described previously, in *Section 4.1.3,* the increase at 340 nm has been attributed to monohydroxy terephthalate groups. These species were identified by Pacifici and Straley,[27] and a pathway for their production was proposed by Day and Wiles,[27] which is given in *Chapter 1, Figure 1.28.* The minor increase in absorbance at 400 nm has been attributed to the production of quinone groups and Fechine *et al.* have proposed a mechanistic pathway for their production, given in *Chapter 1, Figure 1.31.* This increase at 400 nm has also been discussed further in *Section 4.1.3.*

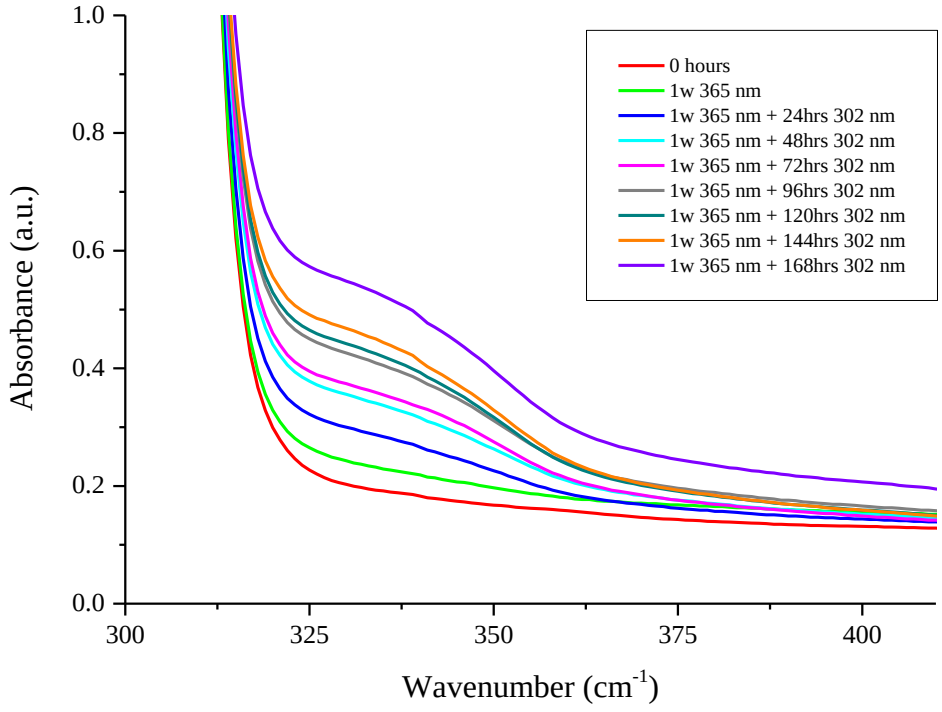

Figure 4.28: UV-visible spectra of 36 µm PET film samples exposed to 365 nm light followed by 302 nm light.

Figure 4.29 shows the change in absorbance at 340 nm for the samples exposed to 365 nm followed by 302 nm and samples exposed to 302 nm light only. Both samples have quite similar trends, but samples pre-exposed to 365 nm light appear to degrade to a slightly lesser extent than samples exposed to 302 nm light only. At short timescales exposing samples to 365 nm light does not seem to have a major effect on further exposure. However, it is thought that after prolonged exposure, differences would be evident. This supports the rates of the photodegradation calculated from the DRIFT data reported in *Section 4.2.2*.

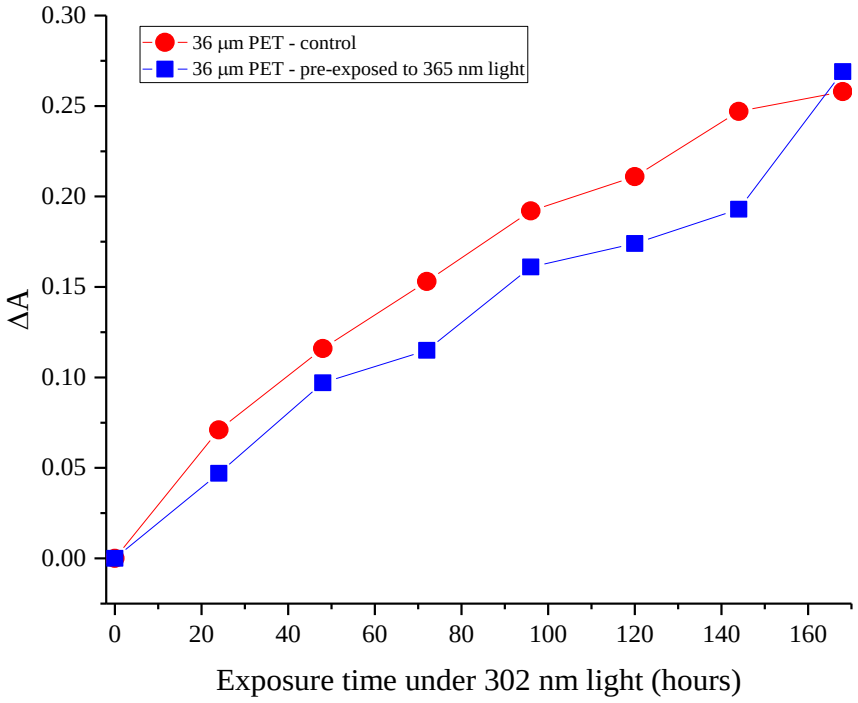

Figure 4.29: Change in absorbance at 340 nm with exposure time under 302 nm light.

4.2.4 Fluorescence spectroscopy

Figure 4.30 shows the fluorescence emission spectra for a control film of PET and samples exposed to 365 nm light followed by 302 nm light. The control sample, depicted by the black line on the graph, shows peaks at 370 and 385 nm and a shoulder

at 410 nm. Both peaks have been studied by various groups and at present, the peak at 370 nm has been attributed to an excimer, and the peak at 385 nm with the shoulder at 410 nm are known to be associated with a ground state dimer.[24] The assignments of the peaks have been discussed previously, in more detail, in *Section 4.1.4.*

After exposure to 365 nm light for 1 week, the intensity of the initial emission peak decreases, which has been reported to be due to a loss of interaction between chromophores. There is also the development of a peak centered at 475 nm, after irradiation. This emission peak, at 475 nm, has been previously discussed in *Section 4.1.4.* A mechanistic pathway for the production of these groups was proposed by Day and Wiles, shown in *Chapter 1, Figure 1.87.*[28]

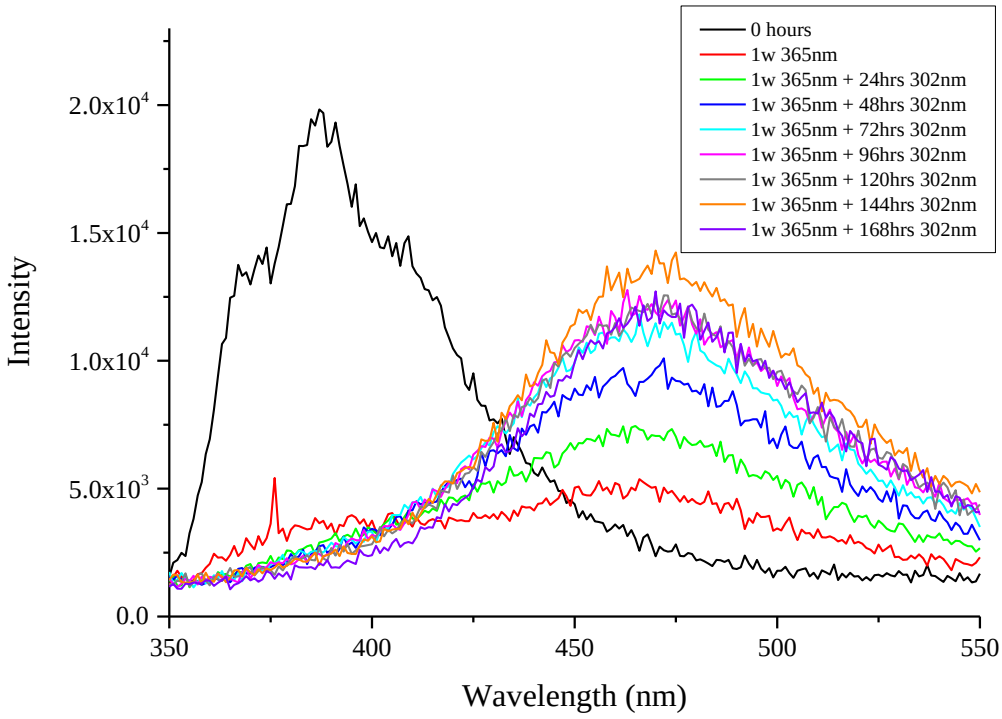

Figure 4.30: Fluorescence spectra of 36 µm PET film samples exposed to 365 nm light followed by 302 nm light.

Although it has been proposed that 365 nm light primarily causes branching and crosslinking, chain scission reactions are still possible under this wavelength range of

light. Considering the reaction pathway, shown in *Chapter 1, Figure 1.26*, the chain scission reactions that take place in steps 3 and 4 can be accomplished when PET is exposed to the 365 nm light range used in this study. This explains why monohydroxy terephthalate groups are produced and why the initial fluorescence emission peaks diminish after exposure to high intensity 365 nm light.

After further exposure to 302 nm light the peak at 475 nm increases with exposure time. At longer hours of exposure with 302 nm light, there is some fluctuation in the intensity of this peak. This is thought to be due to the production and subsequent attack of the new chromophoric groups. A reaction pathway for the breakdown of these groups has been discussed in *Chapter 3, Section 3.3.3* and is given in *Figure 3.20*.

4.2.5 DSC

4.2.5.1 Heating cycle

Figure 4.25 shows the first heating cycle for samples exposed to 365 nm light followed by 302 nm light. After exposure to 365 nm light for 1 week, there is no notable change in the melting temperature. After further exposure to 302 nm light, there is still no meaningful change in the melting temperature. A small decrease in the onset temperature of the melting peak was observed. This indicates that at prolonged hours of exposure a decrease in melting temperature may occur.

The same observations were made for samples exposed to 302 nm light, with no pre-exposure (*Chapter 3, Section 3.4.4*). This indicates that exposing samples to 365 nm light before exposing to 302 nm light has no effect on the melting temperature of the polymer.

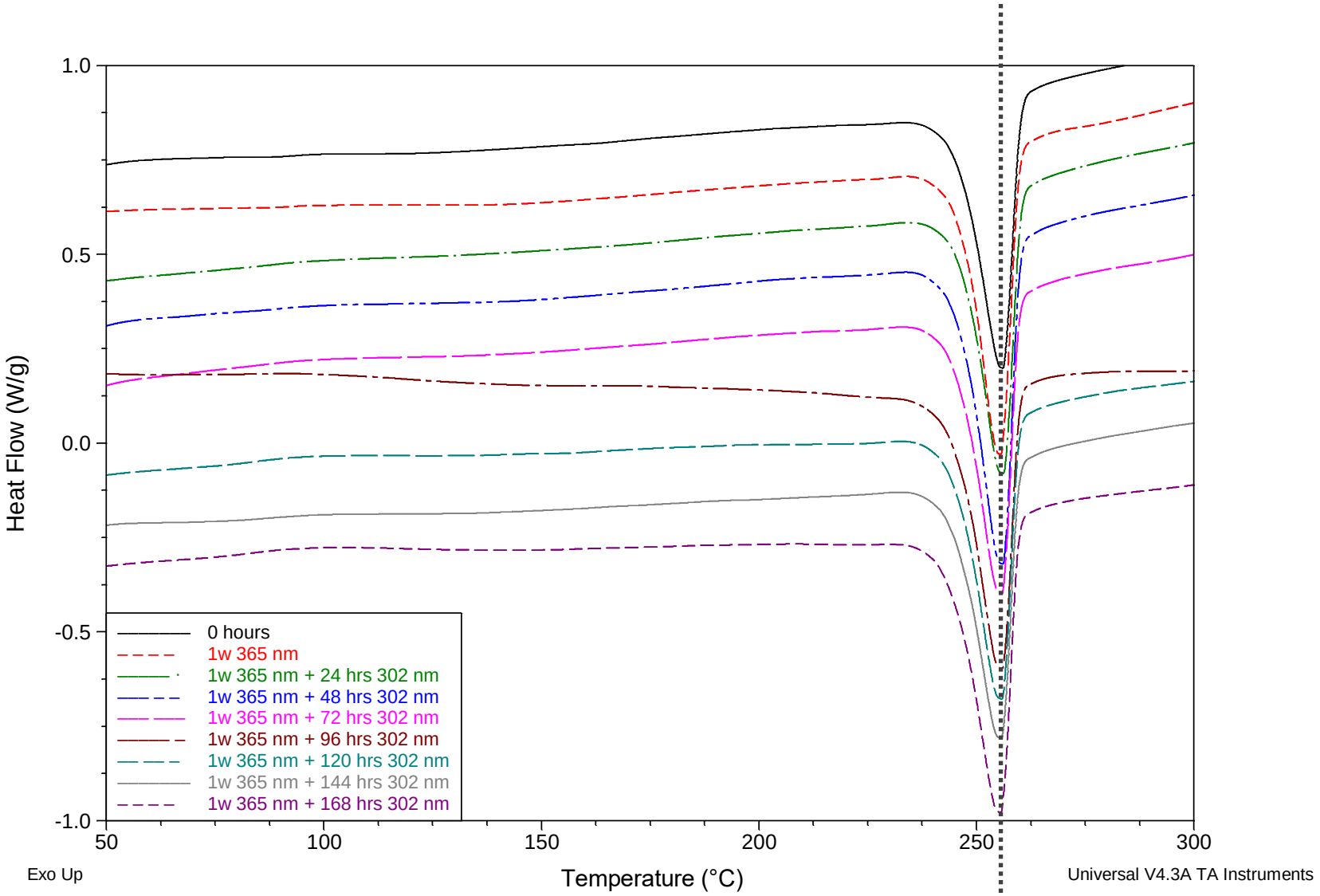

Figure 4.25: Heating cycle of DSC thermogram for PET film exposed to 365 nm light followed by 302 nm light.

4.2.5.2 Cooling cycle

Figure 4.26 shows the cooling cycle for samples exposed to 365 nm light followed by 302 nm light. The data shows no meaningful change in the crystallisation temperature after exposure to 365 nm light for 1 week, which agrees with results reported for samples exposed to 365 nm light only (*Chapter 3, Section 3.4.4*).

After further exposure to 302 nm light there is a slight increase in T_c which indicates that chain scission is occurring during exposure. Chain scission reactions lead to the production of shorter chain fragments which can easily crystallise upon cooling. Therefore, the T_c increases due to the exposed polymer being able to crystallise more easily than the control sample during the cooling cycle.

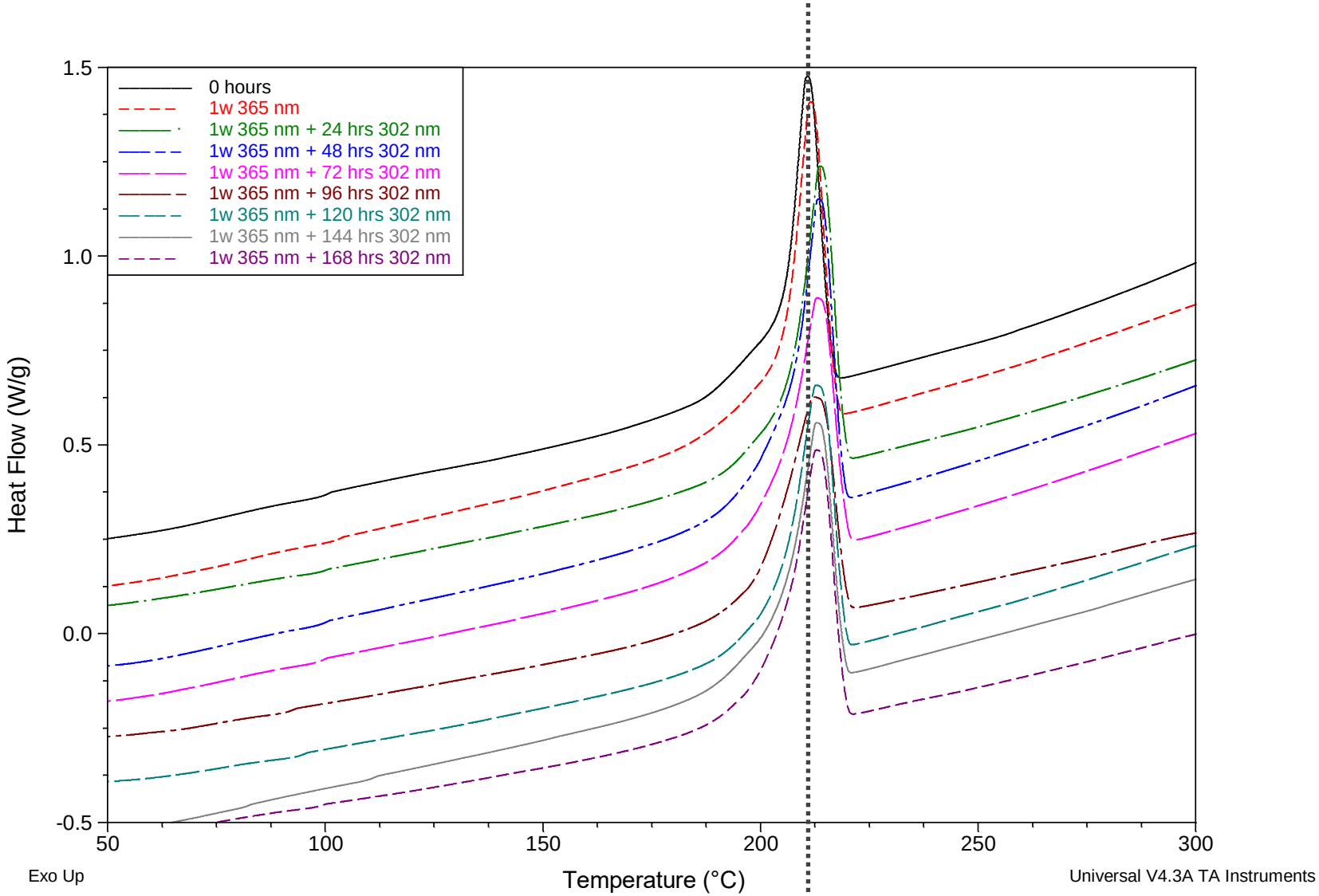

Figure 4.26: Cooling cycle of DSC thermogram for PET film exposed to 365 nm light followed by 302 nm light.

Although there is an increase in T_c with exposure to 302 nm light (after exposure to 365 nm light), the increase is not as large compared to samples that have only been exposed to 302 nm light.

As previously stated, it is believed that 365 nm light primarily causes branching and crosslinking reactions in the polymer, during exposure. However, as discussed there was no meaningful change in the crystallisation peak after the sample was exposed to 365 nm light for 1 week. Therefore, a sample that was exposed to 365 nm light for 4 weeks was analysed using the DSC, shown in *Figure 4.27*. From this, it is apparent that the T_c has started to decrease after exposure, which indicates that branched or crosslinked chains could be produced during exposure.

Considering this, it is thought that exposing PET to 365 nm light could be initiating branching or crosslinking, causing a decrease in the ratio of chain scission to branching and crosslinking, when the sample is subsequently exposed to 302 nm light.

Therefore, if samples were exposed to 365 nm light for longer, before being exposed to 302 nm light, it is thought that this would have a greater effect on the change in crystallisation temperature.

The results reported here also support the theory that short wavelength light causes chain scission to occur, whereas long wavelength light primarily causes branching and crosslinking to occur, during exposure.

4.2.5.3 Reheat cycle

On the second heating cycle, shown in *Figure 4.28*, the melting temperature shows no meaningful change when samples are pre-exposed to 365 nm light followed by 302 nm light. The same observations were made for samples exposed to 302 nm light only (*Chapter 3, Section 3.4.4*).

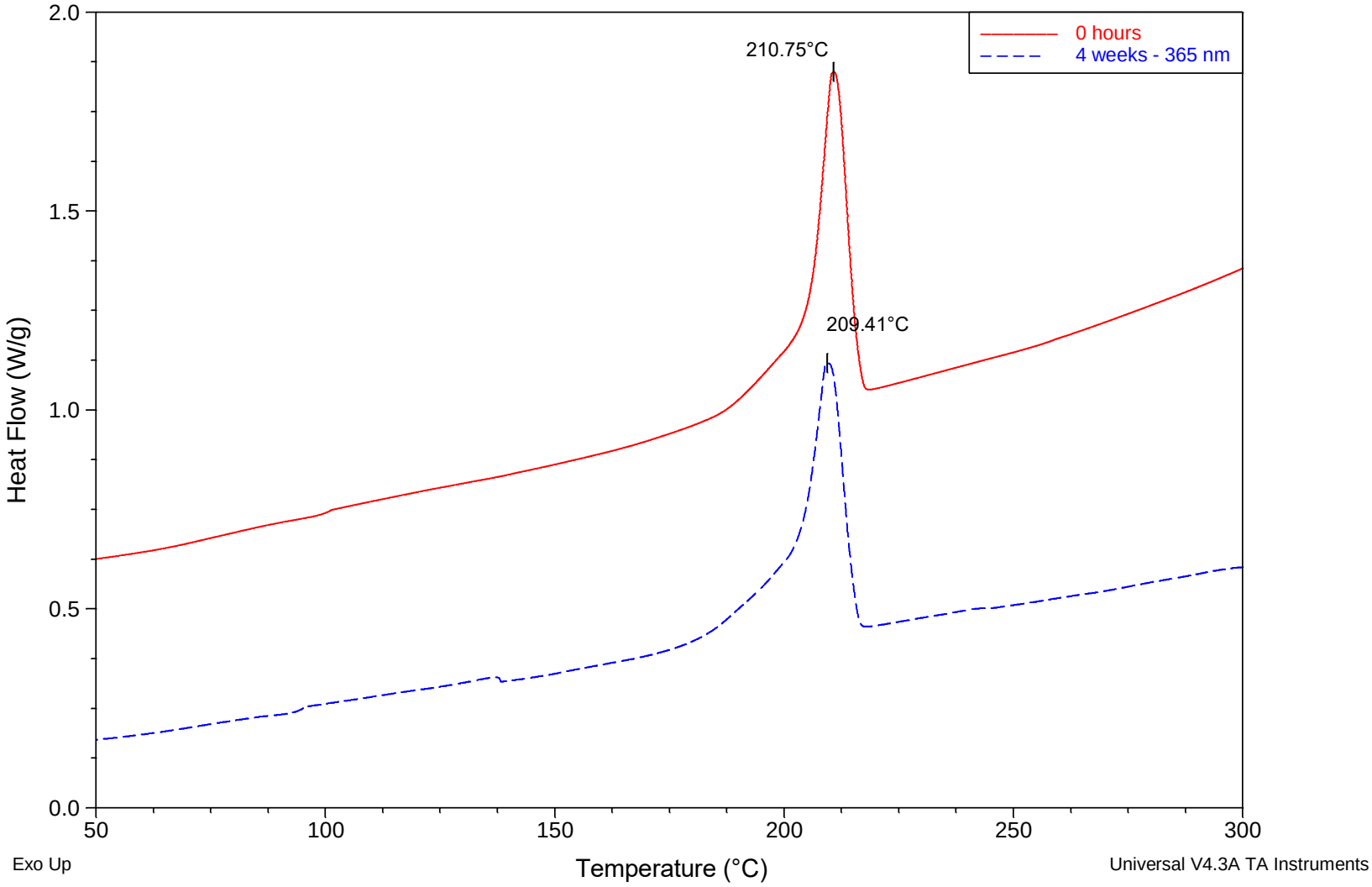

Figure 4.27: Cooling cycle of DSC thermogram for a control sample of PET film and sample exposed to high intensity 365 nm light for 4 weeks.

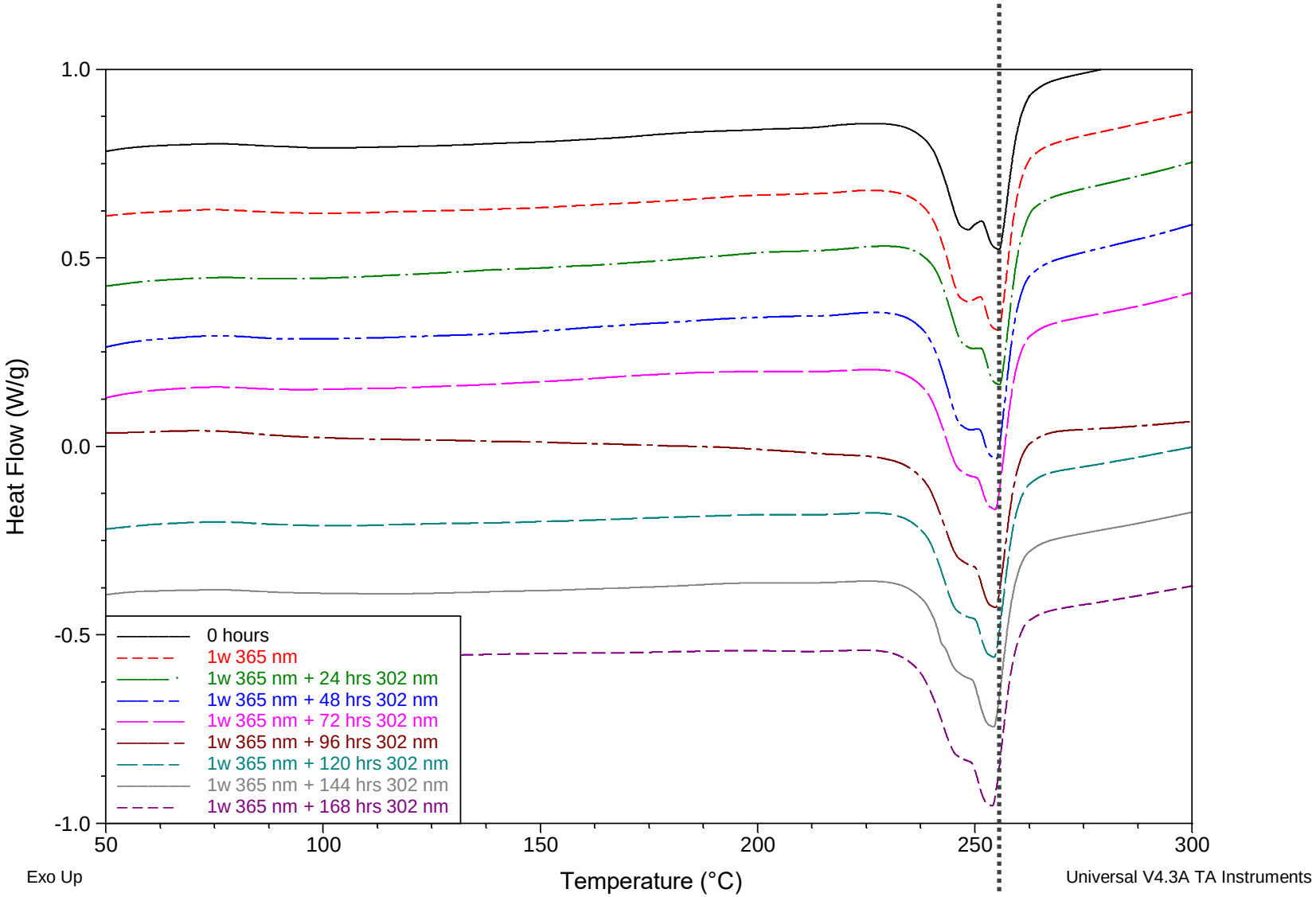

Figure 4.28: Reheat cycle of DSC thermogram for PET film exposed to 365 nm light followed by 302 nm light.

4.2.6 Contact Angle

The contact angle measurement for the front and back sides of PET samples exposed to 365 nm light followed by 302 nm light are given in *Figure 4.31*. A description of the sample names used on the x-axis of the graph in *Figure 4.31* are given in *Table 12*.

After 1 week of exposure to 365 nm light, there is a decrease in contact angle for both the front and back sides of the films *(sample a)*. On the front side of the film this decrease is thought to be due to oxidation reactions which occur under either wavelength of light. From previous results and considering the fact that 365 nm light is absorbed weakly the decrease on the rear side of the film was expected.

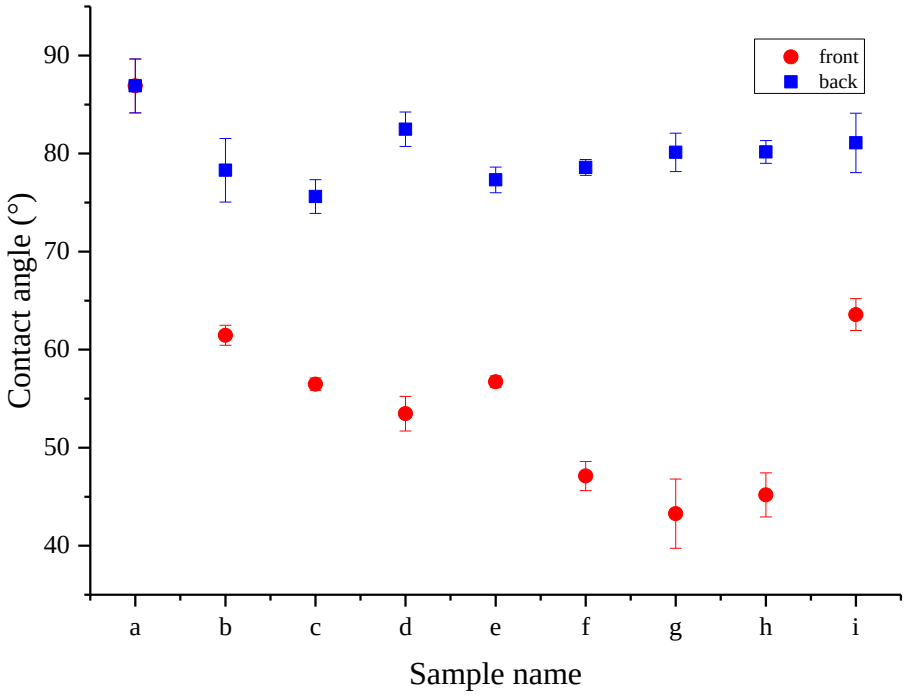

Figure 4.31: Contact angles of front and back side of 36 µm PET films exposed to 365 nm light followed by 302 nm light.

After further exposure to 302 nm light there was a decrease in contact angle on the front side with exposure time, but no notable change on the rear side of the films. The decrease on the front side was expected as 302 nm light causes degradation primarily

at the surface. The fact that there was no notable change on the rear side of the films is thought to be because 302 nm light is weakly penetrating and therefore does not cause any chemical change on the rear side of the film.

A decrease in contact angle indicates that the surface of the sample has become more hydrophilic upon exposure. This agrees with the mechanisms proposed for the photodegradation of PET, where carboxylic acid end groups and mono-hydroxy terephthalate groups are produced. The pathways for the production of these products are given in *Chapter 1, Figure 1.29.*

Table 12: Description of sample name on the x-axis of the graph in Figure 4.31.

Sample name	Sample description
a	0 hrs
b	1w 365 nm
c	1w 365 nm + 24 hrs 302 nm
d	1w 365 nm + 48 hrs 302 nm
e	1w 365 nm + 72 hrs 302 nm
f	1w 365 nm + 96 hrs 302 nm
g	1w 365 nm + 120 hrs 302 nm
h	1w 365 nm + 144 hrs 302 nm
i	1w 365 nm + 168 hrs 302 nm

At longer hours of exposure (*sample i*) the front surface of the films shows an increase in contact angle. This is believed to be due to the heterogeneity of the surface or surface roughness. Contact angles measured on heterogeneous or rough surfaces would not solely reflect surface energies as surface topography would now need to be considered. This has been discussed further in *Section 4.1.6.*

4.2.7 Scanning Electron Microscopy

The SEM images taken before and after exposure to 365 nm light for 1 week and 302 nm for a further week are shown in *Figure 4.32*. This shows that there has been no notable change on the surface of the PET sample after exposure to 365 nm light for 1 week. This indicates that 365 nm light causes no considerable damage to the surface. After further exposure to 302 nm light cracks are visible on the surface after only 24 hours, again showing not only is their chemical change during exposure, physical changes are also occurring. This reaffirms that 365 nm light causes changes in the bulk of the film due to its strongly penetrating nature, whereas 302 nm light primarily causes degradation on the surface as it is weakly penetrating.

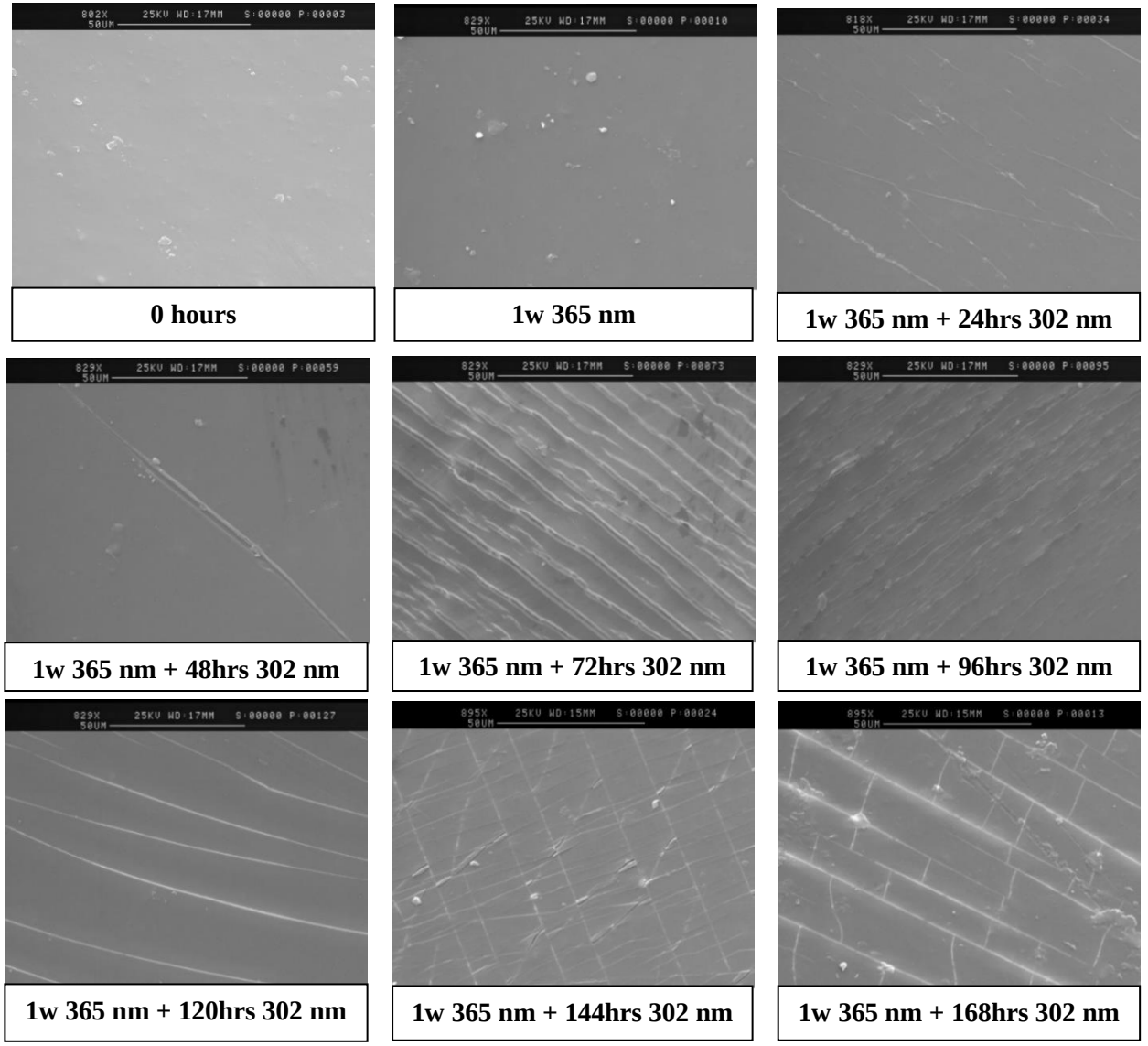

Figure 4.32: SEM images of PET samples exposed to 365 nm light for 1 week followed by 302 nm light for 1 week in 24 hours increments.

4.2.8 Conclusions

The effect of pre-exposing PET films with 365 nm light followed by 302 nm light was analysed using several techniques. After exposure to 302 nm light results indicate the production of various degradation products, including carboxylic acid end groups, dimers, anhydrides, aldehydes and monohydroxy terephthalate groups, as well as the existence of surface cracks. Although no significant changes were identified on the surface of the films after exposure to 365 nm light, techniques that analyse the bulk of the film showed that 365 nm light may have more of an influence on the effect of subsequent exposure to 302 nm light than originally expected. In addition, DSC thermograms provide evidence for the theory that 365 nm light primarily causes branching and crosslinking reactions, whereas 302 nm light causes chain scission reactions to occur. From the data presented it can be concluded that exposing samples to 365 nm light does not significantly influence the effect of subsequent exposure to 302 nm light, at the timescales used in this study. However, it is believed that at prolonged hours of exposure/higher dosages to 365 nm light may influence the effect of subsequent exposure to 302 nm light.

4.3 References

1 G. J. M. Fechine, M. S. Rabello and R. M. Souto-Maior, *Polym. Degrad. Stab.*, 2002, **75**, 153–159.

2 M. Day and D. M. Wiles, *J. Appl. Polym. Sci.*, 1972, **16**, 203–215.

3 N. B. Colthup, L. H. Daly and S. E. Wiberley, *Introduction to Infrared and Raman Spectroscopy*, Academic Press, Third Edition., 2009.

4 P. Delprat and X. Duteurtreb, *Polym. Degrad. Stab.*, 1995, **50**, 1–12.

5 F. B. Marcotte, D. Campbell, J. A. Cleaveland and D. T. Turner, *J. Appl. Polym. Sci. Part A-1*, 1967, **5**, 481–501.

6 C. V Stephenson, C. Lacey and W. S. Wilcox, *J. Polym. Sci.*, 1961, **55**, 477–488.

7 M. Day and D. M. Wiles, *J. Appl. Polym. Sci.*, 1972, **16**, 175–189.

8 Z. Chen, J. N. Hay and M. J. Jenkins, *Eur. Polym. J.*, 2012, **48**, 1586–1610.

9 A. K. Crane, E. Y. L. Wong and M. J. MacLachlan, *CrystEngComm*, 2013, **15**, 9811.

10 J. Scheirs and J. Gardette, *Polym. Degrad. Stab.*, 1997, **56**, 339.

11 M. Edge, R. Wiles, N. S. Allen, W. A. McDonald and S. V Mortlock, *Polym. Degrad. Stab.*, 1996, **53**, 141–151.

12 J. Scheirs and J. L. Gardette, *Polym. Degrad. Stab.*, 1997, **56**, 339–350.

13 A. Rivaton, J. L. Gardette, C. E. Hoyle, M. Ziemer and D. R. Fagerburg, 2000, **41**, 3541–3554.

14 N. B. Colthup, L. H. Daly and S. E. Wiberley, in *Introduction to Infrared and Raman Spectroscopy*, 1990, pp. 289–325.

15 J. V. Gulmine, P. R. Janissek, H. M. Heise and L. Akcelrud, *Polym. Degrad. Stab.*, 2003, **79**, 385–397.

16 G. A. Cordell, *The Alkaloids*, Academic Press, 1997.

17 N. Grassie and G. Scott, *Polymer Degradation and Stabilisation*, Cambridge University Press, 1985.

18 C. F. Ladasiu Ciolacu, N. Roy Choudhury and N. K. Dutta, *Polym. Degrad. Stab.*, 2006, **91**, 875–885.

19 B. J. Holland and J. N. Hay, *Polymer*, 2002, **43**, 1835–1847.

20 J. F. Rabek, *Polymer Photodegradation: Mechanisms and Experimental Methods*, Chapman & Hall, 1995.

21 P. de Donato, J. M. Cases, B. Humbert, P. Lutgen and G. Feyder, *J. Polym. Sci. Part B Polym. Phys.*, 1992, **30**, 1305–1310.

22 T. Berndt and O. Boge, *Phys. Chem. Chem. Phys.*, 2001, **3**, 4946–4956.

23 J. F. Rabck, *Polymer photodegradation. Mechanisms and experimental methods.*, London: Chapman and Hall, 1995.

24 G. J. M. Fechine, M. S. Rabello, R. M. Souto Maior and L. H. Catalani, *Polymer*, 2004, **45**, 2303–2308.

25 L. Chen, X. Jin, J. Du and R. Qian, *Makromol. Chem.*, 1991, **192**, 1399–1408.

26 N. Fukazawa, K. Yoshioka, H. Fukumura and H. Masuhara, *J. Phys. Chem.*, 1993, **97**, 6753–6759.

27 J. G. Pacifici and J. M. Straley, *Polym. Lett.*, 1969, **7**, 7–9.

28 M. Day and D. M. Wiles, *J. Appl. Polym. Sci.*, 1972, **16**, 191–202.

29 T. Kijchavengkul, R. Auras and M. Rubino, *Polym. Test.*, 2008, **27**, 55–60.

30 S. S. Hosseini, S. Taheri, A. Zadhoush and A. Mehrabani-Zeinabad, *J. Appl. Polym. Sci.*, 2007, **103**, 2304–2309.

31 C. Sammon, J. Yarwood and N. Everall, *Polym. Degrad. Stab.*, 2000, **67**, 149–158.

32 D. Kint and S. Munoz-Guerra, *Polym. Int.*, 1999, **48**, 346–352.

33 F. Khabbaz, A.-C. Albertsson and S. Karlsson, *Polym. Degrad. Stab.*, 1999,

63, 127–138.

34 M. Jayakannan and S. Ramakrishnan, *J. Appl. Polym. Sci.*, 1998, 59–66.

35 G. Li, S. L. Yang, J. M. Jiang and C. X. Wu, *Polymer*, 2005, **46**, 11142–11148.

36 M. S. Rabello and J. R. White, *Polym. Compos.*, 1996, **17**, 691–704.

37 W. K. Fisher and J. C. Corelli, *J. Polym. Sci. Polym. Chem. Ed.*, 1981, **19**, 2465–2493.

38 C. W. Extrand, *Langmuir*, 2004, **20**, 4017–4021.

39 L. Gao and T. J. Mccarthy, *Langmuir*, 2006, **22**, 6234–6237.

40 D. Murakami, H. Jinnai and A. Takahara, *Langmuir*, 2014, **30**, 2061–2067.

5 Investigating the role of wavelength, temperature, and atmosphere on the photodegradation of PDEGT

This chapter discusses the photodegradation behaviour of PDEGT. In this study, the effects of temperature, atmosphere, and wavelength of light were considered.

Irradiations were performed using UVP XX-series bench lamps of wavelengths 302 nm and 365 nm and a Hönle Cube 100 UV lamp of wavelength 365 nm. A weatherometer was also used to expose samples to a broad wavelength range of light, replicating outdoor exposure, between 290-800 nm. A photodegradation cell was used to expose samples at different temperatures and atmospheres. After exposure, the extent of degradation was analysed using ATR FT-IR, DRIFT and UV-Vis-NIR. The instrumentation and analysis techniques used in this study have been discussed further in *Chapter 2*.

PDEGT is only distinguishable from PET due to the monomer unit used in synthesis; PDEGT synthesis uses DEG, whereas PET uses EG. It has been reported that the ether linkages in PDEGT are the weak links during thermal degradation, and it is thought that this could be the same during photodegradation and therefore PDEGT would degrade to a greater extent than PET.

5.1 Characterisation of PDEGT

Purified PDEGT used in this study was characterised using ATR FT-IR, DRIFT, DSC and UV-visible spectroscopy.

The ATR and DRIFT spectra for purified PDEGT are shown in *Figure 5.01 (a)* and *(b)*, respectively. The band assignments for the peaks in these spectra are given in *Table 1*.

Table 1: Band assignments for the ATR FT-IR and DRIFT spectra of PDEGT.

Wavenumber (cm^{-1})		Assignment
ATR FT-IR	**DRIFT**	
3630	3620	Aqueous O-H stretching vibration[1]
3550	3540	Alcoholic O-H stretching vibration[1]
3430	3425	First overtone of the carbonyl peak[1]
3100-3060	3100-3060	Aromatic C-H stretching[1]
2955, 2875	2955, 2875	Aliphatic CH_2 stretching[2]
1950	1950	Aromatic summation band
1720, 1713	1720	Amorphous and crystalline carbonyl stretching[2]
1614, 1453, 1439, 1409	1612, 1451, 1436, 1409	Aromatic skeletal stretching bands[2]
1578, 1505	1577, 1504	Amorphous and crystalline ring stretching[2]
1265	1265	C(O)-O stretching of ester group[2]
1173, 1115, 1017	1173, 1117, 1017	Indicative of aromatic 1, 4-substitution pattern[2]
1095	1104	C-O stretching vibration of aliphatic ester
980	980	O-CH_2 stretching of ethylene glycol segment[2]
940	940	O-CH_2 stretching of diethylene glycol segment[2]
873	874	Isolated hydrogen on aromatic ring[3]
845	845	C-H deformation of two adjacent hydrogens on the terephthalic ring[3]
726	727	Out of plane deformation of the two carbonyl substituents on the aromatic ring[2]

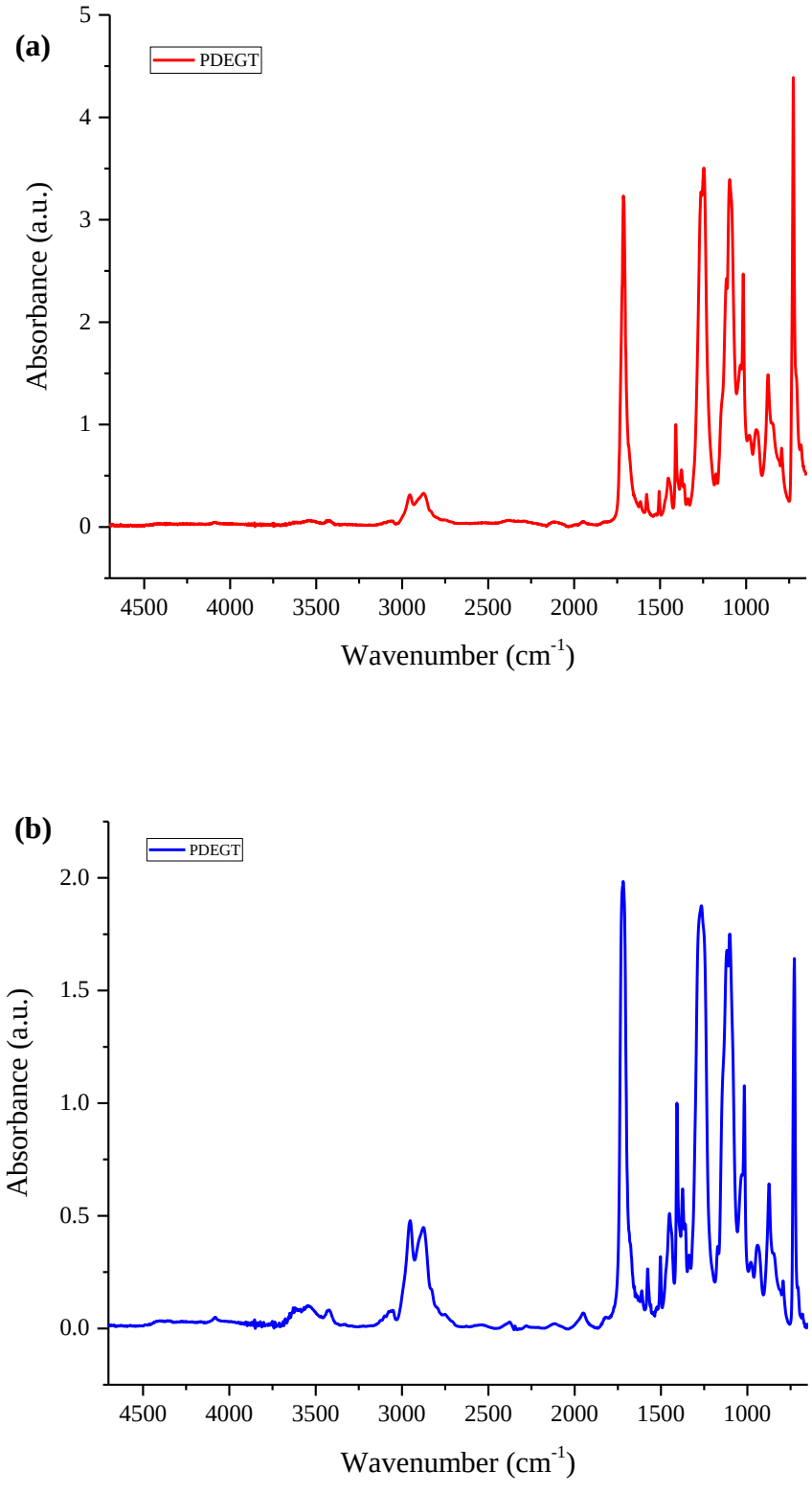

Figure 5.01: (a) ATR FT-IR and (b) DRIFT spectra of purified PDEGT.

The UV-visible spectrum of PDEGT is given in *Figure 5.02*. This shows that short wavelengths, between 280-325 nm, are absorbed strongly, whereas longer wavelengths, between 325-450 nm, are absorbed weakly by PDEGT.

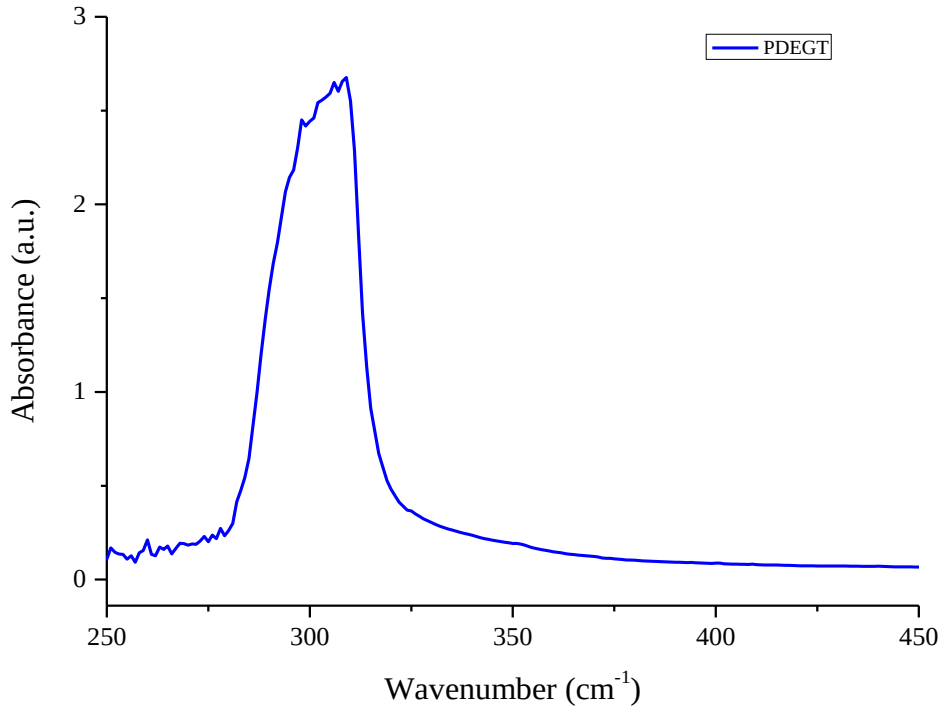

Figure 5.02: UV-visible spectrum of PDEGT between 250-450 nm.

Figure 5.03 (a) and (b) show the DSC thermograms for purified PDEGT before and after solvent casting, respectively. Three transitions were observed in the DSC of purified PDEGT, before solvent casting (*Figure 5.03 (a)*). A T_g occurs at 25°C and two melting endotherms at 58°C and 92°C. These two endotherms correspond to two different crystalline forms in the polymer.

When the polymer was solvent cast as a film a further DSC was taken, given in *Figure 5.03 (b)*, which shows a T_g at 25°C. The T_g, in cycle 3, shows an overlapping endothermic peak which is known as enthalpy relaxation. This time, however, there was no melting endotherms observed, confirming that the cast film was amorphous.

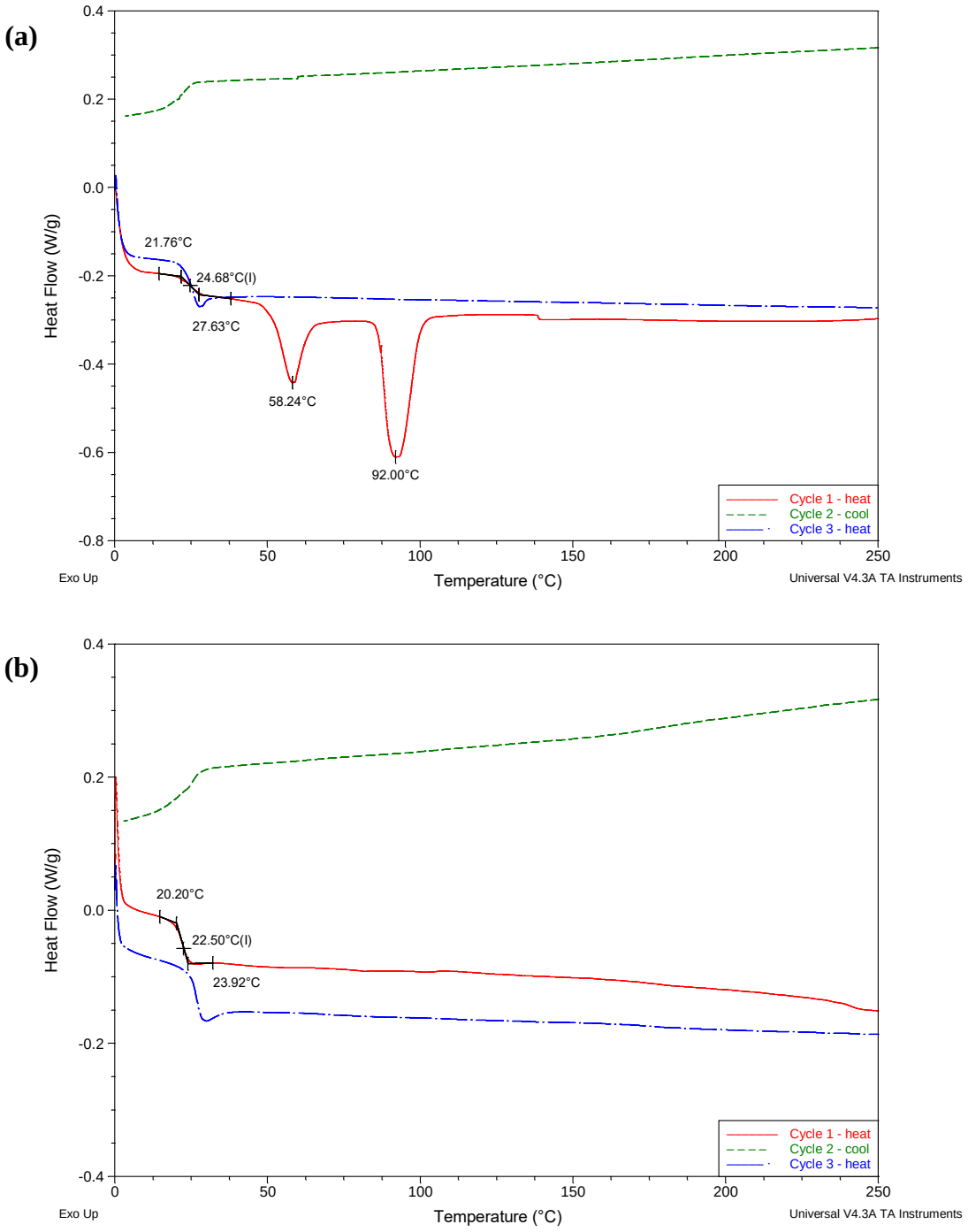

Figure 5.03: DSC thermograms of PDEGT, (a) before and (b) after solvent casting.

5.2 Weatherometer irradiations

PDEGT samples were irradiated in an Atlas Suntest XLS+ weatherometer with a spectral range from 290-800 nm, and a temperature of (37.5 ± 2.5)°C. The weatherometer was used to attempt to replicate outdoor exposure.

Samples were placed in the weatherometer for various time periods and degradation was monitored using ATR FT-IR, DRIFT and UV-Vis-NIR.

5.2.1 Weekly weatherometer exposures

5.2.1.1 ATR FT-IR

Samples of PDEGT film were irradiated in the weatherometer for 6 weeks (equivalent to a dosage of approximately 3.7×10^5 W m^{-2} hr^{-1}) and analysed every week (equivalent to a dosage of approximately 6.1×10^4 W m^{-2} hr^{-1}) using ATR FT-IR. *Figure 5.04* shows the ATR spectra for PDEGT after every week of exposure. One week of irradiation in the weatherometer is approximately 7.5 weeks outdoors. After only 1 week of exposure, there are substantial changes in the spectra in the region between 3800-2100 cm^{-1}, as well as the carbonyl and fingerprint regions.

The spectra of the region between 3800-2100 cm^{-1} of the control and the PDEGT sample irradiated for 6 weeks are shown in *Figure 5.05.* The peaks within this region have been assigned and are given in *Table 2*.

The peak at 3290 cm^{-1} has been assigned to the hydroxy of the carboxylic acid group and has developed during irradiation. The increase in absorbance of this peak indicates that carboxylic acid end groups have been produced during exposure. A mechanistic pathway for the production of these groups, during the photodegradation of PET, have been proposed, and it is thought that these groups could be produced during irradiation of PDEGT in the same way. The reaction is shown in *Chapter 1*, *Figure 1.29*.

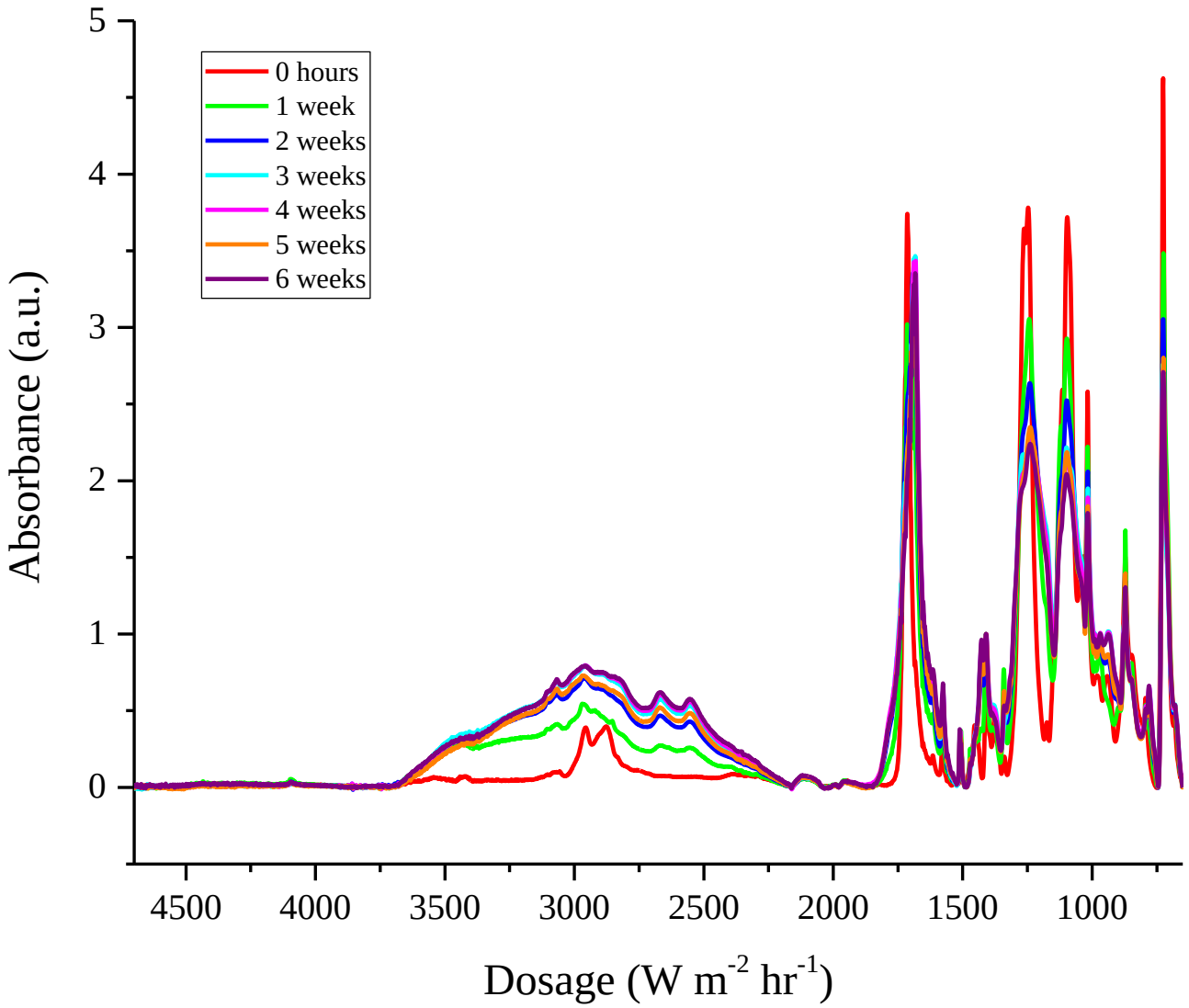

Figure 5.04: ATR FT-IR spectra of PDEGT films irradiated in the weatherometer for 6 weeks, in 1 week increments.

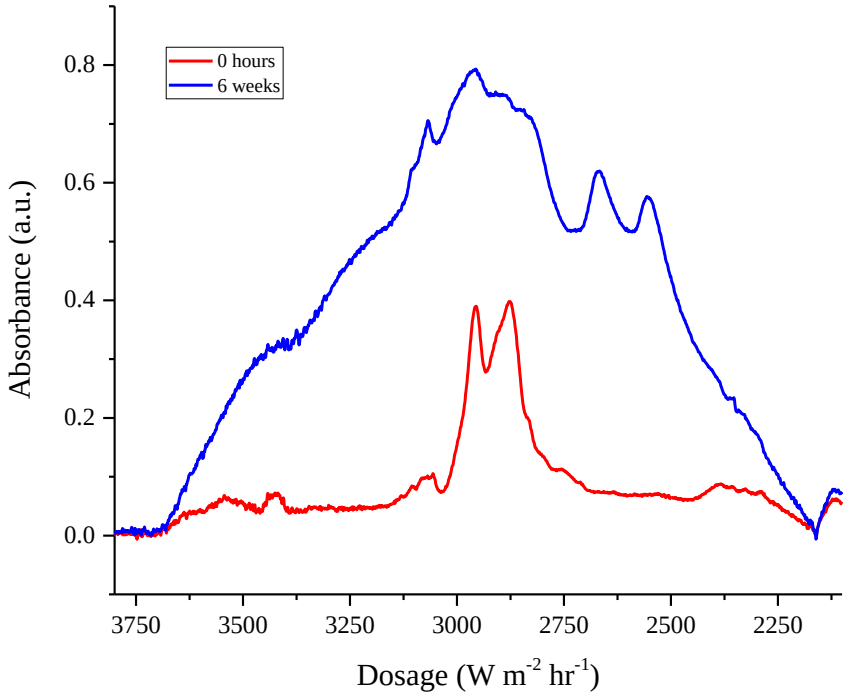

Figure 5.05: ATR FT-IR spectra of PDEGT irradiated in the weatherometer, in the region between 3800-2100 cm^{-1}.

Table 2: Band assignments for the region between 3800-2100 cm^{-1} of the ATR FT-IR spectrum of PDEGT.

Peak (cm^{-1})	Assignment
3630	Aqueous O-H stretching vibration[1]
3550	Alcoholic O-H stretching vibration[1]
3430	First overtone of the carbonyl peak[1]
3290	Carboxylic acid end groups[1]
3100 – 3060	Aromatic C-H stretching[4]
2955, 2875	Asymmetric and symmetric aliphatic C-H stretching[2]
2920	C-H symmetric stretching vibration associated with the Ar-CH_3 group[5]
2665, 2550	Characteristic of the carboxylic acid dimer[6]

In addition, there are two peaks that have evolved at 2665 and 2550 cm^{-1} and are representative of the carboxylic acid dimer.[6] The production of these groups has been reported when changes have been acknowledged in the carbonyl peak during photodegradation of PET. It is thought that these peaks have never been attributed to the carboxylic acid dimer during the photodegradation of PDEGT materials.[7]

Peaks attributed to the stretching modes of the four aromatic C-H bonds of the terephthalate ring between 3100 and 3060 cm^{-1} have shown a change in absorbance and area with exposure.[4] The increase in absorbance could be due to the peaks being overlapped with the growing hydroxy. The change in area and shape of the peak is thought to be due to the production of mono-substituted rings, which would result in another aromatic C-H bond on the terephthalate ring.

From *Table 2*, the peaks assigned to the aliphatic C-H stretching vibrations have decreased in height with exposure time. The peak at 2875 cm^{-1} is more intense compared to the peak in PET, which is most likely due to the additional C-H environment in the diethylene glycol segment of the PDEGT.[2] The decrease in height of these peaks is due to absorption of light by the ester carbonyl, which leads to bond breakage and subsequently the breakdown of the polymer. The peak at 2875 cm^{-1} appears to decrease in height further than the peak at 2955 cm^{-1}, which indicates the breakdown of the ether link of the diethylene glycol segment. The apparent decrease in the size of these peaks could also be due to the peaks being overlapped with the growing hydroxy.

After exposure, another new peak has developed at 2920 cm^{-1} and has been assigned to the C-H stretching vibration associated with the Ar-CH_3 group. It is thought that phenyl and methyl radicals could be produced and combine to form an Ar-CH_3 group. These radicals have been shown to be produced during the photodegradation of other polyesters.[8]

The change in the carbonyl peak after irradiation in the weatherometer for 6 weeks is shown in *Figure 5.06*. Six weeks of irradiation in the weatherometer is approximately 11 months outside. The peaks contained within the carbonyl peak before and after exposure are given in *Table 3*.

After exposure there is general broadening of the carbonyl peak, as seen in *Figure 5.06*, indicating the production of new carbonyl groups. This broadening at higher wavenumbers has been assigned to the formation of anhydride groups. The formation of anhydride groups has been reported by Scheirs and Gardette during the photo-oxidation of PEN.[9] However, anhydride groups have also been shown to occur in the photo-oxidation of PET, in *Chapter 3, Section 3.3.1*. It is thought that anhydrides could also be produced during the exposure of PDEGT as exposures were performed at temperatures which provide an ideal environment for anhydride production.

Development of a peak at 1740 cm^{-1} has been assigned, in *Table 3*, to the carbonyl stretch of an aliphatic aldehyde. Aldehydes have been reported to be produced during the photodegradation of other polyesters.[10]

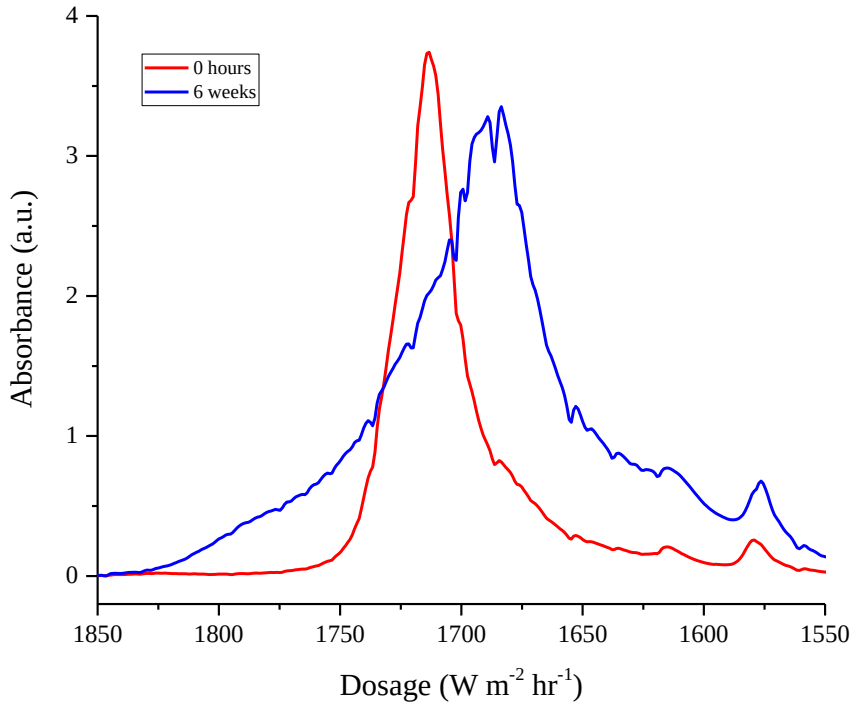

Figure 5.06: ATR FT-IR spectra of PDEGT irradiated in the weatherometer, in the carbonyl region between 1850-1550 cm^{-1}.

Peaks present in the control spectrum, shown in *Figure 5.06*, at 1721 and 1713 cm^{-1} have been assigned to the amorphous and crystalline carbonyl stretch from the ester.[4] These peaks have shown a decrease in absorbance with exposure time. This was expected as chain scission reactions can occur at the ester group, as shown in PET, and so this decrease indicates the breakdown of the ester group upon exposure.

Table 3: Band assignments for the carbonyl region of the ATR FT-IR spectrum of PDEGT.

Peak (cm^{-1})	Assignment
1785	Carbonyl stretch from anhydride carbonyl[9,11]
1740	Carbonyl stretch from aliphatic aldehyde[5]
1721	Amorphous carbonyl stretch from ester[4]
1713	Crystalline carbonyl stretch from ester[4]
1700	Carbonyl stretch from carboxylic acid dimer[7,11,12]
1695	Carbonyl stretch from carboxylic acid end groups[13]
1690	Carbonyl stretch from quinone groups[14,15]
1685	Carbonyl stretch from terephthalic acid

The broadening of the carbonyl peak at shorter wavenumbers is due to the development of peaks at 1700, 1695, 1690 and 1685 cm^{-1}. These peaks have been attributed to the carboxylic acid dimer, end groups, quinone groups and terephthalic acid. Carboxylic acid dimers have been reported in the literature by Delprat *et al.* during the photodegradation of copolymers but have not been described for PDEGT.[7] The production of carboxylic acid end groups has been reported in the literature for PET materials but, again, not for PDEGT.[1,10,16] Fechine *et al.* has proposed a pathway for the production of these groups during the photo-oxidation of PET, shown in *Chapter 1, Figure 1.29.*[17] The mechanism is thought to be the same during the photodegradation of PDEGT. Quinone groups have been identified during the photodegradation of PET by Edge *et al.* reporting changes in IR spectra and Fechine *et al.* showing changes in UV-visible spectra. Mechanistic pathways have been proposed for their production, as shown in *Chapter 1, Figure 1.31.* The peak at 1685

cm^{-1}, assigned to terephthalic acid, indicates the breakdown of the polymer into its monomer units. A spectrum of terephthalic acid and irradiated PDEGT were overlaid to identify this peak.

The extent of photodegradation of PDEGT was measured in the same way as for PET; the change in area of the region between 3800-2100 cm^{-1} and the carbonyl peak with dosage. *Figure 5.07* shows the change in area of the peaks, with dosage, for PDEGT and 36 μm PET irradiated in the weatherometer. Both graphs show an initial sharp increase, followed by a more moderate increase, in the change in area, for PDEGT. In comparison to PDEGT, PET shows only minor increases with dosage. This shows that PDEGT degrades to a much greater extent than PET during irradiation in the weatherometer. This is thought to be due to the presence of the ether link within the PDEGT.

Wang *et al.* reported that the photodegradation process of PET takes place in two steps; a very rapid initial step, due to the scission of weak links, followed by the degradation of normal links. The author reported that the rate constants of degradation for weak links were higher than that for normal links, as the weak links are more easily broken.[18] It is thought that this is also the case for PDEGT. In PDEGT, the weak links are believed to be the ether links of the DEG segment, as this is known to be the weak link in PET during thermal degradation.[19]

A related point to consider is that PDEGT was exposed in the weatherometer at (37.5 ± 2.5)°C, which is above the T_g of this polymer. This could also explain the greater extent of degradation of PDEGT compared to PET, as although PET was irradiated in the weatherometer at the same temperature, this is below the T_g of PET. Exposing PDEGT above its T_g could increase the samples extent of photodegradation, which will be examined further in *Section 5.5*.

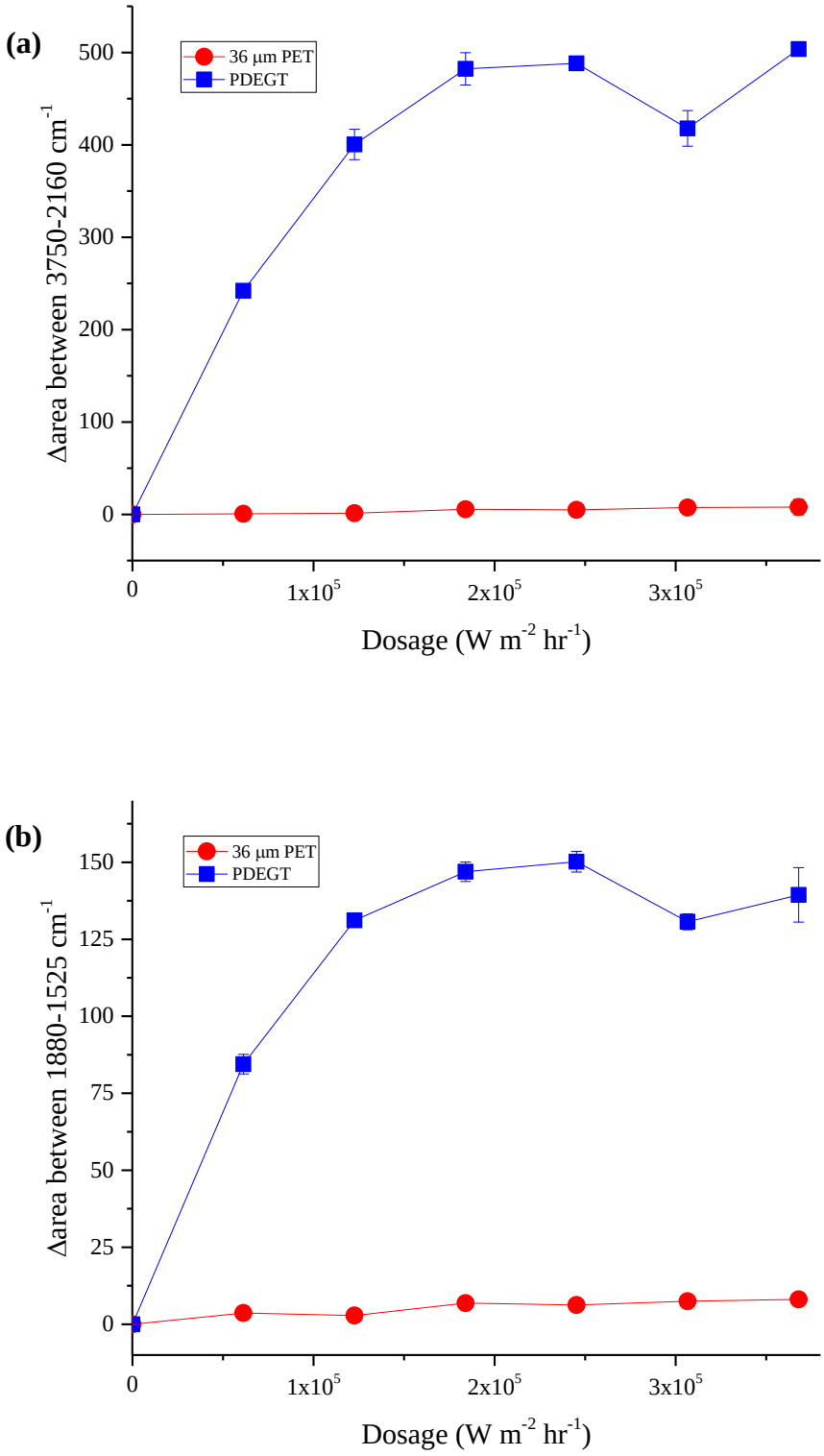

Figure 5.07: Extent of photodegradation of PDEGT measured by the change in area of peaks between (a) 3750-2160 cm^{-1} and (b) 1880-1525 cm^{-1}(carbonyl).

Figure 5.08 shows the fingerprint region of a control and a film irradiation in the weatherometer for 6 weeks. The various peaks that have changed or developed during exposure have been assigned in *Table 4*.

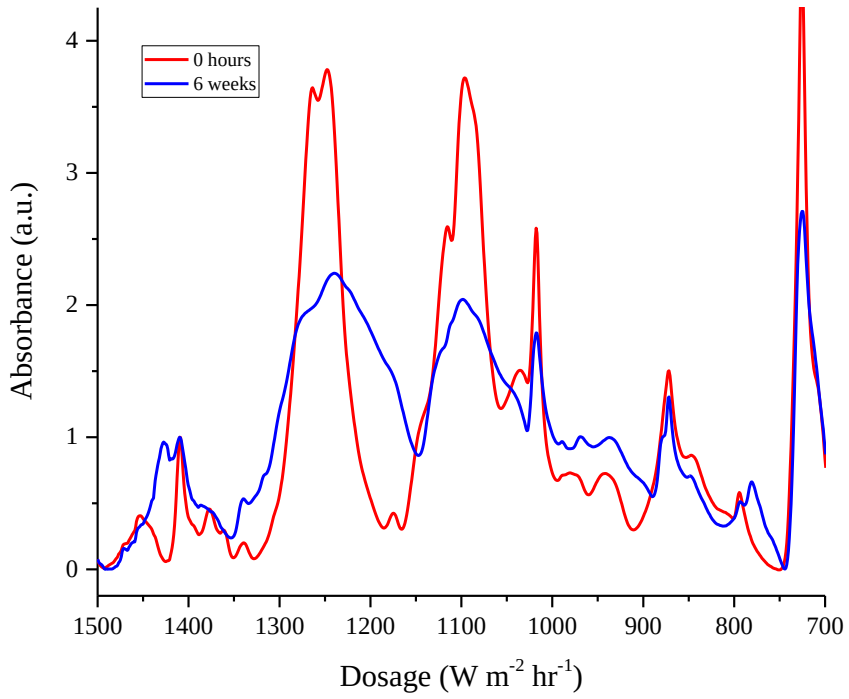

Figure 5.08: ATR FT-IR spectra of PDEGT irradiated in the weatherometer, in the fingerprint region between 1500-700 cm^{-1}.

The evolution of peaks at 1430 and 1220 cm^{-1} are associated with the production of carboxylic acid dimers. As far as is known these peaks have never been reported in literature after exposure of PDEGT.

Peaks at 1265 and 1095 cm^{-1}, associated with the ester group show a decrease in absorbance with exposure time, as shown in *Figure 5.08*. This indicates that chain scission reactions have occurred during exposure, leading to the breakdown of the ester group.

Figure 5.08, shows the reduction in size of the peaks at 980 and 940 cm^{-1}, assigned to the O-CH_2 stretching of the ethylene glycol and diethylene glycol segments,

respectively.[2] The reduction in size of these peaks indicates the breakdown of the ester and ether units during degradation.

Table 4: Band assignments for the fingerprint region of the ATR FT-IR spectrum of PDEGT.

Peak (cm^{-1})	Assignment
1430	Combination band due to C-O stretching and O-H deformation vibration, associated with carboxylic acid dimer.[5]
1265	C(O)-O stretching of ester group[2]
1220	C-O stretching vibration, associated with carboxylic acid dimer.[5]
1095	C-O stretching vibration of ester group[5]
980	O-CH_2 stretching of ethylene glycol segment.[2]
940	O-CH_2 stretching of diethylene glycol segment.[2]
845	C-H deformation of two adjacent hydrogens on the terephthalic ring (indicates 1, 4 substitution)[3]
780	Out-of-plane deformation vibrations of mono-substituted rings[5]
758	Out of plane deformation vibrations of 1, 2, 4-substituted rings[5]

The region between 850-750 cm^{-1} is sensitive to changes in the substitution pattern of the terephthalic ring. After exposure, there has been change in the peak at 845 cm^{-1} and development of peaks at 778 and 758 cm^{-1}. From *Figure 5.08*, it is apparent that there has been a small reduction in the size of the peak at 845 cm^{-1} assigned to the C-H deformation of two adjacent hydrogens on the terephthalic ring. This suggests that substitution has occurred on the ring.[2,3] This is further supported by the development of the peaks at 758 cm^{-1} assigned to the 1, 2, 4-substituted ring.[5] The change and evolution of these peaks support the formation of monohydroxy terephthalate groups.

The development of the peak at 778 cm^{-1}, after exposure, has never been assigned in the literature, during the irradiation of PDEGT or PET, but it is thought to be due to mono-substituted rings. The peak that has developed is also larger compared to the evolution of the peak during irradiation of PET. In PET, this group is thought to be produced from the phenyl radical being able to abstract a hydrogen atom from the

backbone of the polymer chain. In PDEGT there are more hydrogen atoms available in the main chain, due to the incorporation of the diethylene glycol segment. This means that it will be easier for the phenyl radical to abstract a hydrogen and thus more mono-substituted rings will be produced, causing an increase in peak height.

5.2.1.2 DRIFT

The DRIFT spectra of PDEGT films irradiated in the weatherometer for 6 weeks (equivalent to a dosage of approximately 3.7 x 10^5 W m^{-2} hr^{-1}) and analysed every week (equivalent to a dosage of approximately 6.1 x 10^4 W m^{-2} hr^{-1}) are shown in *Figure 5.09*. This shows change in the region between 3800-2100 cm^{-1} and the carbonyl and fingerprint regions, after exposure. DRIFT spectra differ from ATR spectra as DRIFT analyses the whole thickness of the film, whereas ATR only analyses the surface of the film samples.

Figure 5.10 shows the region of the DRIFT spectra between 3800-2100 cm^{-1} for the control sample and PDEGT irradiated in the weatherometer for 6 weeks. The assignments for the peaks in this region are given in *Table 5*.

Peaks assigned to the aqueous, alcoholic and carboxylic acid hydroxy stretches, show an increase in absorbance with exposure time, shown in *Figure 5.10*. This increase indicates the production of new hydroxy groups, including the carboxylic acid end groups. These groups are known to be produced during the photodegradation of PET, and it is believed that these groups are also produced during the exposure of PDEGT. The peak at 3430 cm^{-},[1] assigned to the overtone of the carbonyl peak, has also increased with exposure time which is thought to be due to the overlap with the growing hydroxy peaks.

After exposure, the peaks assigned to the C-H stretching vibrations, in *Table 5*, appear to show an increase in absorbance and a reduction in height. The decrease in height of these peaks could be due to the absorption of light by the ester carbonyl, which leads to bond breakage and subsequently the breakdown of the polymer. The changes could also be due to the peaks being overlapped with the growing hydroxy peaks.

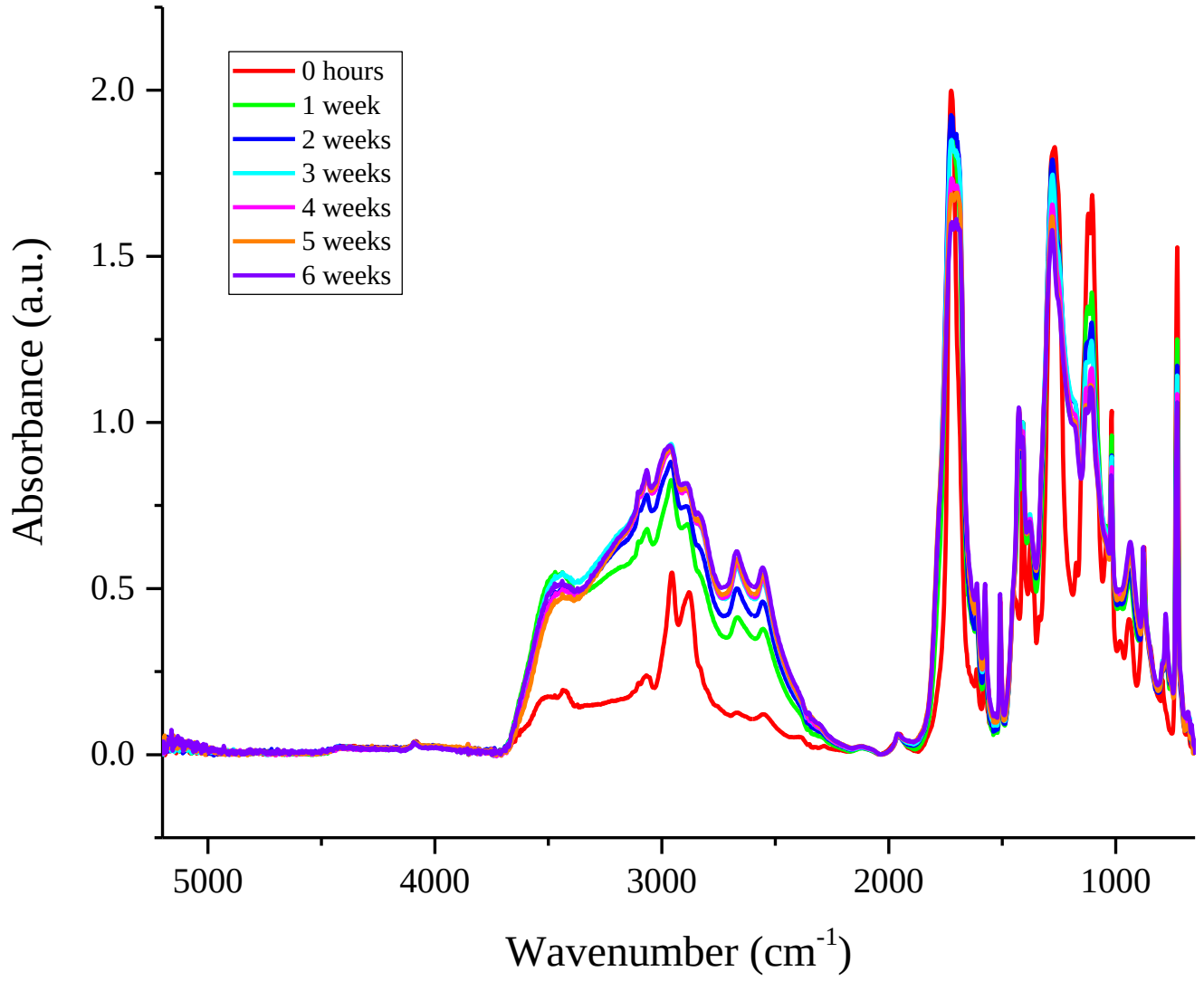

Figure 5.09: DRIFT spectra of PDEGT films irradiated in the weatherometer for 6 weeks, in 1 week increments.

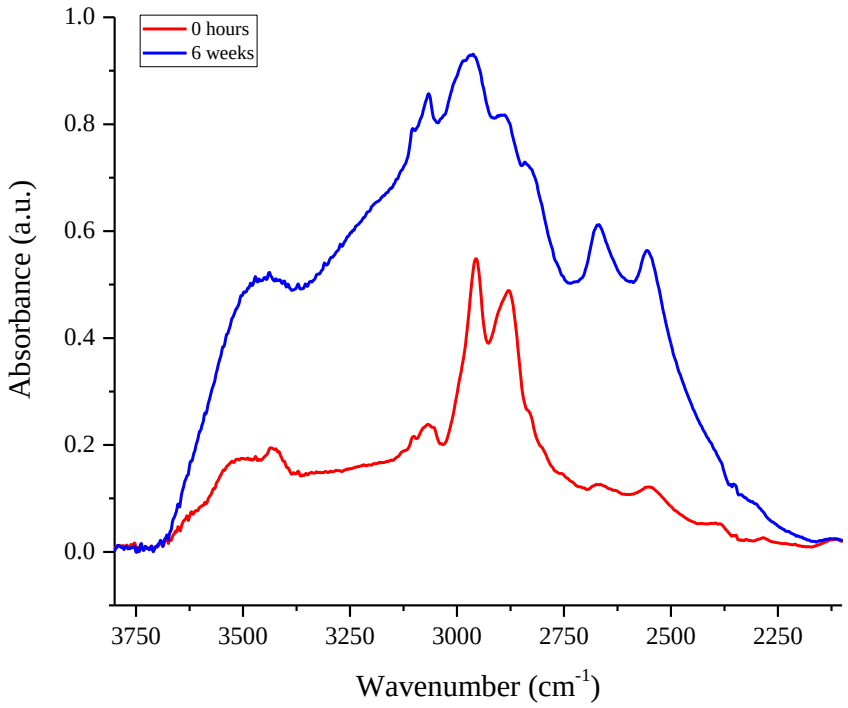

Figure 5.10: DRIFT spectra of PDEGT irradiated in the weatherometer, in the region between 3800-2100 cm^{-1}.

The development of a further two peaks at 2670 and 2555 cm^{-1}, is apparent from *Figure 5.10*. These peaks have been assigned to the carboxylic acid dimer and have been previously discussed due to their development in the ATR spectra in *Section 5.2.1.1*. Interestingly, these peaks have developed during the photodegradation of PET, but have only been identified in the ATR spectra and not in the DRIFT spectra. This indicates that PDEGT is degrading much more rapidly than PET, in the bulk of the film, during irradiation in the weatherometer.

Table 5: Band assignments for the region between 3800-2100 cm^{-1} of the DRIFT spectrum of PDEGT.

Peak (cm^{-1})	Assignment
3630	Aqueous O-H stretching vibration[1]
3550	Alcoholic O-H stretching vibration[1]
3430	First overtone of the carbonyl group in ester[1]
3290	Carboxylic acid end groups[1]
3125, 3100, 3068, 3050	Aromatic C-H stretching[4]
2955 2875	Amorphous aliphatic CH_2 stretching[4]
2830	Crystalline aliphatic CH_2 stretching[4]
2670, 2555	Characteristic of the carboxylic acid dimer[6]

The carbonyl region of the spectra, between 1900-1550 cm^{-1}, for a control film and a sample of PDEGT irradiated in the weatherometer for 6 weeks, are shown in *Figure 5.11*. The assignments for the peaks contained within the carbonyl region are given in *Table 6*.

It is apparent, from *Figure 5.11*, that there is general broadening of the carbonyl peak, after exposure. This indicates the production of new carbonyl species during exposure. At higher wavenumbers, this broadening is due to the production of anhydride groups.[20] As explained in *Section 5.2.1.1,* anhydrides can be produced during the photodegradation of PDEGT, as irradiations were performed at a temperature that provides an ideal environment for anhydride formation to occur.

The peak observed in the control spectrum at 1725 cm^{-1} has been assigned to the carbonyl stretching vibration of the ester group. *Figure 5.11* shows that this peak decreases in absorbance with exposure time. This indicates the breakdown of the ester group during exposure.

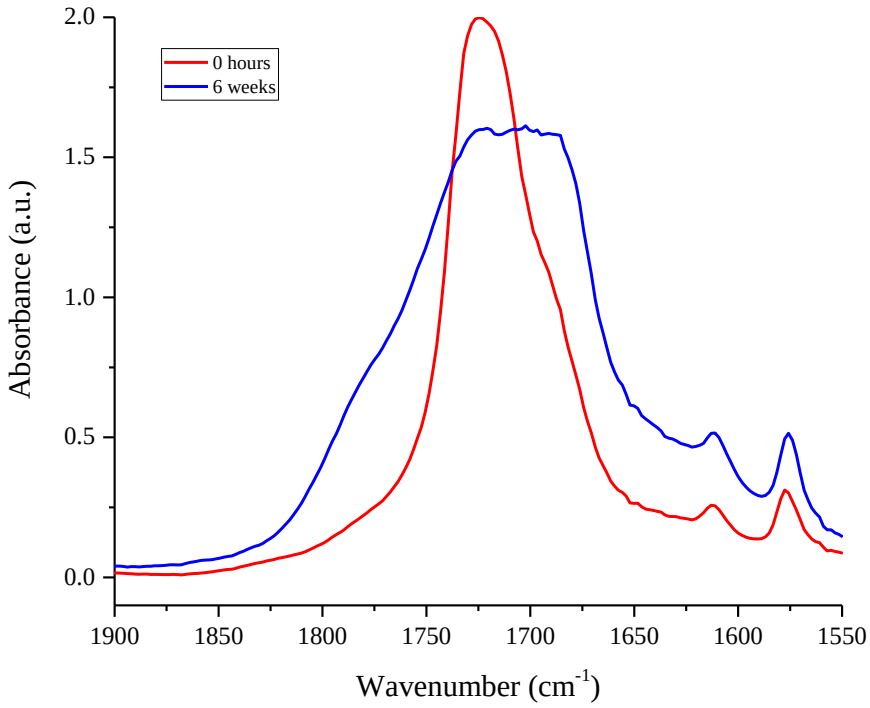

Figure 5.11: DRIFT spectra of PDEGT irradiated in the weatherometer, in the carbonyl region between 1850-1550 cm^{-1}.

Table 6: Band assignments for the carbonyl region of the DRIFT spectrum of PDEGT

Peak (cm^{-1})	Assignment
1785	Carbonyl stretch from anhydride carbonyl[9]
1725	Carbonyl stretching vibration of an ester[21]
1685	Carbonyl stretch from terminal acid end groups[21]

In the initial control spectrum, there is a shoulder at 1685 cm^{-1} which have developed into a peak after exposure. This peak has been assigned, in *Table 6*, to the carbonyl stretch from a terminal acid end group. Donato *et al.* first reported this peak during the degradation of PET.

Another peak that has developed upon exposure at 1702 cm^{-1} has been reported to be present in the DRIFT spectra of PET materials but it has never been assigned.[21] As discussed in *Chapter 3, Section 3.3.2,* this peak is thought to be due to carboxylic acid dimers. The spectra in *Figure 5.11* further supports this assignment as the peak at 1702 cm^{-1} is not present in the control film and has only developed upon exposure.

Using the DRIFT spectra, the extent of photodegradation of PDEGT was measured in the same way as for PET; the change in area of the region between 3800-2100 cm^{-1} and the carbonyl peak with dosage. *Figure 5.12 (a) and (b)* shows the change in area of these peaks, with dosage, for PDEGT and 36 µm PET irradiated in the weatherometer. Both graphs show an initial sharp increase, followed by a more moderate increase, in the change in area, for PDEGT. In comparison to PDEGT, PET shows minor increases with dosage. This shows that PDEGT degrades to a much greater extent than PET during irradiation in the weatherometer. This is thought to be due to the presence of the ether link within the PDEGT.

Wang *et al.* reported that the photodegradation process of PET takes place in two steps; a very rapid initial step, due to the scission of weak links, followed by the degradation of normal links.[18] It is thought that this is also the case for PDEGT. In PDEGT, the weak links are believed to be the ether links of the DEG segment, as this is known to be the weak link in PET during thermal degradation.[19]

However, the extent of photodegradation of PET indicates that a one step process is occurring in the bulk of the film, whereas the PDEGT results indicate a two step process, agreeing with the ATR data, in *Section 5.2.1.1.* This indicates that the surface of the PDEGT films breaks down more rapidly than PET and therefore UV light can affect the bulk of the film faster compared to PET.

Again, the fact that PDEGT degrades to a much greater extent compared to PET could also be because PDEGT was irradiated in the weatherometer above its T_g, whereas PET was not. Exposing PDEGT above its T_g could increase the rate of photodegradation of the sample. The effect of temperature will be examined further in *Section 5.5.*

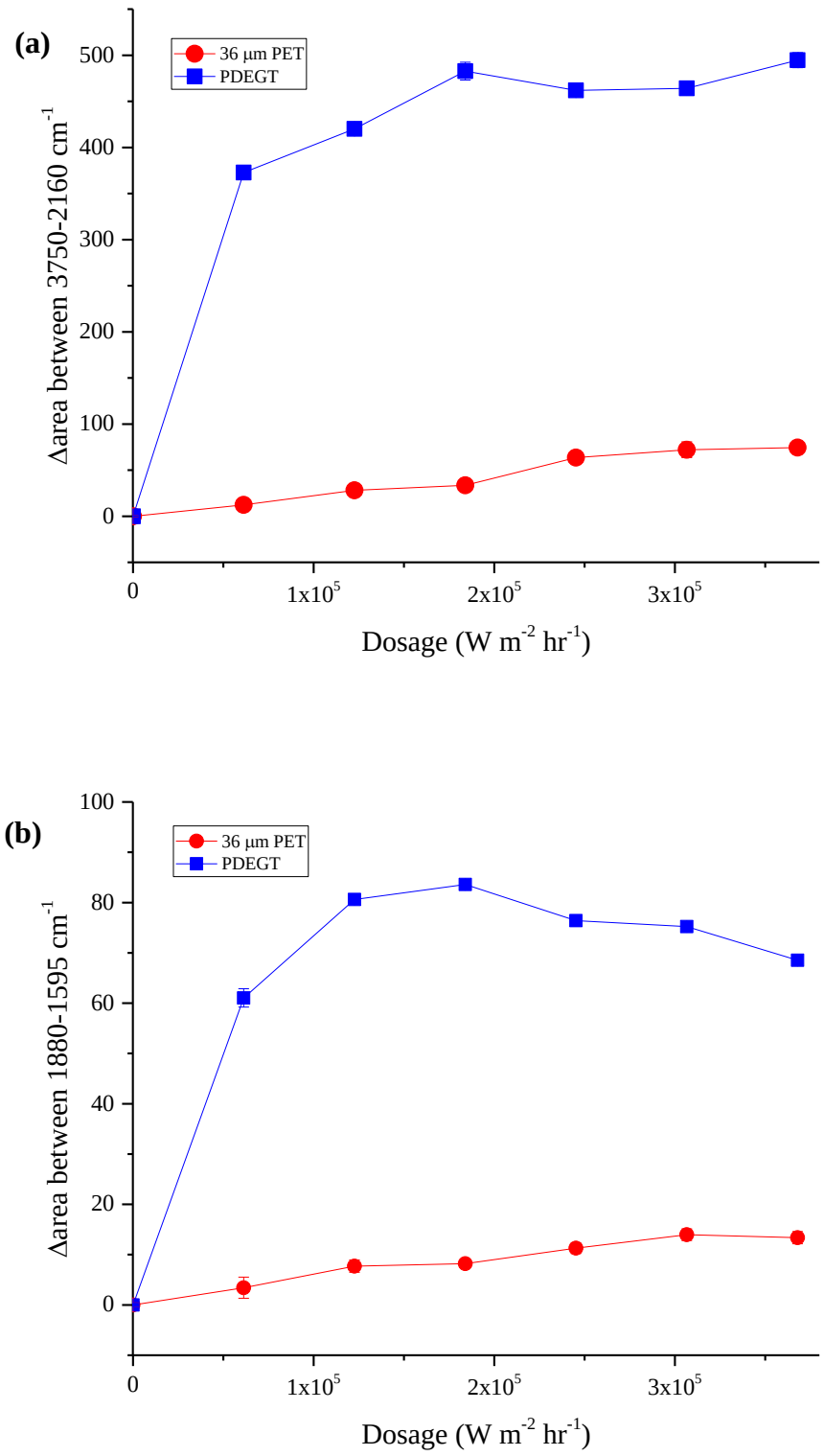

Figure 5.12: Extent of photodegradation of PDEGT measured by the change in area of peaks between (a) 3750-2160 cm^{-1} and (b) 1880-1595 cm^{-1}(carbonyl).

Figure 5.13 shows the change in the fingerprint region after irradiation in the weatherometer for 6 weeks. The various peaks that have changed or developed during exposure have been assigned in *Table 7*.

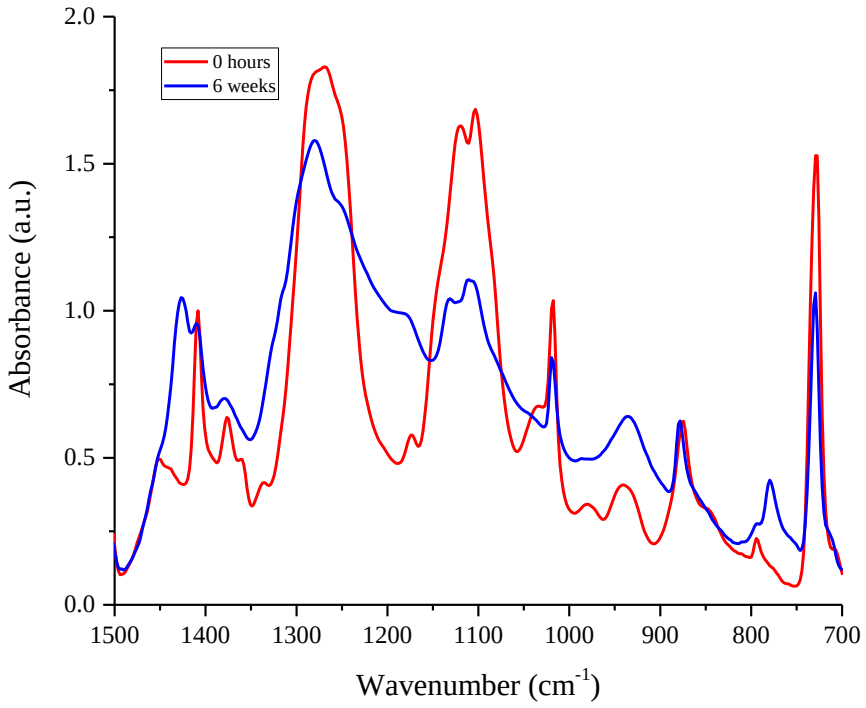

Figure 5.13: DRIFT spectra of PDEGT irradiated in the weatherometer, in the fingerprint region between 1500-700 cm^{-1}.

The evolution of peaks at 1430 and 1220 cm^{-1} are associated with the production of carboxylic acid dimers. As far as is known these peaks have never been reported in literature after exposure of PDEGT.

Peaks at 1265 and 1104 cm^{-1}, associated with the ester group show a decrease in absorbance with exposure time, as shown in *Figure 5.13*. This indicates the breakdown of the ester group due to chain scission reactions occurring during exposure.

Figure 5.13 shows the reduction in the size of the peaks at 980 and 940 cm^{-1}, assigned to the O-CH_2 stretching of the ethylene glycol and diethylene glycol segments, respectively.[2] This reduction in size indicates the breakdown of the ether units during degradation. The peak at 845 cm^{-1} assigned to the C-H deformation of two adjacent hydrogens on the terephthalic ring is almost unidentifiable after exposure. This suggests that substitution has occurred on the ring.[2,3] which could indicate the formation of monohydroxy terephthalate groups.

Table 7: Band assignments for the fingerprint region of the DRIFT spectrum of PDEGT.

Peak (cm^{-1})	Assignment
1430	Combination band due to C-O stretching and O-H deformation vibration, associated with carboxylic acid dimer.[5]
1265	C(O)-O stretching of ester group[2]
1220	C-O stretching vibration, associated with carboxylic acid dimer.[5]
1117	Indicative of aromatic 1, 4-substitution pattern[2]
1104	C-O stretching vibration of aliphatic ester[5]
980	O-CH_2 stretching of ethylene glycol segment.[2]
940	O-CH_2 stretching of diethylene glycol segment.[2]
845	C-H deformation of two adjacent hydrogens on the terephthalic ring (indicates 1, 4 substitution)[3]
780	Out-of-plane deformation vibrations of mono-substituted rings[5]

The development of the peak at 780 cm^{-1}, after exposure, has never been assigned in the literature, during the irradiation of PDEGT or PET, but it is thought to be due to mono-substituted rings. Interestingly, this peak has developed during the photodegradation of PET and PDEGT but has only been identified in the ATR spectra and not in the DRIFT spectra. This, again, indicates that PDEGT is degrading much more rapidly than PET, in the bulk of the film, during irradiation in the weatherometer.

5.2.2 Shorter weatherometer exposures

One week of exposure in the weatherometer is equal to only 7.5 weeks outside, in England. After 2 weeks of exposure, (equivalent to a dosage of approximately 1.2 x 10^5 W m^{-2} hr^{-1}) there is moderate change and then very little noticeable change thereafter. Therefore, thin films of PDEGT were exposed in the weatherometer again, but this time the samples were analysed every 24 hours (equivalent to a dosage of approximately 8.8 x 10^3 W m^{-2} hr^{-1}).

Figure 5.14 (a) and (b) shows that after only 24 hours in the weatherometer there are significant changes in both the ATR and DRIFT spectra, respectively. Again, the trends that were seen in the spectra after exposure are the same as the samples discussed in *Section 5.2.1*, but to a lesser extent.

As there were still substantial changes after 24 hours, the PDEGT samples were exposed in the weatherometer once again, but this time the samples were analysed every 4 hours (equivalent to a dosage of approximately 1.5 x 10^3 W m^{-2} hr^{-1}). The ATR and DRIFT spectra for samples exposed for 24 hours, in 4 hour increments, are shown in *Figure 5.15 (a) and (b)*, respectively. Analysing samples every 4 hours showed moderate changes in the ATR and DRIFT spectra with irradiation time. This allowed for the extent of initial degradation to be studied and compared to samples of PET.

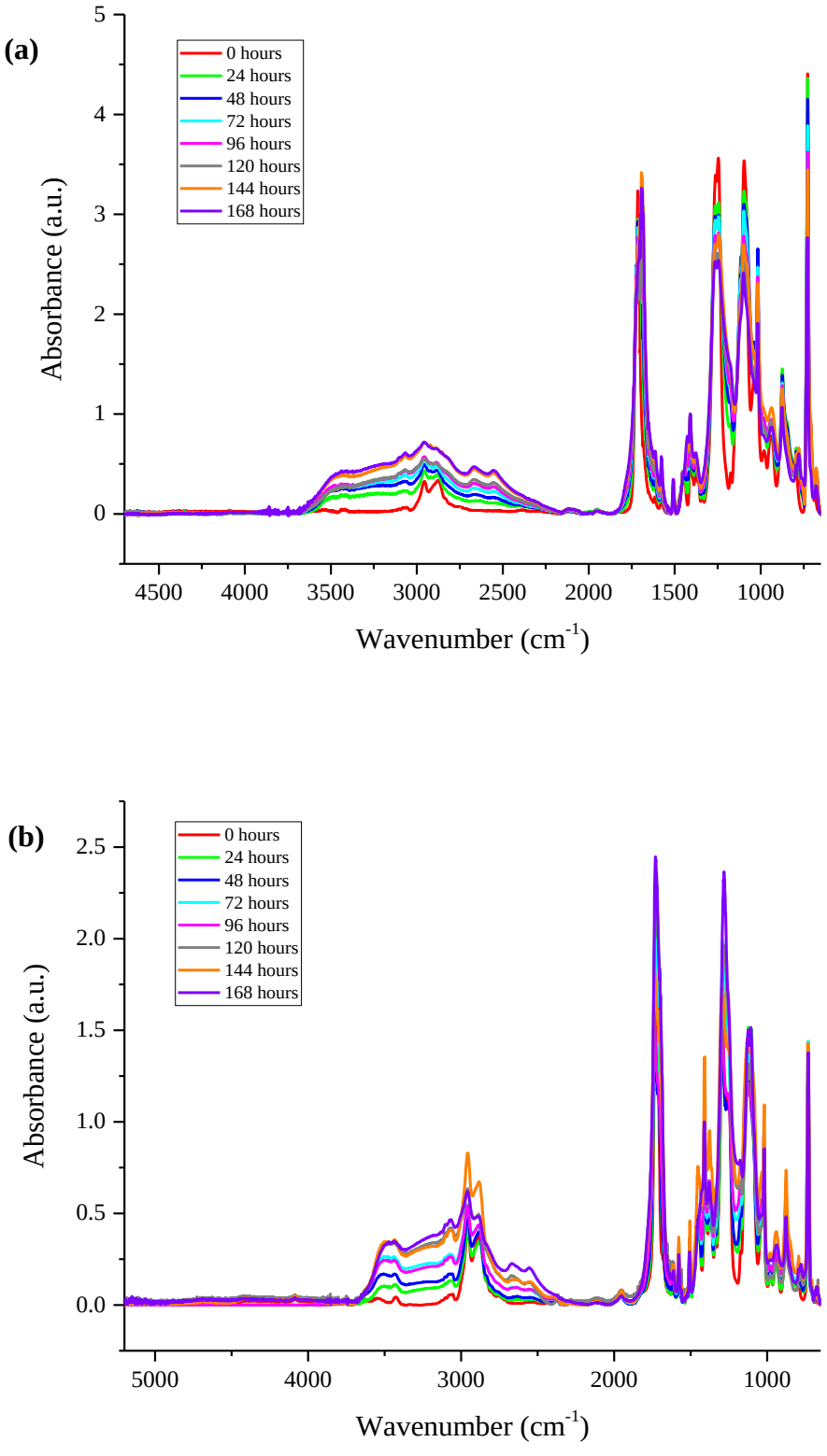

Figure 5.14: (a) ATR FT-IR spectra and (b) DRIFT spectra of PDEGT irradiated in the weatherometer from 0 to 1 week.

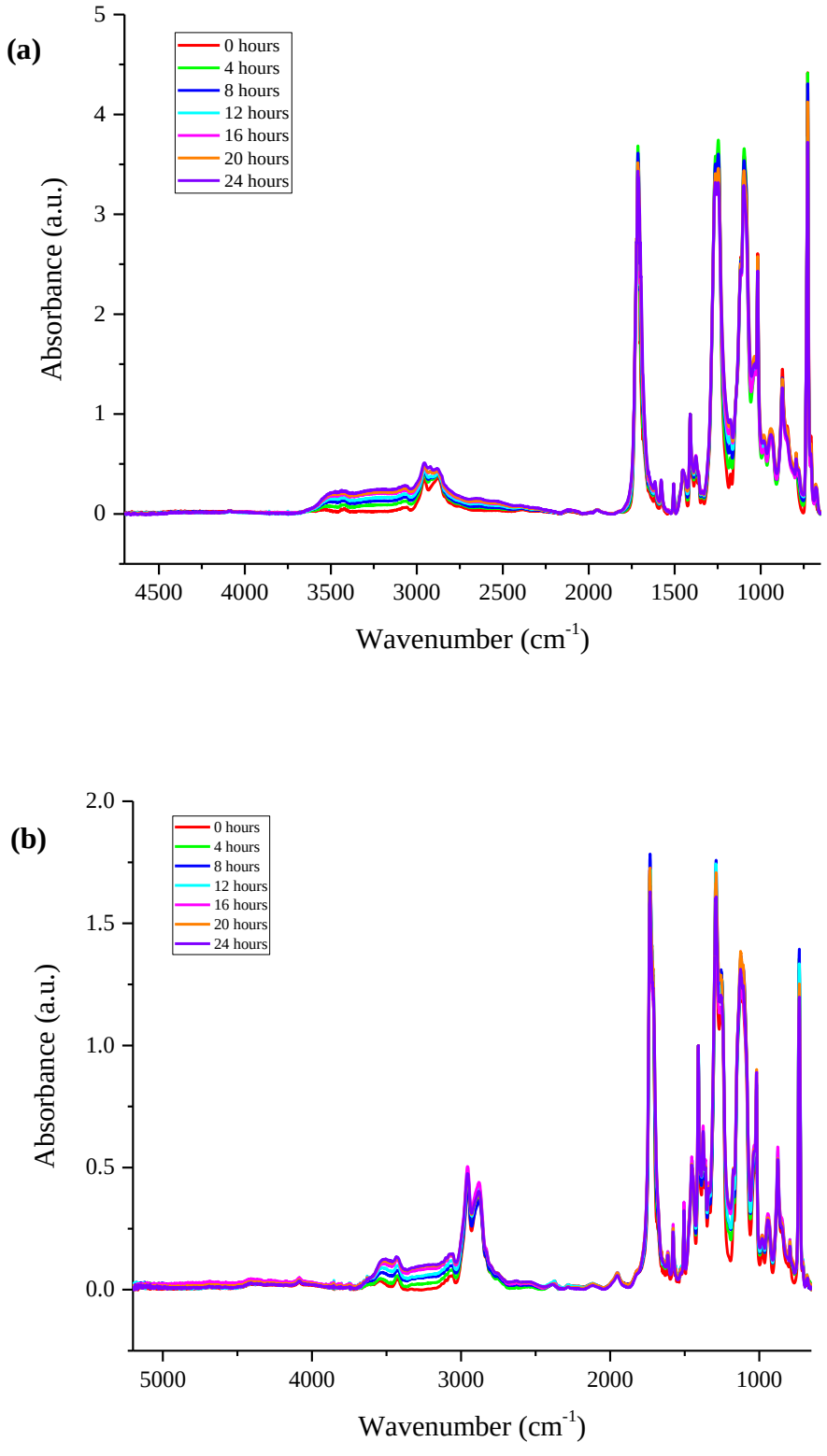

Figure 5.15: (a) ATR FT-IR spectra and (b) DRIFT spectra of PDEGT irradiated in the weatherometer from 0 to 24 hours.

As previously mentioned, the extent of photodegradation was measured by the change in area of the region between 3800-2100 cm^{-1} and the carbonyl peak with dosage. Fi*gure 5.16 and 5.17* shows the change in area of these peaks, with dosage, for PDEGT and 36 µm PET irradiated in the weatherometer, from ATR and DRIFT spectra, respectively. The graphs show the change in the extent of degradation in the first week of exposure. Both figures show that the change in areas for PDEGT increase steadily with dosage, which agrees with the trends shown in *Figures 5.07 and 5.12* of samples analysed weekly. *Figure 5.17 (b)* shows some fluctuation in the change in area of the carbonyl peak of PDEGT, which is thought to be because each spectrum was taken on a separate sample of PDEGT film.

Throughout the exposure, PDEGT degrades to a greater extent than the PET film, which is true for the surface and the bulk of the PDEGT sample. The fact that PDEGT degrades to a greater extent is thought to be due to the instability of the ether linkage and the temperature at which the exposures were carried out ((37.5 ± 2.5)°C is above the T_g of PDEGT).

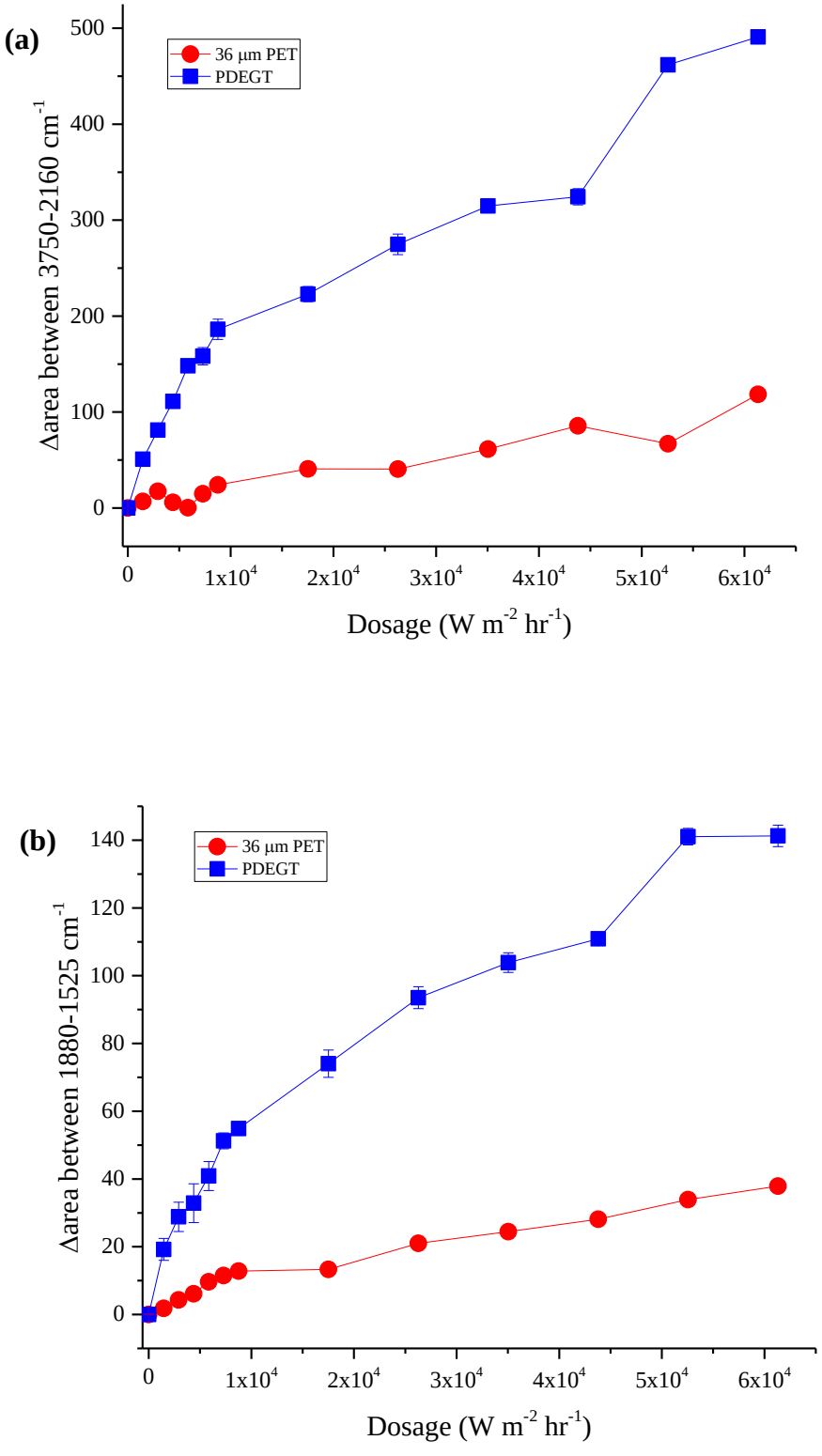

Figure 5.16: Extent of photodegradation of PDEGT measured by the change in area of peaks between (a) 3750-2160 cm^{-1} and (b) 1880-1525 cm^{-1}(carbonyl), from the ATR spectra.

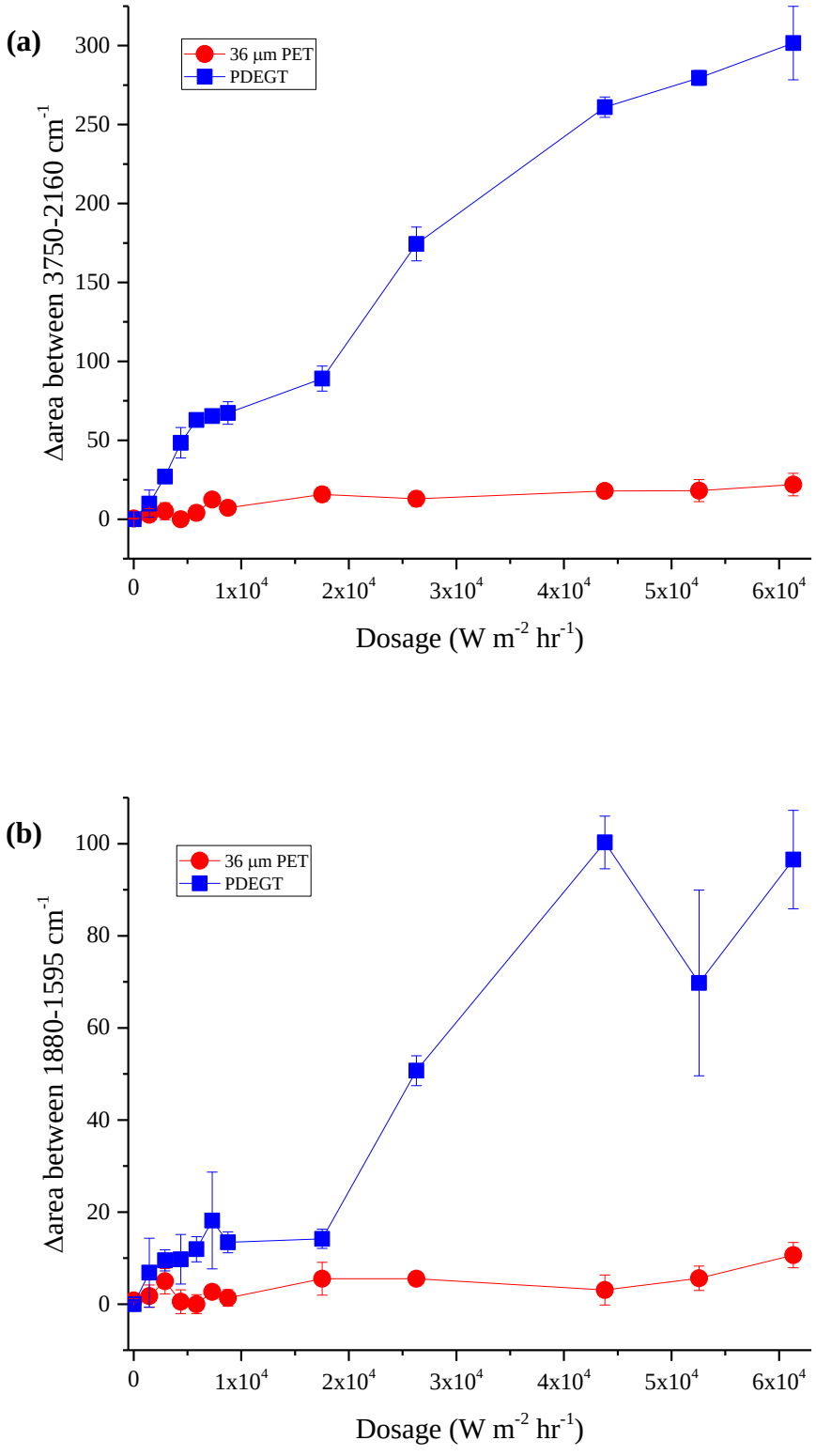

Figure 5.17: Extent of photodegradation of PDEGT measured by the change in area of peaks between (a) 3750-2160 cm^{-1} and (b) 1880-1595 cm^{-1}(carbonyl), from the DRIFT spectra.

5.2.3 UV-Vis-NIR

Figure 5.18 shows the UV-Vis-NIR spectra of samples irradiated in the weatherometer for 24 hours and 1 week. The peaks in the spectra have been assigned in *Table 8.* Peaks at 2265 and 2450 nm have been assigned to a combination C-H stretching, while 1715, 1660 and 845 nm have been assigned to the first overtone and third overtone of the C-H stretching.

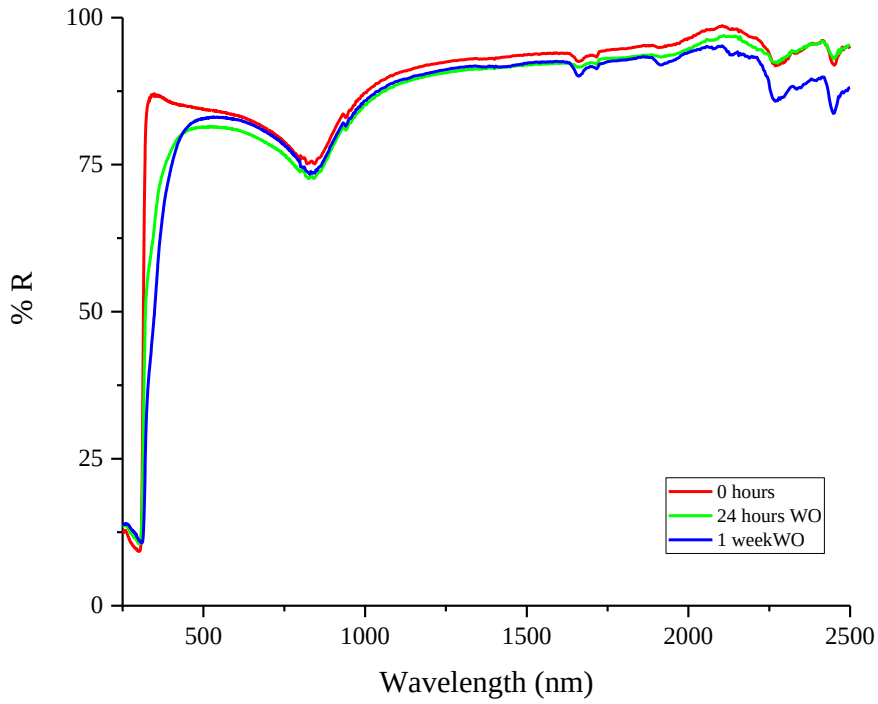

Figure 5.18: UV-Vis-NIR spectra of PDEGT samples irradiated in the weatherometer.

After 1 week of exposure it is apparent, from *Figure 5.18,* that there has been a development of a peak at 1925 nm which has been assigned to the combination O-H stretching peak. This indicates the production of new hydroxy groups during the photodegradation of PDEGT, which could include carboxylic acid end groups.

After exposure, there is the appearance of a shoulder between 450-320 nm. This indicates the production of monohydroxy terephthalate groups and quinone species, as discussed in the UV-visible spectra in *Chapter 3, Section 3.3.3*. The monohydroxy

terephthalate groups were first identified by Pacifici and Straley,[22] and a mechanism was proposed for their formation by Day and Wiles.[23] This mechanism is given in *Chapter 1, Figure 1.28.* The formation of the quinone species has been studied by Edge *et al.* and Fechine *et al.* and mechanistic pathways for their production have been proposed.[24,25] These mechanisms are given in *Chapter 1, Figures 1.31.*

Table 8: Band assignments for the UV-Vis-NIR spectra of PDEGT.

Wavelength (nm)	Assignment
2265, 2450	Combination C-H stretching
1925	Combination O-H stretching
1715, 1660	First overtone C-H stretching
845	Third overtone C-H stretching

5.2.4 Conclusions

The photodegradation reactions taking place in PDEGT, during exposure to conditions simulating outdoors, were investigated. Results show the production of carboxylic acid end groups, dimers, anhydrides, monohydroxy terephthalate groups and quinone species. The production of these groups suggests that chain scission reactions are occurring during degradation. Mono-substituted rings have also been shown to be produced by the development of a peak in both the ATR and DRIFT spectra.

Initially, PDEGT degrades under a broad spectrum of light due to its high absorbance at shorter wavelengths, this is then followed by the degradation products absorbing longer wavelengths of light which causes another scheme of reactions. PDEGT degrades to a greater extent than PET, when irradiated in the weatherometer at the same temperature and time. This is thought to be due to the instability of the ether linkage. However, this difference could also be due to the fact that the exposures in the weatherometer were run at (37.5 ± 2.5)°C, which is above the T_g of PDEGT but

below the T_g of PET. Both the ether linkage and the temperature are thought to play a part in PDEGT degrading to a greater extent than PET. As shown with PET, it is incredibly difficult to determine the role of each wavelength of light in the degradation process using a broad spectrum of light. Thus, narrow wavelength ranges were used to study the influence of different wavelengths of light on the photodegradation of PDEGT.

5.3 Effect of wavelength on the photodegradation of PDEGT

PDEGT was exposed to two wavelength ranges of UV light; UV-A (365 nm) and UV-B (302 nm), at room temperature. This allowed for the analysis of the effect of different wavelengths of light on the photodegradation of PDEGT. Samples were analysed using ATR FT-IR, DRIFT and UV-Vis-NIR.

5.3.1 ATR FT-IR

Thin films of PDEGT were exposed to 365 nm and 302 nm light independently for 1 week, (equivalent to a dosage of approximately 4.8 x 10^3 W m^{-2} hr^{-1} and 4.2 x 10^3 W m^{-2} hr^{-1}, respectively) in 24 hours increments (equivalent to a dosage of approximately 8.3 x 10^2 W m^{-2} hr^{-1} and 6.1 x 10^2 W m^{-2} hr^{-1}, respectively). *Figures 5.19 and 5.20* show the ATR spectra for the PDEGT samples exposed to 302 nm and 365 nm light, respectively.

After only 24 hours of exposure to 302 nm light there are major changes identified in the spectra of PDEGT, shown in *Figure 5.19*. Changes have occurred in the region between 3800-2100 cm^{-1} and the carbonyl and fingerprint regions. However, samples exposed to 365 nm light show only minor changes in the ATR spectra with exposure time, as shown in *Figure 5.20*.

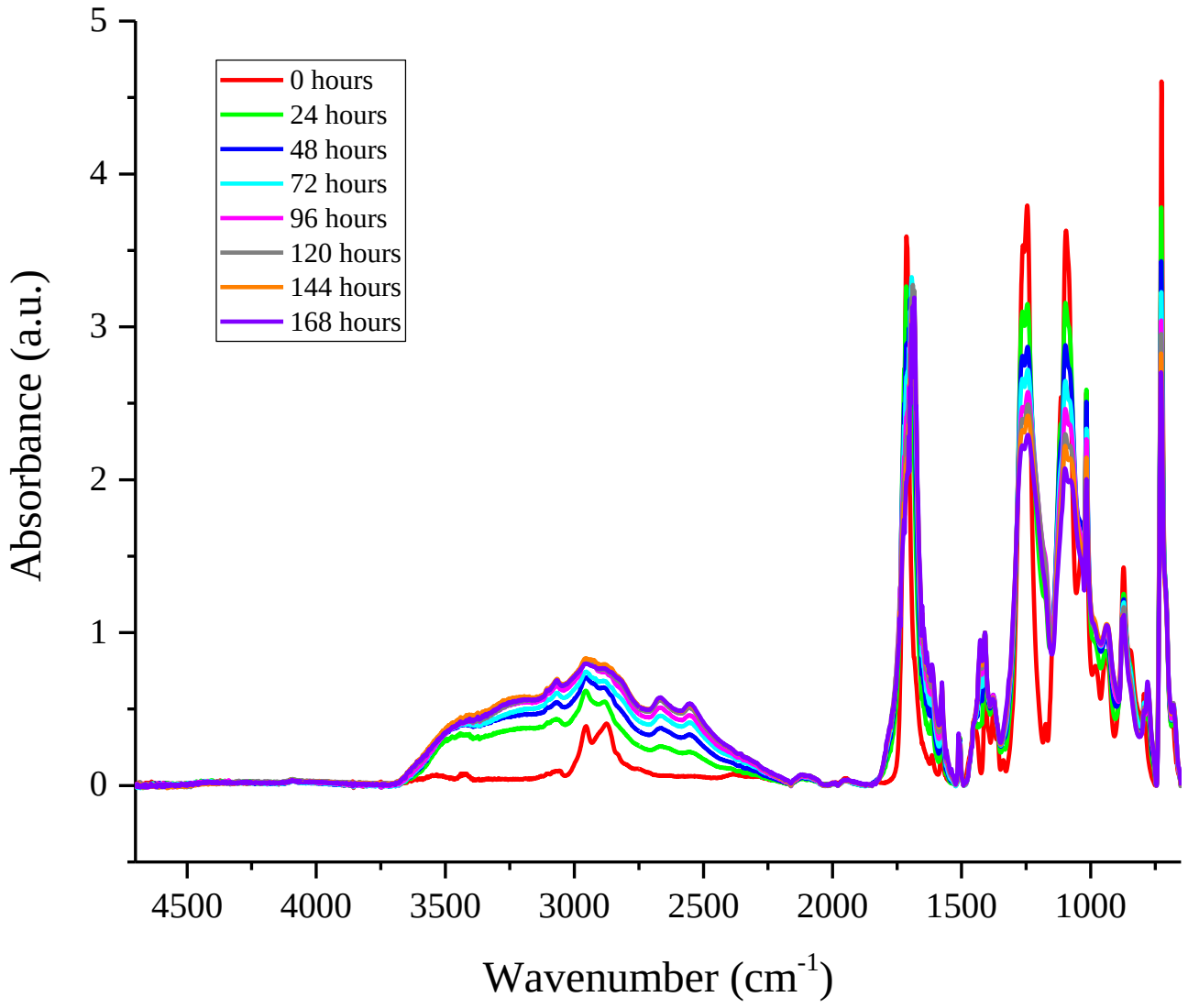

Figure 5.19: ATR FT-IR spectra of PDEGT films exposed to 302 nm light for 1 week, in 24 hour increments.

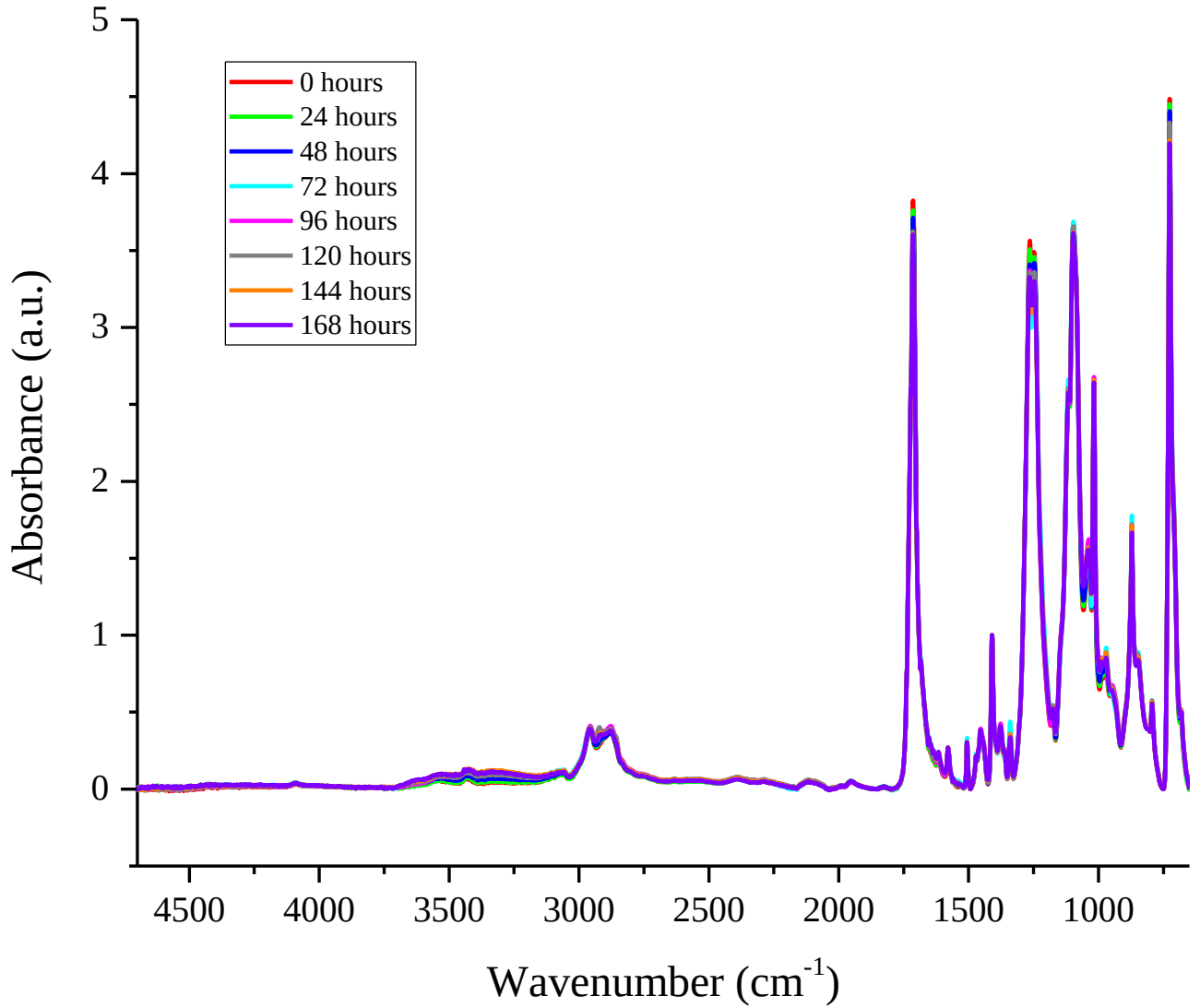

Figure 5.20: ATR FT-IR spectra of PDEGT films exposed to 365 nm light for 1 week, in 24 hour increments.

Figure 5.21 shows the region of the ATR spectra of samples exposed to 302 nm light, between 3800-2100 cm^{-1}, containing the hydroxy peaks as well as the aromatic and aliphatic C-H stretching peaks. The peaks present in this region, before and after exposure, have been assigned in *Table 9*.

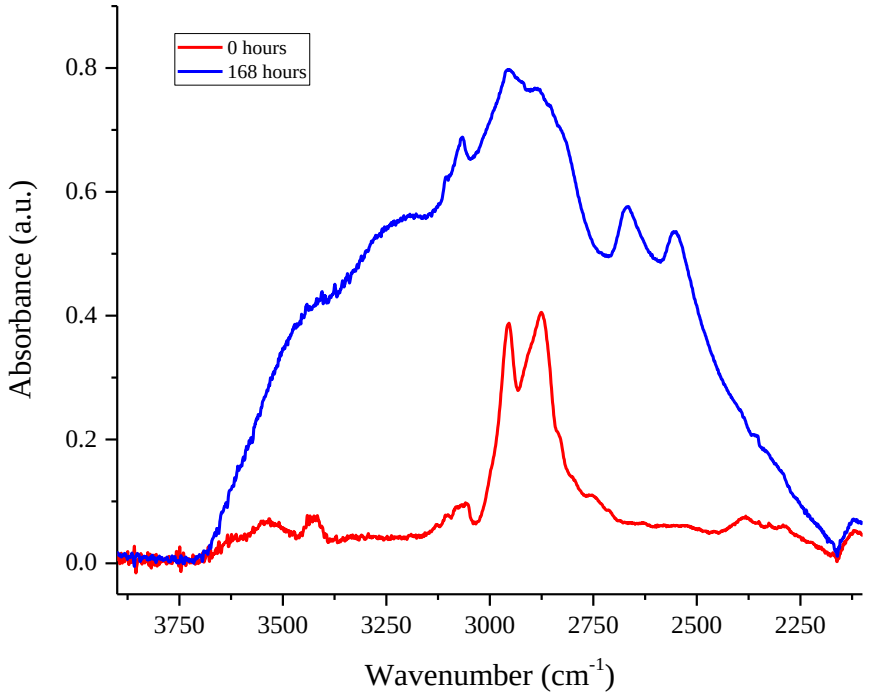

Figure 5.21: ATR FT-IR spectra of PDEGT exposed to 302 nm light, in the region between 3800-2100 cm^{-1}.

Peaks associated with the carboxylic acid end groups and dimers as well as Ar-CH_3 groups have developed upon exposure to 302 nm light. There has also been change in other peaks in this region, including the size of the peaks associated with the aromatic C-H stretching due to the production of mono-substituted rings which results in another aromatic C-H bond on the terephthalic ring. There has also been a decrease in height of the peaks assigned to the aliphatic C-H stretching vibrations, which can be

explained due to the chain scission reactions taking place during degradation. The peaks in this region of the spectra have been discussed in detail in *Section 5.2.1.1*.

Table 9: Band assignments for the region between 3800-2100 cm^{-1} of the ATR FT-IR spectrum of PDEGT.

Peak (cm^{-1})	Assignment
3630	Aqueous O-H stretching vibration[1]
3550	Alcoholic O-H stretching vibration[1]
3430	First overtone of the carbonyl peak[1]
3290	Carboxylic acid end groups[1]
3100 – 3060	Aromatic C-H stretching[4]
2955, 2875	Asymmetric and symmetric aliphatic C-H stretching[2]
2920	C-H symmetric stretching vibration associated with the Ar-CH_3 group[5]
2665, 2550	Characteristic of the carboxylic acid dimer[6]

The carbonyl peak of a control sample and a sample exposed to 302 nm light for 1 week, from the ATR spectra, are shown in *Figure 5.22*. The various peaks contained within the carbonyl region have been assigned and are given in *Table 10.*

After exposure to 302 nm light, the carbonyl peak shows general broadening indicating the production of new carbonyl groups. At higher wavenumbers, this broadening has been attributed to the production of anhydride and aliphatic aldehyde groups. Peaks assigned to carboxylic acid dimers, end groups, quinone species and terephthalic acid have all shown an increase in absorbance after exposure and cause the broadening of the peak at lower wavenumbers. The decrease in absorbance of peaks associated with the ester carbonyl and the development of peaks assigned to degradation products appears to happen simultaneously during exposure. The various peaks contained with the carbonyl region have been discussed in detail in *Section 5.2.1.1*.

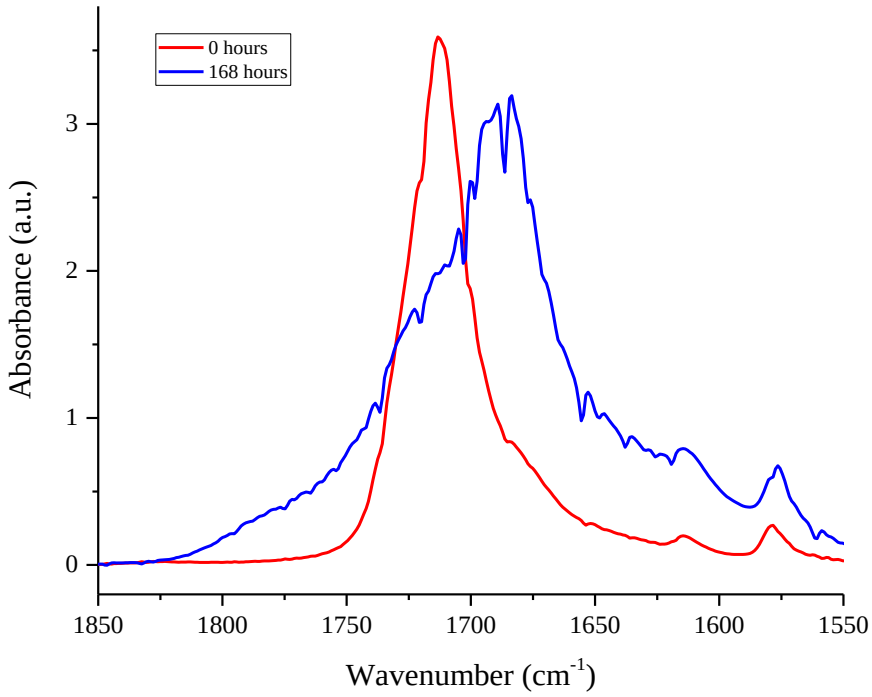

Figure 5.22: ATR FT-IR spectra of PDEGT exposed to 302 nm light, in the carbonyl region between 1850-1550 cm^{-1}.

Table 10: Band assignments for the carbonyl region of the ATR FT-IR spectrum of PDEGT.

Peak (cm^{-1})	Assignment
1785	Carbonyl stretch from anhydride carbonyl[9,11]
1740	Carbonyl stretch from aliphatic aldehyde[5]
1721	Amorphous carbonyl stretch from ester[4]
1713	Crystalline carbonyl stretch from ester[4]
1700	Carbonyl stretch from carboxylic acid dimer[7,11,12]
1695	Carbonyl stretch from carboxylic acid end groups[13]
1690	Carbonyl stretch from quinone groups[14,15]
1685	Carbonyl stretch from terephthalic acid

As discussed in *Section 5.2.1.1* the extent of photodegradation of PDEGT was measured by the change in area of the peaks in the region between 3800-2100 cm^{-1} and the carbonyl peak. *Figure 5.23 (a) and (b)* shows the change in area of these peaks, with dosage, for PDEGT and 36 µm PET exposed to 302 nm and 365 nm light. Both graphs show that PDEGT exposed to 302 nm light degrades to a greater extent than PET exposed to 302 nm light. This, again, indicates that the ether linkage is the weak link in PDEGT, as this is the only structural difference between the two polymers. PDEGT also displays degradation to a greater extent when exposed to 302 nm light compared to 365 nm light. This was expected as PDEGT shows a much stronger absorbance at shorter wavelengths. Samples of PDEGT and PET exposed to 365 nm light degrade to similar extents.

Although the mechanism for photodegradation is thought to be similar to that of PET, there must be another photo-oxidative process taking place during exposure to account for PDEGT degrading to a greater extent.

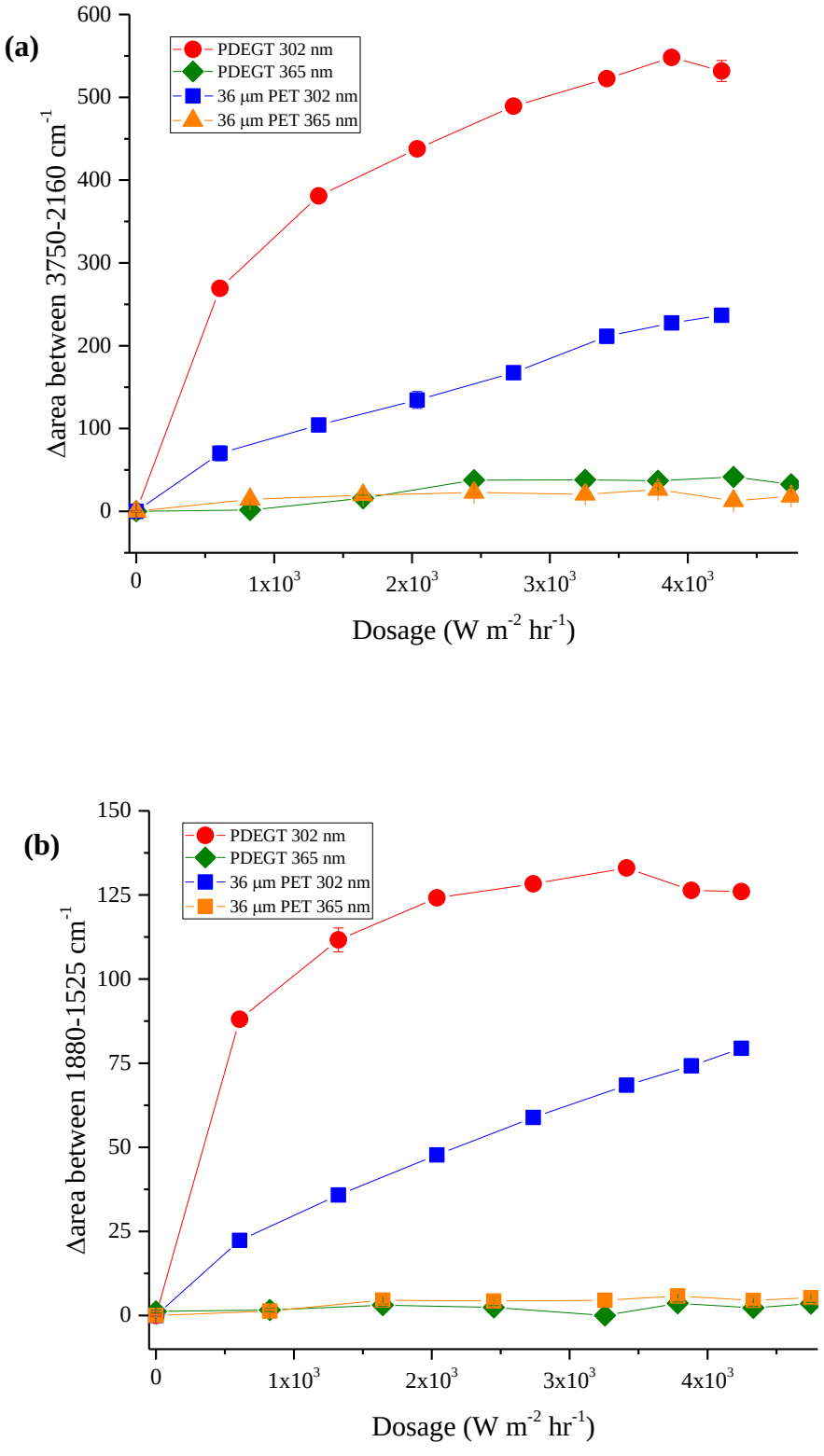

Figure 5.23: Extent of photodegradation of PDEGT measured by the change in area of peaks between (a) 3750-2160 cm^{-1} and (b) 1880-1525 cm^{-1}(carbonyl), from the ATR spectra.

The fingerprint region of the control film and PDEGT exposed to 302 nm light are shown in *Figure 5.24.* Peaks that have changed or developed in this region have been assigned in *Table 11*.

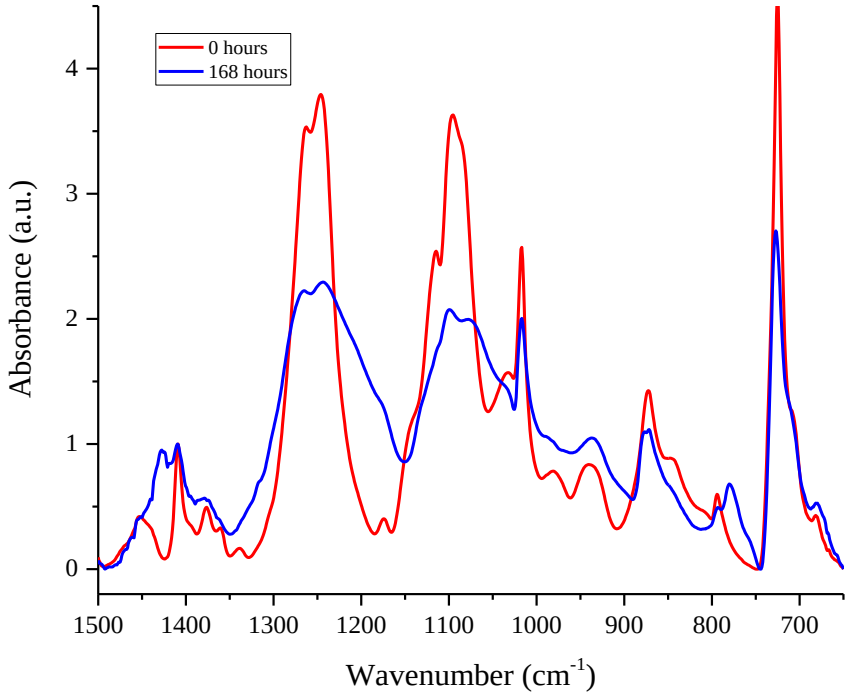

Figure 5.24: ATR FT-IR spectra of PDEGT exposed to 302 nm light, in the fingerprint region between 1500-700 cm^{-1}.

After exposure, peaks have developed at 1430 and 1220 cm^{-1} associated with carboxylic acid dimers. Peaks at 1265 and 1095 cm^{-1} associated with the ester group show a decrease in absorbance, due to chain scission reactions leading to the breakdown of the ester group. There has also been a reduction in the size of the peaks at 980 and 940 cm^{-1} which indicate the breakdown of the ester and ether units during degradation. *Figure 5.24* shows a decrease in absorbance of the peak at 845 cm^{-1} and the development of the peak at 758 cm^{-1}, which indicate a change in substitution pattern of the terephthalic ring. The peak that has evolved at 778 cm^{-1} has not been reported in the literature, during the irradiation of PDEGT or PET, but is thought to be

due to the production of mono-substituted rings. The peaks in the fingerprint region have been discussed in detail in *Section 5.2.1.1*.

Table 11: Band assignments for the fingerprint region of the ATR FT-IR spectrum of PDEGT.

Peak (cm^{-1})	Assignment
1430	Combination band due to C-O stretching and O-H deformation vibration, associated with carboxylic acid dimer.[5]
1265	C(O)-O stretching of ester group[2]
1220	C-O stretching vibration, associated with carboxylic acid dimer.[5]
1095	C-O stretching vibration of ester group[5]
980	O-CH_2 stretching of ethylene glycol segment.[2]
940	O-CH_2 stretching of diethylene glycol segment.[2]
845	C-H deformation of two adjacent hydrogens on the terephthalic ring (indicates 1, 4 substitution)[3]
778	Out-of-plane deformation vibrations of mono-substituted rings[5]
758	Out of plane deformation vibrations of 1, 2, 4-substituted rings[5]

5.3.2 DRIFT

The DRIFT spectra of PDEGT films exposed to 365 nm and 302 nm light for 1 week, (equivalent to a dosage of approximately 4.8 x 10^3 W m^{-2} hr^{-1} and 4.2 x 10^3 W m^{-2} hr^{-1}, respectively) in 24 hour increments (equivalent to a dosage of approximately 8.3 x 10^2 W m^{-2} hr^{-1} and 6.1 x 10^2 W m^{-2} hr^{-1}, respectively) are shown in *Figure 5.25 and 5.26*. The spectra of samples exposed to 302 nm light show that changes are apparent in the region between 3800-2100 cm^{-1}, as well as the carbonyl and fingerprint regions, after exposure. However, samples exposed to 365 nm light (*Figure 5.26)* show only minor changes in the spectra, with exposure time.

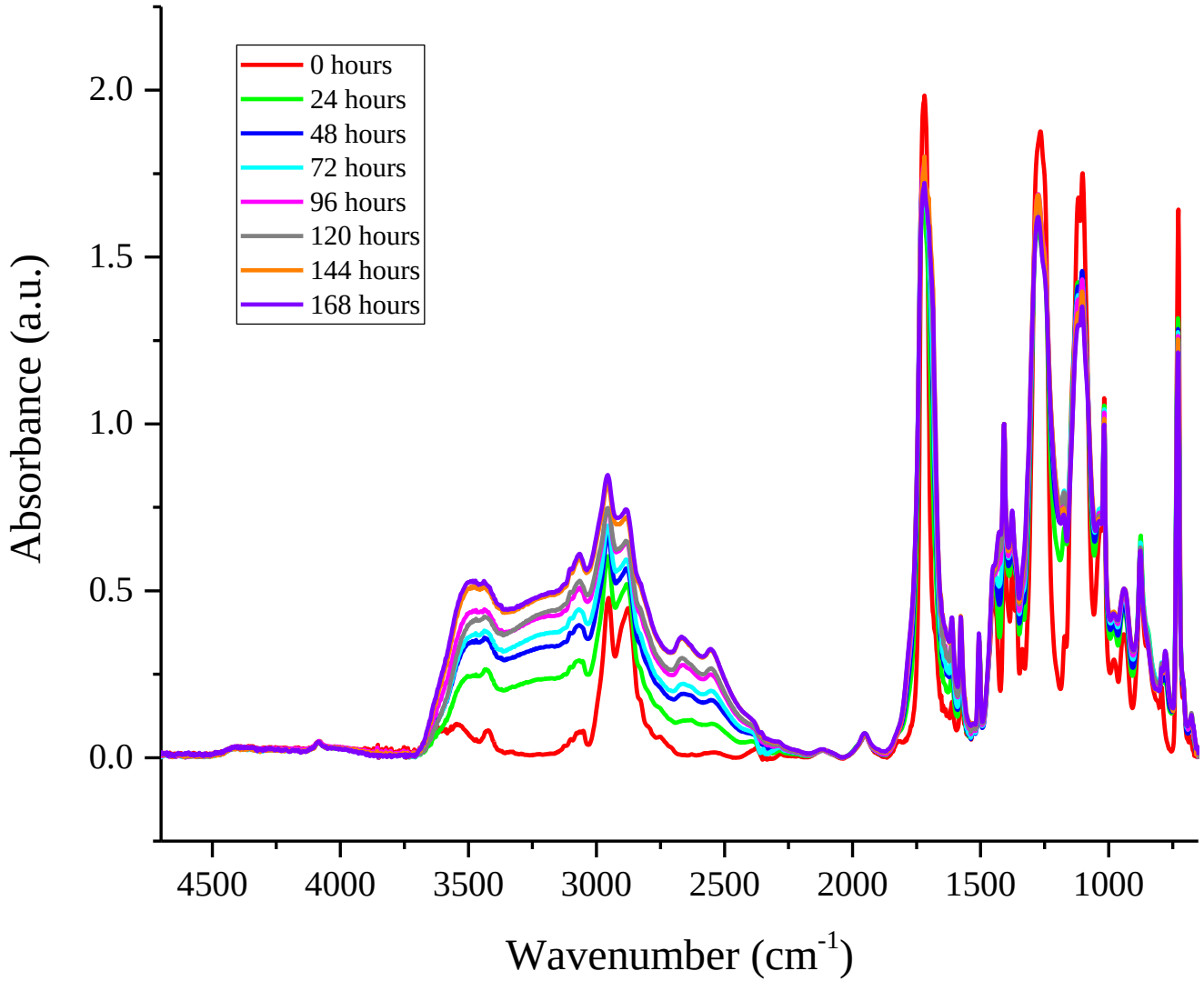

Figure 5.25: DRIFT spectra of PDEGT films exposed to 302 nm light for 1 weeks, in 24 hour increments

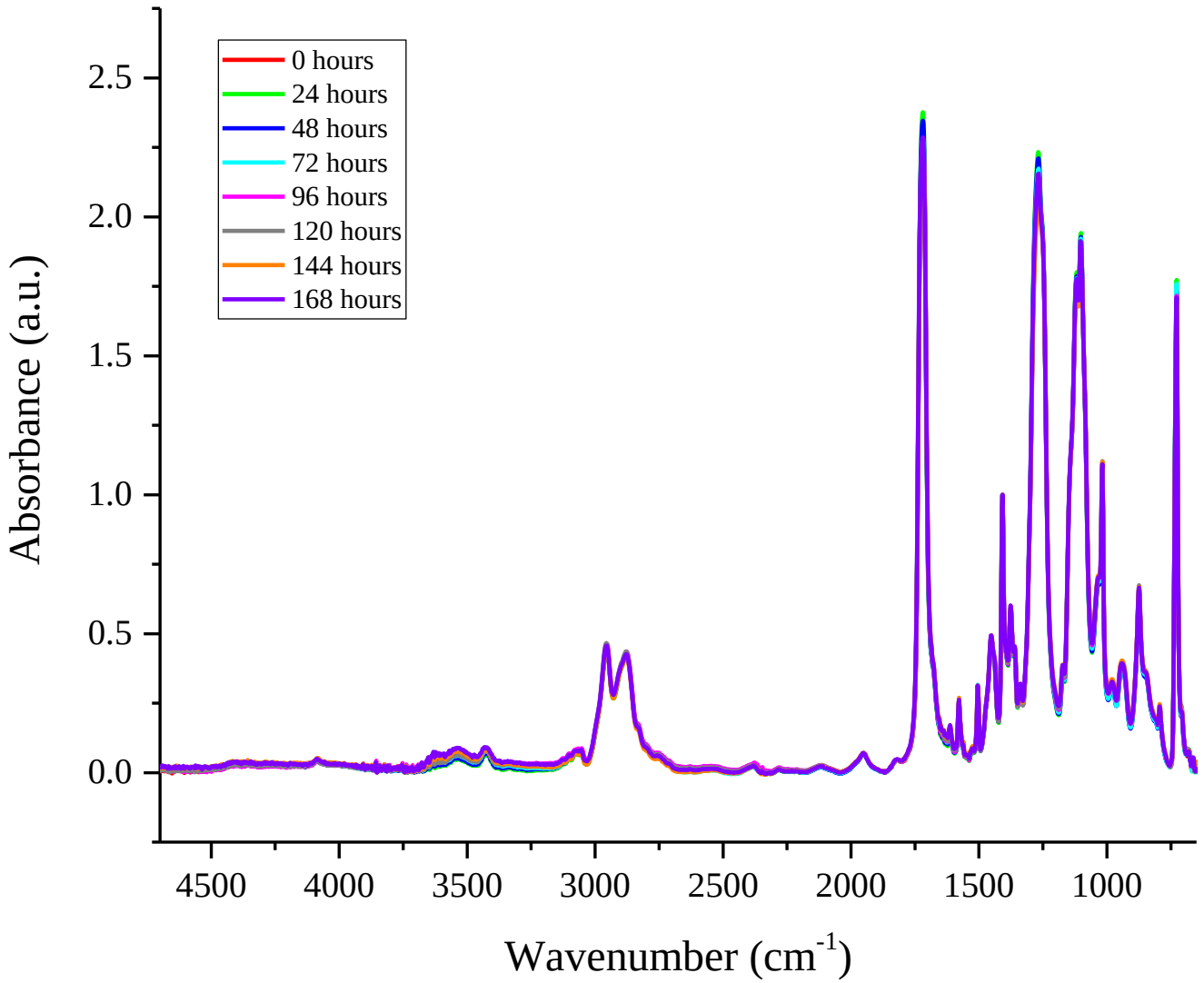

Figure 5.26 DRIFT spectra of PDEGT films exposed to 365 nm light for 1 week, in 24 hour increments.

The assignments for peaks in the region between 3800-2100 cm^{-1} for samples exposed to 302 nm light are given in *Table 12*. The main change in this region is the increase in absorbance of the peaks assigned to the aqueous, alcoholic and carboxylic acid hydroxy stretches. This indicates the production of new hydroxy groups during exposure, including carboxylic acid end groups. This region has been discussed in detail in *Section 5.2.1.2.*

Table 12: Band assignments for the region between 3800-2100 cm^{-1} of the DRIFT spectrum of PDEGT.

Peak (cm^{-1})	Assignment
3630	Aqueous O-H stretching vibration[1]
3550	Alcoholic O-H stretching vibration[1]
3430	First overtone of the carbonyl group in ester[1]
3290	Carboxylic acid end groups[1]
3125, 3100, 3068, 3050	Aromatic C-H stretching[4]
2955 2875	Amorphous aliphatic CH_2 stretching[4]
2830	Crystalline aliphatic CH_2 stretching[4]
2670, 2555	Characteristic of the carboxylic acid dimer[6]

Assignments for the various peaks contained within the carbonyl region of the DRIFT spectra (*Figure 5.25*) are given in *Table 13*. The control sample shows a peak at 1725 cm^{-1} assigned to the carbonyl stretching vibration of the ester. After exposure, the peak has broadened at higher wavenumbers due to the production of anhydride groups. The broadening at lower wavenumbers has been attributed to the formation of carboxylic acid end groups during degradation. The peaks in this region have been discussed in detail in *Section 5.2.1.2*.

Table 13: Band assignments for the carbonyl region of the DRIFT spectrum of PDEGT.

Peak (cm^{-1})	Assignment
1785	Carbonyl stretch from anhydride carbonyl[9]
1725	Carbonyl stretching vibration of an ester[21]
1685	Carbonyl stretch from terminal acid end groups[21]

The extent of photodegradation was measured by the change in area of the peaks in the region between 3800-2100 cm^{-1} and the carbonyl peak, from the DRIFT spectra. *Figure 5.27 (a) and (b)* shows the change in area of these peaks, with dosage, for PDEGT and 36 µm PET exposed to 302 nm and 365 nm light. Both graphs show that PDEGT exposed to 302 nm light degrades to a greater extent compared to PET exposed to 302 nm light. This indicates the breakdown of the ether unit, during degradation, as this is the only structural difference between the polymers. It is also interesting to note that PDEGT degrades to a greater extent under 302 nm light than 365 nm light, due to the polymer's strong absorbance at shorter wavelengths of light. PDEGT and PET films degrade to similar extents when exposed to 365 nm light.

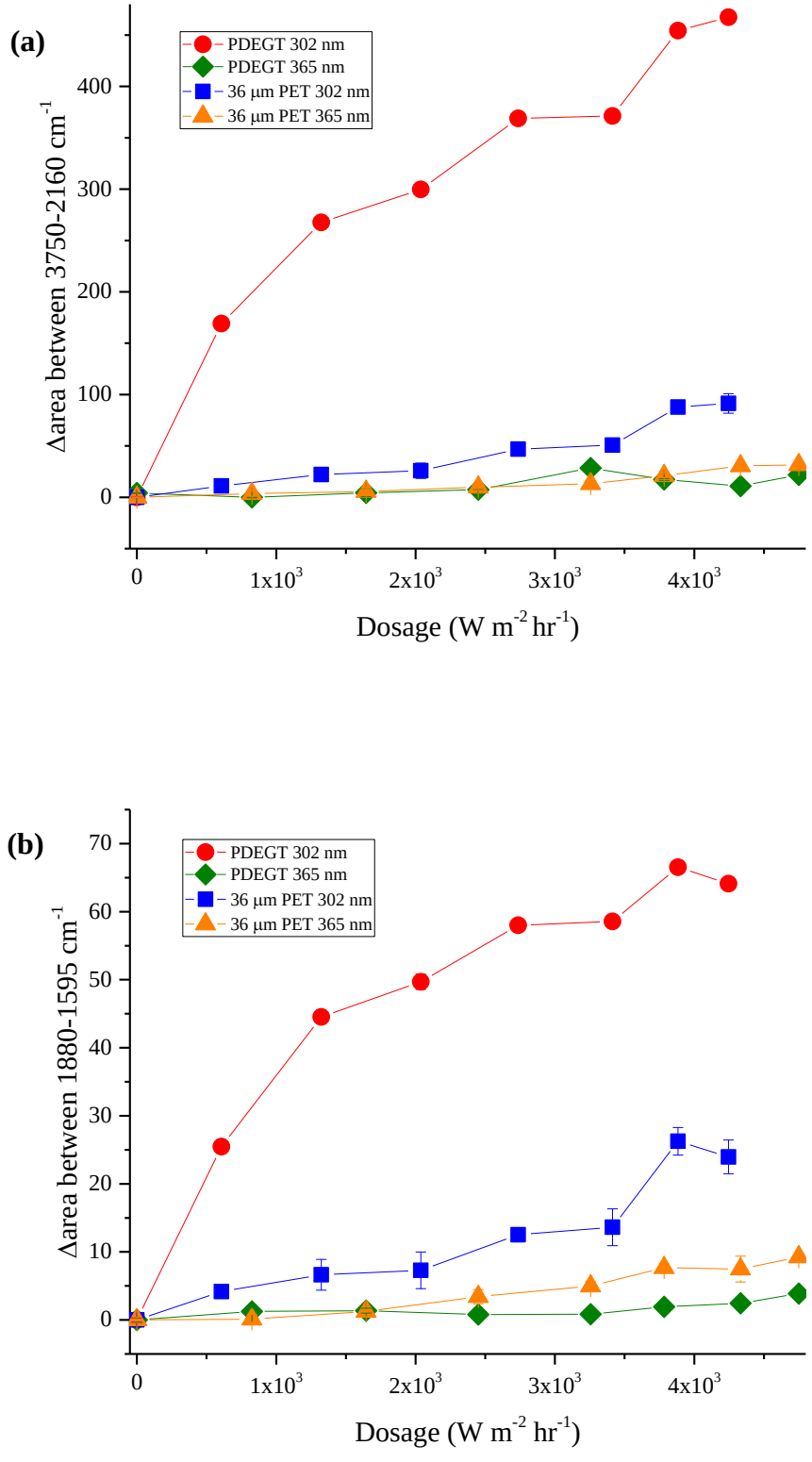

Figure 5.27: Extent of photodegradation of PDEGT measured by the change in area of peaks between (a) 3750-2160 cm^{-1} and (b) 1880-1595 cm^{-1}(carbonyl), from the DRIFT spectra.

Table 14 shows the assignments for peaks that have changed or developed in the region of the spectra between 1500-750 cm^{-1}. Peaks at 1430 and 1220 cm^{-1} have developed upon exposure and have been associated with the production of carboxylic acid dimers. The decrease in absorbance of peaks associated with the ester group indicates the breakdown of the ester during exposure. There has also been a reduction in the size of the peaks assigned to the $O\text{-}CH_2$ stretching of the ethylene glycol and diethylene glycol segment, respectively, indicating the breakdown of the ester and ether units.

Table 14: Band assignments for the fingerprint region of the DRIFT spectrum of PDEGT.

Peak (cm^{-1})	Assignment
1430	Combination band due to C-O stretching and O-H deformation vibration, associated with carboxylic acid dimer.[5]
1265	C(O)-O stretching of ester group[2]
1220	C-O stretching vibration, associated with carboxylic acid dimer.[5]
1117	Indicative of aromatic 1, 4-substitution pattern[2]
1104	C-O stretching vibration of aliphatic ester[5]
980	$O\text{-}CH_2$ stretching of ethylene glycol segment.[2]
940	$O\text{-}CH_2$ stretching of diethylene glycol segment.[2]
845	C-H deformation of two adjacent hydrogens on the terephthalic ring (indicates 1, 4 substitution)[3]
778	Out-of-plane deformation vibrations of mono-substituted rings[5]
758	Out of plane deformation vibrations of 1, 2, 4-substituted rings[5]

The peak at 845 cm^{-1} has also shown a reduction in size, indicative of substitution on the terephthalic ring. This is further supported by the development of the peaks at 758 cm^{-1} assigned to the 1, 2, 4-substituted ring.[5]

The development of the peak at 778 cm^{-1}, has never been assigned in the literature during exposure of PDEGT or PET but is believed to be associated with the formation

of mono-substituted rings. The peaks contained within the region between 1500-700 cm^{-1} have been discussed in detail in *Section 5.2.1.2*.

5.3.3 UV-Vis-NIR

UV-Vis-NIR was used to analyse PDEGT samples exposed to 302 nm and 365 nm light after 1 week. The spectra are shown in *Figure 5.28*.

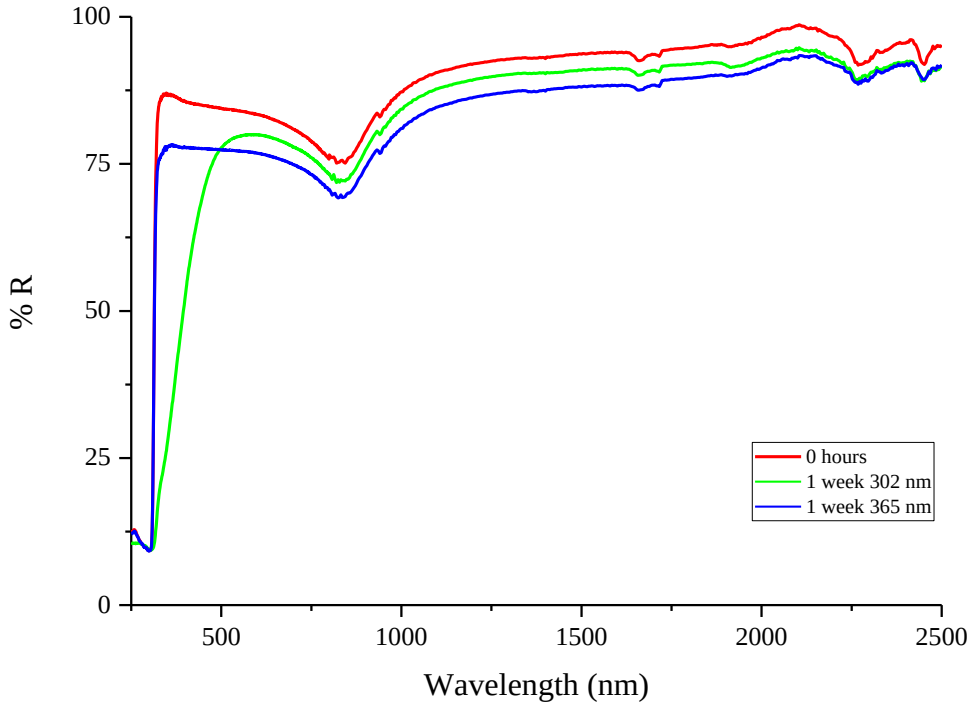

Figure 5.28: UV-Vis-NIR spectra of PDEGT samples exposed to 302 nm and 365 nm light.

Table 15 gives the assignments for the peaks present in the spectra in *Figure 5.28*. Peaks at 2265 and 2450 nm have been assigned to a combination C-H stretching, while 1715, 1660 and 845 nm have been assigned to the first overtone and third overtone of the C-H stretching. After exposure to 302 nm light, there has been development of a small peak at 1925 nm, which is assigned to the combination O-H stretching vibration. This suggests that there has been production of new hydroxy groups, including

carboxylic acid end groups, during exposure. The sample exposed to 302 nm light also shows the appearance of a shoulder between 450-320 nm, indicating the production of monohydroxy terephthalate groups and quinone species. The production of these groups has been discussed in detail in *Chapter 3, Section 3.3.3.*

The spectrum for the PDEGT sample exposed to 365 nm light, depicted by the blue line in *Figure 5.28*, shows no meaningful change.

Table 15: Band assignments for the UV-Vis-NIR spectra of PDEGT.

Wavelength (nm)	Assignment
2265, 2450	Combination C-H stretching
1925	Combination O-H stretching
1715, 1660	First overtone C-H stretching
845	Third overtone C-H stretching

5.3.4 Conclusions

The effect of exposing PDEGT to different wavelengths of light was studied, using 302 nm and 365 nm light. PDEGT samples exposed to 302 nm light showed production of carboxylic acid end groups, dimers, anhydrides, quinones, monohydroxy terephthalate groups and mono-substituted rings. The production of these groups suggests that chain scission and substitution reactions have occurred during exposure. Results show that PDEGT photodegrades faster under 302 nm light compared to 365 nm light, of similar intensity, under oxidative conditions. This was expected as the UV-visible spectrum of PDEGT shows that longer wavelengths are absorbed weakly, whereas short wavelengths are absorbed strongly, with a λ_{max} of approximately 306 nm. Samples exposed to 365 nm light showed minor changes with exposure time. Upon exposure to light, PDEGT seems to degrade more rapidly when exposed to short wavelength light compared to long wavelength light of the same intensity.

5.4 Exposing PDEGT to high intensity 365 nm light

PDEGT films were exposed to high intensity 365 nm light at approximately (43 ± 2)°C. The lamp used in this study is approximately 26 times more intense than the previous 365 nm lamp. As minor changes were identified when PDEGT was exposed to 365 nm light at an average intensity of (31.7 ± 4.0) W m^{-2}, a more intense lamp, with an average intensity of (825.5 ± 20) W m^{-2}, was used to allow for any minimal changes to be highlighted. Samples were analysed, before and after exposure, using ATR FT-IR, DRIFT and UV-Vis-NIR.

5.4.1 Infrared

The ATR and DRIFT spectra of PDEGT exposed to high intensity 365 nm light, for 6 weeks (equivalent to a dosage of approximately 8.3 x 10^5 W m^{-2} hr^{-1}) in 1 week increments, (equivalent to a dosage of approximately 1.4 x 10^5 W m^{-2} hr^{-1}) are shown in *Figures 5.29 and 5.30*, respectively. Peak assignments for the ATR and DRIFT spectra of PDEGT have already been discussed in detail in *Sections 5.2.1.1 and 5.2.1.2*, respectively. Both spectra show change in the region between 3800-2100 cm^{-1} and the carbonyl and fingerprint regions. The changes identified in both the ATR and DRIFT spectra follow the same trends as those seen in *Section 5.2.1.1 and 5.2.1.2*.

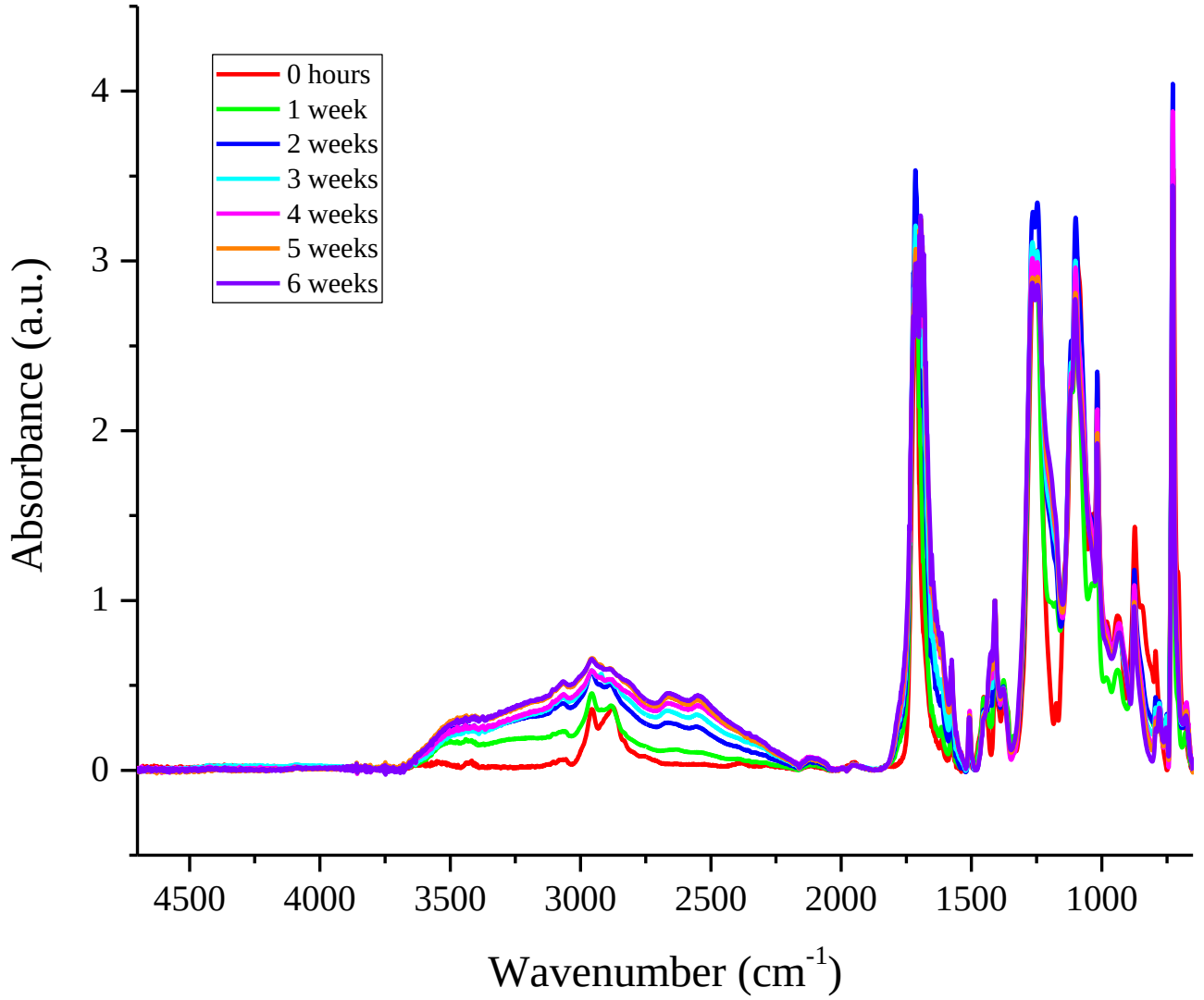

Figure 5.29: ATR FT-IR spectra of PDEGT exposed to 365 nm light for 6 weeks, in 1 week increments.

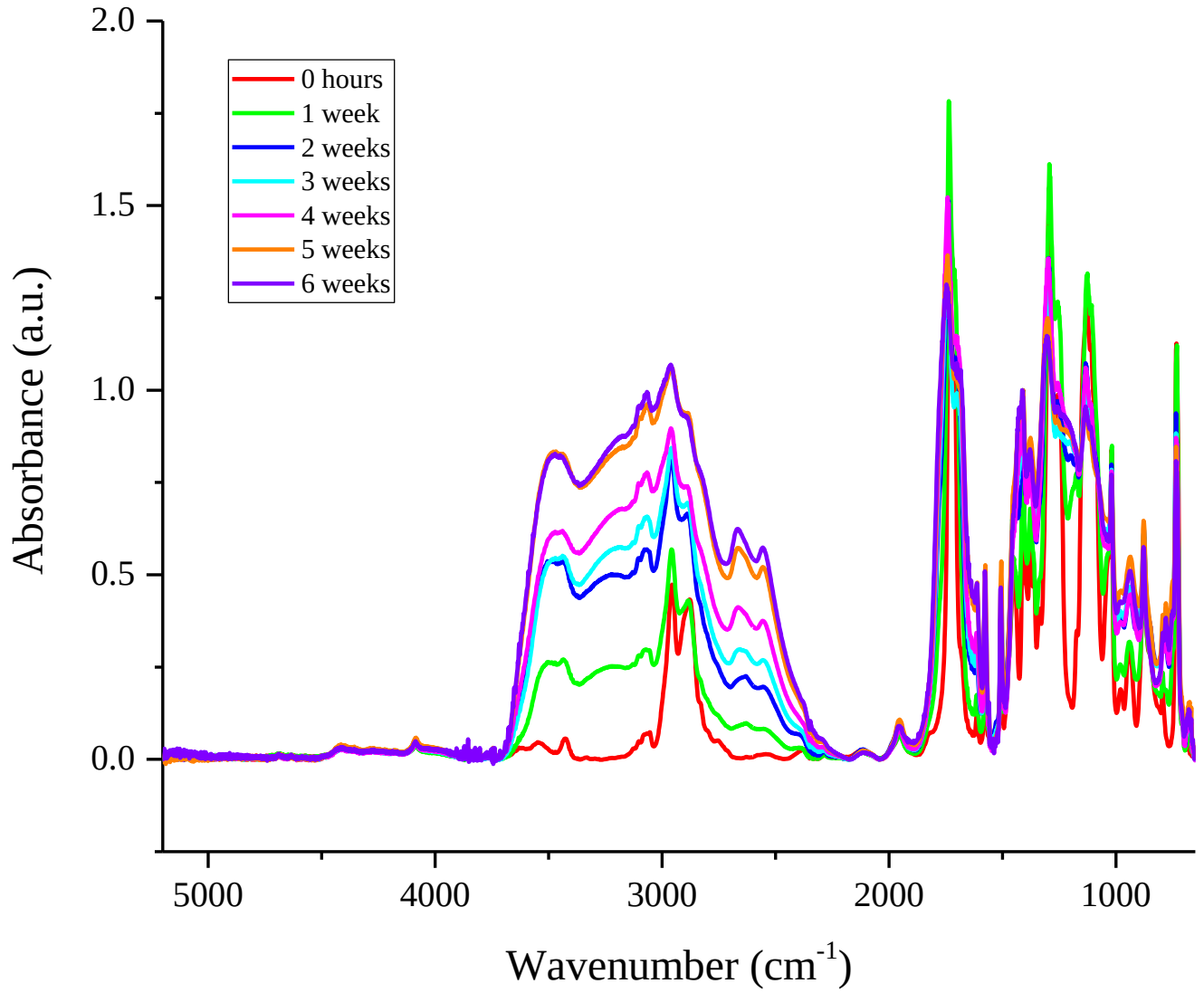

Figure 5.30: DRIFT spectra of PDEGT exposed to 365 nm light for 6 weeks, in 1 week increments.

Figure 5.29 shows that high intensity 365 nm light has had a significant effect on the surface of the PDEGT film. The DRIFT spectra, shown in *Figure 5.30*, also shows that 365 nm light has a major effect on the bulk of the PDEGT sample. PET has also been exposed to 365 nm light, shown in *Chapter 3, Section 3.5*, but does not show such a marked increase in the extent of degradation as seen with the PDEGT. However, PDEGT does show greater changes in the DRIFT spectra compared to the ATR spectra, which agrees with the spectra reported for PET. It is important to note that the temperature of the irradiation chamber was (43 ± 2)°C, during exposures. This means that although PET was still below its T_g, PDEGT was exposed above its T_g. Temperature is shown to influence the extent of degradation on the surface and in the bulk in *Section 5.5*. However, the results in *Section 5.5* do not show such a noticeable change in the extent of degradation with temperature. This is thought to be because the temperature sensor was wrapped in tin foil during exposure (to stop the degradation of the rubber buttons) and therefore would record a lower temperature than the temperature that the PDEGT film was exposed too.

5.4.2 UV-Vis-NIR

Figure 5.31 shows the UV-Vis-NIR spectra for a control film and a PDEGT sample exposed to high intensity 365 nm light for 6 weeks. The peaks assignments for the UV-Vis-NIR spectra of PDEGT have been discussed in *Section 5.2.3*. The development of the peak at 1925 nm, assigned to the combination O-H stretching, indicates the production of new hydroxy groups, such as carboxylic acid end groups. After exposure, the spectra also show the appearance of a shoulder between 450-320 nm. This suggests the presence of monohydroxy terephthalate groups and quinone species. The production of these groups has been discussed in further detail in *Chapter 3, Section 3.3.3*.

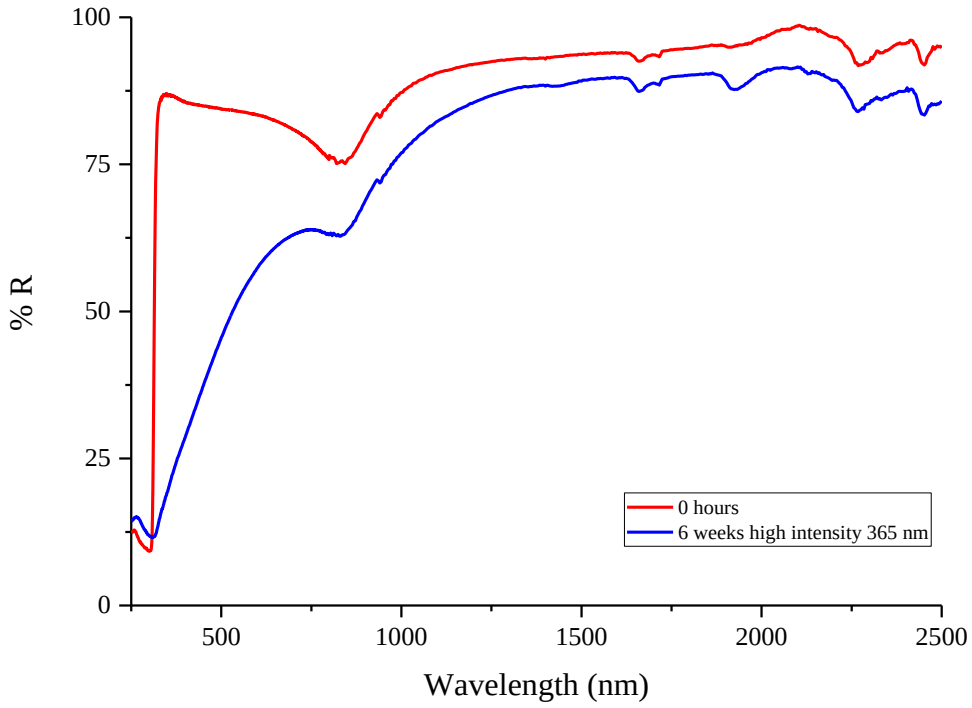

Figure 5.31: UV-Vis-NIR spectra of PDEGT before and after exposure to high intensity 365 nm light for 6 weeks.

5.4.3 Images of exposed PDEGT

During the exposure of PDEGT to intense 365 nm light, there was a noticeable colour change. Photographs of this colour change before and after exposure are given in *Figure 5.32*. Microscope images of PDEGT were also taken, which show the colour change and surface cracks after exposure, given in *Figure 5.33*.

The discoloration of the films is thought to be largely due to the production of quinone species during photodegradation. These species are also fully conjugated. Quinone species have been proven to be produced during the photodegradation of PET and the mechanism for their production, proposed by Fechine *et al.* is given in *Chapter 1, Figure 1.27.*

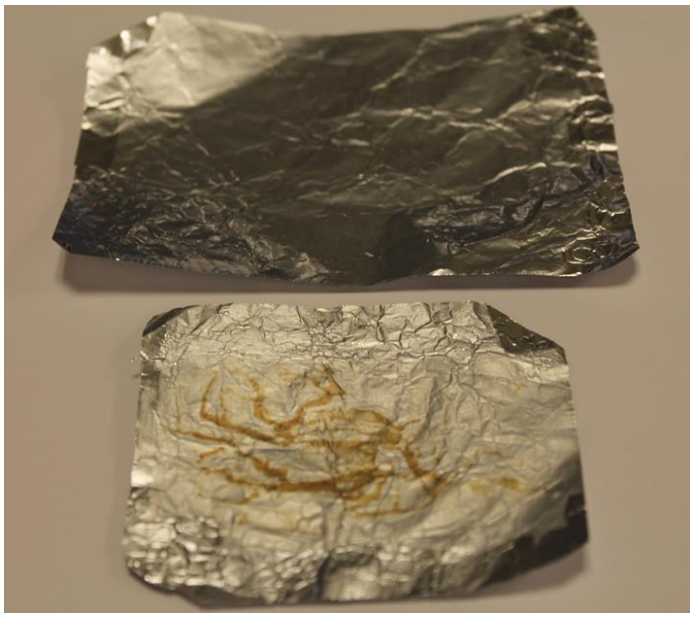

Figure 5.32: Photographs of PDEGT before (top) and after (bottom) exposure to high intensity 365 nm light for 4 weeks.

Figure 5.33: Microscope images of PDEGT after exposure to high intensity 365 nm light for 4 weeks.

5.4.4 Conclusions

PDEGT films were exposed to high intensity 365 nm light to allow for any minimal changes to be accentuated. Both the surface and the bulk of the PDEGT films showed significant changes in the spectra after exposure. This marked increase in the extent of degradation, on both the surface and in the bulk, is thought to be due to the instability of the ether linkage and temperature. The temperature of the irradiation chamber was approximately (43 ± 2)°C, which means that PDEGT was exposed above its T_g. An increase in temperature would influence the extent of photodegradation. In future experiments, the photodegradation cell (shown in *Chapter 2, Figure 2.06)* was used to control the temperature of the sample.

5.5 Effect of temperature

The effect of temperature on the photodegradation of PDEGT was investigated. The photodegradation cell (shown in *Chapter 2, Figure 2.06*) was used along with a chiller unit to heat and cool the sample. The PDEGT sample was exposed to 302 nm light above its T_g, at 40°C, and below its T_g, at 6°C, and was analysed using ATR FT-IR, DRIFT and UV-Vis-NIR.

5.5.1 Infrared results

5.5.1.1 Exposure above T_g

PDEGT was exposed to 302 nm light at 40°C; above the T_g of the polymer. The ATR and DRIFT spectra for samples exposed for 1 week (equivalent to a dosage of approximately 1.8 x 10^3 W m^{-2} hr^{-1}) in 24 hour increments (equivalent to a dosage of approximately 2.4 x 10^2 W m^{-2} hr^{-1}) are given in *Figures 5.34 and 5.35*. The spectra show change in the carbonyl and fingerprint region, as well as the region between 3800-2100 cm^{-1}. Changes in the spectra show the production of carboxylic acid end groups, dimers, quinone species and mono-substituted rings during exposure. The spectra also indicate that chain scission and substitution reactions have occurred. Peak assignments for the ATR and DRIFT spectra are given in *Sections 5.2.1.1 and 5.2.1.2,* respectively, and have been discussed in detail in these sections.

From the IR spectra, shown in *Figures 5.34 and 5.35*, exposure of PDEGT at 40°C and exposure at room temperature appear to show degradation occurring to similar extents.

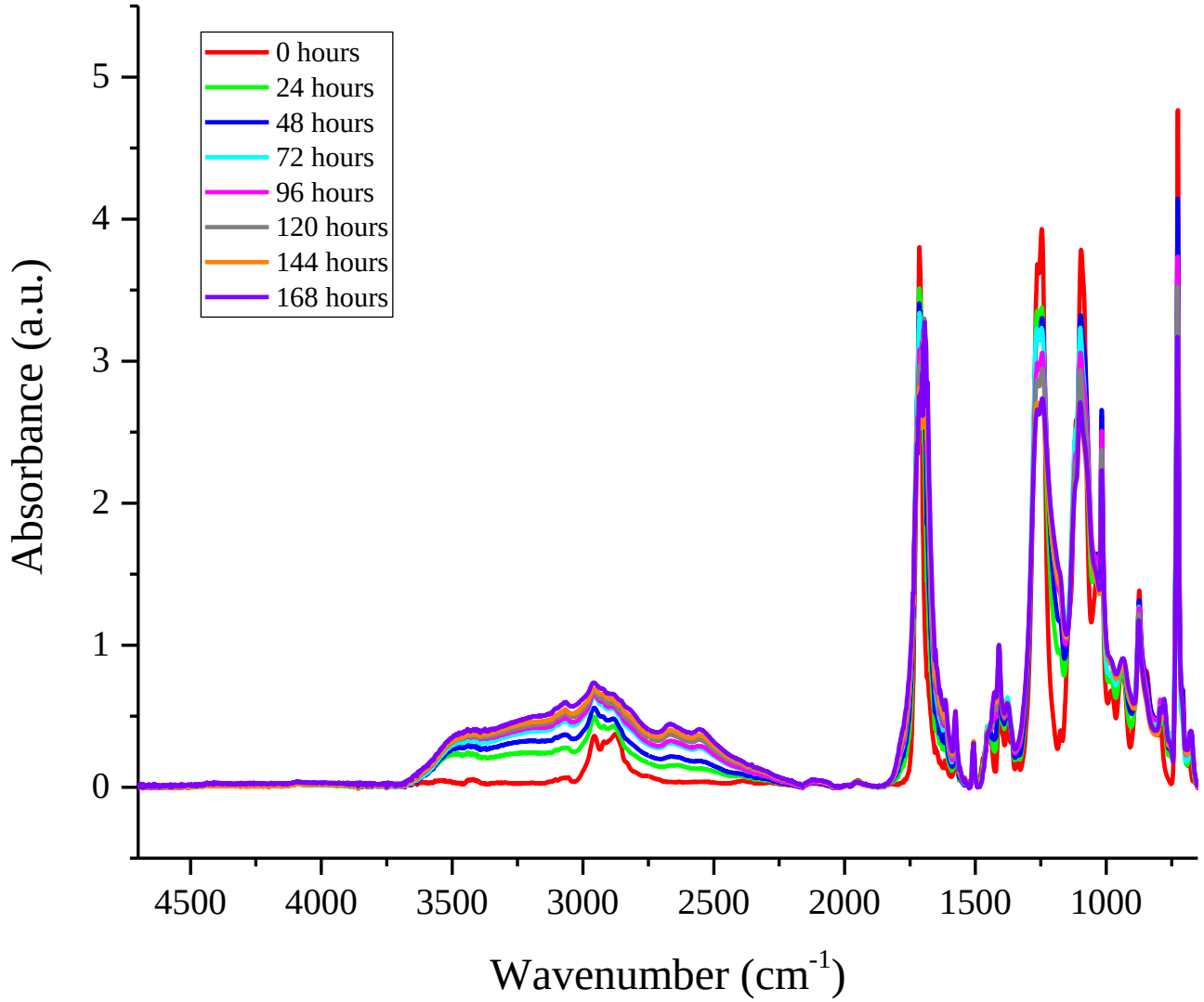

Figure 5:34: ATR FT-IR spectra of PDEGT exposed to 302 nm light at 40°C (above T_g) for 1 week, in 24 hour increments.

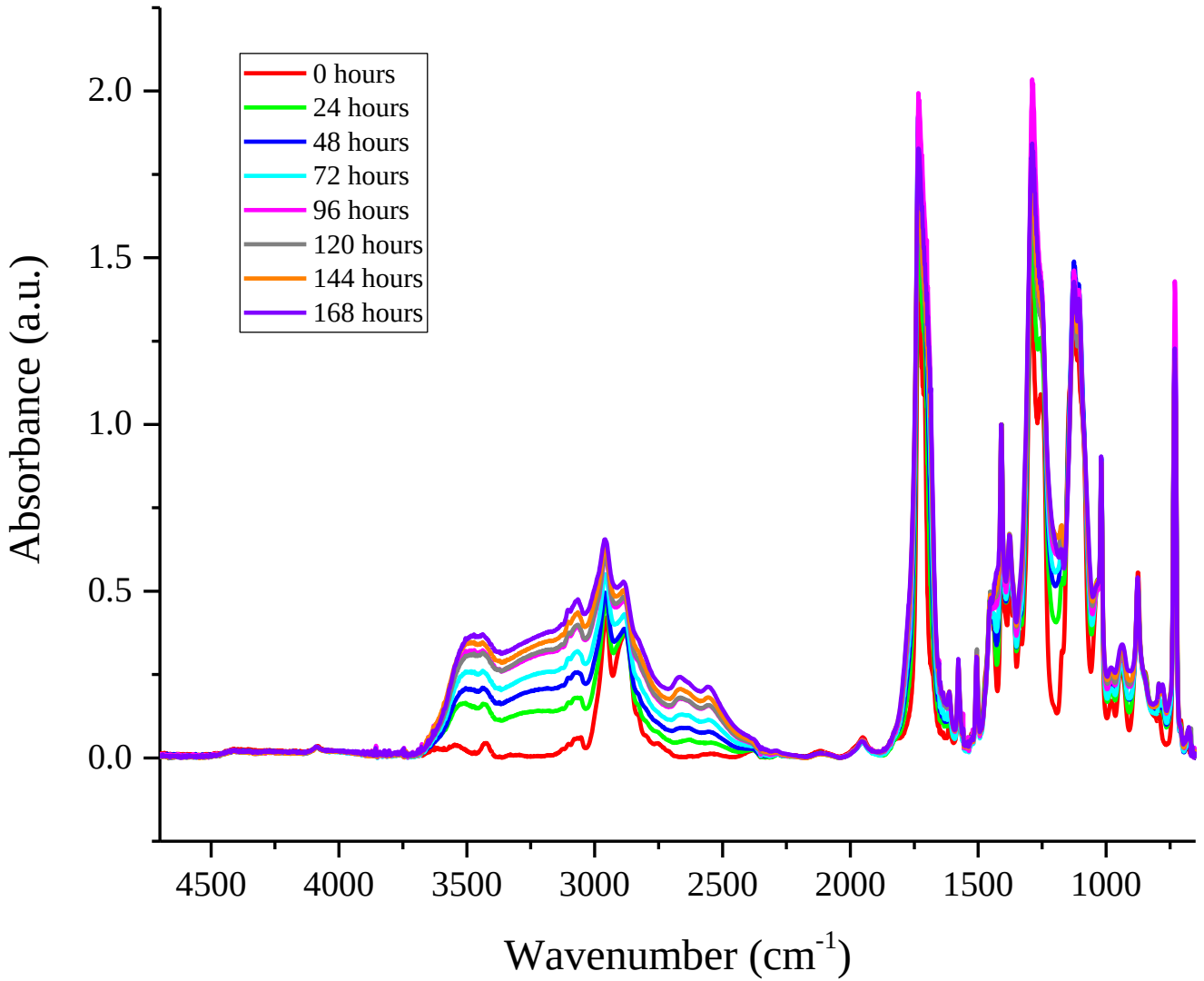

Figure 5.35: DRIFT spectra of PDEGT exposed to 302 nm light at 40°C (above T_g) for 1 week, in 24 hour increments.

5.5.1.2 Exposure below T_g

Films of PDEGT were exposed to 302 nm light at 6°C (below the T_g of the polymer) for 1 week (equivalent to a dosage of approximately 1.9 x 10^3 W m^{-2} hr^{-1}) in 24 hour increments (equivalent to a dosage of approximately 2.6 x 10^2 W m^{-2} hr^{-1}). The ATR and DRIFT spectra, shown in *Figures 5.36 and 5.37*, respectively, show change in the region between 3800-2100 cm^{-1}, as well as the carbonyl and fingerprint regions. Changes in the spectra indicate that chain scission and substitution reactions have taken place, as well as the production of carboxylic acid end groups, dimers, quinones and mono-substituted rings. The peak assignments for the ATR and DRIFT spectra have been discussed in detail in *Sections 5.2.1.1 and 5.2.1.2*.

The spectra show the same trends as seen with PDEGT exposed at room temperature (*Section 5.3)* but appear to show degradation to a lesser extent compared to samples exposed above the T_g.

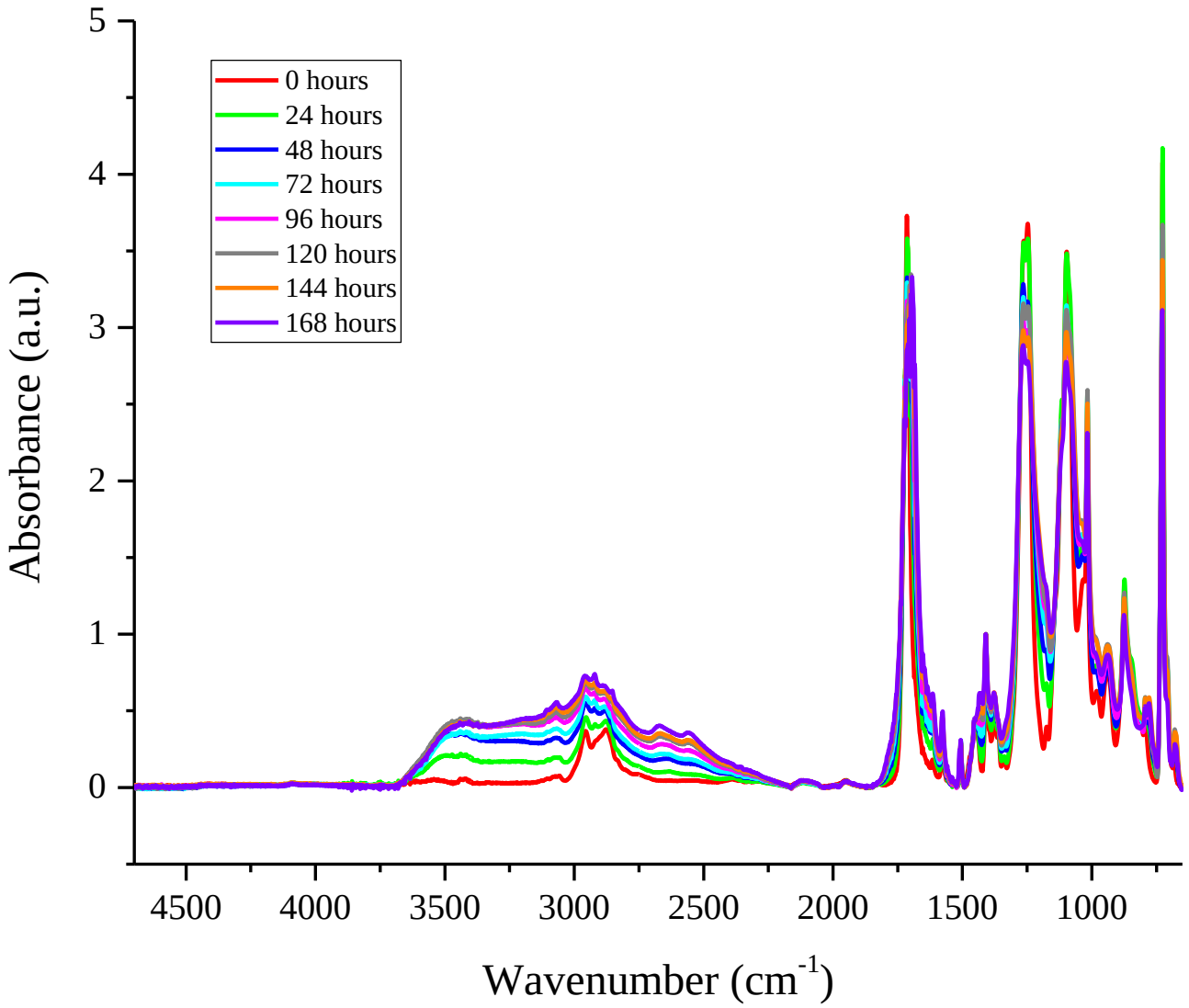

Figure 5.36: ATR FT-IR spectra of PDEGT exposed to 302 nm light at 6°C (below T_g) for 1 week, in 24 hour increments.

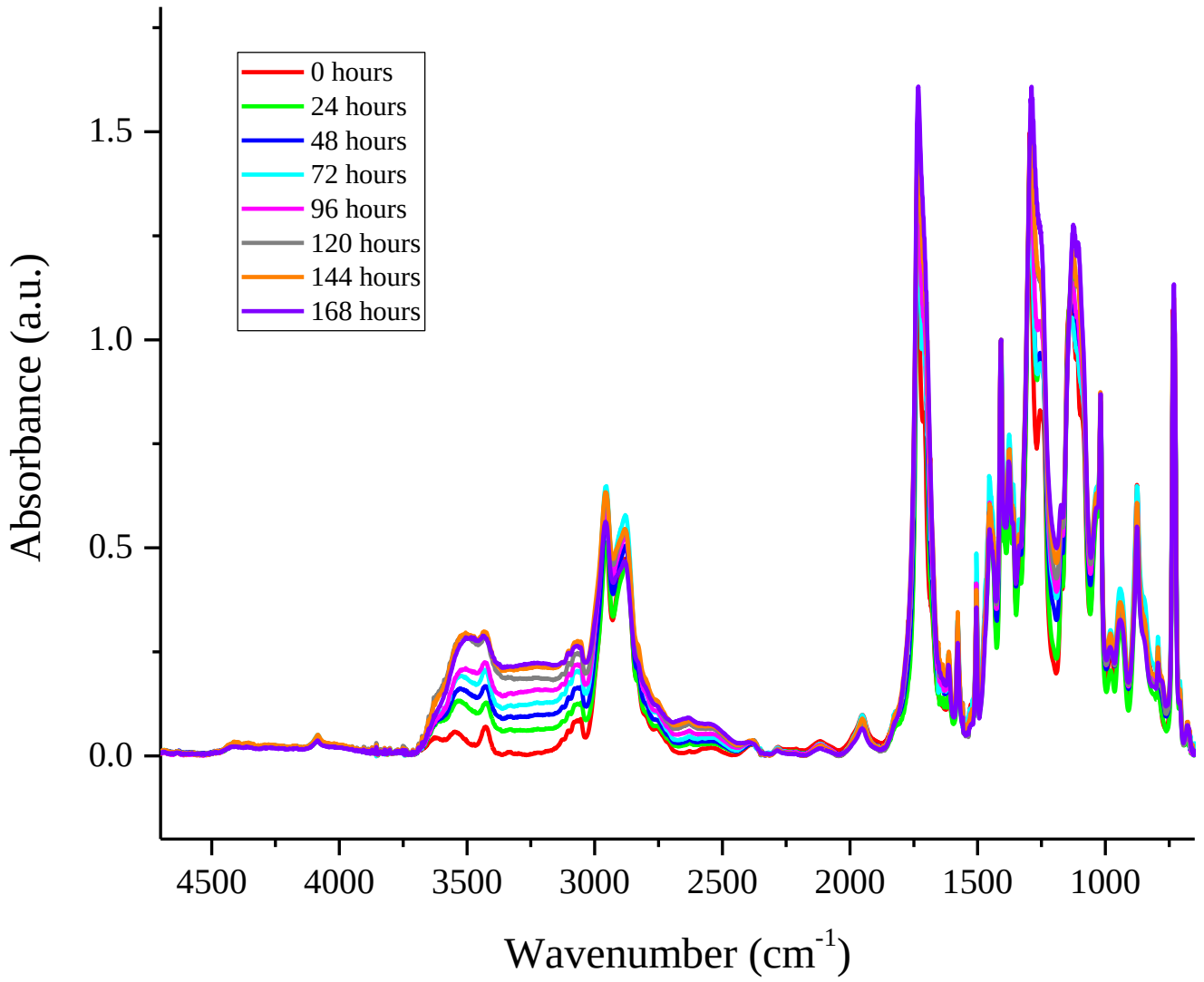

Figure 5.37: DRIFT spectra of PDEGT exposed to 302 nm light at 6°C (below T_g) for 1 week, in 24 hour increments.

5.5.1.3 Extent of photodegradation

As stated previously, the extent of photodegradation of PDEGT was measured by the change in area of the peaks in the region between 3800-2100 cm^{-1} and the carbonyl peak. *Figure 5.38* shows the change in area of these peaks, with dosage, for PDEGT exposed to 302 nm and 365 nm light at room temperature and those exposed to 302 nm light above and below the T_g, determined from the ATR spectra. *Figure 5.39* shows the extent of degradation calculated from the DRIFT spectra.

Figure 5.38 (a) and (b) show that PDEGT films, exposed to 302 nm at different temperatures, all showing degradation to a similar extent. There are some differences, in the extent of degradation, with temperature and it is thought that at higher dosages these differences would be accentuated. The samples are thought to degrade to a similar extent due to the presence and accessibility of oxygen at the surface of the films.

Based on the graphs shown in *Figure 5.38 (a) and (b)* it has been concluded that temperature has a minimal effect on the extent of photodegradation on the surface of PDEGT films, at short timescales. ATR FT-IR measures only the surface of the PDEGT samples.

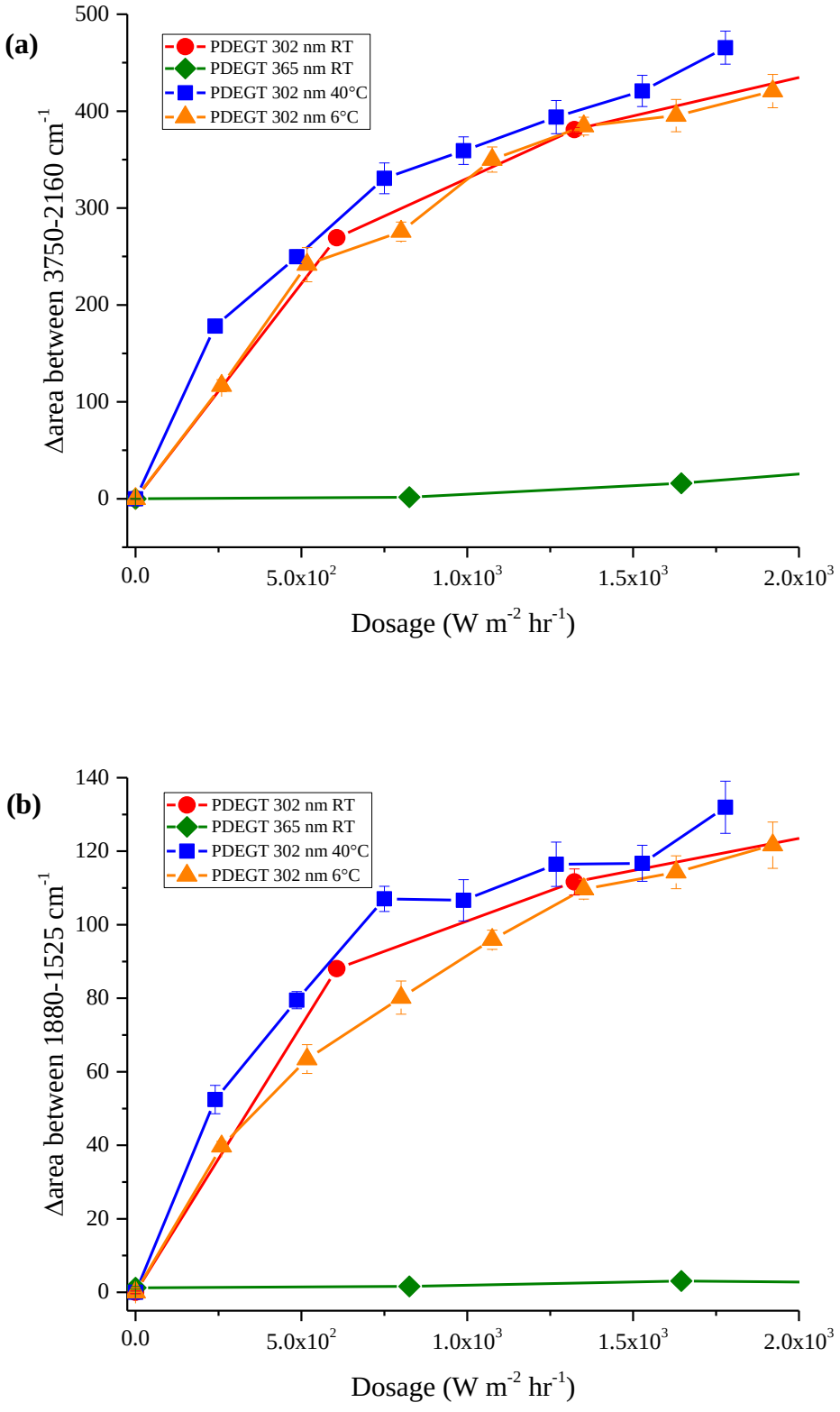

Figure 5.38: Extent of photodegradation of PDEGT measured by the change in area of peaks between (a) 3750-2160 cm^{-1} and (b) 1880-1525 cm^{-1}(carbonyl), from the ATR spectra.

The graphs in *Figure 5.39 (a) and (b)* show that the extent of degradation in the bulk of the PDEGT films has been influenced by temperature. *Figure 5.39* shows that samples exposed to 302 nm light at 6°C degrade the least, followed by the samples at room temperature and those exposed at 40°C. Degradation to a lesser extent, in the bulk of the film, when PDEGT is exposed below the T_g, is thought to be due to oxygen diffusion. Below the T_g, the polymer chains are rigid, whereas above the T_g the polymer chains become more flexible. Therefore, below the T_g, oxygen cannot diffuse into the bulk of the film as easily as when the polymer is above the T_g. Subsequently, photo-oxidative reactions are restricted below the T_g.

This also further explains why the surface of the sample does not show such a noticeable change with temperature. Although oxygen diffusion is a problem in the bulk of the film at different temperatures, oxygen will always be present and accessible at the surface of the film.

The lines depicting the samples exposed to 302 nm light at room temperature and 40°C (above T_g), in *Figure 5.39 (a)*, display degradation to similar extents. This is thought to be because the T_g of PDEGT is approximately 25°C which means that experiments undertaken at room temperature, specifically at (22.5 ± 2.5)°C, would mean the PDEGT film was exposed at a temperature either around or above the T_g. This means that the PDEGT could be showing degradation to a similar extent as PDEGT exposed at 40°C; above the T_g.

Figure 5.38 and 5.39 also show that the extent of degradation on the surface is faster than in the bulk of the sample. This could be due to lesser amounts of oxygen in the deeper positions of the film.

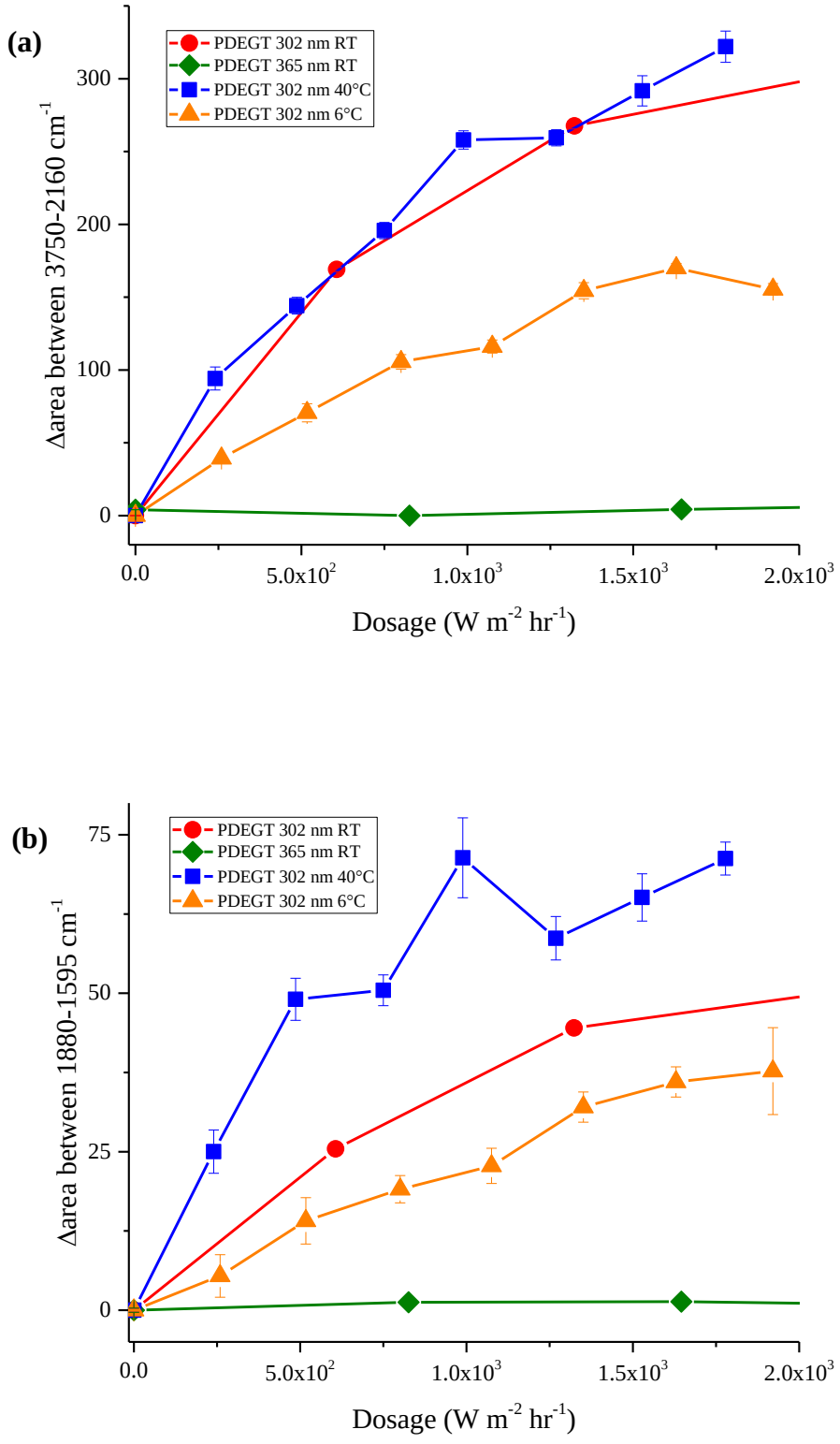

Figure 5.39: Extent of photodegradation of PDEGT measured by the change in area of peaks between (a) 3750-2160 cm^{-1} and (b) 1880-1595 cm^{-1}(carbonyl), from the DRIFT spectra.

5.5.2 UV-Vis-NIR

Figure 5.40 shows the UV-Vis-NIR spectra for samples exposed to 302 nm light at 40°C (above the $T_{g)}$ and 6°C (below the T_g). The peak assignments are given in *Section 5.2.1.3*. After exposure to 302 nm light at both temperatures, a peak at 1925 nm has appeared, which has been assigned to the combination O-H stretching. This suggests that new hydroxy groups have been produced during exposure, such as carboxylic acid end groups. The spectra also show the development of a shoulder between 450-320 nm, indicating the presence of monohydroxy terephthalate groups and quinone species. The formation of these groups during exposure have been discussed in *Chapter 3, Section 3.3.3.*

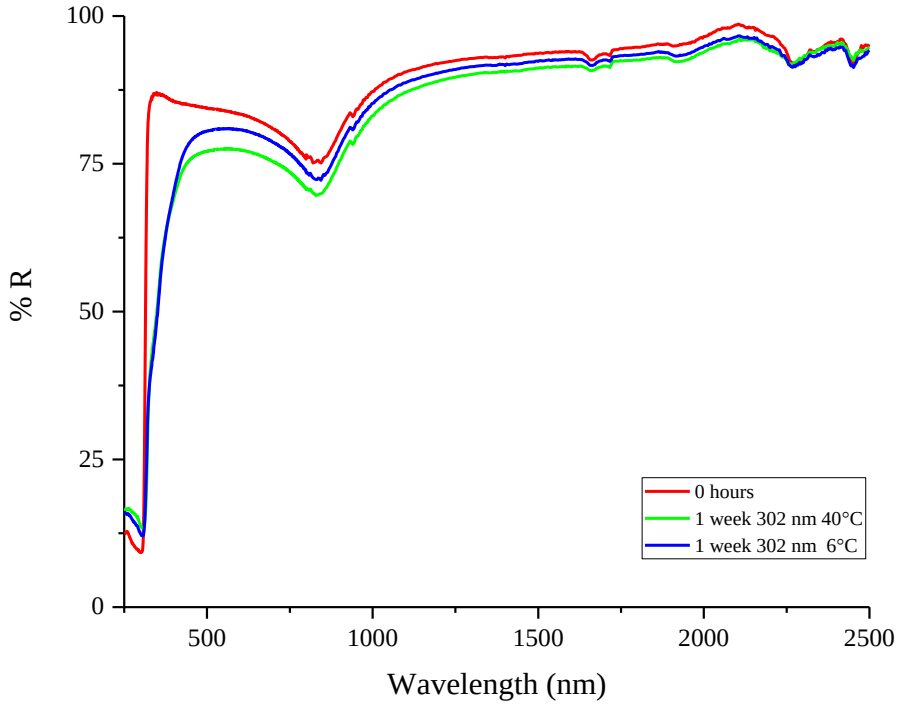

Figure 5.40: UV-Vis-NIR spectra of PDEGT exposed to 302 nm light at 40°C (above T_g) and 6°C (below T_g), for 1 week.

From *Figure 5.40*, there does not appear to be any major differences between the sample exposed above the T_g compared to the sample exposed below the T_g. This is

because UV-Vis-NIR is a surface technique. The IR spectra have shown that temperature influences the bulk, but not surface reactions. Therefore, if the temperature has no effect on the surface and UV-Vis-NIR only analyses the surface, then no change in the spectra is expected.

5.5.3 Conclusions

PDEGT was exposed to 302 nm light at different temperatures, above and below its T_g, to study the effect of temperature on the photodegradation process. ATR data shows that the extent of degradation on the surface of the PDEGT films is not affected by temperature. However, the DRIFT data shows that the extent of degradation in the bulk of the PDEGT films is affected by temperature, due to oxygen diffusion. Below the T_g, the polymer chains are rigid, whereas above the T_g the polymer chains are more flexible, meaning that oxygen can diffuse into the polymer film more easily when the polymer is above its T_g. Therefore, degradation occurs to a greater extent in samples exposed above their T_g.

5.6 Effect of degradation atmosphere

In this part of the study, the effect of degradation atmosphere on the photodegradation of PDEGT was explored. The photodegradation cell (shown in *Chapter 2, Figure 2.06*) was used to run exposures under nitrogen. Again, a chiller unit was attached to the cell to expose the sample above and below its T_g under non-oxidative conditions. The samples were analysed using ATR FT-IR and DRIFT before and after exposure.

5.6.1 Infrared results

5.6.1.1 Exposures above T_g under a non-oxidative atmosphere

The ATR and DRIFT spectra for PDEGT samples exposed to 302 nm light at 40°C (above the T_g) under nitrogen are shown in *Figure 5.41 and 5.42*. Samples were exposed for 1 week (equivalent to a dosage of approximately 1.6 x 10^3 W m^{-2} hr^{-1}) in 24 hour increments (equivalent to a dosage of approximately 2.7 x 10^2 W m^{-2} hr^{-1}). From the spectra, it is apparent that there are changes in the region between 3800-2100 cm^{-1} as well as the carbonyl and fingerprint regions. Other changes identified in the spectra suggest that carboxylic acid end groups, dimers, quinones and mono-substituted rings have been produced during exposure. Chain scission and substitution reactions are also believed to occur. The peaks present in the ATR and DRIFT spectra have been assigned and discussed in *Section 5.2.1.1*.

The spectra, given in *Figure 5.41 and 5.42*, appear to show degradation to a lesser extent than samples exposed under oxidative conditions.

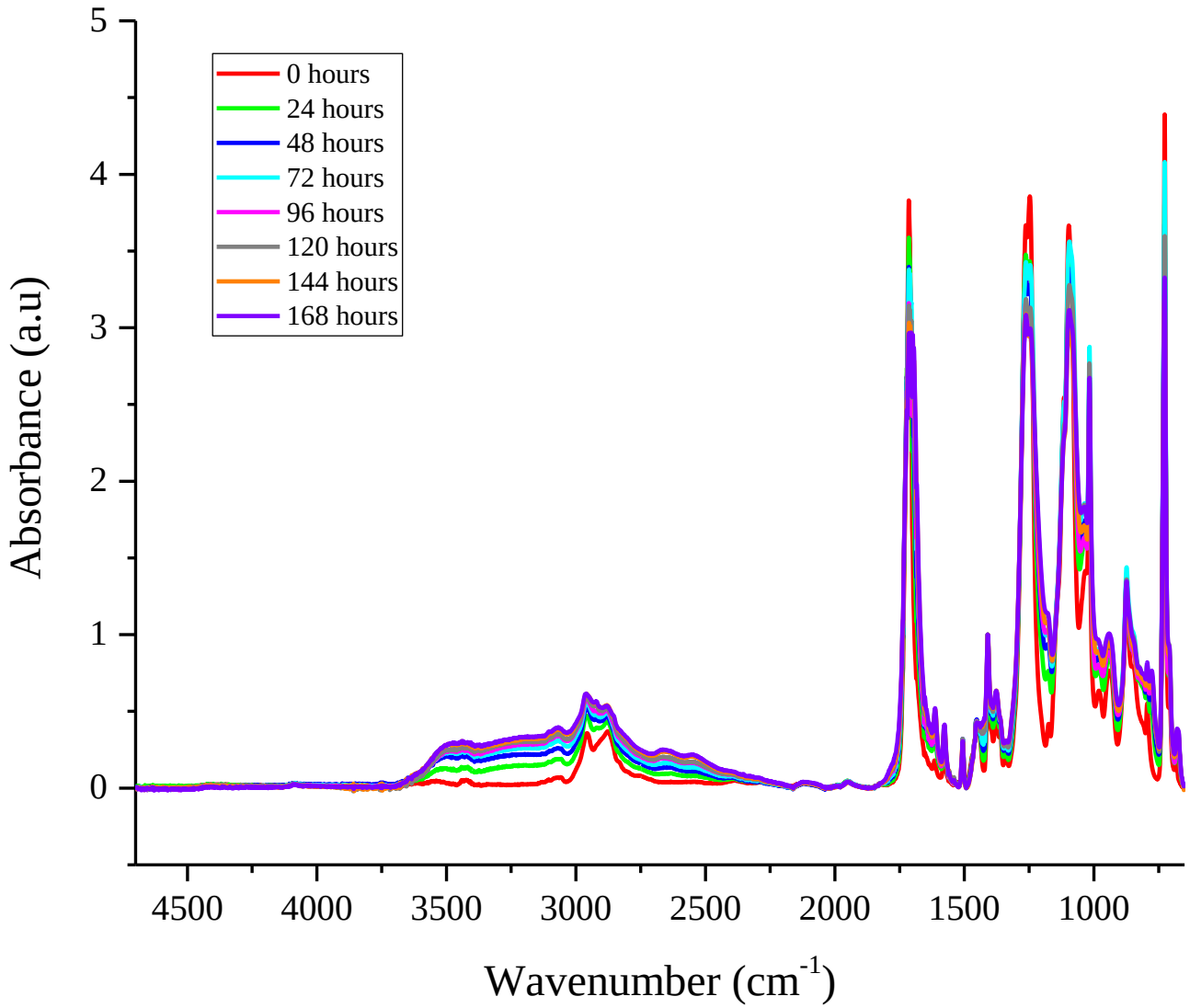

Figure 5.41: ATR FT-IR spectra of PDEGT exposed to 302 nm light at 40°C (above T_g) under nitrogen for 1 week, in 24 hour increments.

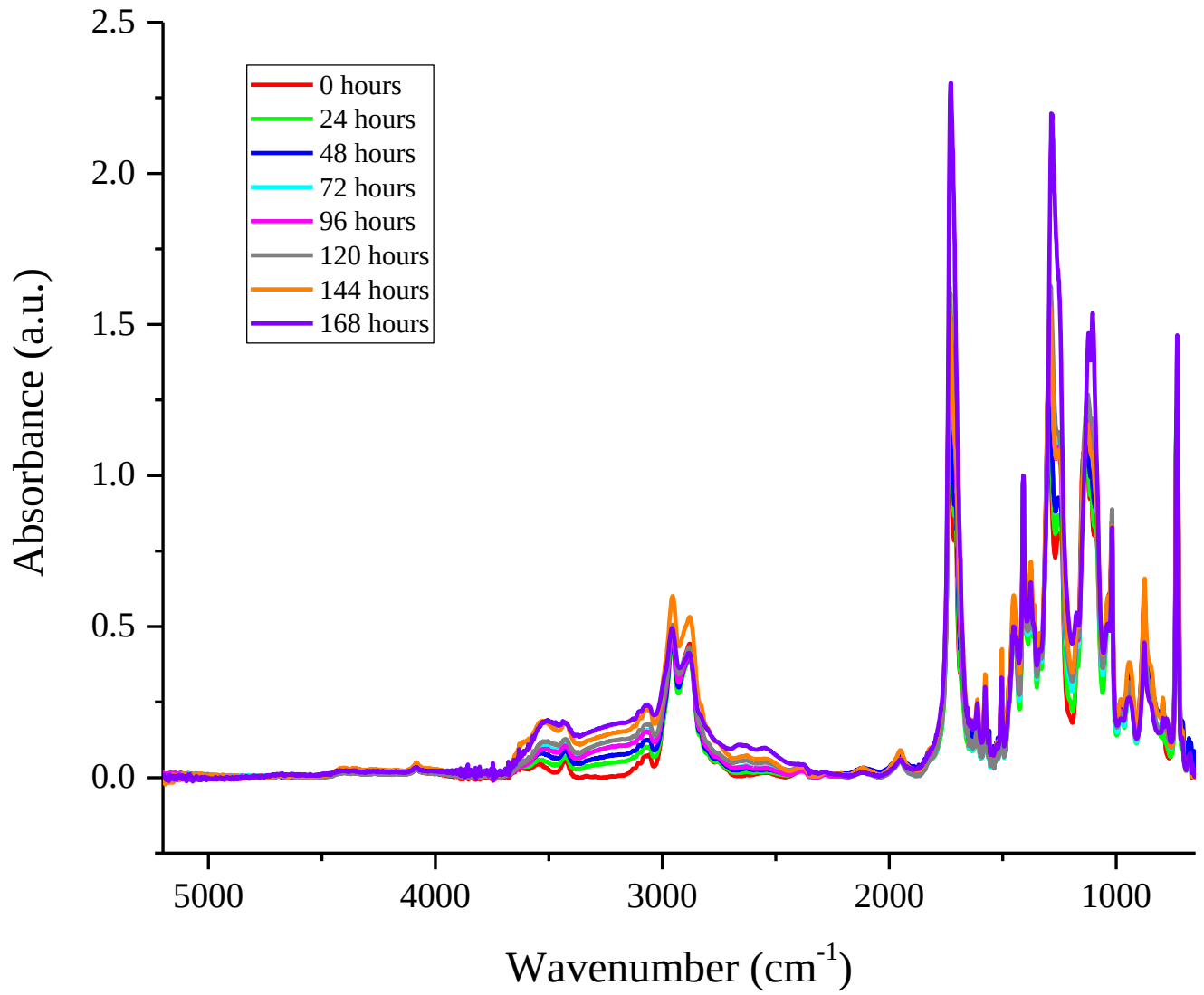

Figure 5.42: DRIFT spectra of PDEGT exposed to 302 nm light at 40°C (above T_g) under nitrogen for 1 week, in 24 hour increments.

5.6.1.2 Exposures below T_g under a non-oxidative atmosphere

PDEGT films were exposed to 302 nm light at 6°C (below T_g) under nitrogen, for 1 week (equivalent to a dosage of approximately 1.8 x 10^3 W m^{-2} hr^{-1}) in 24 hour increments (equivalent to a dosage of approximately 2.6 x 10^2 W m^{-2} hr^{-1}). The ATR and DRIFT spectra, shown in *Figure 5.43 and 5.44*, respectively, show change in the carbonyl and fingerprint regions, as well as the region between 3800-2100 cm^{-1}. These changes suggest that chain scission and substitution reactions have occurred, as well as the formation of carboxylic acid end groups, dimers, and mono-substituted rings, during exposure. The peaks have been assigned and discussed in detail, for the ATR and DRIFT spectra, in *Section 5.2.1.1*.

The spectra, given in *Figure 5.43 and 5.44*, show the same trends as seen with PDEGT exposed at room temperature but appear to show degradation to a lesser extent than samples exposed under oxidative conditions.

The ATR spectra (*Figure 5.43*) shows the development of a peak at 778 cm^{-1}. This peak has been observed before during exposure of PET and PDEGT, and under oxidative and non-oxidative conditions, and is believed to be due to the production of mono-substituted rings. Although this peak has been observed before, under these conditions the absorbance is unusually high. As the sample was exposed below the T_g is it thought that the chemistry has been interrupted, radicals cannot recombine, and the products have been quenched in place. It is thought that the peak is not as large during the exposure of PET below the T_g as there are more hydrogen atoms for the phenyl radical to abstract from the backbone in PDEGT, compared to PET. Below the T_g abstracting a hydrogen atom would be more favourable, in PDEGT, than radical recombination. This being said, if this was the only reason for the more intense peak at 778 cm^{-1} then this would also be present in the spectra of samples exposed below the T_g under oxidative conditions (*Figure 5.5*), but this is not the case. This suggests that the degradation atmosphere also has a part to play in the intensity of this peak. It is thought that degradation products can migrate throughout the polymer during exposure under oxidative conditions. This would explain why there is an increased concentration of this product during exposure under nitrogen.

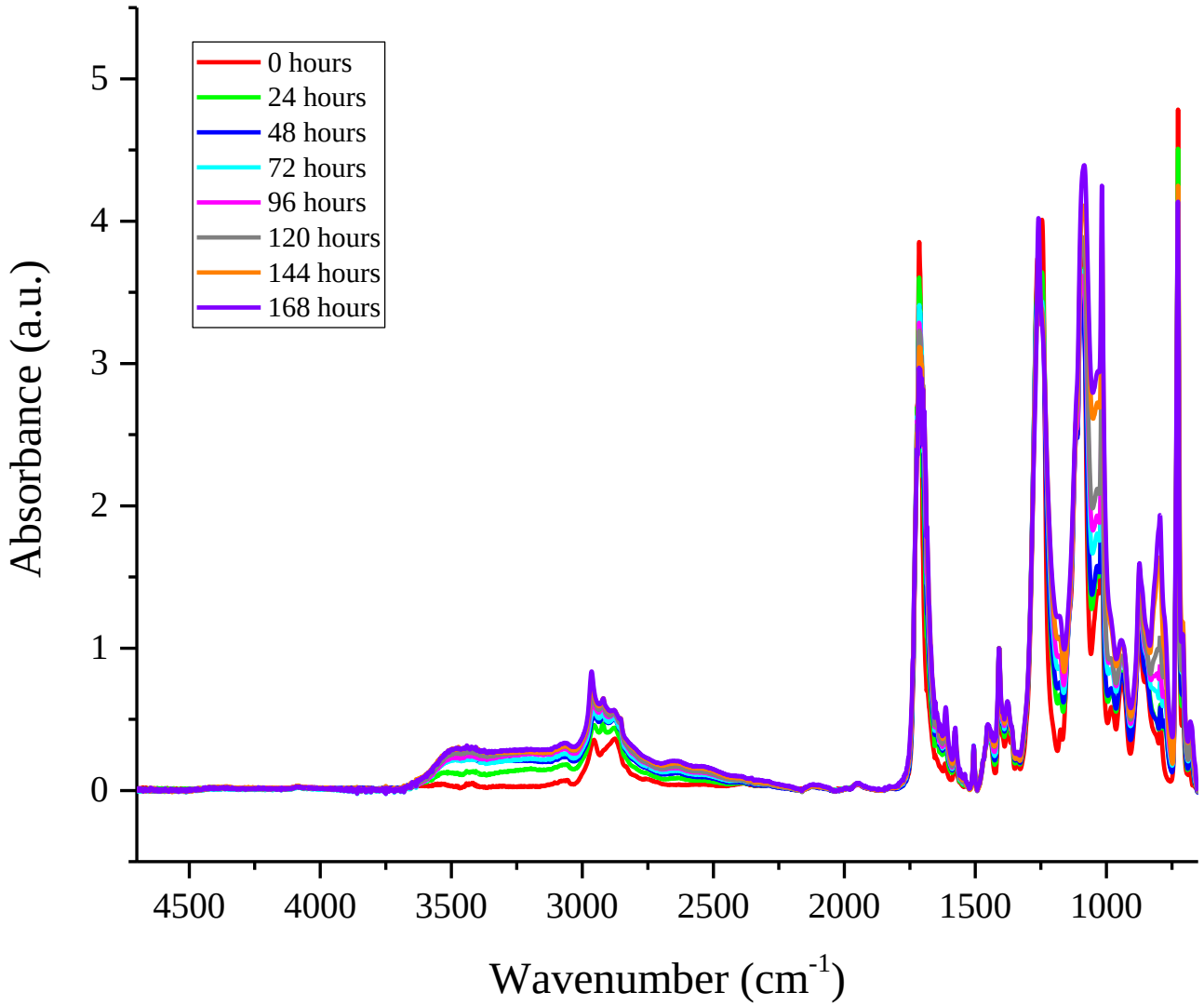

Figure 5.43: ATR FT-IR spectra of PDEGT exposed to 302 nm light at 6°C (below T_g) under nitrogen for 1 week, in 24 hour increments.

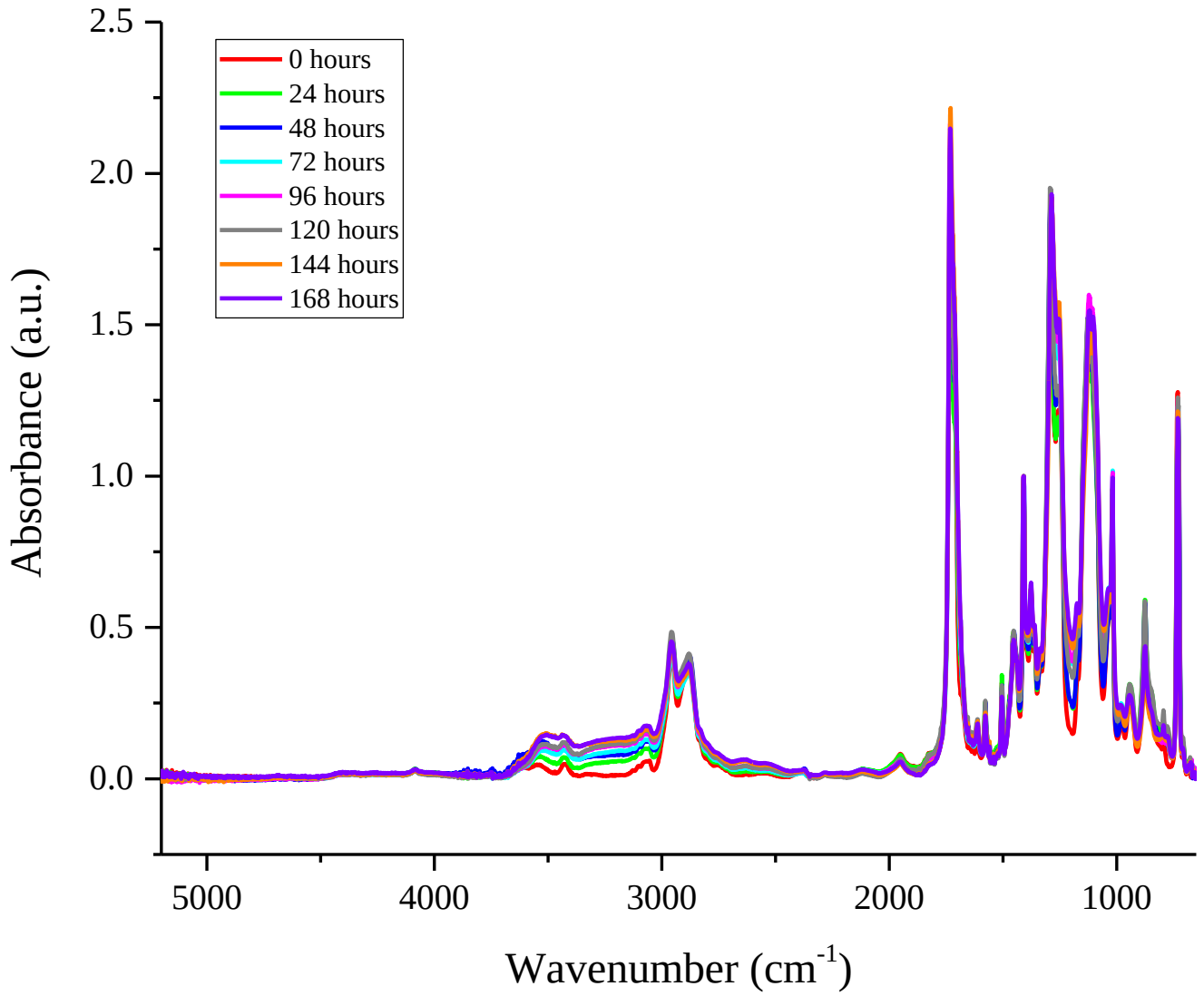

Figure 5.44: DRIFT spectra of PDEGT exposed to 302 nm light at 6°C (below T_g) under nitrogen for 1 week, in 24 hour increments.

5.6.1.3 Extent of photodegradation

As previously defined, the extent of photodegradation for PDEGT was measured by the change in area of the peaks in the region between 3800-2100 cm^{-1} and the carbonyl peak. *Figure 5.45* shows the change in area of these peaks, with dosage, for PDEGT exposed to 302 nm light above and below the T_g, under oxidative and non-oxidative conditions, determined from the ATR spectra. *Figure 5.46* shows the extent of degradation, calculated from the DRIFT spectra.

Figure 5.45 (a) and (b) show that the extent of degradation on the surface of the film has been affected by degradation atmosphere. PDEGT samples exposed under nitrogen show degradation to a lesser extent compared to those exposed under oxidative conditions, due to the absence of oxygen. Oxygen is no longer part of the degradation reactions when PDEGT is exposed under nitrogen and therefore shows degradation to a lesser extent.

Initially, the graph indicates that temperature does not influence the extent of degradation, which agrees with the ATR data reported for samples exposed at different temperatures under oxidative conditions (*Figure 5.38*). However, at higher dosages differences start to become apparent. The samples exposed under nitrogen at different temperatures show that PDEGT exposed above the T_g degrades to a greater extent compared to the sample exposed below the T_g. This could suggest that under oxidative conditions the presence of oxygen primarily affects the extent of degradation compared to the change in temperature, on the surface, at short timescales. Whereas, under non-oxidative conditions, the temperature and atmosphere are both important parameters.

Although the samples were exposed under nitrogen, it is thought that the cell was not allowed to flush with nitrogen for long enough, meaning that some oxygen may still be present during exposure. This suggests that PDEGT samples exposed under non-oxidative conditions may degrade to a lesser extent than reported.

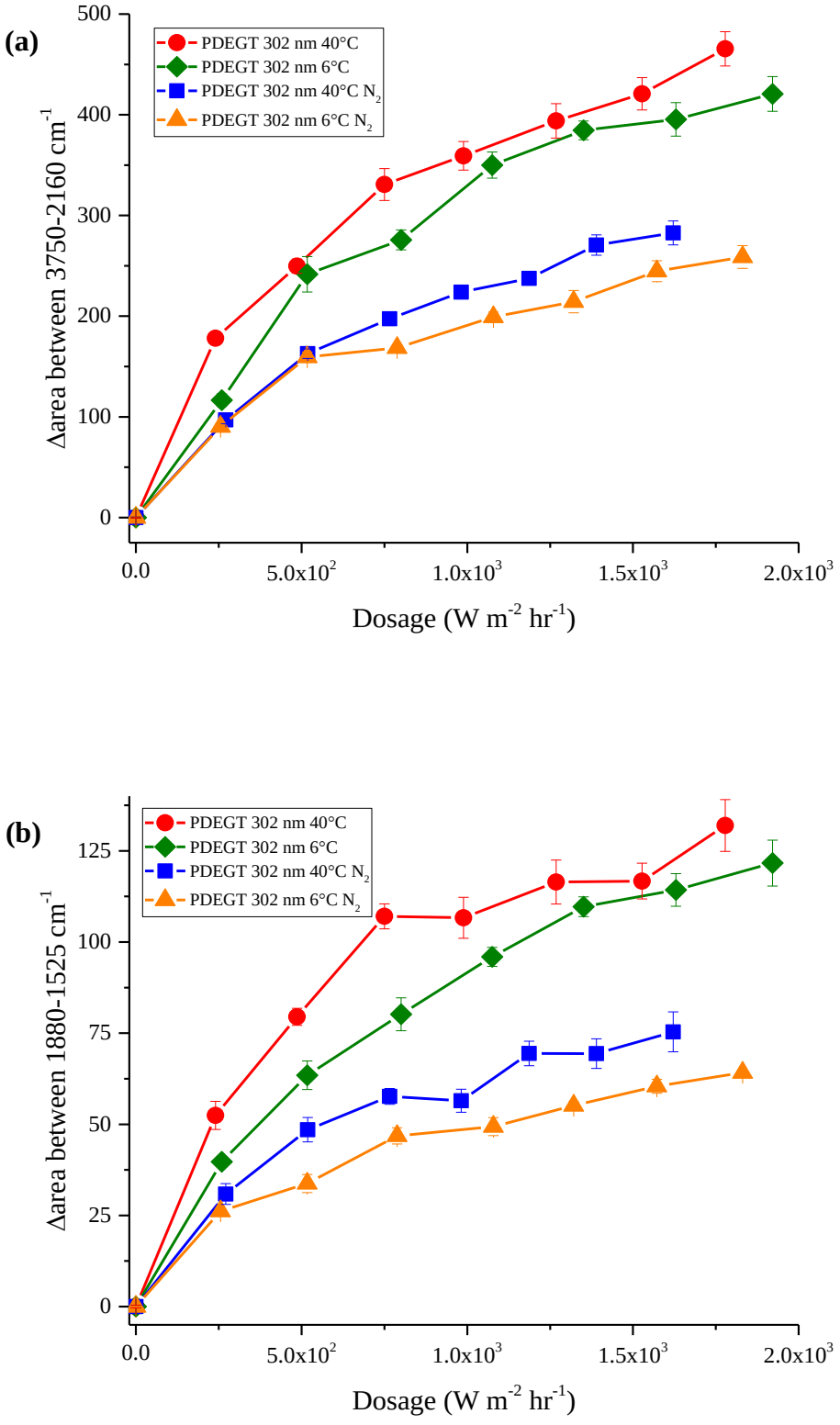

Figure 5.45: Extent of photodegradation of PDEGT measured by the change in area of peaks between (a) 3750-2160 cm^{-1} and (b) 1880-1525 cm^{-1}(carbonyl), from the ATR spectra.

The graphs in *Figure 5.46 (a) and (b)* show that the extent of degradation in the bulk of the PDEGT films has been influenced by degradation atmosphere. Samples of PDEGT exposed under oxidative conditions have a greater extent of degradation for a given irradiation dosage compared to those exposed under nitrogen. This agrees with the extent of degradation shown in *Figure 5.45,* determined from the ATR spectra.

At short timescales, the graphs indicate that temperature does not have an effect on the extent of degradation when the samples are exposed under nitrogen. However, at higher dosages, differences become apparent with the sample exposed below the T_g degrading to a lesser extent compared to the sample exposed above the T_g. This supports data reported in *Section 5.5.* It is thought that temperature influences the extent of degradation in the bulk of the sample due to oxygen diffusion. On the other hand, these samples have been exposed under nitrogen, it is therefore thought that the cell was not allowed to flush with nitrogen for long enough before beginning exposure experiments, and thus oxygen was still present in deeper positions of the film.

From analysing the graphs in *Figure 5.46,* it could be suggested that samples exposed under oxidative conditions the temperature and presence of oxygen are both important parameters. Whereas, under non-oxidative conditions, the absence of oxygen primarily affects the extent of degradation compared to the change in temperature, in the bulk of the film, at short timescales.

Figure 5.45 and 5.46 also show that on the surface, degradation occurs to a greater extent than in the bulk of the sample. This could be because 302 nm light has been shown to preferentially affect the surface of the film compared to the bulk, and in this case, the same could be said under non-oxidative conditions.

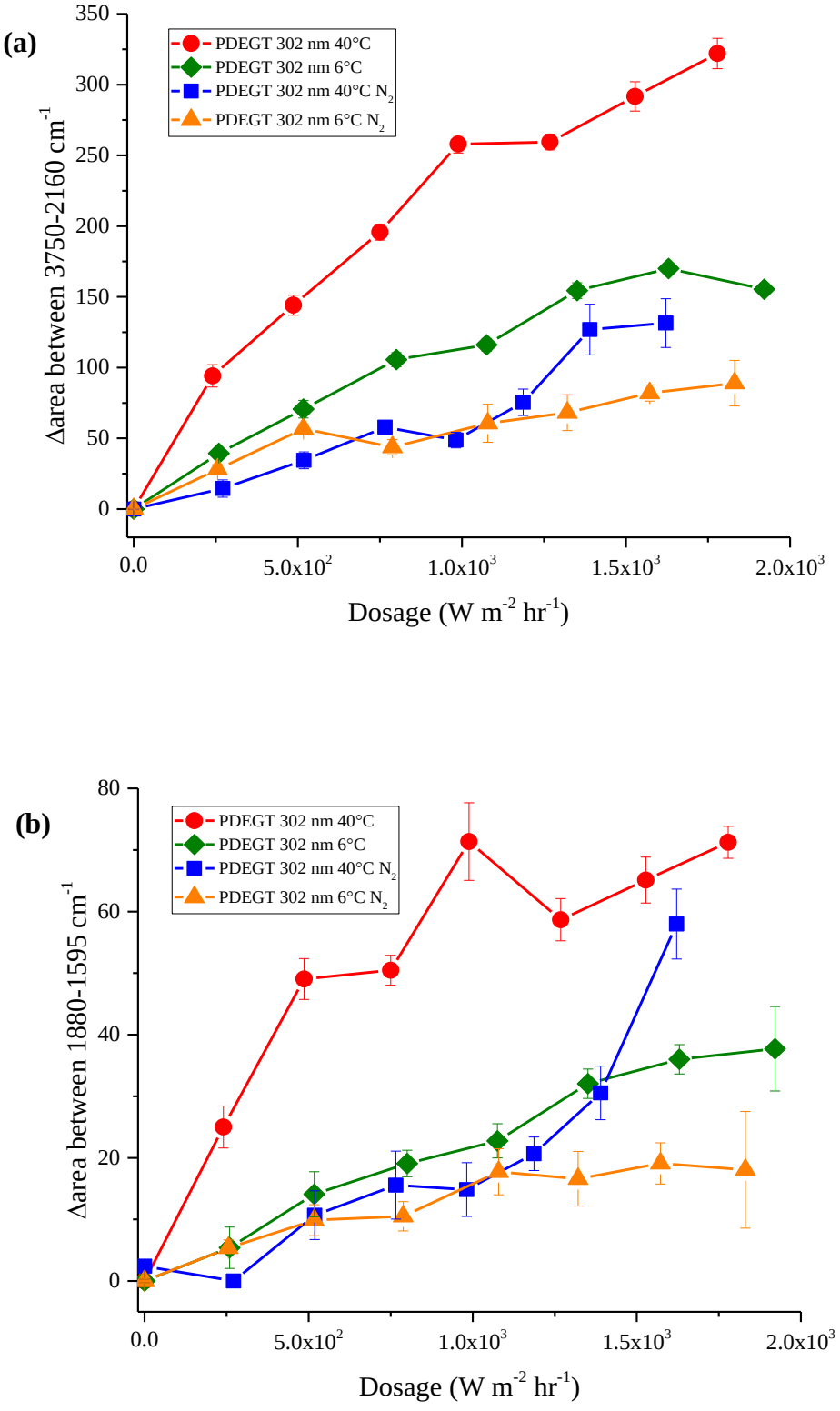

Figure 5.46: Extent of photodegradation of PDEGT measured by the change in area of peaks between (a) 3750-2160 cm^{-1} and (b) 1880-1595 cm^{-1}(carbonyl), from the DRIFT spectra.

5.6.2 Conclusions

Using ATR FT-IR and DRIFT the effect of atmosphere on the photodegradation reactions taking place in PDEGT, during exposure, was investigated. The results show that when PDEGT is exposed to 302 nm light under nitrogen degradation occurs to a lesser extent, compared to exposures in air, on the surface and in the bulk of the sample. PDEGT samples exposed under non-oxidative conditions degrade to a lesser extent compared to those exposed under oxidative conditions due to the absence of oxygen in the system.

5.7 Mechanistic pathways for the photodegradation of PDEGT

5.7.1 Oxidative conditions

Figure 5.47 shows the proposed initiation free radical reactions as well as the mechanistic pathway for the photo-oxidation reactions occurring during the degradation of PDEGT. This mechanism was proposed by Bei *et al.* for the photodegradation of polycaprolactone-poly(ethylene glycol) block copolymer[26] Bei *et al.* reported that pure poly(ethylene glycol) could not be photodegraded alone but increasing its content in the copolymer increased the rate of photodegradation. The authors concluded that this was due to the carbonyl groups in the poly(ε-caprolactone) segment catalysing the breakage of the poly(ethylene glycol) chains through UV initiated free radical reactions.

5.7.2 Non-oxidative conditions

The mechanistic pathway, shown in *Figure 5.48*, was originally suggested for the photodegradation of PET under vacuum by Day and Wiles.[23] Here it has been adapted for the photodegradation reactions taking place in PDEGT under non-oxidative conditions, with the proposal of reaction 9. Reaction 9 has been suggested here to account for the appearance of the new peak at 780 cm^{-1} in the ATR data, associated with the formation of mono-substituted rings. This reaction is dependent upon temperature.

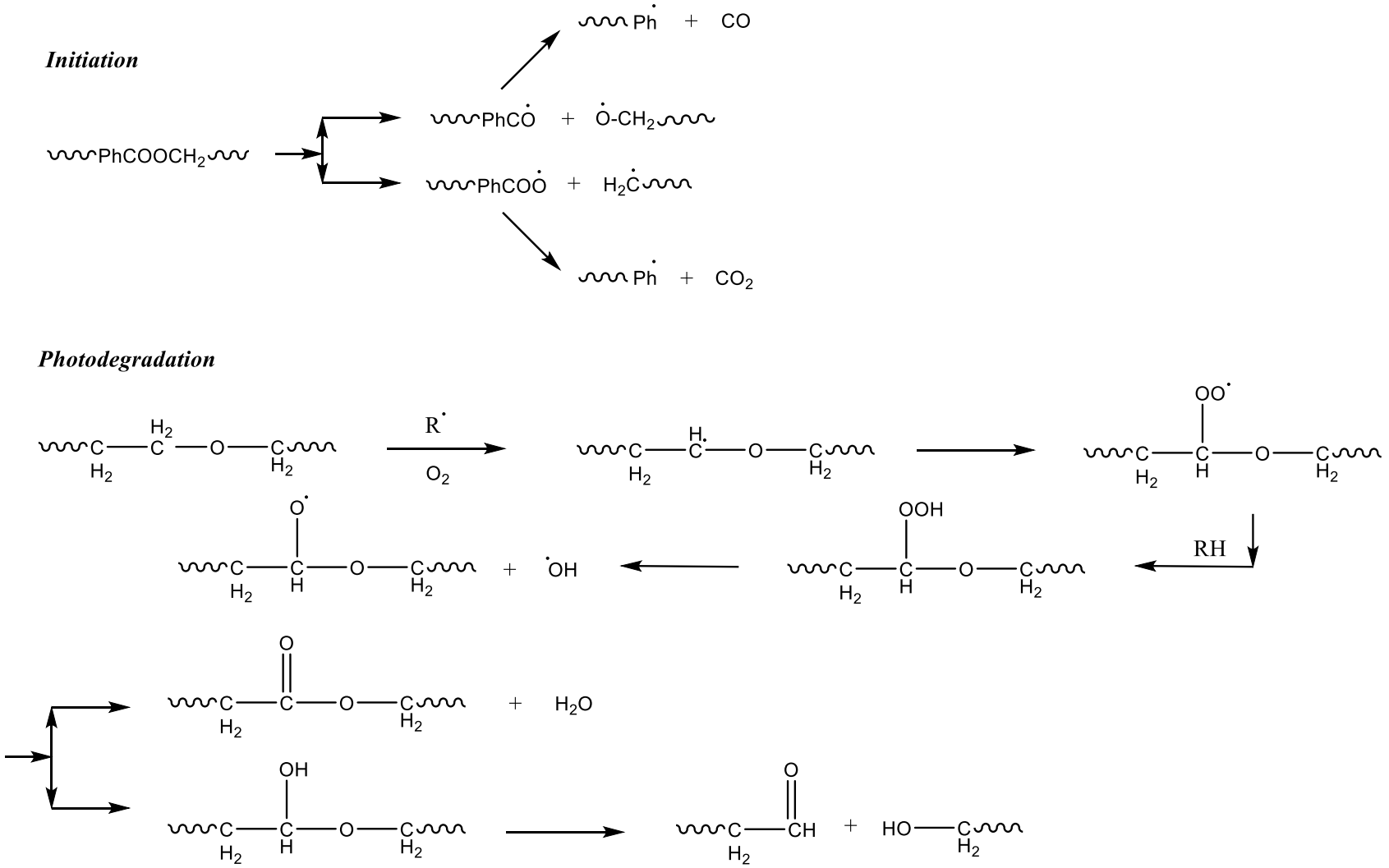

Figure 5.47: Mechanistic pathway for the photodegradation of PDEGT under oxidative conditions.

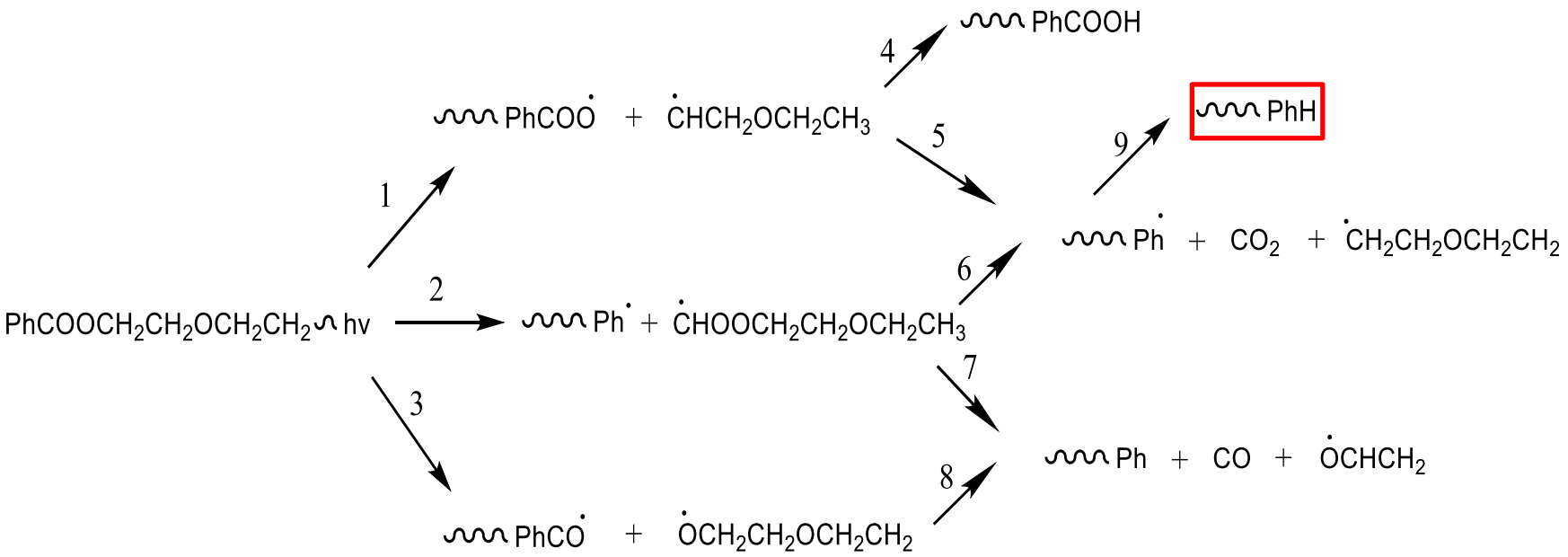

Figure 5.48: Mechanistic pathway for the photodegradation of PDEGT under non-oxidative conditions.

5.8 References

1 M. Day and D. M. Wiles, *J. Appl. Polym. Sci.*, 1972, **16**, 175–189.

2 B. J. Holland and J. N. Hay, *Polymer*, 2002, **43**, 1835–1847.

3 C. F. Ladasiu Ciolacu, N. Roy Choudhury and N. K. Dutta, *Polym. Degrad. Stab.*, 2006, **91**, 875–885.

4 Z. Chen, J. N. Hay and M. J. Jenkins, *Eur. Polym. J.*, 2012, **48**, 1586–1610.

5 N. B. Colthup, L. H. Daly and S. E. Wiberley, *Introduction to Infrared and Raman Spectroscopy*, Academic Press, Third Edition., 2009.

6 A. K. Crane, E. Y. L. Wong and M. J. MacLachlan, *CrystEngComm*, 2013, **15**, 9811.

7 P. Delprat and X. Duteurtreb, *Polym. Degrad. Stab.*, 1995, **50**, 1–12.

8 C. V Stephenson, C. Lacey and W. S. Wilcox, *J. Polym. Sci.*, 1961, **55**, 477–488.

9 J. Scheirs and J. L. Gardette, *Polym. Degrad. Stab.*, 1997, **56**, 339–350.

10 M. Day and D. M. Wiles, *J. Appl. Polym. Sci.*, 1972, **16**, 191–202.

11 A. Rivaton, J. L. Gardette, C. E. Hoyle, M. Ziemer and D. R. Fagerburg, 2000, **41**, 3541–3554.

12 N. B. Colthup, L. H. Daly and S. E. Wiberley, in *Introduction to Infrared and Raman Spectroscopy*, 1990, pp. 289–325.

13 J. V. Gulmine, P. R. Janissek, H. M. Heise and L. Akcelrud, *Polym. Degrad. Stab.*, 2003, **79**, 385–397.

14 M. Edge, R. Wiles, N. S. Allen, W. A. McDonald and S. V Mortlock, *Polym. Degrad. Stab.*, 1996, **53**, 141–151.

15 G. A. Cordell, *The Alkaloids*, Academic Press, 1997.

16 N. S. Allen, M. Edge, M. Mohammadian and K. Jones, *Polym. Degrad. Stab.*,

1994, **43**, 229–237.

17 G. J. M. Fechine, M. S. Rabello, R. M. Souto Maior and L. H. Catalani, *Polymer*, 2004, **45**, 2303–2308.

18 W. E. I. Wang, A. Taniguchi, M. Fukuhara and T. Okada, 1998, 306–310.

19 H. A. Pohl, *J. Am. Chem. Soc.*, 1951, **73**, 5660–5661.

20 J. Scheirs and J. Gardette, *Polym. Degrad. Stab.*, 1997, **56**, 339.

21 P. de Donato, J. M. Cases, B. Humbert, P. Lutgen and G. Feyder, *J. Polym. Sci. Part B Polym. Phys.*, 1992, **30**, 1305–1310.

22 J. G. Pacifici and J. M. Straley, *Polym. Lett.*, 1969, **7**, 7–9.

23 M. Day and D. M. Wiles, *J. Appl. Polym. Sci.*, 1972, **16**, 203–215.

24 M. Edge, N. S. Allen, R. Wiles, W. McDonald and S. V. Mortlock, *Polymer*, 1995, **36**, 227–234.

25 G. J. M. Fechine, M. S. Rabello and R. M. Souto-Maior, *Polym. Degrad. Stab.*, 2002, **75**, 153–159.

26 J. Bei, W. He, X. Hu and S. Wang, *Polym. Degrad. Stab.*, 2000, **67**, 375–380.

6 Conclusions and Future Work

6.1 Conclusions

At the outset, some fundamental exposure studies were carried out to explore the photodegradation reactions occurring when PET was exposed to UV light. Stacks of 12, 23 and 36 μm PET films were used to understand if a stack of films would degrade in the same way as a single film of the same thickness. This could then be used for depth profiling analyses. Unfortunately, it was reported that scattering was occurring at the interface of each layer in a stack of films, which means that using a stack of thin films is not a reliable way to study the depth profile of a single film of the same thickness.

Samples of 23 and 36 μm PET were exposed to broad band light (290-800 nm) in the weatherometer, where 1 week of exposure is approximately equal to 7.5 weeks outdoors. After exposure, results showed the production of various degradation products, including carboxylic acid end groups, anhydrides, quinones and monohydroxy terephthalate groups, as well as mono-substituted rings. In addition, there was evidence of substitution, chain scission, branching and crosslinking reactions. From the results collected it was clear that, even though the films showed some degradation, it was near impossible to determine the role of each wavelength in the degradation.

For this reason, narrow wavelength ranges of light (302 nm and 365 nm) were used to study the role of different wavelengths. Films exposed to 302 nm light showed production of carboxylic acid end groups, dimers, anhydrides, aldehydes, quinones and monohydroxy terephthalate groups. Furthermore, results indicated substitution and chain scission reactions, as well as surface cracks, occurring in the samples exposed to 302 nm light, while samples at 365 nm light showed only minor changes. Results from these experiments showed that PET degrades to a greater extent when exposed to 302 nm light compared to 365 nm light of the same intensity.

However, there were some minor changes identified when PET was exposed to 365 nm light, so a high intensity 365 nm light was used to accentuate any minimal changes.

In the literature, it has been reported that longer wavelength light has no meaningful effect on PET, but reports have only focused on the surface of the films. Although absorbed weakly, it was evident, using DRIFT, that 365 nm light preferentially affected the bulk of the film rather than the surface. In addition, PET samples were also exposed to 302 nm light under nitrogen, which showed that peaks evolved that have not been reported during exposure under air. These peaks are associated with changes in the substitution patterns on the ring and the build-up of conjugated aromatic structures. Results show that degradation occurs to a lesser extent under non-oxidative conditions compared to oxidative conditions, due to the absence of oxygen in the system.

Exposing samples to broad and narrow band light demonstrated that PET degrades to a greater extent under short wavelength light compared to longer wavelength light and under oxidative conditions compared to non-oxidative conditions. However, at this point in the study, it was believed that long wavelength light could be having more of a detrimental effect than previously reported; due to some differences identified in the results of samples exposed to broad band compared to those exposed to narrow band light.

Samples of PET were exposed to different wavelengths of light sequentially in an effort to study the reactions that occur simultaneously outdoors. Samples were exposed to 302 nm light followed by 365 nm light and vice versa. Results show the production of numerous degradation products including, carboxylic acid end groups, dimers, anhydrides, aldehydes and monohydroxy terephthalate groups.

Exposing samples to 302 nm light first produces new chromophoric groups which allow the polymer to absorb longer wavelengths of light. Additionally, results indicate that 302 nm light is causing chain scission, whereas 365 nm light is primarily causing branching and crosslinking reactions to occur. From the data, it is reasonable to conclude that exposure to 302 nm light does influence the effect of subsequent exposure to 365 nm light.

Samples were also exposed to 365 nm light first, and although changes were identified on the surface of the films after exposure to 365 nm light, techniques that analyse the bulk of the film showed that 365 nm light may have more of an influence on the effect

of subsequent exposure to 302 nm light than originally expected. In addition, results provided evidence for the theory that 365 nm light primarily causes branching and crosslinking reactions, whereas 302 nm light causes chain scission reactions to occur. From the data presented, it can be concluded that 365 nm light did not significantly influence the effect of subsequent exposure to 302 nm light, at the timescales used in this study. Exposing samples to different wavelengths of light consecutively has proven to be a new, effective way of studying the reactions that occur simultaneously outdoors.

Finally, the effect of wavelength, temperature, and atmosphere on the photodegradation reactions occurring in PDEGT, during irradiation, have been investigated. Results show that PDEGT degrades to a greater extent than PET when exposed to broad band light (290-800 nm) in the weatherometer. This is thought to be due to the instability of the ether linkage, however, this could also be due to the fact that PDEGT was exposed above its T_g. PDEGT also degrades to a greater extent when exposed to 302 nm light compared to 365 nm light. However, samples exposed to high intensity 365 nm light showed spectral changes on the surface and in the bulk. Exposing PDEGT above and below its T_g showed that the surface was not affected by temperature, but the bulk was affected, whereas exposing samples under nitrogen affected both the surface and the bulk of the film. Considering all the results reported in this study, mechanistic pathways have been proposed for the oxidative and non-oxidative reactions occurring when PDEGT is exposed to UV light.

6.2 Future Work

Although the photodegradation reactions have been studied during exposure of PET and PDEGT films, there remains some research to be undertaken to build a full picture of what is believed to be occurring. These include:

- Carry out more tests exposing PET to specific wavelengths of light under a non-oxidative environment and consider exposing samples above the T_g, and samples of different thickness and crystallinities.
- This research would also benefit from pre-treating the samples with one wavelength of light for longer before exposing to a different wavelength of light. It would also be interesting to expose samples to 302 nm light and then expose to a longer wavelength of light, for example, 405 nm.
- It would be advantageous to explore a more efficient way to expose the samples under a non-oxidative environment, as from results shown in this thesis the error bars are larger for samples exposed using the photodegradation cell.
- Another area of interest would be to synthesis PET containing different percentages of DEG segments to analyse if samples with a higher DEG content would degrade more extensively compared to those with a low DEG content.
- A more efficient way to create the PDEGT films should be considered, as a more consistent thickness across the width of the film would be beneficial.
- An additional, interesting area would be to carry out a pre-treatment study, like the one reported in *Chapter 4*, using PDEGT films.